warwick.ac.uk/lib-publications

The Role of the staphylococcal Type VII secretion system in the modulation of host responses

by

Kate Eloise Watkins

BSc (Hons). MSc.

─────────────

Thesis submitted for the degree of

Doctor of Philosophy

in Interdisciplinary Biomedical Research

─────────────

Warwick Medical School

University of Warwick

Supervisors: Dr. Meera Unnikrishnan and Dr. Marco Polin

Table of Contents

I.   List of figures

II. List of Tables

III. Acknowledgements

I would like to express my deepest gratitude to my supervisor Dr Meera Unnikrishnan for her invaluable mentorship and assistance during this project. Your devotion to science has continued to inspire my own ambitions. Even at the most frustrating of times I always left a meeting with you with a smile on my face. In addition, to the WMS MRC DTP team, thank you for awarding me this opportunity. The Doctoral Training Programme created a wonderfully supportive environment which has given me confidence in my work and most importantly a set of friends for life.

I would like to thank a previous member of the Unnikrishnan group, Dr Arnaud Kengmo Tchoupa, for teaching me the ropes and for being a guiding hand, but especially, for the endless jokes in the lab. To the rest of the MIU, I could not have wished to be part of a more cohesive and collaborative group. Thank you for the all the fun times, help and friendship. I would like to specifically thank Grace Taylor-Joyce for being a fantastic housemate, friend and invaluable colleague, together we helped each other through a tough thesis write-up and pandemic lockdown.

To my dearest friend Sophie, thank you for being a beacon of positivity and encouragement. I have missed you being close by, but seeing you was always the break I needed from work. I will try to permanently move back down South now! Finally, thank you to my amazing family for your immeasurable love and support throughout my PhD. I especially thank my Mum for being my rock and for keeping me sane through this whole experience.

Onwards and upwards!

IV. Declaration

This thesis is submitted to the University of Warwick in support of my application for the degree of Doctor of Philosophy. It has been composed by me and has not been submitted in a previous application for any degree.

The work presented (including data generated and data analysis) was carried out by the author except for the following things:

- The Δ*esxC S. aureus* USA300 JE2 strains was made prior to this project by Arnaud Kengmo Tchoupa.
- The histological embedding, sectioning and hematoxylin and eosin staining of mouse abscesses were carried out by Manchester University Core Histology Facility.

Signed:……   ……….

Date:…………30/03/2021…………………

V. Summary

The staphylococcal type VII secretion system (T7SS) is responsible for the export of several virulence factors. Some T7SS effectors are associated with long-term persistence of *Staphylococcus aureus* in murine models and modulation of epithelial and dendritic cell death, although the molecular mechanisms underlying T7SS-mediated modulation of cellular processes remain unclear. The aim of this study was to investigate the role of staphylococcal T7SS during macrophage infection. Isogenic mutants lacking either single or multiple secretion substrates of the T7SS (EsxC, EsxB, EsaE and EsxD) or EssC, an ATPase driving protein export were studied in comparative *in vitro* assays using THP-1 macrophages and *in vivo* mouse models.

Time-lapse microscopy over the course of 24 hrs revealed that intracellular *S. aureus* caused the formation of pore-induced intracellular traps (PIT)-like structures, indicative of lytic cell death, in macrophages. Wild type (WT) *S. aureus* infections resulted in an early peak in cell death and inflammatory cytokine release which was absent or markedly shifted with T7SS mutant infections. WT induced early cell death was attributed to the T7SS promotion of the necroptosis pathway. Importantly T7SS mutants were not defective at causing necroptosis, but promotion of this pathway appeared to occur at later timepoints, suggesting other *S. aureus* virulence factors can also cause the onset of necroptosis in macrophages. Interestingly, in low-dose skin infections, T7SS mutants survived better than the WT and demonstrated enhanced dissemination to distal sites. However, WT was more successful in high-dose infections which indicates dose dependent changes in the effect of the T7SS. Finally, using interdisciplinary techniques a microfluidic air-way-blood-vessel-on-a-chip was designed, fabricated and evaluated for the investigation of *S. aureus*-host interactions under shear stress. Overall, this project provided insight into specific roles of the T7SS in macrophages and questions whether that the T7SS is always beneficial for *S. aureus* during infection.

VI.   List of Abbreviations

Agr	Accessory gene regulator
ASC	Apoptosis-associated speck-like protein containing caspase activation and recruitment domains
ATCC	American Type Culture Collection
ATP	Adenosine Triphosphate
ATPase	Adenosine Triphosphatase
BCG	*Mycobacterium bovis* Calmette-Guérin
BirA	Biotin ligase
BCL2	B-cell lymphoma 2
BMDM	Bone-marrow-derived macrophage
BSA	Bovine serum albumin
CA-MRSA	Community associated methicillin resistant Staphylococcus aureus
CFP-10	Culture filtrate protein 10 kDa
CFU	Colony forming unit
c-GSDMD	Cleaved gasdermin D
Chlor-10	Chloramphenicol 10 µg/mL
ClfB	Clumping factor B
CLR	C-type lectin receptor
CWA	Cell wall-anchored protein
DAMP	Danger associated molecular patterns
DAPI	4′,6-Diamidino-2-phenylindole
DCF	2′, 7′-Dichlorofluorescein
DCF-DA	2′,7′-Dichlorofluorescin diacetate
DMEM	Dulbecco's Modified Eagle Medium
ECM	Extracellular matrix
EHEC	Enterohemorrhagic *E. coli*
EIEC	Enteroinvasive *E. coli*
ESAT-6	Early secreted antigenic target 6 kDa
ESCRT	Endosomal sorting complexes required for transport
Ess	ESAT-6-like secretion system

ETEC	Enterotoxigenic *E. coli*
FBS	Fetal bovine serum
FnBP	Fibronectin binding protein
GM-CSF	Granulocyte-macrophage colony-stimulating factor
GSDMD	Gasdermin-D
H&E	Hematoxylin and eosin
HA-MRSA	Hospital associated methicillin resistant Staphylococcus aureus
HIV	Human immunodeficiency virus
HMGB1	High Mobility Group Box 1
HUVEC	Human umbilical vein endothelial cell
IFN	Interferon
IgG	Immunoglobulin G
IL	Interleukin
ILR	Interleukin receptor
JNK	c-Jun N-terminal kinase
LA	Linoleic acid
LAC	Los Angeles County jail
LAMP-1	Lysosomal associated membrane protein-1
LDH	Lactate dehydrogenase
LTA	Lipoteichoic acid
LPS	Lipopolysaccharide
LUKAB	Leukocidin A/B
MAPK	Mitogen-activated protein kinase
MCL1	Myeloid cell leukaemia 1
MCP-1	Monocyte chemoattractant protein 1
METs	Macrophage extracellular traps
MHC-II	Major histocompatibility complex class II
MIP-1α	Macrophage inflammatory protein-1α
MLKL	Mixed lineage kinase domain-like protein
MOI	Multiplicity of infection
MprF	Multiple peptide resistance factor

MRSA	Methicillin resistant *Staphylococcus aureus*
MSCRAMM	Microbial surface components recognizing adhesive matrix molecules
MSD	Meso Scale Discovery
MSSA	Methicillin sensitive *Staphylococcus aureus*
Mtb	*Mycobacterium tuberculosis*
MyD88	Myeloid differentiation primary response 88
NADPH	Nicotinamide adenine dinucleotide phosphate
Nec-1	Necrostatin-1
NET	Neutrophil extracellular trap
NGS	Normal goat serum
NLR	NOD-like receptor
NLRC	NOD-like receptor csaspase activation and recruitment domains
NLRP	NOD-like receptor with pyrin domain
NOD	Nucleotide-binding oligomerization domain
NOX	NADPH oxidase
NSA	Necrosulfonamide
OD	Optical Density
PAMP	Pathogen associated molecular patterns
PBS	Phosphate-buffered saline
PBMCs	Peripheral blood mononuclear cells
PCR	Polymerase chain reaction
PDMS	Poly dimethyl siloxane
PE	Proline-glutamic acid protein families
PFA	Paraformaldehyde
PMA	phorbol 12-myristate 13-acetate
p-MLKL	Phosphorylated mixed lineage kinase domain-like protein
PMNs	polymorphonuclear leukocytes
PI	Propidium iodide
PIT	Pore-induced intracellular trap
PPE	Proline-proline-glutamic acid protein families

PRR	Pattern recognition receptors
PSM	Phenol-soluble modulin
PVL	Panton–Valentine leukocidin
QPI	Quantitative phase imaging
RBCs	Red Blood Cells
RIG	Retinoic acid-inducible
RIPA	Radioimmunoprecipitation assay buffer
RIPK	Receptor-interacting serine/threonine-protein kinase
RNS	Reactive nitrogen species
ROS	Reactive oxygen species
RPMI	Roswell Park Memorial Institute
SARM	sterile alpha and HEAT/Armadillo motif
SaeRS	*S. aureus* exoprotein expression RS
SCV	Small colony variant
Sec	General Secretion pathway
SigB	Alternative sigma factor B
SpA	Staphylococcal protein A
SR-A	Scavenger receptor A
SSTI	Skin and soft tissue infection
Tat	Twin-arginine translocation
TCS	Two-component system
TE	Tris-EDTA
TEER	Transepithelial/endothelial electrical resistance
TIR	Toll-interleukin receptor
Th	T-helper cell
TLR	Toll-like receptor
TNF-α	Tumor necrosis factor alpha
TE	Tris-Ethylenediaminetetraacetic acid
TSB	Tryptic soy broth
T7	Type VII
T7SS	Type VII secretion system

UK	United Kingdom
ULvWF	Ultra-large von Willebrand factor
USA	United States of America
VISA	Vancomycin-intermediate resistant *Staphylococcus aureus*
vWF	Von willebrand factor
WHO	World Health Organisation
YFP	Yellow fluorescent protein

1 Chapter 1: Introduction

1.1 *Staphylococcus aureus*

Staphylococcus aureus is a Gram-positive spherical bacterium first isolated in 1880 from pus in a surgical abscess of the knee by Scottish surgeon Sir Alexander Ogston. Its etymology, from the Greek *staphyle* (bunch of grapes) and *kokkos* (berry), is accurate in describing is microscopic appearance. Later in 1884 the German physician Friedrich Julius Rosenbach differentiated the bacteria from other staphylococci by its distinct yellow colony pigmentation: *Staphylococcus aureus* (from the Latin *aurum*, gold) (Sejvar, 2013) .

S. aureus is very successful facultative human pathogen that is associated with both hospital and community settings. It causes a wide spectrum of infections in humans ranging from mild skin abscesses and impetigo to life-threatening septicaemia and endocarditis (Naber, 2009; Tong et al., 2015). In addition to this, it is found to colonise approximately 30% of humans as a commensal (H. F. Wertheim et al., 2005). The increasing occurrence of antibiotic resistant strains, including methicillin and vancomycin-intermediate resistant (MRSA, VISA) strains have resulted in major treatment challenges and increased costs across healthcare systems worldwide (C. Liu & Chambers, 2003; Turner et al., 2019). A great concern is the high rates of recurrence of many *S. aureus* infections, which has been attributed largely to the ability of *S. aureus* to adapt to the host environment by formation of biofilms and small colony variants or surviving within host cells (Fraunholz & Sinha, 2012; Barbara C. Kahl et al., 2016; Kiedrowski & Horswill, 2011). A large proportion of *S. aureus* disease involves extracellular bacteria, for example in biofilms formed on indwelling medical devices. In fact, although it was long thought that *S. aureus* were only capable of extracellular infections, it is now generally accepted that *S. aureus* survives within host cells and therefore has a facultative intracellular lifestyle (Fraunholz & Sinha, 2012). *S. aureus* is armed with an extraordinary repertoire of virulence factors. Its elaborate armoury is intricately controlled by a network of regulators

which enables *S. aureus* to adapt to the variety of challenges that come with extracellular and intracellular growth (Horn et al., 2017; Jenul & Horswill, 2019).

1.2 Epidemiology

The first observations of MRSA were reported soon after methicillin was introduced into the clinic in 1961 (Barber, 1961). Although it has been suggested that resistance was acquired in the mid-1940s due to the wide-spread use of penicillin (Harkins et al., 2017). Vancomycin, a cell wall biosynthesis inhibiting antibiotic, remains a drug of choice for treatment of acute MRSA infections. *S. aureus* strains exhibiting increased resistance to vancomycin were discovered in the 1990s (McGuinness et al., 2017). The emergence of *S. aureus* strains that are highly resistant to antimicrobials is a major public health concern and places a substantial financial burden on healthcare systems (Chambers & Deleo, 2009; Enright et al., 2002). *S. aureus* is one of six ESKAPE pathogens (*Enterococcus faecium, Staphylococcus aureus, Klebsiella pneumoniae, Acinetobacter baumannii, Pseudomonas aeruginosa, and Enterobacter* species), identified as the most common causes of life-threatening nosocomial infections amongst immunocompromised, critically ill patients (Rice, 2008). Furthermore, VISA and MRSA are included in the World Health Organisation (WHO) list of high priority pathogens for research and development of new antibiotics (Shrivastava et al., 2018).

MRSA has been categorised into community-associated (CA-MRSA) or hospital-associated (HA-MRSA) strains. Patients with CA-MRSA infections often lack risk factors known for patients with HA-MRSA infections, such as hospitalization, nursing-home residence, dialysis, and other co-morbid conditions associated with health-care settings (Huang et al., 2006). CA-MRSA strains are resistant to beta-lactam antibiotics however they are typically susceptible to other anti-staphylococcal therapies and characteristically encode the exotoxin Panton-Valentine Leukocidin (PVL) (Vandenesch et al., 2003). In recent years, several countries have introduced 'at risk' patient screening for MRSA as a preventative

measure. Patients who are found to be colonised are often treated with topical antibiotics before hospitalization, however more effective and less damaging ways of decolonisation of nasal sites are desperately required (Bode et al., 2010). In addition, attempts to bring a vaccine against *S. aureus* to the clinic have thus far been unsuccessful but is urgently needed to reduce epidemics (Giersing et al., 2016; Redi et al., 2018).

In North America, epidemic community-associated strains of MRSA have been largely responsible for the increase in the incidence of MRSA bacteraemia (Klevens et al., 2007; Laupland et al., 2008). USA300 LAC (Los Angeles county jail) was the leading cause of community-associated *S. aureus* SSTIs in the early-to-mid 2000s (Tong et al., 2015) and by 2011, USA300 was the most common MRSA isolated from infections at all body sites (Diekema et al., 2014). This particular *S. aureus* superbug gained media coverage as it was the cause of skin abscesses in several USA professional athletes (Kazakova et al., 2005). In the United Kingdom (UK), epidemic hospital-associated strains of MRSA, EMRSA-15 and EMRSA-16, have been responsible for the majority of MRSA bacteraemia cases (Johnson et al., 2005). In the UK as with many other industrialised countries bacteraemia is perhaps the best studied manifestation of *S. aureus* infection. Public Health England has carried out enhanced surveillance of both MRSA and methicillin sensitive *S. aureus* (MSSA) bacteraemia in recent years. While the number of cases of MRSA were halved between 2004 and 2011 due to the implementation of hospital infection control procedures (Johnson et al., 2012), the cases of MSSA are much higher and appear to be on the rise (Public Health England, 2019), as shown in Figure 1.1.
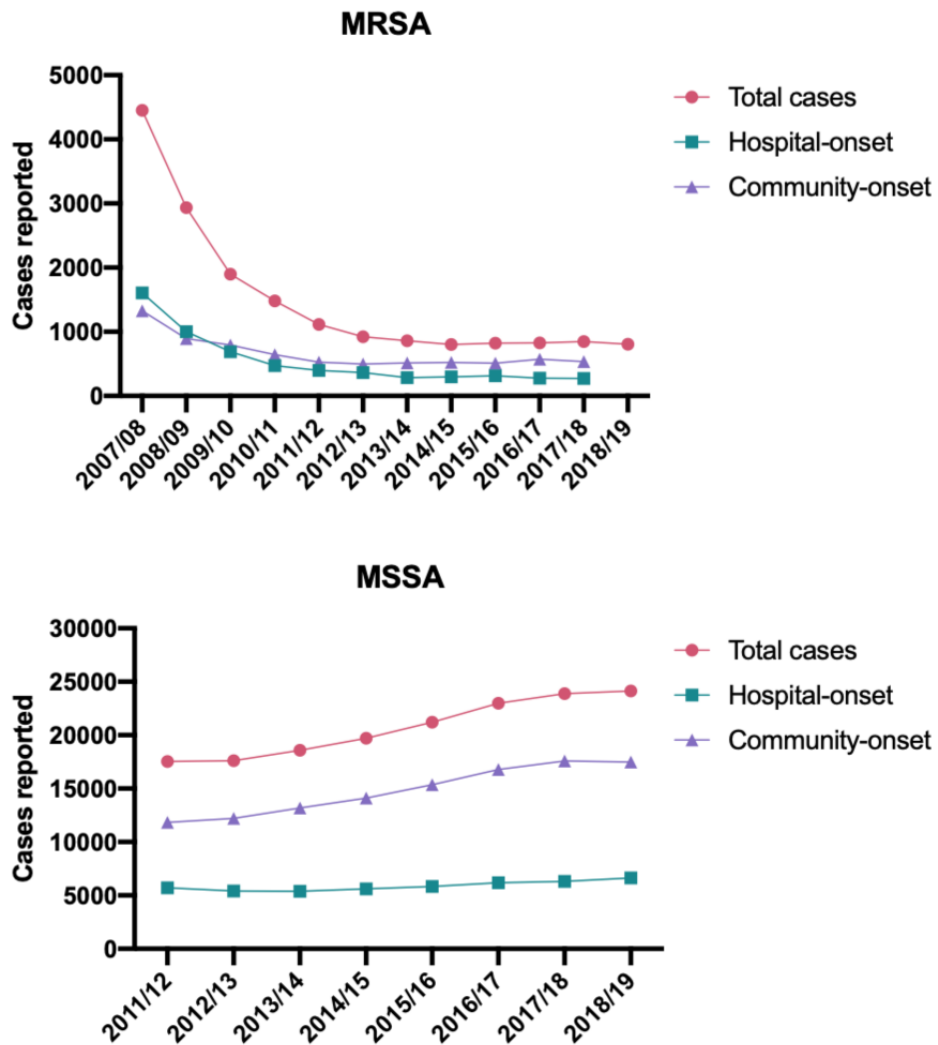
Figure 1.1: Public Health England reported cases of MRSA and MSSA bacteraemia in the United Kingdom.

Cases reported are from Public health England mandatory enhanced surveillance of methicillin resistant (MRSA) and methicillin sensitive (MSSA) *Staphylococcus aureus* bacteraemia cases across the United Kingdom between 2011 and 2019. Data acquired from (Public Health England, 2019).

1.3 *S. aureus colonisation*

S. aureus can colonise sites such as the skin and the nares in healthy individuals, who often remain asymptomatic (Krismer et al., 2017). The capacity of *S. aureus* to colonise has been associated with the composition of the nasal microbiota (Krismer et al., 2017). Anterior nares are the main site of colonisation by *S. aureus*; here it can undergo a commensal to pathogen transition usually due to suppressed host immune defences or mechanical damage (Z. Li et al., 2015). This opportunistic pathogen can cause fatal nosocomial infections such as soft-tissue infections (SSTI), life-threatening endocarditis, pneumonia, chronic osteomyelitis and bacteraemia among other diseases (F D Lowy, 1998; Tong et al., 2015). Age, immune status and presence of other medical conditions like diabetes or human immunodeficiency virus (HIV) infections, are some of the major risk factors associated with invasive *S. aureus* infections (F D Lowy, 1998).

Over 80% of hospital-associated *S. aureus* bacteraemia is caused by invasion of the endogenous colonizing strain, and a particularly strong link has been shown between other severe staphylococcal infections like pneumonias and complicated SSTIs with previous *S. aureus* colonisation (Brown et al., 2014; Safdar & Bradley, 2008; H. F. Wertheim et al., 2005). Underlying reasons for high rates of colonisation and recurrence are not very clear, although studies indicate that it is influenced by multiple factors including pathogen physiology, host immune status and local environment (Creech et al., 2015).

S. aureus can colonise the nasal or skin epithelial cells through attachment to host cells or mucosal components. Several bacterial factors have been shown to be involved in colonisation of the nasal mucosa including cell wall associated fibronectin binding proteins and clumping factor B (ClfB) (Clarke & Foster, 2006; Foster et al., 2014; Mulcahy et al., 2012), which are discussed later. Upon successful colonisation, *S. aureus* is proficient at forming biofilms, which provide a niche for bacteria to survive in the presence of antibiotics and immune responses, and thus have been strongly associated with chronic or recurrent or

infections (Moormeier & Bayles, 2017; Otto, 2018). More recently, the intracellular lifestyle of *S. aureus* has been highlighted as another mechanism that the bacterium utilizes to survive and thrive within the host. *S. aureus* also ensures their survival by successfully manipulating the complex interplay of innate and adaptive immune responses during chronic infection (Scherr et al., 2014).

1.3.1 S. aureus skin and soft tissue infections

A particularly important and prevalent infection caused by *S. aureus* is skin and soft tissue infections (SSTIs). In the UK, between 1991 and 2006, admission rates for abscesses and cellulitis increased 3-fold which was accompanied with a climb in the numbers of prescriptions for anti-staphylococcal antibiotics from primary care settings (Hayward et al., 2008; Saxena et al., 2010). SSTIs are promoted by skin barrier disruption and manifest in a diverse array of clinical presentations, varying from superficial, harmless to complicated and life-threatening. *S. aureus* represents the most frequent cause of SSTIs in industrialised countries such as the USA (Ray et al., 2013). The hallmark of S*. aureus* SSTI is generally a cutaneous abscess, however other manifestations include cellulitis, impetigo staphylococcal scalded skin syndrome, erysipelas and folliculitis as shown in Figure 1.2A (Olaniyi et al., 2017; Ray et al., 2013). Colonisation status is particularly important in SSTI, which is commonly caused by CA-MRSA strains (Creech et al., 2015; Yang et al., 2010). Studies in the United States reveal that 72% of all *S. aureus* SSTIs were caused by MRSA, and ~85% of these were caused by USA300 (Talan et al., 2011). Up to 70% of patients with SSTI have recurrent infections, often requiring repeated courses of antibiotic therapy (McNeil & Fritz, 2019). In many cases of SSTI several members of the same household are colonised with MRSA. *S. aureus* SSTIs are associated with the development of serious complications, as bacteria can gain access to deeper tissue and disseminate to the bloodstream causing invasive disease like endocarditis, osteomyelitis, deep tissue abscesses, sepsis and pneumonia (Tong et al., 2015). *S. aureus* is also the leading cause of surgical site infections (Humphreys et al., 2016).
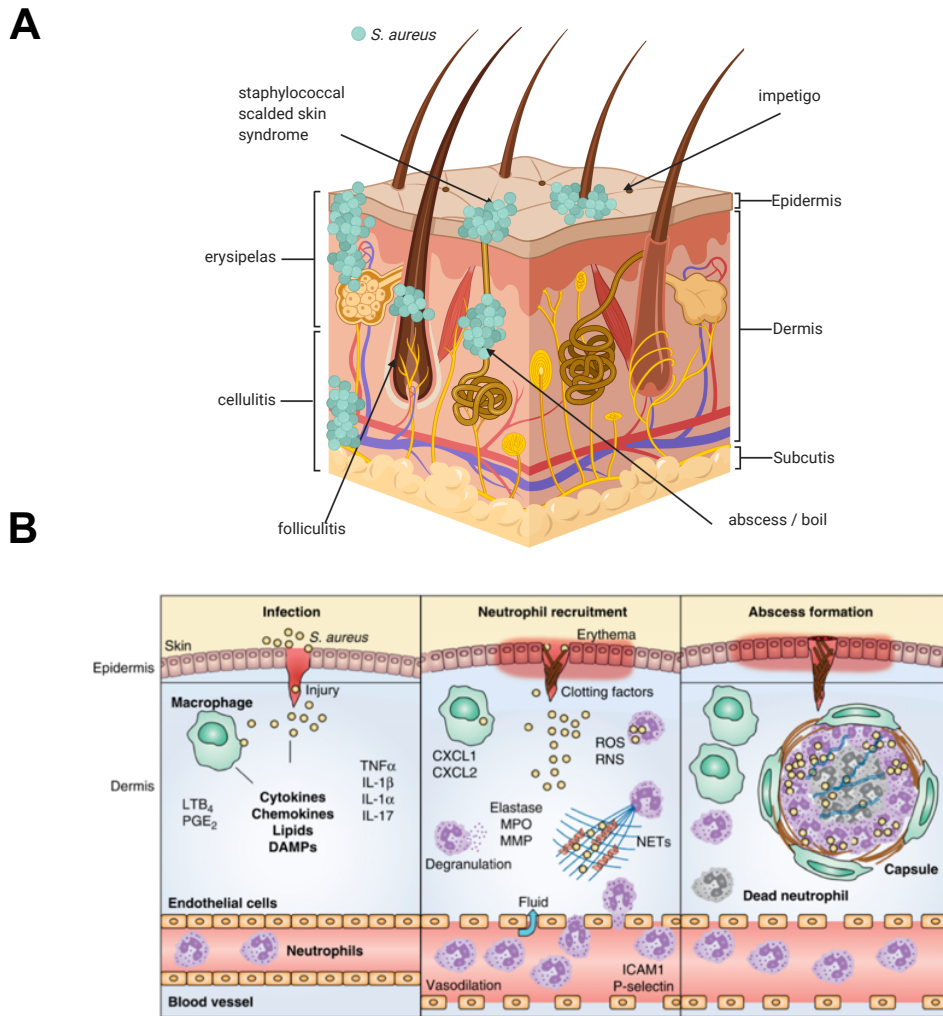
Figure 1.2: *S. aureus* skin and soft tissue infections.

(A) The different manifestations and locations of *S. aureus* skin and soft tissue infections. Based on figure from (Olaniyi et al., 2016). (B) Staphylococcus abscess formation and maturation. Left panel, *S. aureus* breaches the epithelial layers to launch the infection. Tissue-resident macrophages and other phagocytes begin clearance of bacteria and together with keratinocyte cells they produce inflammatory signals to promote neutrophil responses. Middle panel, recruited neutrophils use several mechanisms to kill bacteria such as phagocytosis, degranulation, and production of extracellular traps. Right panel, viable *S. aureus* and infected cells or cell corpses are contained by abscess formation. Fibrous material encapsulates the abscess and macrophages surround the area. Figure from (Brandt et al., 2018).

During skin invasion, *S. aureus* likely utilises its numerous cell wall-anchored proteins, T cell antigens, and membrane damaging toxins to aid in its colonisation and evasion of the immune system, but there is still much to learn on their specific roles during SSTIs (Lacey et al., 2016). Skin-resident immune cells such as Langerhans cells, macrophages, dendritic cells, mast cells, several T lymphocytes, plasma cells, and NK cells participate in the recognition and response to the invading pathogens. The close interplay and communication between immune cells and neighbouring keratinocytes and fibroblasts is also of great importance (Matejuk, 2018). Tissue-resident macrophages are one of the main contributing phagocytes in the clearance of bacteria in the skin, and in conjunction with dendritic cells and Langerhans cells they recruit and activate neutrophils and T cells (Kashem et al., 2017; Tamoutounour et al., 2013). Toll like receptor- 2 (TLR-2) is highly expressed on resident macrophages and recruited neutrophils and monocytes, TLR-2 is known to promptly respond to *S. aureus* and further stimulate cytokine production and phagocytosis, however the role of TLR2 in skin infection is controversial. TLR2 has been shown to be both dispensable (Miller et al., 2006) and important (Hoebe et al., 2005) in the resolution of *S. aureus* skin infections in mice. Dermal macrophages secrete different chemoattractants that provide signals for neutrophil recruitment in a manner dependent on interleukin-1 receptor (IL-1R) and myeloid differentiation primary response 88 (MyD88) (Miller et al., 2006).

Inflammatory lesions called abscesses often form during *S. aureus* infection and function to restrain and eliminate the pathogen (Figure 1.2B) (Brandt et al., 2018; Cheng et al., 2011; Kobayashi et al., 2015). The characteristic pus-filled core of the abscess contains fibrin, viable and necrotic polymorphonuclear leukocytes (PMNs), tissue debris, along with live bacteria. Abscess maturation involves the formation of a fibrous capsule at the periphery; but, bacterial access to the bloodstream and systemic spread may still occur if the abscess is not contained (Brandt et al., 2018; Cheng et al., 2011; Kobayashi et al., 2015). Interestingly, macrophages are localized near the fibrous capsule at the periphery of the abscess, where they can regulate the recruitment of neutrophils and monocytes

to the site of infection (Brandt et al., 2018; Kobayashi et al., 2015). Macrophages expressing MyD88 have been implicated in the contribution to *S. aureus* abscess maturation (Feuerstein et al., 2015) and neutrophil-derived interleukin-1 β (IL-1β) is required for abscess formation (Cho et al., 2012). More recently Brandt et *al.* (2018) showed that macrophage-derived leukotriene B4 is essential for orchestrating the chemoattractant gradient for neutrophil migration to the infectious focus, fibrous capsule formation and microbial killing.

1.4 *S. aureus* virulence

The success of *S. aureus* as a pathogen has been consistently attributed to its huge array of multifaceted virulence factors. The production of virulence factors must be adapted in order to suit the stage of infection or the location the pathogen. The expression of virulence factors is therefore regulated by an intricately bound network involving two-component systems (TCSs) able to sense environmental cues. Of the sixteen different TCSs encoded by *S. aureus* (Mihaila et al., 2010) only some are linked to virulence such as accessory gene regulator (*agr*), *sae*RS and *arl*RS . (Jenul & Horswill, 2019). The best studied of these *agr*, which encodes a quorum-sensing system that acts as a master virulence regulator (Jenul & Horswill, 2019). A number of cytoplasmic regulators couple with TCSs to aid in virulence regulation, among the most important are the SarA protein family of transcriptional regulators and the alternative sigma factors (SigB and SigH) (Jenul & Horswill, 2019). The list of *S. aureus* virulence factors is extensive, as shown in Figure 1.3. A selection of prominent and well-studied members of the *S. aureus* weaponry are described in more detail below.
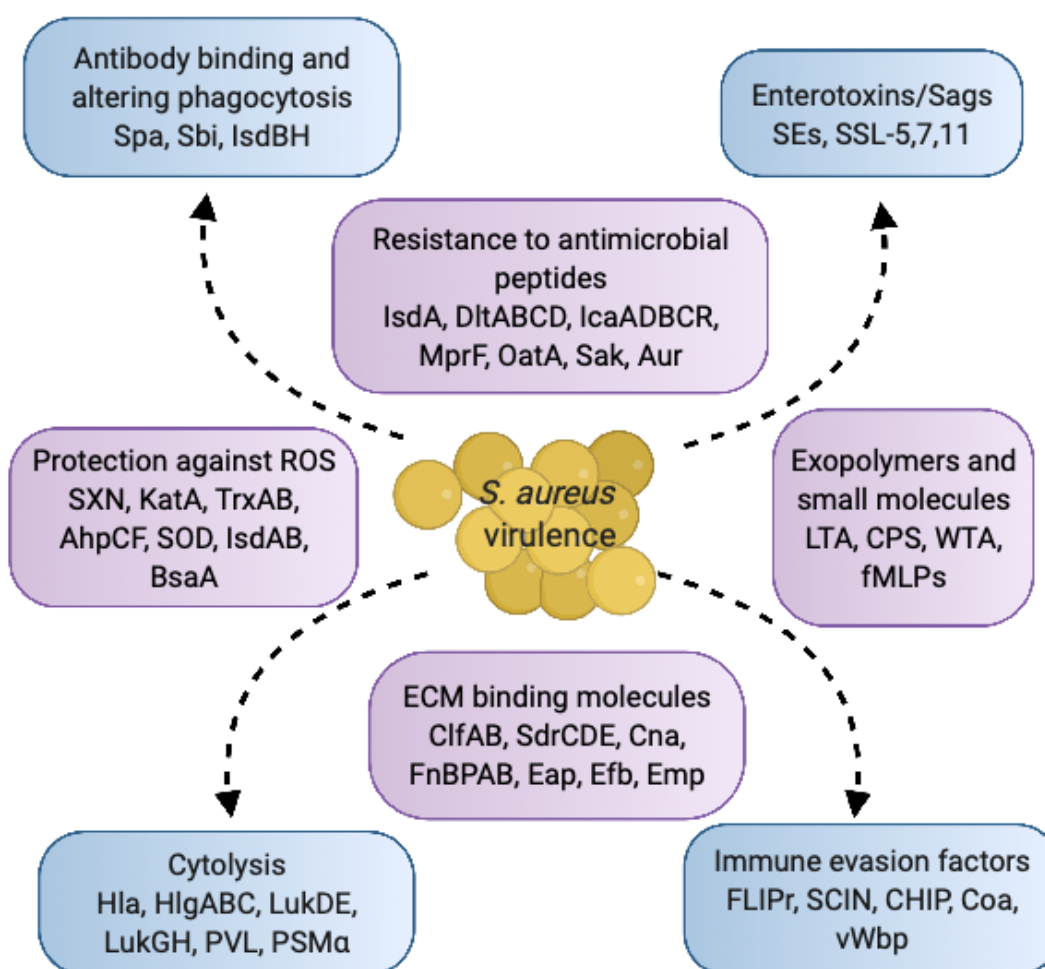
Figure 1.3: *S. aureus* virulence factors grouped by function.

AhpCF, alkyl hydroperoxide reductase subunits C and F; Aur, aureolysin; BsaA, glutathione peroxidase; CHIPS, chemotaxis inhibitory protein of staphylococcus; Clf, clumping factor; Cna, collagen adhesin; Coa, coagulase; CPS, capsule; Eap, extracellular adherence protein; ECM, ectracellular matrix; Emp, extracellular matrix protein; Efb, extracellular fibrinogen binding protein; FLIPr, formyl peptide receptor-like 1 inhibitory protein; fMLP, N-formyl-methionyl-leucyl-phenylalanine; FnBPAB, fibronectin binding protein A and B; Hla, α-hemolysin/α-toxin; HlgABC, gamma-hemolysin subunits A, B, and C; IcaADBCR, intercellular adhesin subunits A, D, B, C, and R; Isd, iron-regulated surface determinant; KatA, catalase; LTA, lipoteichoic acid; Luk, leukocidin; MprF, multiple peptide resistance factor; OatA, O-acetyltransferase A; PSM, phenol-soluble modulin; PVL,

Panton-Valentine leukocidin; ROS, reactive oxygen species; Sak, staphylokinase; Sbi, staphylococcal IgG-binding protein; SCIN, staphylococcal complement inhibitor; SdrCDE, Ser-Asp rich fibrinogen/bone sialoprotein-binding protein subunits C, D, and E; SE, staphylococcal enterotoxin; SOD, superoxide dismutase; Spa, staphylococcal protein A; SSL, staphylococcal superantigen-like protein; SXN, staphyloxanthin; TrxAB, thioredoxin (TrxA) and thioredoxin reductase (TrxB); vWbp, von Willebrand factor binding protein; WTA, wall techoic acid. Figure adapted from Kobayashi et al. 2015.

1.4.1 Cell wall-anchored proteins

S. aureus utilize a repertoire of 25 known cell wall-anchored (CWA) proteins to carry out multiple functions (Foster et al., 2014). As the name suggests they are exposed on the cell wall, attached covalently to peptidoglycan, which enables their direct contact with the host. Thus, they perform functions involved with colonisation and immune evasion with some redundancy between proteins (Foster et al., 2014). One function of CWA proteins is to adhere to extracellular matrix (ECM) proteins or to host cells directly (Schwarz-Linek et al., 2004). The most prevalent staphylococcal CWA proteins are the group collectively termed MSCRAMMs (microbial surface component recognizing adhesive matrix molecules). Two MSCRAMMs known as fibronectin-binding proteins A and B (FnBP-A and FnBP-B) enable *S. aureus* binding to ECM protein fibronectin (Fn) creating a molecular bridge that links FnBP-expressing *S. aureus* with the host cell integrin $\alpha5\beta1$ (Fowler et al., 2000; Jonsson et al., 1991; Schwarz-Linek et al., 2003). Importantly this interaction induces internalisation of *S. aureus* into host cells. (Agerer et al., 2003; Fowler et al., 2000; Sinha et al., 1999, 2000).

Clumping factor B (ClfB) is another example of an important MSCRAMM for colonisation. It binds to fibrinogen, cytokeratin 10, and loricrin (Mulcahy et al., 2012; Walsh et al., 2004, 2008) and facilitates *S. aureus* nasal colonisation in rodents and humans (Mulcahy et al., 2012; H. F. L. Wertheim et al., 2008). Recently ClfB was shown to be crucial in determining abscess structure and bacterial burden in infection in a loricrin dependent manner (Lacey et al., 2019). Deregulation of expression of loricrin within the damaged tissue has been suggested to facilitate binding of *S. aureus* via ClfB, which ultimately promotes the development of the abscess (Lacey et al., 2019). So far the effect of ClfB on abscess formation appears to be unique to skin infections as no defects in kidney abscess formation were observed in systemic infection when using strains with mutated *clfb* (Cheng et al., 2009).

One of the most well studied immune evasion CWA proteins is Protein A (SpA), which is both secreted and cell wall associated (Buchan et al., 2019). SpA disrupts

the process of opsonization by binding the Fcγ effector portion of immunoglobulin G (IgG), leading to IgG bound to bacteria in the incorrect orientation (Buchan et al., 2019; Graille et al., 2000; Lindmark et al., 1983). This prevents binding of C1q to antibody–antigen complexes as part of the classical complement pathway and ultimately decreases recognition of the pathogen by neutrophils (Foster, 2005). SpA is also implicated in the progression of inflammatory pneumonia by directly binding the Tumor necrosis factor-α (TNF-α) receptor TNFR1 (Gómez et al., 2004). TNFR1 activates mitogen-activated protein kinase (MAPK) pathways, resulting in the expression of inflammatory cytokines such as IL-8 and consequent recruitment of polymorphonuclear leukocytes (Gómez et al., 2004). Furthermore, Spa acts as a B cell toxin, able to bind VH3+ immunoglobulins on the surface of B cell receptors and induce apoptosis (Goodyear & Silverman, 2003). The deletion of B cells results in reduced capacity to produce antibodies and to develop robust adaptive immune responses (Goodyear & Silverman, 2003).

1.4.2 Membrane-disrupting toxins

Key members of the *S. aureus* virulence factor arsenal are its set of seven distinct multicomponent β-barrel pore forming toxins, including α-hemolysin (Hla) and six bicomponent leukocidins (Alonzo & Torres, 2014; Berube & Wardenburg, 2013). Hla also known as α-toxin, was discovered over 80 years ago (Glenny & Stevens, 1935), and is encoded in the core genome of most sequenced strains (Vandenesch et al., 2012). *S. aureus* Hla is secreted as a water-soluble monomer, capable of binding and oligomerizing into a heptameric perforating pore on the cell membrane (Berube & Wardenburg, 2013). The pore causes the unwanted flow of Ca^{2+}, K^+, adenosine triphosphate (ATP), and low molecular weight molecules though the host membrane (Bhakdi & Tranum-Jensen, 1991). Hla targets cells such as monocytes, neutrophils, B-cells and T-cells (Nygaard et al., 2012), its broad specificity stems from its ability to bind to the nearly universal host a disintegrin and metalloproteinase-10 or ADAM10 (Wilke & Wardenburg, 2010).

Increased *hla* expression enhances virulence. The epidemic strain USA300 that was the dominant USA CA-MRSA strain in the early 2000s, was found to be significantly more virulent and lethal than the previously dominant USA400 strain, correlating with significant increases in *hla* expression (Montgomery et al., 2008). Hla is a major virulence factor in numerous murine infection models including skin (Kennedy et al., 2010; Tkaczyk et al., 2013), sepsis and vascular injury (Menzies & Kernodle, 1996; Powers et al., 2012) and pneumonia (Wardenburg et al., 2007). Moreover, individuals colonised or infected with *S. aureus* develop serum antibody titres consistent with Hla expression (Fritz et al., 2013; Kolata et al., 2011).

While leukotoxic and haemolytic activities are the prominent consequence of *S. aureus* pore forming toxin action, studies in recent years have demonstrated specific cellular responses to sub-lytic concentrations of Hla and the alteration of cell signalling pathways associated with cell proliferation (Haugwitz et al., 2006), inflammatory responses, cytokine secretion (Craven et al., 2009) and programmed cell death (Nygaard et al., 2012). Hla is also recorded to be required for *S. aureus* escape from the phagosome of a cystic fibrosis bronchial epithelial cell line (Jarry et al., 2008; Jarry & Cheung, 2006). The pore forming toxin's potential to disrupt cellular processes suggests a deeper manipulation of host responses, which could explain how *S. aureus* is often able to coexist in homeostasis with host cells (Rudkin et al., 2017).

Surfactant-like phenol-soluble modulins (PSMs) are another important group of membrane damaging toxins and to date, have been found to be expressed exclusively by staphylococcal species (Cheung et al., 2014). It is likely that their surfactant characteristic originally evolved due to their important role in channel formation within biofilms, then later they evolved the ability to aggregate in host lipid bilayers causing cytolysis. (Periasamy et al., 2012). PSMs are expressed by virtually all strains of *S. aureus*, and are encoded in the core genome; this includes PSMα1-4, PSMβ1-2 and δ-toxin (also known as PSMγ) (R. Wang et al., 2007).

Unlike other staphylococcal toxins, PSM activity is non-specific and receptor-independent and therefore targets a greater range of cell types (Cheung et al., 2014). They have an exceptionally high capacity to lyse human neutrophils (Cheung et al., 2014) but other roles for PSMs have also been described. Abscess size and number appear to be dependent on PSMα in rabbit and mouse infection models (Kobayashi et al., 2011; R. Wang et al., 2007). Staphylococcal escape from the phagosome is thought to be promoted by PSMs, which facilitates cytoplasmic replication and survival inside phagocytes (Grosz et al., 2014). At sub-cytolytic concentrations PSMs are highly inflammatory peptides that induce migration and activation in both macrophages and neutrophils, and stimulate the release of pro-inflammatory cytokines (Kretschmer et al., 2010; R. Wang et al., 2007). Beyond their impact on host cells and responses PSMs have been implicated in bacterial dissemination through biofilm detachment and dispersal (Periasamy et al., 2012) and in killing or inhibiting rival bacteria (Joo et al., 2011).

The classical virulence factors mentioned here have been extensively studied and reviewed in the context of many infections (Brown et al., 2014; Foster, 2005; Oliveira et al., 2018; Rudkin et al., 2017). There are several other understudied secreted factors produced by *S. aureus* that have been associated with bacterial virulence; one of these is the type-VII secretion system and associated proteins, which have been linked with virulence since 2005 (Burts et al., 2005).

1.5 *S. aureus* type-VII secretion system

1.5.1 Bacterial protein secretion systems

The transport of proteins from the bacterial cytoplasm into the extracellular environment is an essential prokaryotic cell function (Green & Mecsas, 2016). The transport of cargo between locations often involves the use of dedicated protein secretion systems. In some cases, these secretion systems are employed by bacterial pathogens to manipulate the host and/or compete with neighbouring bacteria to establish a replicative niche (Green & Mecsas, 2016). A

small number of the known secretion systems have been discovered in almost all bacteria and secrete a wide variety of substrates, for example the general secretion pathway (Sec) and the twin-arginine translocation (Tat) pathway (Papanikou et al., 2007). Others secretion systems are limited to a small number of species or secrete only one or a few proteins (Green & Mecsas, 2016).

Gram-negative bacteria need specialised systems to transport proteins across two phospholipid membranes in order to reach their final extracellular destination. Often the Sec or Tat secretion systems deliver the protein to the periplasm, then a second transport system moves the protein across the outer membrane (Natale et al., 2008). Well-studied Gram-negative systems include Type1 -Type 6 secretion systems. Gram-positive bacteria contain only one lipid bilayer and are surrounded by a very thick cell wall. These fundamental differences in cell structure mean Gram-positive bacteria require extra mechanisms of extracellular protein secretion. Secretion systems unique to Gram-positive bacteria include SecA2 pathway, sortase, injectosome and type VII secretion systems (T7SS) (Green & Mecsas, 2016). *S. aureus* translocates virulence factors using several different secretion systems (Sibbald et al., 2006) including, the Sec pathway and accessory Sec2 system (Siboo et al., 2008), the Tat pathway (Biswas et al., 2009), and the type VII-like secretion pathway (Unnikrishnan et al., 2017).

1.5.2 Type VII secretion systems

The Type VII secretion system (T7SS) is specialized protein secretion machinery found mostly in representatives of the Actinobacteria and Firmicutes phyla, such as *M. tuberculosis, S. aureus*, *Bacillus subtilis* and *Bacillus anthracis* as shown in Figure 1.4 (Gey Van Pittius et al., 2001; Houben et al., 2014; Pallen, 2002). Across these two phyla there are two defining features of the core T7SS loci. The first is the presence of genes that encode proteins from the WXG100 superfamily. These secreted proteins are approximately 100 amino acids in length and include the conserved Trp-X-Gly (WXG) motif in the centre of the polypeptide that

contributes to their helix-turn-helix structures (Pallen, 2002; Renshaw et al., 2005). Examples of these include EsxA/ESAT-6 (6-kDa early secreted antigenic target) and EsxB/CFP-10 (Culture filtrate protein 10 kDa), in mycobacteria and EsxA and EsxB in *S. aureus*. The second is the presence of genes that encode FtsK–SpoIIIE-like adenosine triphosphatase (ATPase) family transmembrane proteins (Pallen, 2002). Other than these two features, the T7SSs seem to have been individually moulded by evolutionary processes such as gene duplication, diversification and horizontal gene transfer over a long period of time (Dumas et al., 2016; Tekaia et al., 1999). Genomic analysis has even uncovered the presence of WXG100 proteins in the Gram-negative bacterium *Helicobacter pylori* and members of other Gram-negative phyla (S. B. Jang et al., 2009; Pallen, 2002; Sutcliffe, 2011).

The first T7SS identified was in *M. tuberculosis*. The discovery was made during comparative and functional genomic studies involving pathogenic *M. tuberculosis* and attenuated vaccine strains *Mycobacterium bovis* Calmette-Guérin (BCG) and *Mycobacterium microti* (Leung & Finlay, 1991; Lewis et al., 2003; Pym et al., 2002, 2003; Stanley et al., 2003). Researchers found that the *M. tuberculosis* vaccine strains lack *esxA*, the gene encoding the key T7SS WXG-100 EsxA protein and these strains of mycobacteria are restricted within the phagosomes without cytosolic escape. Since then, it has been revealed that EsxA is secreted by a T7SS in named ESX-1. Mycobacterial genomes encode up to five of these transport systems named ESX-1 through to ESX-5 (Gröschel et al., 2016).

Figure 1.4: Distribution of key components of type VII secretion system across phyla.
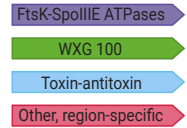
Components of the type VII secretion system clusters in species representative of Firmicutes: *Staphylococcus aureus, Listeria monocytogenes, Streptococcus agalactiae, Bacillus subtilis* and *Bacillus anthracis*; Actinobacteria: *Mycobacterium tuberculosis* and *Streptomyces coelicor*; *Helicobacter pylori*. Arrows represent relative length of the genes and direction of transcription. Figure adapted from (Unnikrishnan et al., 2017).

ESX-1 is the most extensively researched mycobacterial T7SS. It plays a role in the induction of macrophage phagosomal rupture, releasing bacteria into the host cell cytosol therefore enabling bacterial persistence inside phagosomes (van der Wel et al., 2007). ESX-1 secretes EsxA (formerly known as ESAT-6), a 6 kDa early secreted antigenic target, and EsxB (CFP-10), a 10 kDa culture filtrate protein, which exhibits highly immunogenic properties. ESX-1 associated phagosomal rupture and *M. tuberculosis* cytosolic access has been suggested to be responsible for inducing major host cellular responses (K.-W. Wong, 2017) including, activation of Nucleotide-binding oligomerization domain 2 (NOD2) signalling, cytosolic inflammasome receptor (NOD-like receptor protein) NLRP3, the onset of cell death, , type I interferon production, and autophagy (Dallenga et al., 2017; Mishra et al., 2010; Romagnoli et al., 2012; Stanley et al., 2007; K. W. Wong & Jacobs, 2011).

There is no current evidence of active secretion in ESX-2 systems and functions are currently unknown (Roy et al., 2020). The presence of the ESX-2 locus has been associated with slow-growing mycobacterial species. ESX-2 genes are transcriptionally coregulated in *M. tuberculosis* with genes encoding other ESX systems and appear to be necessary for survival within dendritic cells (Mendum et al., 2015) .

ESX-3 effector proteins have separate roles in iron acquisition and virulence. The secretion of ESX-3 associated EsxG and EsxH is co-dependent on the secretion of proline-glutamic acid (PE) and proline-proline-glutamic acid (PPE) protein families, PE5–PPE4 and PE15–PPE20. PE5–PPE4 was found to be critical for the siderophore-mediated iron-acquisition functions of ESX-3, thought to be a mechanism of counteracting host defense mechanisms that restrict iron availability (Tufariello et al., 2016). PE15–PPE20 are important for iron uptake and modulate virulence in an iron-independent fashion (Tufariello et al., 2016). Additionally, EsxH, in complex with EsxG, disrupts ESCRT (endosomal sorting complexes required for transport) proteins and impairs phagosome maturation and repair (Mehra et al., 2013; Mittal et al., 2018). ESCRT-III proteins are

recruited to *M. tuberculosis* phagosomes in an ESX-1 dependent manner (Mittal et al., 2018). ESCRT proteins are required to direct cargo in the multi-vesicular bodies to fuse with lysosomes and more recently have been shown to respond to pathogen-induced membrane damage in the form of closing holes in the membrane (Skowyra et al., 2018). The ability of EsxG-EsxH to antagonize ESCRT seems to block major histocompatibility complex class II (MHC-II) antigen presentation (Portal-Celhay et al., 2016).

The ESX-4 system is involved in the conjugation process, particularly in the mycobacterial recipient strains. In a *M. smegmatis* donor: recipient co-culture study, ESX-1 mediated expression of ESX-4 genes was essential for DNA transfer to recipient cells. While neither secretory apparatus provides the physical channel for DNA transfer they may secrete cell-surface "mating factor" receptors (Gray et al., 2016). Further work showed that the extracytoplasmic σ factor, SigM, is a cell contact-dependent activator of ESX-4 expression (Clark et al., 2018). Although in most mycobacterium strains ESX-4 is not associated with virulence, the ESX-4 system in *Mycobacterium abscessus* is responsible for virulence-associated phagosomal rupture and cytosolic escape of mycobacteria, both in human macrophages and amoeba (Laencina et al., 2018). In this case researchers speculate that ESX-4 operates as a surrogate of ESX-1 as *M. abscessus* lacks an ESX-1 locus.

ESX-5 is involved in capsule integrity and virulence through its secreted substrates PPE and PE. Mycobacterial ESX-5 mutants fail to secrete PE and PPE protein repertoires, rendering them avirulent and inducing a small colony phenotype (Abdallah M. Abdallah et al., 2009; Ates et al., 2015). ESX-5 impacts mycobacterial capsule composition, affecting its integrity and consequently modulating cytokine responses in macrophages, apoptosis induction and caspase-independent cell death (A. M. Abdallah et al., 2008; Abdallah M. Abdallah et al., 2011; Ates et al., 2016).

1.5.3 The staphylococcal T7SS locus organisation

Type VII systems have been found in several close relatives of *M. tuberculosis* within the high-C+G bacterial species, Actinobacteria. These include *Streptomyces coelicolor* and *Corynebacterium diphtheriae* (Gey Van Pittius et al., 2001). EsxA homologues have also been identified in bacteria of the more distantly related low-C+G group, the Firmicutes*.* These include *Staphylococcus aureus, Streptococcus agalactiae, Bacillus subtilis, Bacillus anthracis, Bacillus cereus, Bacillus thuringiensis, Rhodococcus equi,* and *Clostridium acetobutylicum* (Baptista et al., 2013; Burts et al., 2005; Callahan et al., 2010; Desvaux et al., 2005; Huppert et al., 2014; Letek et al., 2010; Pallen, 2002; Poulsen et al., 2014)*.* T7SS in Firmicutes are distinct from those of Actinobacteria due to its simpler esx gene organisation; as a result they are classified as type VIIb or type-VII-like secretion systems (Unnikrishnan et al., 2017). The staphylococcal type-VII secretion system is the most extensively explored T7SS after mycobacterium, although there is still much to learn.

From the analysis of 153 whole genome sequences of *S. aureus* isolates it has been established that the locus encoding staphylococcal T7SS, also known as the ESAT6 secretion system (Ess*)* is one of the few core variable regions in the *S. aureus* genome, although there is modularity and organisational variation across the species as well as transcriptional variation (Warne et al., 2016). Core components of the T7SS are shown in Figure 1.5. Overall, the locus comprise of four distinct modules (Warne et al., 2016).
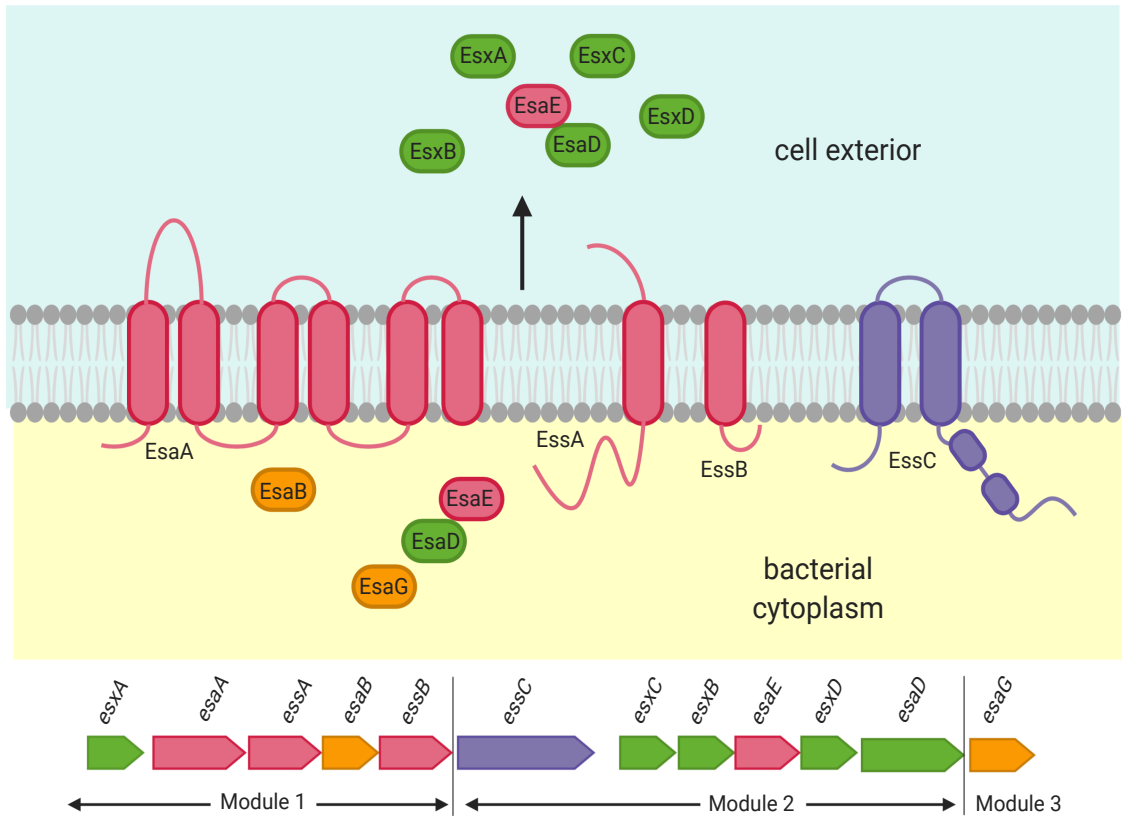
Figure 1.5: The staphylococcal type VII secretion system core components
Suggested model of the core type VII secretion machinery, accessory proteins and secreted substrates. Membrane-associated proteins (pink), FtsK/SpoIII ATPase (purple), secreted substrates (green), cytoplasmic proteins (orange). Figure adapted from (Unnikrishnan et al., 2017).

The 5' module 1 contains genes encoding the soluble proteins EsxA and EsaB plus three membrane anchored proteins EsaA, EssA and EssB. EsaB is a small cytosolic protein that behaves as a regulator of the expression of a subset of the T7SS substrates (Burts et al., 2008). In the case of *S. aureus* Newman and USA300, *esaB* seems to act as a negative regulator of EsxC, however in the background of RN6390 *esaB* appears to be essential for both EsxA and EsxC secretion (Burts et al. 2005; Kneuper et al. 2014). EsxA is the only other soluble protein found in module 1, it is a highly abundant WXG100 secreted effector protein also required for the secretion of other T7SS substrates (Warne et al. 2016; Kneuper et al. 2014). Each of the module 1 genes are highly conserved between strains and functional analysis suggests they make up five of the six core machinery proteins that are integral for regulation and secretion through the staphylococcal T7SS (Burts et al., 2005; Kneuper et al., 2014; Pallen, 2002; Warne et al., 2016). Immediately upstream of module 1, and therefore EsxA, lies the more recently discovered member of the T7SS locus *ess*H, which encodes for a peptidoglycan hydrolase. The hydrolase activity of EssH is thought to sufficiently break down the bacterium's own cell wall envelope by cleaving the pentaglycine cross bridge and the amide bond of N-acetylmuramyl-L-alanine to enable type VIIb secretion (Bobrovskyy et al., 2018).

The gene encoding the sixth core protein, *essC*, resides in module 2. The resulting EssC protein is a membrane-anchored FtsK/SpoIIIE ATPase that likely energizes protein secretion and may form part of the channel for cargo transportation (Mietrach et al., 2020). The 5' region of *essC* is conserved across strains, but the 3' section displays sequence variability; four variations have been identified, *essC*1 through *essC*4, with *essC1* being the most frequent (90 out of 153 strains, including USA300) (Jäger et al., 2018; Warne et al., 2016). In USA300, module 2 includes essC1 as well as genes esxC, esxB, esxD, and essD in addition to essE (esaE) (Figure 1.5), which are co-transcribed with core protein genes from module 1 (Kneuper et al. 2014). Three of these genes, *esxC*, *esxB* and *esxD* encode small secreted substrates (up to 15 kDa) (Anderson et al., 2013; Burts et al., 2005,

2008). e*saD* encodes a large protein with a C-terminal nuclease domain that acts as a secreted toxin by targeting and degrading the DNA of *S. aureus* strains lacking an antitoxin. *esaE,* encodes for a protein that interacts with EsaD and is required for its secretion or stability (Cao et al., 2016).

Module 3 represents the most variable module and includes a number of predicted transmembrane proteins scattered with hypothetical protein encoding genes that have the functionally unknown DUF600 domain (Warne et al., 2016). EsaG from the DUF600 family, encoded in module 3 directly downstream of *esaD,* has the ability to bind the nuclease domain of the toxin EsaD in the cytoplasm resulting in neutralisation (Cao et al., 2016). Together, EsaD and EsaG form a toxin-antitoxin pair. Module 4 includes two genes that encode suspected transmembrane proteins that are conserved among all *S. aureus* isolates. The function or requirements of the two module 4 genes for T7SS in are, however, unknown

1.5.4 Regulation and expression of T7SS

High levels of heterogeneity were found in transcription profiles of the T7SS locus across different staphylococcal isolates*. esxA,* in module 1 is monocistronic transcript that is not co-transcribed with the downstream *ess* genes in strain Newman and RN6390, however, in strains COL, USA300 and SA113 all genes in module 1, 2 and 3 form part of the same transcriptional operon (Kneuper et al., 2014; Schulthess et al., 2012; Warne et al., 2016). In line with this, a likely promoter sequence has been identified in the *esxA*-*esaA* intergenic region in strain RN6390 but not USA300 (Kneuper et al., 2014).

Despite the ess genes forming a single operon in USA300, COL and SA113 transcript levels still vary between genes (Kneuper et al., 2014). The highest T7SS related transcript levels were consistently associated with *esxA,* which is up to 100 times higher than that of the *essC* gene. The *esaA* gene immediately

downstream of *esxA,* is also more highly expressed than *essC*, (around 10 times), while esxB is expressed to similar levels as essC (Kneuper et al., 2014). For strains COL and RN6390 secretion of EsxA and EsxC could be detected at optical density (OD)$_{600}$ 1, whereas secretion of these proteins was not detected until cultures had reached an OD600 2 for USA300 (Kneuper et al., 2014). *esx*A has been shown to be subject to complex regulation by the alternative sigma factor σB involving staphylococcal accessory regulator SarA, the ArlRS two- component system and SpoVG (Schulthess et al., 2012). Interestingly, the Chinese ST398 isolates exhibited significantly increased expression of T7SS genes as compared to other common hospital-associated strains, researchers suggest this is likely due to its increased expression of *agr* system (Y. Wang et al., 2016).

1.5.5 T7SS Molecular architecture

The precise molecular structure of the staphylococcal T7SS has not yet been elucidated although the integral membrane proteins EsaA, EssA, EssB, and EssC are thought to make up the core T7 secretion machinery (Burts et al., 2005; Chen et al., 2012; Jäger et al., 2018; M. Zoltner et al., 2016). Interaction is thought to occur between two of these integral membrane proteins EssB and EsaA (Ahmed et al., 2018). The recent resolution of the crystal structure of the ATPase domain D3 of EssC aided in determining that substrate binding occurs at the adjacent ATPase domain D2, and that substrates bound to D2 require domain D3 for further transport (Mietrach et al., 2020). EsxB was also reported to interact with the D3 domain of T7SSa FtsK/SpoIII like ATPase (Mietrach et al., 2020). EsaE seems to form a complex with other members of the T7SS secretion pathway and its substrates, promoting the secretion of EsxA, EsxB, EsxC, EsxD and EsaD (Anderson et al., 2017). EsaE has been found in both cytoplasmic and membrane cell fractions, and membrane-bound EsaE has the ability to interact with EssC, implicating EsaE in targeting substrates to the T7SS (Cao et al., 2016). The overall functional assembly of the type VII secretion machinery, in *S. aureus*, was reported be assisted by the flotillin homolog FloA within functional membrane microdomains (Mielich-Süss et al., 2017).

1.5.6 T7SS secreted proteins

esxA, esxC, esxB and *esxD* encode small substrates (11-15 kDa) that are transported to the extracellular environment via the T7SS (Anderson et al., 2013; Burts et al., 2005, 2008). A feature of type VII systems, is that effectors influence secretion of each other (Unnikrishnan et al., 2017). EsxC secretion appears to depend upon the presence of both *esxB* and *esxA* (Kneuper et al., 2014). Deletion of esxD abrogated the production of EsxB altogether and affected the secretion, but not the production, of EsxA and EsxC (Anderson et al., 2013). Other T7 secreted proteins include EsaD, the large anti-bacterial toxin, with a nuclease domain at its C terminus and, EsaE, which binds to the non- nuclease part of EsaD and appears to target the EsaDG complex to the secretion machinery before its own secretion (Cao et al., 2016).

The Missiakas group showed through bacterial two-hybrid analyses that unlike the *Mycobacterium* ESAT-6 and CFP-10, staphylococcal EsxA and EsxB do not interact (Anderson et al., 2013). Instead, EsxB can associate with, EsxD and appear to function as a heterodimer exclusively. EsxA and EsxC can both form homodimers with themselves and heterodimers with each other (Abd El-Fatah et al., 2018; Anderson et al., 2013; Sundaramoorthy et al., 2008). EsxC and EsxD do not share sequence features of WXG100 proteins like EsxA and EsxB, but EsxD carries the C terminal motif YxxxD/E that was proposed to target T7SS substrates for secretion in mycobacteria (Anderson et al., 2013). EsxA can form elongated cylindrical structures created from side-by-side α-helices linked with a hairpin bend formed by the WXG motif (Sundaramoorthy et al., 2008). Structural analysis suggests EsxA could play a role as transport module or chaperone to assist export of proteins by the T7SSb (Sundaramoorthy et al., 2008).

1.5.7 Biological functions of staphylococcal type VII secretion

A small number of biological functions for the T7SS have so far been uncovered. As previously mentioned, a T7SS associated toxin-antitoxin (EsaD-EsaG) pair was

reported recently (Cao et al., 2016; Ulhuq et al., 2020) Like many other toxin-antitoxin systems this pair is designed to kill bacterial competition whilst providing protection from self-intoxication (Page & Peti, 2016). Bacterial competition assays showed that there is an approximately two-log decrease in recovered prey cells when they are co-cultured with a T7SS positive strain COL compared with a T7SS mutant strain (Cao et al., 2016). Approximately 50% of *S. aureus* strains do not carry the *esaD* toxin but they do encode at least two homologues of the antitoxin *esaG* close to their T7SS locus, suggesting they may produce EsaG-like proteins to protect against killing by EsaD-producing strains (Cao et al., 2016).

A role for the RN6390 T7SS in the acquisition of iron has been suggested (Casabona, Kneuper, et al., 2017). With strain RN6390 the transcription of T7SS is activated by supplementing the growth medium with haemoglobin and its cofactor haemin. The deletion of essC, causing loss of T7SS secretion, resulted in upregulation of genes required for iron acquisition (Casabona, Kneuper, et al., 2017). These finding were not replicated in the other T7SS expressing staphylococcal strains tested (Casabona, Kneuper, et al., 2017)

Staphylococcal T7SS expression is known to be initiated by various host factors including serum, nasal secretions, and pulmonary surfactant (Burts et al., 2008; Ishii et al., 2014; Lopez et al., 2017). A significant component of each of these factors is unsaturated fatty acids (Lopez et al., 2017). In 2017 it was found that host-specific cis- unsaturated fatty acids are major stimulatory factors (Lopez et al., 2017). More specifically, host fatty acid incorporation into bacterial biosynthetic pathways by the *S. aureus* fatty acid kinase complex significantly increased T7SS expression. Linoleic acid (LA), an essential fatty acid for humans required as a component of cell membranes, induced a dose-dependent increase in EsxA protein levels in USA300 *S. aureus*. Incorporated cis-unsaturated fatty acids decrease *S. aureus* membrane fluidity, which is at least part of the signal for the transcriptional changes induced by the host environment and increases virulence (Lopez et al., 2017). However, the link between the T7SS induction and

fatty acid incorporation in this study is unclear. High levels of unsaturated fatty acids can have a toxic effect on *S. aureus* by disruption of the cell membrane, leading to leakage of cell contents (Parsons et al., 2012). Work completed in our lab demonstrate that *S. aureus* lacking T7SS components are more susceptible to host-derived antimicrobial fatty acids such as LA. We show that initial LA binding to *S. aureus* was unaffected by the deletion of *esxC* but the mutant was less able to incorporate LA into its membrane phospholipids when compared to WT (Kengmo Tchoupa et al., 2020). Together these finding indicate that T7SS expression is upregulated by the unsaturated fatty acid-rich host environment, then functions to contribute to the maintenance of *S. aureus* membrane integrity and homeostasis (Kengmo Tchoupa et al., 2020).

1.5.8 The role of the staphylococcal type VII secretion in virulence

Although little is known about specific T7SS functions during infection, it is clear that the secretion system is required for virulence and persistence. Table 1.1 summarises the T7SS associated proteins and their role during infection or biological function. With the use of murine models, it has been shown that *S. aureus* mutants defective in the production of EsxA, EsxB, EsaD, EssE produce a diminished infection in kidneys and/or liver with fewer abscess lesions and lower bacterial load when compared to wild-type strains (Anderson et al., 2011, 2017; Burts et al., 2005; Ohr et al., 2017) . It was further shown that *esaB, esxC,* and *esaD* mutants were less able to elicit a persistent infection compared to the wild-type strain in the similar intravenous mouse models (Anderson et al., 2011; Burts et al., 2008). More work has been carried out with a pneumonia mouse models where the whole *ess* loci are deleted or just *essC,* these strains demonstrated a reduced ability to colonise the nasal cavities and cause mouse mortality (Ishii et al., 2014; Kneuper et al., 2014). Skin abscess and bloodstream models have shown that deletion of EsxX or EssB in the emerging Chinese strain ST398 decreased virulence of *S. aureus* (Dai et al., 2017; Y. Wang et al., 2016)

A mouse bloodstream infection suggests the T7SS modulates mouse cytokine and macrophage responses (Anderson et al., 2017). In murine infections with *ΔessE* mutant, serum concentrations of IL-1β and IL-12 (p40/70) were significantly reduced compared to WT USA300, however the release of RANTES in the bloodstream was increased (Anderson et al., 2017). Immunohistochemical analysis of thin-sectioned renal tissues revealed that WT infections caused a distinct distribution of macrophages around lesions. In contrast to this, during *ΔessE* mutant infections macrophages penetrated lesions (Anderson et al., 2017). The T7SS clearly has immunostimulatory characteristics as EsxA and EsxB can elicit high titers of anti-EsxA and anti-EsxB antibodies in humans and mice (Zhang et al., 2015; H. Zhou et al., 2013). EsxA and EsxB were previously incorporated into a vaccine against *S. aureus* named the 4C-Staph Vaccine (GlaxoSmithKline, GSK2392102A), which was shown to elicit a robust murine antibody and Th1 and Th17 response (Bagnoli et al., 2015; Mancini et al., 2016a; Torre et al., 2015). This vaccine is however no longer featured in the GlaxoSmithKline pipeline.

Table 1.1: Functions of *S. aureus* Type-VII secretion system proteins. Suggestions of function with little or no associated experimental evidence are represented with the symbol ?.

T7SS Protein	Location	Function	Strain	Literature
EssH	Secreted	Peptidoglycan hydrolase. Enables T7SS secretion across cell wall	USA300 LAC	(Bobrovskyy et al., 2018)
EsxA	Secreted and membrane	Assists in export of other T7SS proteins; associated with *in vivo* virulence and immune modulation; regulates apoptosis in epithelial and dendritic cells	USA300 LAC, SA 113, Newman	(Burts et al., 2005; Cruciani et al., 2017; Korea et al., 2014; Sundaramoorthy et al., 2008)

EsaA	Membrane	T7SS machinery/ assembly factor?	Newman, *E. coli* DH5α	(Ahmed et al., 2018; Burts et al., 2005)
EssA	Membrane	T7SS machinery	Newman, RN6390	(Burts et al., 2005; Kneuper et al., 2014)
EsaB	Membrane and cytoplasm	T7SS machinery?; stable expression of secreted T7SS polypeptides, persistent infection *in vivo*	Newman, *E. coli* DH5α	(Ahmed et al., 2018; Anderson et al., 2011; Burts et al., 2008; Casabona, Buchanan, et al., 2017)
EssB	Membrane	T7SS machinery?	USA300 LAC, Newman, *E. coli* DH5α	(Ahmed et al., 2018; Chen et al., 2012)
EssC	Membrane	Essential T7SS machinery; ATPase likely driving secretion; associated with *in vivo* virulence	RN6390, Newman and USA300	(Burts et al., 2005; Ishii et al., 2014; Jäger et al., 2018; Kneuper et al., 2014)
EsxC	Secreted and membrane	chaperone to assist export/ adaptor protein?; associated with *in vivo* virulence and persistence	Newman, USA300	(Anderson et al., 2013; Burts et al., 2008; Kengmo Tchoupa et al., 2020)
EsxB	Secreted	Role in T7SS secretion?; associated with *in vivo* virulence; *S. aureus* release from epithelial cells; immunoregulation in dendritic cells;	Newman, USA300	(Burts et al., 2005; Cruciani et al., 2017; Korea et al., 2014)
EsaE	Cytoplasm and membrane	Secretion chaperone; associated with manipulation of *in vivo* immune responses	RN6390, USA300 LAC	(Cao et al., 2016)

EsxD	Secreted	Unknown; role in T7SS protein secretion?		(Anderson et al., 2013)
EsaD	Secreted	Nuclease targeting staphylococcal species without the EsaG antitoxin; IL-12 signaling during bloodstream infection; associated with virulence and persistence *in vivo*	RN6390, Newman, USA300	(Anderson et al., 2011; Cao et al., 2016; Ohr et al., 2017)
EsaG	Cytoplasm	An antitoxin to neutralise EsaD	RN6390	(Cao et al., 2016)
EsxX (ST398 only)	Secreted	Promotes neutrophil lysis and contributes to evasion of host innate immune response; associated with virulence *in vivo*	ST398	(Dai et al., 2017)

1.5.9 Host modulatory functions of Staphylococcal T7SS associated proteins

Although it is well established that the staphylococcal T7SS is required for virulence, mechanisms by which T7SS associated proteins modulate host-bacterial interactions remain largely unclear. Invasion assays using human cell lines have provided some insights into the cellular mechanisms of Esx proteins. Korea et al. (2014) demonstrated that in the presence of EsxA, lung epithelial cells have increased protection against apoptotic cell death and EsxA overexpression in these cells is sufficient to alleviate staurosporine-induced apoptosis. The absence of both EsxA and EsxB was shown to decrease bacterial escape from lung epithelial cells, suggesting a finely tuned interaction with the host (Korea et al., 2014). Cruciani et al. (2017) confirmed the involvement of EsxA in dysregulation of host apoptosis in dendritic cells and went on show that infection with *ΔesxB. S.*

aureus conferred an increased capacity for dendritic cells to release IL-12, TNF-α, IL-6, and IL-1β, cytokines that are heavily involved in T-helper cell-1/17 (Th1/Th17) immune responses (Cruciani et al., 2017). Expression of T7SS in the Chinese *S. aureus* isolate ST398 has been associated with resistance to elimination by neutrophils (Dai et al., 2017; Y. Wang et al., 2016). In this same isolate the newly discovered EsxX, a WXG family protein conserved only in ST398 was found to promote neutrophil lysis and contribute to evasion of innate immune responses (Dai et al., 2017).

1.6 *S. aureus*-host cell interactions

1.6.1 Host cell internalisation of S. aureus

Barrier forming host cells, such as epithelial and endothelial cells, have a fairly high capacity to internalise *S. aureus* (Strobel et al., 2016). These cells likely function as non-professional phagocytes that remove bacteria from vital parts of the body, for example the cardiovascular system or the lungs. Keratinocytes, located in the outer most layer of the skin, function to form a fundamental barrier against invading pathogens but still ingest *S. aureus* at low levels (Bur et al., 2013; Strobel et al., 2016). Evidence shows that *S. aureus* has the capacity to invade other cells in internal organs such as osteoblasts and fibroblasts, but at a lower efficiency (Strobel et al., 2016). The internalisation of *S. aureus* can be both beneficial and detrimental to the bacterium, something likely dependent on how well the host cell is equipped to recognize and kill an intracellular pathogen. An intracellular niche can be associated with evasion of the human humoral and cellular immune responses and increased accessibility to nutrients. The intracellular fate of *S. aureus* is multifaceted, as shown in Figure 1.6, and likely dependent on host cell type and bacterial strain.
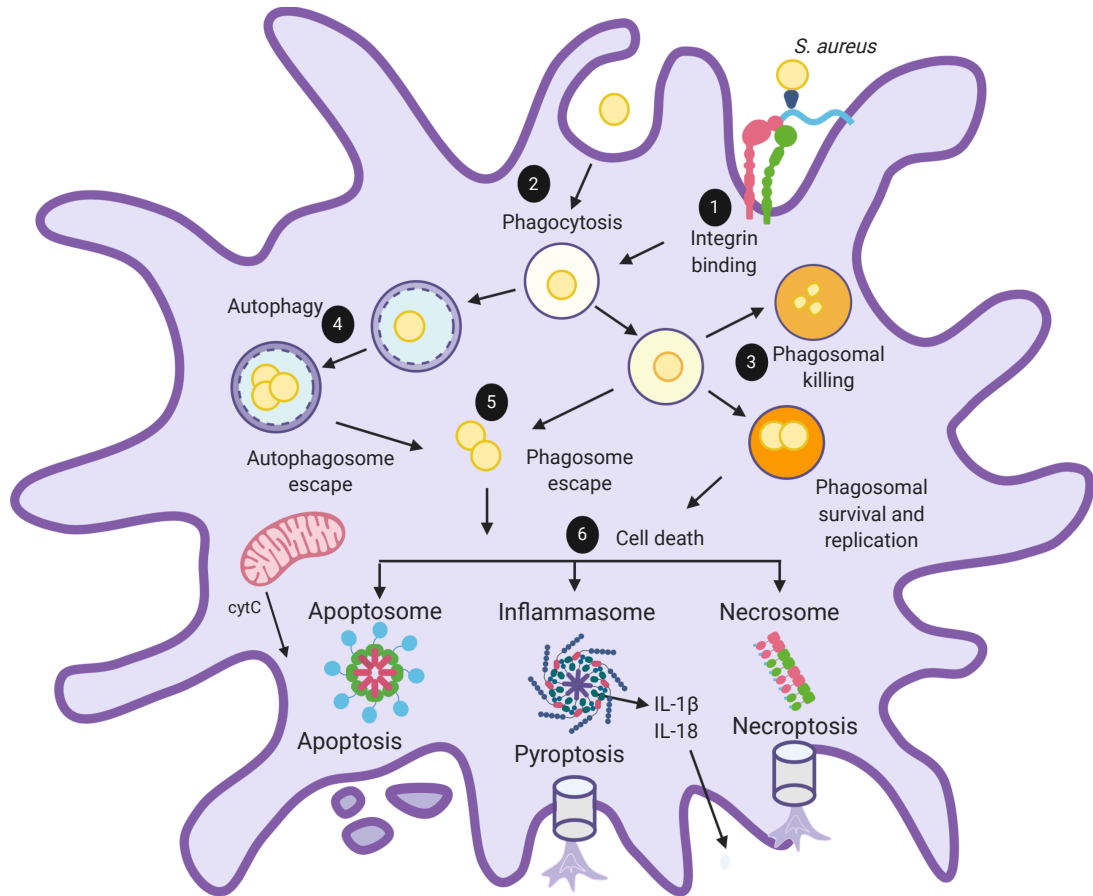
Figure 1.6: Intracellular fates of *S. aureus*.

(1) *S. aureus* internalisation into host cells is initiated by formation of a staphylococcal FnBP-A and FnBP-B-fibronectin-α5β1 integrin bridge. (2) Professional phagocytes can internalize *S. aureus* via phagocytosis. (3*) S. aureus* has been shown to overcome host antibacterial factors during phagosomal maturation, enabling survival, and in some cases replication inside the phagosome. (4) *S. aureus* has been associated with both canonical autophagy and the selective xenophagy machinery, with some reports of autophagosomes providing a niche for replication. (5) *S. aureus* can escape to the cytoplasm from autophagosomes and endosomes where it can replicate. (6) Programmed cell death pathways, apoptosis, pyroptosis and necroptosis, are induced by *S. aureus* and promote pathogen dissemination. Figure adapted from (Watkins and Unnikrishnan, 2020).

In order to initiate its own internalisation into host cells, *S. aureus* utilizes a repertoire of adhesins exposed on their surface to adhere to various host cell ECM components or to host cells directly (Schwarz-Linek et al., 2004). The group of adhesins termed MSCRAMMs, are the most prevalent. MSCRAMMs have adjacent IgG-like folded domains (Patti et al., 1994). Clinical isolates of *S. aureus* often express two MSCRAMMs, FnBP-A and FnBP-B, which create tight repeats of β-zipper structures with the ECM protein fibronectin (Fowler et al., 2000; Jonsson et al., 1991; Schwarz-Linek et al., 2003). Once associated with the surface of the bacteria Fn serves as a molecular bridge linking FnBP-expressing *S. aureus* with the host cell integrin $\alpha_5\beta_1$ Fn receptor (Fowler et al., 2000). Upon formation of the FnBP-Fn-α5β1-integrin bridge clustering of host integrins occurs, triggering the assembly of protein complexes on the intracellular tails of the integrins (Fowler et al., 2000; Lamkanfi & Dixit, 2010; Sinha et al., 1999, 2000). FnBP-Fn triggered events are a prerequisite to the internalisation of the bacteria into non-professional phagocyte cells (Agerer et al., 2003; Fowler et al., 2000; Sinha et al., 1999, 2000). The efficiency of adhesion via FnBR varies between cell types and bacterial strains (Josse et al., 2017), which likely explains trends in host cell capacities to internalise. Three FnBRs are required for adhesion to keratinocytes (Edwards et al., 2011) whilst a single high-affinity FnBR is sufficient for adhesion to endothelial cells (Edwards et al., 2010).

Indeed *S. aureus* is also known to be internalised via phagocytosis by professional phagocytic cells, including macrophages, neutrophils, dendritic cells and mast cells (R. S. Flannagan et al., 2016; van Kesse et al., 2014). Classically, phagocytes are thought to use Fc receptors (FcR) and complement receptors to induce phagocytosis (van Kesse et al., 2014). In the case of *S. aureus,* endocytosis via these mechanisms may be limited as this pathogen produces many factors that interfere in complement activity and opsonization, such as protein A and Efb that function to neutralize host complement protein C3b and IgG (Dossett et al., 1969; Ko et al., 2013). Other host receptors may therefore play a more prominent role in endocytosis of *S. aureus* into professional phagocytes. Both type I and II class A scavenger receptors (SR-A) and CD36, have been shown to mediate opsonin-

independent phagocytosis into macrophages (Blanchet et al., 2014; Stuart et al., 2005).

Once internalised by host cells, *S. aureus* can persist for extended periods of time (Hamill et al., 1986; Kubica et al., 2008; Lowy et al., 1988; Tuchscherr et al., 2011). Extensive interactions of this pathogen with a number of host response pathways such as phagosomal killing, autophagy, inflammasome activation and cell death pathways have been demonstrated. The fate of *S. aureus* is largely dependent on a variety of factors, including host cell capacity to produce antimicrobial responses, the differential susceptibility of host cells to virulence factors, the staphylococcal strain and growth phase (Krut et al., 2003; Schwartz et al., 2009; Strobel et al., 2016), as well as multiplicity of infection (MOI) (Fraunholz & Sinha, 2012; Jubrail et al., 2016; Schwartz et al., 2009).

1.6.2 *S. aureus* survival in phagosomes

Phagocytosis is essential for the capture and elimination of bacterial pathogens. Pathogen pattern recognition at a phagocyte cell surface triggers the uptake of that pathogen into a membrane bound phagosome (R. S. Flannagan et al., 2009). The phagosome undergoes a sequence of highly choreographed fusion and fission events with other endosomes which enable it to develops antibacterial properties such as low pH, and recruitment of degradative enzymes (Uribe-Quero & Rosales, 2017; Yates et al., 2005). The last step in the phagosomal pathway is the fusion of phagosome with lysosomal compartments to develop the highly destructive phagolysosome (Flannagan et al., 2009). Classical phagocytosis is associated with professional phagocytes however, non-professional phagocytes can also encapsulate pathogens during endocytosis. In this instance, the bacteria are initially taken up into endosomes that bare resemblance to the phagosomes of phagocytes. These endosomes are decorated with phagosomal markers and will acidify to pH 4.5 in addition to displaying some antibacterial properties; but they lack key phagosomal characteristics, for example accumulation of some antimicrobial peptides (Giese et al., 2009).

Overcoming the inhospitable environment of a phagosome in order to find even a brief intracellular niche can be invaluable to the extension of pathogen survival. Evidence suggests that *S. aureus* has the ability to overcome host antibacterial factors while residing inside early Rab5 associated endosomes which quickly mature into acidic phagosomes supporting proteins such as Rab7 and late phagosomal marker lysosome-associated membrane protein-1 (LAMP-1) (Flannagan et al., 2016; Grosz et al., 2014; Jarry & Cheung, 2006; Lacoma et al., 2017; Lâm et al., 2010; Lowy, 1998; Tranchemontagne et al., 2015). However, there is little agreement in descriptions of phagosomal acidification and fusion with the lysosome in the presence of *S. aureus,* the reason for which is likely host cell type and strain specific effects.

It has been demonstrated that this highly adaptive pathogen can tolerate acidic environments and promote its survival by modifying its membrane components (Weinrick et al., 2004). *S. aureus* has the ability to secrete a number of different products to deal with acidic stress including urease, ammonia, nitrite and nitrate reductase (Lacoma et al., 2017). As seen for other pathogens, phagosomal acidification has been reported to be essential for the survival of *S. aureus,* although this seems to be specific (Lacoma et al., 2017; Rathman et al., 1996). In macrophages, acidification has been strongly linked to triggering *S. aureus* virulence factors, as it promotes the expression *agr* system, a global virulence regulator (Kubica et al., 2008; Pang et al., 2010; Schnaith et al., 2007; Shompole et al., 2003; Tranchemontagne et al., 2015). Disrupting the acidification of phagosomes had a critical impact on the survival of *S. aureus* USA300 in THP-1 macrophages (Tranchemontagne et al., 2015) but intracellular survival of *S. aureus* Newman had was not affected by phagosomal acidification (Lacoma et al., 2017). A selection of studies report normal acidification of *S. aureus* containing phagosomes, while others report the inhibition of acidification and in some instances even the lack of phagolysosomal maturation (C. Zhou et al., 2019). In the latter situation, a fully functional phagolysosomal microenvironment failed to be reached due to the absence of lysosomal hydrolases beta-glucuronidase and

cathepsin D (Jubrail et al., 2016; B. C. Kahl et al., 2000; Tranchemontagne et al., 2015). *S. aureus* may sense acidic pH and directly perturb the acquisition or activation of lysosomal hydrolases which show pH-dependent activity (Jubrail et al., 2016; Tranchemontagne et al., 2015).

The two-component regulatory system GraRS is essential for *S. aureus* to adapt and replicate within acidified phagolysosomes (Bewley et al., 2011; Jubrail et al., 2016; Tranchemontagne et al., 2015). GraRS-dependent upregulation of multiple peptide resistance factor (MprF) instigates the addition of L-lysine to staphylococcal phosphatidylglycerol. The modified phosphatidylglycerol provides membrane resistance against host defensins, likely through repulsion of the cationic peptides (Peschel et al., 2001). Another important staphylococcal membrane armour against defensins and other antimicrobial peptides are the D-alanylated teichoic acids. Proteins responsible for D-alanylation are encoded for by the *dlt* operon (Flannagan et al., 2018; Peschel et al., 2001). Meanwhile, the staphylococcal peptidoglycan O-acetyltransferase, generates copious amounts of O-acetylated peptidoglycan which denies the contact between membrane degrading lysozymes and bacterial peptidoglycan (Bera et al., 2005).

S. aureus must also overcome robust oxidative burst events involving the release of degrading oxygen species (ROS) and reactive nitrogen species (RNS) by phagocytes. *S. aureus* is armed with enzymes such as catalase, superoxide dismutase, and peroxiredoxins to protect against or neutralize these harmful events (Cosgrove et al., 2007; Karavolos et al., 2003; Richardson et al., 2008). Carotenoid staphyloxanthin, the molecule that gives *S. aureus* its characteristic golden pigment, also plays a role in protection against oxidative stress (Clauditz et al., 2006). Notably, *S. aureus* can form small colony variants (SCVs) which generally have mutations in the *agr* locus. Although this means SCVs fail to produce a number of quorum sensing-controlled virulence factors they instead display a thick cell wall, grow slowly and up-regulate alternative sigma-factor σB, creating a version of *S. aureus* more resistant to a variety of environmental stressors and antibiotics (Horsburgh et al., 2002; Sendi & Proctor, 2009).

Despite the arsenal of *S. aureus* virulence factors, ingestion by phagocytes is often associated with at least a proportion of bacteria initially dying (Clauditz et al., 2006). Other factors also play a role in bacterial survival, for example, continuous exposure of *S. aureus* leads to a bottle-neck in the capacity of the macrophage to take up and clear intracellular bacteria through the phagolysosomal pathway (Clauditz et al., 2006). It was shown that *S. aureus* is able to replicate within these "exhausted" macrophages and eventually emerge through host-cell lysis (Flannagan et al., 2015; Jubrail et al., 2016; Lacoma et al., 2017; Tranchemontagne et al., 2015). However, extracellular *S. aureus* can be phagocytosed again, and this cycle of uptake and escape could maintain a viable *S. aureus* pool within cells like macrophages (R. Flannagan et al., 2015; R. S. Flannagan et al., 2016; Jubrail et al., 2016). The survival of *S. aureus* within motile phagocytes is hypothesized to cause dissemination of bacteria to other host sites, (Jubrail et al., 2016). Lehar et al (2015) demonstrated this well by comparing mice intravenously injected with either murine peritoneal macrophages which had previously engulfed *S. aureus* or planktonic bacteria. Researchers observed higher levels of dissemination of the intracellular *S. aureus* to the kidneys and brain when compared to planktonic bacteria (Lehar et al., 2015).

1.6.3 Intracellular bacterial replication

It is now widely accepted that *S. aureus* has the ability to multiply intracellularly, but the subcellular location of replication is dependent on host cell type (Thwaites & Gant, 2011). Studies show that in a number of professional phagocytes such as murine RAW macrophages, M-CSF-derived human macrophages, and THP-1 macrophages, *S. aureus* not only persists but also replicates within PS- and LAMP-1-positive acidic phagosomes (Flannagan et al., 2016; Grosz et al., 2014; Kahl et al., 2000; Kubica et al., 2008; Lowy et al., 1988; Qazi et al., 2001). Moreover, when inside neutrophils, replicating *S. aureus* bacteria were observed to be bound by a phagosomal membrane until host cell lysis; only few bacteria were found in the cytosol of infected murine PMNs

(Blättner et al., 2016; Das et al., 2016; Gresham et al., 2000; Voyich et al., 2005). Conversely, in another study the viable intracellular *S. aureus* found in murine PMNs did not replicate intracellularly (Gresham et al., 2000; Kobayashi et al., 2010). In non-professional phagocytes *S. aureus* can either translocate from the endosome into the cytoplasm for replication or replicate within autophagosomes (Horn et al., 2017; Mestre et al., 2010).

Another factor could offer an explanation for the array of different *S. aureus* fates observed within host cells, this involves the type of vacuoles/endosomes that encapsulate the bacteria, as suggested by Sinha and Fraunholz (2010). During multiple studies researchers have observed replicating *S. aureus* to be in "spacious" compartments/ phagosomes of professional phagocytes (Gresham et al., 2000; Kubica et al., 2008). Similar descriptions of "spacious" compartments have been reported in non-professional phagocytes, such as HeLa cells, where Cowan I, a non-haemolytic strain was found in found in "spacious" vacuoles while the haemolytic strain 6850 was observed only in "tight vacuoles" (Sinha & Fraunholz, 2010). A *sar-* strain that lacks the expression of virulence factors due to a deletion of the global regulator *sar* was primarily found to reside in "tight" phagosomes of PMNs, whereas *sar+* strains were located in "spacious" phagosomes (Gresham et al., 2000). Spacious compartments encapsulating *S. aureus* resemble spacious Listeria-containing phagosomes in macrophages, which display LAMP-1 markers but are non-acidic and non-degradative (Birmingham et al., 2008).

1.6.4 Phagosomal escape

Phagosomal escape is yet another strategy to avoid bacterial damage or demise during the phagolysosomal pathway and is used by a variety of different intracellular pathogens (Grosz et al., 2014). As a consensus, when within professional phagocytes, the majority of *S. aureus* remain associated with phagosomes until programmed cell death is triggered, but knowledge of an intricate timeline of events is lacking (Hybiske & Stephens, 2008; Moldovan &

Fraunholz, 2019). However phagosomal escape in the THP-1 monocyte cell line has been reported (Grosz et al., 2014).

In non-professional phagocytes such as, endothelial cells (Bayles et al., 1998; Giese et al., 2011; Grosz et al., 2014), epithelial cells (Münzenmayer et al., 2016), and keratinocyte cell lines (Strobel et al., 2016) it is evident that *S. aureus* escapes the endosome and subsequently replicates in the cytoplasm. Strobel et al. (2016) suggests that endosomal escape is likely a strain specific trait as after endocytosis many virulent *S. aureus* strains were able to exit the endosome of epithelial cells but the noncytotoxic strain Cowan I lacked this ability. Critically, endosomal escape of *S. aureus* in non-professional phagocytes appears to be a prerequisite for induction of host cell death, as expression of lysostaphin in the cytoplasm of HeLa cells protected the host cell from induction of cell death by internalised strain ATCC29213 (Klein et al., 2006).

The global virulence regulator Agr is the factor most frequently associated with *S. aureus* phagosomal/endosomal escape as *agr* mutants do not translocate to the host cell cytoplasm and encapsulated bacterial *agr*-expression increases prior to escape into the cytosol (Chi et al., 2014; Strobel et al., 2016). Of the many virulence factors Agr controls, PSMα is key to the endosomal escape process in clinical *S. aureus* strains (Blättner et al., 2016; Grosz et al., 2014; Jarry et al., 2008; B. C. Kahl et al., 2000; Qazi et al., 2001; Shompole et al., 2003; Strobel et al., 2016). PSMs are membrane associated, short amphiphilic peptides that possess cytolytic activity (Grosz et al., 2014). The α-type PSMs include the staphylococcal δ-toxin (*hld*) and the *psmα* operon (R. Wang et al., 2007). Expression of PSMs was shown to mirror that of *agr* expression (Cheung et al., 2014; Grosz et al., 2014) with its highest levels occurring just prior to phagosomal escape (Qazi et al., 2001). Although evidence emphasises the importance of PSMs for passage to the cytoplasm, PSMα production alone is not sufficient for inducing phagosomal escape (Giese et al., 2011). A collaborating factor for PSMα-mediated escape is still unknown, however it was shown that *S. aureus* escape from phagosomes occurred when either δ-toxin or PSMβ were coexpressed together with the

phospholipase β-toxin (Giese et al., 2011). Bacterial use of pore-forming toxins and phospholipases for destruction of the phagosomal compartment has been described for several other bacterial species, for example *Listeria monocytogenes*, *Shigella*, and *Rickettsia* (Hybiske & Stephens, 2008).

S. aureus α-toxin, is another key *agr*-controlled pore-forming toxin found to mediate staphylococcal survival within human monocyte-derived macrophages (Kubica et al., 2008). *S. aureus* vesicle escape in the cystic fibrosis airway cell line CFT-1 was found to be α-toxin dependent (Jarry et al., 2008). However, it is likely not solely sufficient to permeabilise the phagolysosomal membrane (Giese et al., 2009).

Additional phagosomal escape factors have been identified including a non-ribosomal peptide synthetase in HeLa cells (Giese et al., 2011) and a Tet38 efflux pump in A549 lung alveolar epithelial cells (Blättner et al., 2016). Furthermore, while PVL was not involved in *S. aureus* escape from phagosomes of epithelial cells (Jarry et al., 2008), the pore-forming toxin was responsible for phagosomal escape of *S. aureus* in keratinocytes, where PVL toxin itself was found associated with the endosomal membrane (Blättner et al., 2016; Grosz et al., 2014; Münzenmayer et al., 2016). Thus, phagolysosomal escape is likely a multifactorial, host cell specific process.

1.6.5 *S. aureus* and the autophagy pathway

Autophagy is an evolutionarily conserved intracellular cargo degradation process that is responsible for the elimination of unwanted and superfluous cytoplasmic components such as misfolded proteins, damaged organelles and other macromolecules (Proctor et al., 1995, 2006; Tuchscherr et al., 2011). Cells scavenge their own cytoplasmic contents through sequestration into an autophagosome which eventually fuses with lysosomes for degradation in a process called autophagic flux (Dikic & Elazar, 2018). Canonical autophagy is important for maintaining homeostasis by providing the cell with energy but also

gets induced by various environmental cues, including stress and pathogen stimulation (Dikic & Elazar, 2018).

Staphylococcus aureus has been shown to elicit an autophagic response in non-professional phagocytes as well as dendritic cells, macrophages and neutrophils (Fang et al., 2014; Neumann et al., 2016; O'Keeffe et al., 2015; Schnaith et al., 2007). *S. aureus* is reported to inhibit the autophagosomal maturation process therefore allowing the bacteria to survive and thrive in an intracellular niche (Dortet et al., 2011; Mulcahy et al., 2020; O'Keeffe et al., 2015; Romagnoli et al., 2012). However, there are discrepancies between mechanistic details during *S. aureus* infection such as maturation and acidification of autophagosomes (Bravo-Santano et al., 2018; Lopez de Armentia et al., 2017; Mestre et al., 2010; Neumann et al., 2016; Schnaith et al., 2007).

1.6.6 Pathogen induced host cell death

During infection host cell death can be an effective programmed defence mechanism that demolishes the replicative niche of intracellular pathogens and induces an immune attack. Major studied modes of programmed-cell death include apoptosis, necroptosis and pyroptosis, as shown in Figure 1.7A. Together these pathways play a critical role in defence against microbial infection (Jorgensen et al., 2017). Cell death pathways can function to either eliminate pathogens at early stages of infection without eliciting an immune response (apoptosis) or to emit alarm signals to initiate an inflammatory response (pyroptosis and necroptosis) (Ashida et al., 2011; Jorgensen et al., 2017). Programmed cell death pathways are interweaved with multiple points of crosstalk (Figure 1.7B), this creates hugely complex signalling networks that cross-guard each other from foreign manipulation in the evolutionary 'arms race' with pathogens (Jorgensen et al., 2017).

Programmed cell death can also benefit intracellular pathogens, induction of cell death can lead to the efficient exit of pathogen from the host cell which enables

its dissemination to neighbouring cells and tissues (Ashida et al., 2011). Many pathogens capable of invading and multiplying within host cells, will actively manipulate the timing and method of host cell death in order to maintain their replicative niche and evade the immune response (Behar et al., 2010; Flieger et al., 2018; Lamkanfi & Dixit, 2010). *S. aureus* has been extensively shown to activate pathways such as apoptosis, pyroptosis and necroptosis through expression of virulence factors (Fraunholz & Sinha, 2012; Kitur et al., 2015, 2016). In parallel to this it has been suggested that *S. aureus* factors can protect cells from immediate demise (Cruciani et al., 2017; Korea et al., 2014; Koziel et al., 2009) although the molecular basis for this is unknown.

1.6.7 Apoptosis

Apoptosis is a well-studied non- inflammatory programmed cell death involving the formation of intact small vesicles called apoptotic bodies that are efficiently taken up by neighbouring phagocytes and degraded within lysosomes (Lamkanfi & Dixit, 2010). There are two variants of apoptosis, the first, extrinsic apoptosis, is initiated by perturbations of the extracellular microenvironment detected by death receptors on the plasma membrane. In contrast, intrinsic apoptosis can be distinguished by mitochondrial outer membrane permeabilization which can be initiated by both intracellular and extracellular perturbations (Lorenzo Galluzzi et al., 2018; Singh et al., 2019). Both apoptotic pathways involve the formation of the supramolecular apoptosome which further propagates the pathway by caspase-8/9 activation and finally caspases-3/7 activation, which executes cell death (Lorenzo Galluzzi et al., 2018). Apoptotic cells exhibit cytoplasmic shrinkage, chromatin condensation, nuclear fragmentation and plasma membrane blebbing, culminating with the formation of apoptotic bodies (Lorenzo Galluzzi et al., 2018; Lamkanfi & Dixit, 2010) (figure 1.7A).

A

B
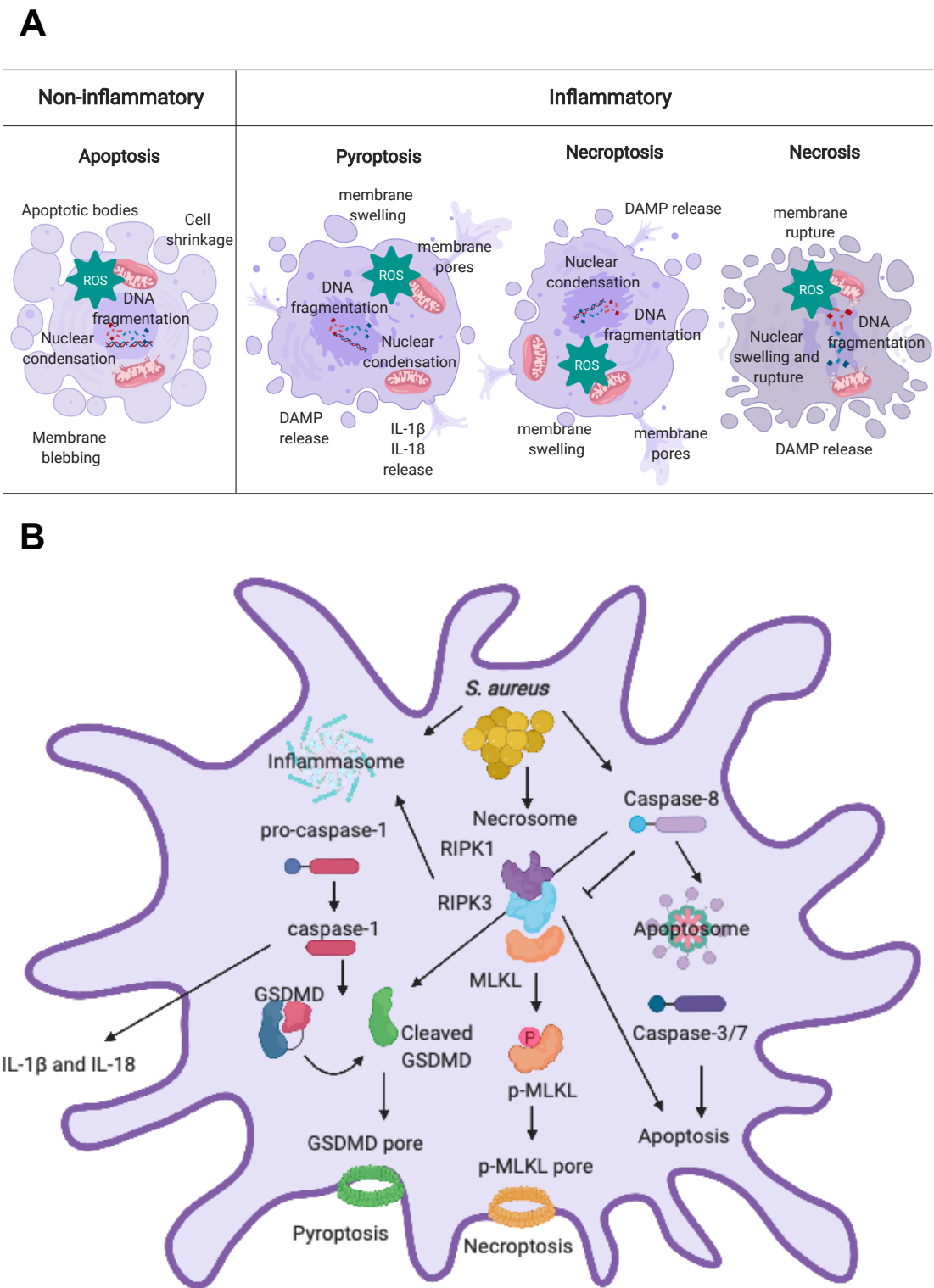
Figure 1.7: Programmed cell death induced by pathogens

(A) Mechanisms of host cell death and associated characteristics. (B) Programmed cell death induced by *S. aureus* and crosstalk between pathways.

In more recent years, modes of programmed cellular demise other than apoptosis have come to light. Pyroptosis and necroptosis are programmed cell death pathways that both cause characteristic cell swelling lysis and are capable of eliciting an inflammatory host response (Behar et al., 2010; Flieger et al., 2018; Lamkanfi & Dixit, 2010) (Behar et al., 2010; Flieger et al., 2018; Lamkanfi and Dixit, 2010).

1.6.8 Pyroptosis

Pyroptosis is dependent on the activation of inflammasomes, such as NOD-like receptor caspase activation and recruitment domain 4 (NLRC4) NOD-like receptor with pyrin domain 3 (NLRP3). Once stimulated the inflammasome initiates the cleavage of procaspase-1 to activated caspase-1. Caspase-1 is a multifunctional proteolytic enzyme which can process two important pro-inflammatory cytokines, IL-1β and IL-18, initiating their release into the extracellular environment (Guo et al., 2015). In addition, caspase-1 can cleave gasdermin-D (GSDMD), a protein key to the completion of pyroptosis (X. Liu et al., 2016; Shi et al., 2015). The N-terminal GSDMD cleavage product assembles into large oligomeric rings that insert into and permeabilise the membrane (X. Liu et al., 2016). GSDMD pores are required for IL-1β transport across an intact lipid bilayer (Lieberman et al., 2019), but if these pores are formed in high abundance, cell swelling occurs due to cellular ion overload and water influx (X. Liu et al., 2016).

The formation of GSDMD pores has been found to be necessary, but not sufficient, for the complete osmotic collapse of cells and pyroptosis (Lieberman et al., 2019; Rühl et al., 2018). Commitment to pyroptotic cell death is thought to also require mitochondrial ROS production, loss of mitochondrial transmembrane potential and a lack of membrane repair (Carty et al., 2019; Lieberman et al., 2019). The cell-intrinsic decision to enter a state of pyroptosis was shown to be associated with the accumulation of SARM (Sterile α and HEAT Armadillo motif-containing protein) at the mitochondrial membrane (Carty et al., 2019). SARM is one of five

TLR adaptor proteins which contains a TIR (Toll-IL-1R) domain and is the only TIR adaptor protein known to downregulate TLR signalling (Carty et al., 2019). SARM-dependent mitochondrial depolarization has been shown to distinguish NLRP3 inflammasome activators that cause pyroptosis from those which do not. Researchers demonstrated that removing SARM from bone-marrow-derived macrophages (BMDMs) protected these cells from undergoing pyroptosis (Carty et al., 2019). SARM accumulation also downregulates inflammasome activation therefore decreasing IL-1β production (Carty et al., 2019). Pyroptotic cells will release a short, large burst of IL-1β at the point of lysis, resulting in a strong local inflammatory response. However due to the abrupt halt in IL-1β production and the transient nature of IL-1β in this circumstance, pyroptotic cells are likely poor inducers of T cell–based adaptive immunity.

When the inflammasome is activated but cells do not undergo pyroptotic cell death, cells may enter an alternative state known as a hyperactive state. A hyperactivated cell remains viable while punctuated with GSDMD pores, which it can use to release high levels of IL-1β over a long period of time (Carty et al., 2019; Evavold et al., 2018). Membrane repair also contributes to the regulation of hyperactivation/pyroptosis downstream of GSDMD pore assembly by removal of GSDMD from the membrane (Rühl et al., 2018). Broz and colleagues revealed the ESCRT-III complex is recruited to areas of GSDMD associated membrane damage and removes GSDMD pores from the plasma membrane via the formation of ectosomes (Rühl et al., 2018).

When GSDMD pores are formed, they can be removed by membrane repair pathways, specifically, through exocytosis or endocytosis via recruitment of ESCRT machinery (Rühl et al., 2018). Some pores will persist in these viable cells over time, and are thought to be the mechanism for long term release of IL-1β (Evavold et al., 2018). Moreover, these viable cells punctuated with GSDMD pores can go on to participate in immunological events which stimulate adaptive immunity, rendering them hyperactive.

The role of pyroptosis during infection goes beyond eliciting an immediate immunological response, the pyroptotic corpse has been shown to efficiently trap viable bacteria in its structure for some time after cell death. These corpse structures were named pore-induced intracellular traps (PITs) (Jorgensen, Zhang, et al., 2016). PITs containing bacteria were observed to be efferocytosed and cleared by neutrophils (Jorgensen, Zhang, et al., 2016).

1.6.9 Necroptosis

Necroptosis is a caspase-independent form of inflammatory cell death. The progression of this pathway requires the formation of the necrosome, a multiprotein complex including receptor- interacting serine/threonine protein kinase (RIPK)1 and RIPK3 and importantly the inhibition of apoptosis-associated caspase-8 (Guo et al., 2015). Activated RIPK3 can phosphorylate mixed lineage kinase domain-like protein (MLKL) which can subsequently oligomerise to form pores in the plasma membrane (Dhuriya & Sharma, 2018). Similar to pyroptosis, necroptosis can be regulated downstream of MLKL pores forming on the membrane by the recruitment of ESCRT-II proteins to the plasma membrane and ectosome removal of pores (Gong et al., 2017). Necroptosis results in the production of damage associated patterns (DAMPs) which elicit an inflammatory response, however direct activation of potent inflammatory cytokines IL-1β and IL-18 are absent from this pathway. While pyroptotic and necroptotic cells undergo cytoplasm swelling caused by plasma membrane leakage, the non-programmed mode of cell death known as necrosis is more like an uncontrolled process of cell explosion or lysis (Dhuriya & Sharma, 2018). Necrosis results from pathogenic invasion or mechanical harm and associated with uncontrolled cell loss as well as inflammation (Dhuriya & Sharma, 2018). The modes of cell death are compared in Table 1.2.

Table 1.2 Comparison of the key features of cell death pathways. Adapted from (Miao et al., 2011).

	Apoptosis	Pyroptosis	Necroptosis	Necrosis
Initiation	Programmed	Programmed	Programmed	Accidental
Key signalling pathway	Caspase-8, caspase-3/7	Caspase-1, GSDMD, Caspase-4/5/11	RIPK1, RIPK3, MLKL	General deregulated activity
Terminal event	Blebbing, non-lytic	Lytic, pore formation	Lytic, pore formation	Lytic
Inflammation?	Non-inflammatory	Inflammatory	Inflammatory	Inflammatory
Cell types	All	Macrophages, dendritic cells, neutrophils	All	All

1.7 *S. aureus* induced host cell death

S. aureus induces cell death in a large range of host cells. A number of early studies describe an apoptotic phenotype caused by intracellular *S. aureus* (Baran et al., 1996, 2001; Bayles et al., 1998; Chi et al., 2014; Esen et al., 2001; Genestier et al., 2005; Bettina Haslinger-Löffler et al., 2005; Haslinger et al., 2003; B. C. Kahl et al., 2000; Menzies & Kourteva, 1998, 2000; Tucker et al., 2006; Wesson et al., 1998, 2000). Later studies report activation of a range of programmed cell death pathways, including pyroptosis and necroptosis (DuMont et al., 2013; R. S. Flannagan et al., 2016; Greenlee-Wacker et al., 2014, 2017; B. Haslinger-Löffler et al., 2006; Kitur et al., 2015, 2016; Kobayashi et al., 2010; Korea et al., 2014; Münzenmayer et al., 2016). Discrepancies observed between studies are likely due to differences in experimental procedures, host cells, *S. aureus* strains and limited knowledge of pathways at the time.

While the majority of studies carried out with non-professional phagocytes report apoptosis execution during intracellular *S. aureus* infection, only few early studies suggest mechanisms behind the onset of apoptosis. Wesson and colleagues showed activation of apoptosis by RN6390 wild type strain in epithelial cells involves caspases 8 and 3, which leads to characteristic apoptotic DNA laddering and cell morphological changes. They also observed that *agr* and *sar* mutant strains did not produce this same onset of cell death as wild type strains, suggesting Agr and/or Sar-regulated products contribute to the onset of apoptosis (Wesson et al., 1998, 2000). However, the *sar* mutant strain ALC136 induced dramatic morphological changes in epithelial cells without DNA laddering, a phenotype more consistent with necrosis (Bayles et al., 1998). Menzies and Kourteva *et al* use two hla-positive *S. aureus* strains and their isogenic hla-deficient mutants to show that expression of α-toxin during endothelial cell invasion by *S. aureus* enhances apoptosis (Menzies & Kourteva, 1998, 2000). Haslinger-Löffler *et al* (2005) also show the importance of α-toxin in apoptosis induction in endothelial cells but also reported that multiple virulence factors are likely involved in activation of apoptosis, as cell death was dependent on the presence of global regulator agr and the alternative sigma factor sigB. Another study conducted by Chi *et al* (2014) demonstrated that a PVL-positive *S. aureus* strain caused significantly more caspase-dependent keratinocyte apoptosis than the isogenic Δ*pvl* mutant.

Studies using professional phagocytes produce less consistent reports on host cell death, with the majority implicating pyroptosis, necroptosis or necrotic pathways and few suggesting apoptosis. It is perhaps not surprising that upon pathogen invasion, immune cells die via a more pro-inflammatory means. Extracellular *S. aureus* LukAB has been shown to be a key factor in inducing a pyroptosis-like mechanism involving the inflammasome components caspase-1, NLR protein 3 (NLRP3) and apoptosis-associated speck-like protein containing a CARD (ASC) in a CD11b dependent manner (Melehani et al., 2015). Staphylococcal induction of cell death from within THP-1 macrophages, primary human monocytes and neutrophils was also dependent on LukAB and its host cell

receptor CD11b, but independent of NLRP3 and ASC which strongly suggests contribution of other factors (DuMont et al., 2013; Melehani et al., 2015; Münzenmayer et al., 2016; Ventura et al., 2010). In human neutrophils staphylococcal PVL was again shown to directly target the mitochondria to induce activation of caspase-9 and caspase-3 causing apoptosis (Genestier et al., 2005). Leukocytes are particularly susceptible to *S. aureus* α-toxin even at low-levels, it is also required and sufficient for induction of either apoptotic or necrotic-like cell death (Bantel et al., 2001; Essmann et al., 2003; Haslinger et al., 2003).

The Prince lab have reported a cohesive map of cell death pathway activation by *S. aureus* in both macrophages and keratinocytes. Their work suggests that all three programmed cell death pathways are indeed induced by *S. aureus,* but despite the activation of apoptosis caspases (caspase-3/7 and -8), necroptosis and pyroptosis are the major pathways executed (Kitur et al., 2015, 2016). The group attribute cell death to staphylococcal toxins Hla, PSMs and lukAB, however, the deletion of the genes encoding these proteins did not completely eliminate the cytotoxic effect of *S. aureus* suggesting other factors are involved in initiating death pathways in these cells (Kitur et al., 2015). It is also not entirely obvious as to whether the effects they report are due to intracellular or extracellular bacteria (Kitur et al., 2015). A number of other studies that focus on intracellular infections suggest that pore forming toxins contribute somewhat to S*. aureus* induced lytic/necroptotic cell death in macrophages, PMNs and neutrophils (Kobayashi et al., 2010; Melehani et al., 2015; Pang et al., 2010; Ventura et al., 2010). Kobayashi *et al*. (2010) describe neutrophils that underwent apoptotic-like mitochondrial membrane depolarization within 4 hrs after phagocytosis of USA300 however the neutrophils went on to rapidly lyse in a rapid RIPK-1-dependent manner, indicative of necroptosis (Kobayashi et al., 2010). Essmann *et al.* report the activation of apoptotic pathways despite apparent necrotic cell death caused by *α*-toxin in both Jurkat T cells and breast carcinoma cells (Greenlee-Wacker et al., 2017). Furthermore, Flannagan *et al.* (2016) show characteristics of both apoptosis and necrosis in *S. aureus* infected macrophages

as lamellipodium retraction, dynamic membranous blebs, osmotic swelling and transient activation of caspase 3/7 were all observed. It is well known that substantial cross-talk occurs between the three prominent cell death pathways (R. S. Flannagan et al., 2016; Jorgensen et al., 2017). Despite multiple conflicting observations in cell death, it is not unreasonable to suggest that all programmed cell death pathways could be activated in *S. aureus*-infected host cells, especially phagocytes, but the fastest or most potent signal succeeds in exterminating the cell.

As seen for many intracellular pathogens, *S. aureus* appears to be able to delay the induction of host cell death, as well as induce it. The fine regulation of cell death often allows for intracellular bacterial multiplication followed by efficient exit (Ashida et al., 2011). Koziel and collegues (2008) have reported that *S. aureus* strain Newman was able to maintain the viability of human monocyte-derived macrophages (hMDM) for days despite the appearance of early apoptotic features, such as phosphatidylserine externalization and decreased mitochondrial membrane potential. *S. aureus* strongly upregulated the expression of *B-cell lymphoma 2* (*BCL2*) and *Myeloid Cell Leukemia 1* (*MCL1)* genes (Koziel et al., 2009, 2013). The resulting proteins, Bcl-2 and Mcl-2, stabilize mitochondrial membrane potential and prevent the release of cytochrome c (Koziel et al., 2009, 2013). Furthermore, *S. aureus* uptake was associated with the activation of caspase-3 only in a subset of infected hMDM cultures and the cryoprotective effects of *S. aureus* was confirmed by demonstrating that *S. aureus*-infected hMDMs were protected from staurosporine-induced apoptosis. (Koziel et al., 2009). A separate lab also report hMDMs are able to maintain an intact plasma membrane up to 5 days post-phagocytosis of *S. aureus* Newman before an explosion of bacterial growth free in the medium and adherent to cell corpses (Kubica et al., 2008). Two more recent studies of epithelial and dendritic cell *S. aureus* infections conclude that EsxA, an effector protein secreted by the staphylococcal T7SS, plays a role in delaying host cell apoptosis (Cruciani et al., 2017; Korea et al., 2014). Δ*esxA S. aureus* increased the levels of late cell death during epithelial and dendritic infections when compared to wild-type (Cruciani

et al., 2017; Korea et al., 2014). When transfected into host cells, esxA caused in a 2.5-fold decrease in the number of apoptotic cells compared to that for control cells (Korea et al., 2014). EsxA alone and/or with other T7SS effectors may block cell apoptosis induced by extracellular or intracellular *S. aureus.* In general, the regulation of *S. aureus* induced cell death timing is understudied. This is highly likely to be a function of local host cell microenvironment, bacterial burden and bacterial expression state among other things.

1.7.1 Host cell detection of pathogens and inflammatory response

The inflammatory response is characterized by rapid signalling to induce the recruitment of immune components to the affected tissue in an attempt to resolve infections and promote healing. Overreaction of the acute inflammatory response may lead to an uncontrolled "cytokine storm", which can induce sepsis and be very detrimental to the host (Polat et al., 2017; Rittirsch et al., 2008). Thus, the immune system must carefully fine-tune the level and timing of inflammation to clear the pathogenic threat while avoiding additional tissue damage. Sepsis-induced mortality rate is 20%–30% in Gram-positive bacterial infections and can be as high as 70%–90% when septic shock is present (Polat et al., 2017).

Host cellular interaction with extracellular bacteria and phagocytosis of microorganisms is accompanied by the production and secretion of inflammatory cytokines that determine both the nature of the adaptive immune response and the recruitment of innate immune cells to the site of infection. These inflammatory cytokines are made in direct response to the engagement of pattern recognition receptors (PRRs) by conserved microbial structures termed pathogen-associated molecular patterns (PAMPs), such as lipopolysaccharide (LPS), lipoteichoic acid (LTA), peptidoglycan, and flagellin (Rittirsch et al., 2008). In addition, PRRs can recognize endogenous molecules produced by damaged cells called damage-associated molecular patterns (DAMPs) (Amarante-Mendes et al., 2018). PRRs that respond to bacterial components include TLRs, NLRs, C-type lectin receptors (CLRs), cytosolic DNA sensors and retinoic acid-inducible

(RIG)-I-like receptors (Rittirsch et al., 2008). The subcellular distribution for each of the PRR classes provides synergy towards recognition of an extensive range of PAMPs with the cumulative effect of differential expression and/or secretion of key pro-inflammatory or anti-inflammatory cytokines (Askarian et al., 2018).

1.7.2 Host cell inflammatory responses specific to *S. aureus*

Important staphylococcal sensing PRRs are located on the plasma membrane and in the cytoplasm and function to initiate signalling pathways associated with the production and release of inflammatory cytokines, as summarised in Figure 1.8. On the plasma membrane of cells such as neutrophils, monocytes/macrophages and dendritic cells are TLR-2 and -6 which recognise staphylococcal PAMPs such as LTA and lipoproteins (Fournier & Philpott, 2005; Iwaki et al., 2002; Schwandner et al., 1999) *S. aureus* deficient in lipoprotein synthesis lose their capability to activate this receptor (Stoll et al., 2005) and TLR2 is of great significance in protection against *S. aureus* strains that produce PSMs (Hanzelmann et al., 2016). In order to avoid immune clearance, *S. aureus* deploys several mechanisms to subvert the fast-acting TLR2 responses through interference with at least three distinct mechanisms. The first involves inhibition of TLR2 heterodimer formation (Koymans et al., 2017; Yokoyama et al., 2012). The second is structural mimicry of the TIR domain (Askarian et al., 2014) and the final known mechanism is through the activation of inhibitory receptor pathways (Nakayama et al., 2007, 2012).
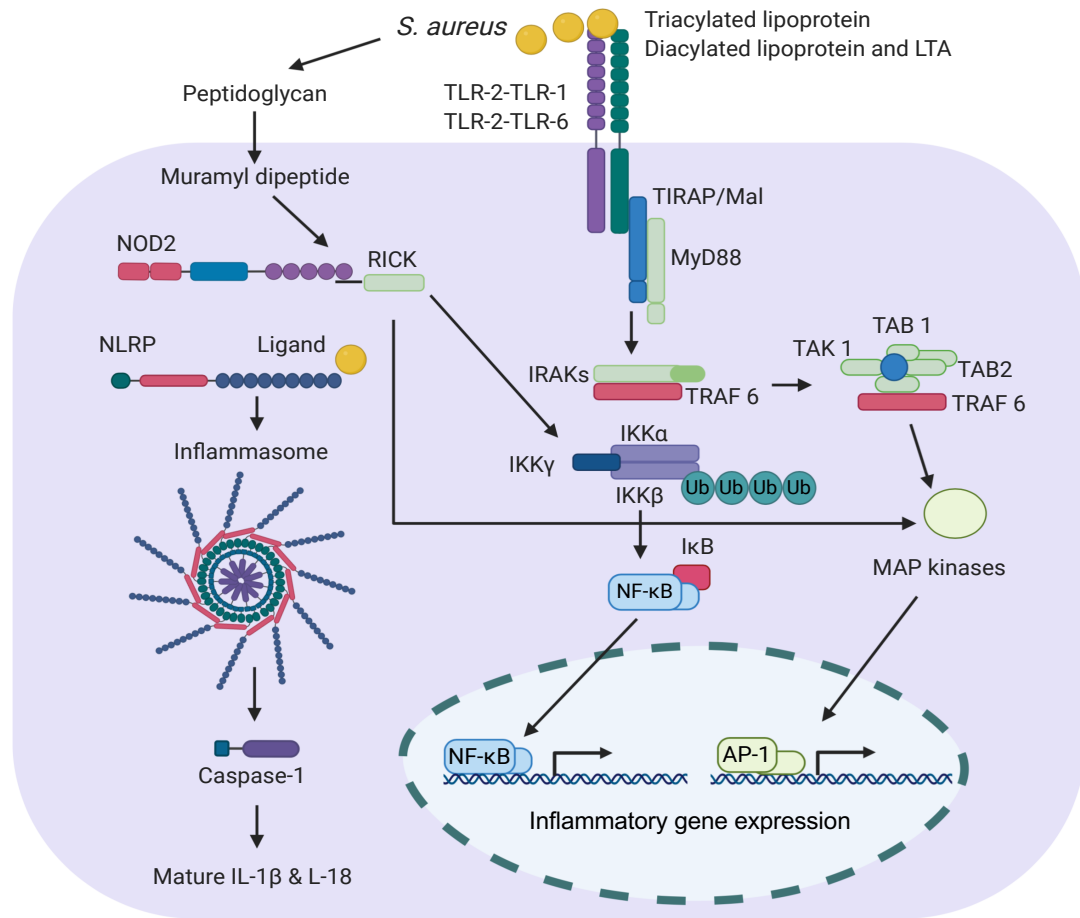
Figure 1.8: Staphylococcal- induced TLR and NLR- mediated signalling. The TLR- pathway is commonly mediated through adapter MyD88. MyD88 recruits IRAKs and TRAF6 which induces NF-κB and AP-1 associated pro-inflammatory responses. NOD2 also induces NF-κB activation through RICK by triggering the polyubiquitination of IKKβ. NLRs induce inflammasome formation resulting in production of mature IL-1β and IL-18. AP-1, activator protein 1; IKK, IkappaB kinase; IRAK, IL-1 receptor associated kinase; MAPK, mitogen activated protein kinase; MyD88, myeloid differentiation factor-88; NF-κB, nuclear factor kappa B; RICK, CARD-containing serine/threonine kinase; TAB, TAK1 binding protein 1; TAK1, growth factor-β-activated kinase-1; TIRAP, TIR associated protein; TRAF, tumour necrosis factor receptor-associated factor. Figure based on (Askarian et al., 2018).

Two specific NLRs have been highlighted for their importance during *S. aureus* intracellular infections, NLR NOD2 and NLRP3. Monomeric peptidoglycan fragments of *S. aureus* and the potent α-hemolysin toxin activate NLR NOD2 (Hruz et al., 2009; Volz et al., 2010). The significance of NOD2-mediated cytokine release, e.g. IL-1β and IL-6 in host defense against *S. aureus* infection, has been demonstrated (Hruz et al., 2009). The NLRP3 inflammasome is shown to be triggered by lysosome-mediated degradation of *S. aureus* peptidoglycan inside phagosomes. To counteract this, *S. aureus* O-acetyl transferase A modifies the peptidoglycan, rendering it more resistant to lysosome-mediated degradation, therefore when O-acetyl transferase A is present, immune responses are blunted (Shimada et al., 2010). A collection of *S. aureus* virulence factors have also been implicated in the activation of NLRP3 including α-hemolysin β- and γ- hemolysins PVL and LukAB (Cho et al., 2012; Holzinger et al., 2012; Kebaier et al., 2012; Muñoz-Planillo et al., 2009). Furthermore, Melehani et al. (2015) have shown that the *S. aureus* activation of NLRP3 inflammasome in monocytes/macrophages results in the secretion of IL-1β and IL-18 and induction of necrotic-like cell death. Overall, however, the role of this NLRP3-driven immune response against *S. aureus in vivo* is controversial. In a murine pneumonia infection model the NLRP3 is not required for bacterial clearance (Kebaier et al., 2012) but in a murine *S. aureus* skin infection model, IL-1β promotes abscess formation and bacterial clearance (Cho et al., 2012).

As previously alluded to, phagocytosis of microbes can cause the activation of both TLRs and NLR inflammasomes but both PRR classes can then in return have an impact on the phagosomal pathway for example, they can trigger phagocytosis, cause phagosome maturation and alert the cell to the cargo it has just encountered (Blander & Medzhitov, 2004; Moretti & Blander, 2014). Upon *S. aureus* infection TLR2 and NOD2 are known to participate in autophagy and phagocytosis activation via JNK (c-Jun N-terminal kinase) signalling pathways (Fang et al., 2014). In the case of macrophages acidification of phagosomes containing *S. aureus* and other Gram-positive bacteria is regulated by the NLRP3-inflammasome and caspase-1. Active caspase-1 accumulates on phagosomes and

acts locally to control the pH by modulating buffering by the Nicotinamide adenine dinucleotide phosphate (NADPH) oxidase 2 (NOX2) (Sokolovska et al., 2013).

1.8 Modelling Staphylococcal infections

1.8.1 *In vivo* models

Animal studies with infectious pathogens aim to provide experimental proof for the molecular basis of pathogenesis, the establishment of innate and adaptive immunity and the molecular mechanisms whereby immunity is achieved. *In vivo S. aureus* infection models span both vertebrates and invertebrates. Invertebrate models of *S. aureus* infection include *Bombyx mori* (silkworms) (Hamamoto et al., 2014), *Drosophila melanogaster* (Needham et al., 2004) and *Caenorhabditis elegans* (Sifri et al., 2003) which have significantly divergent innate immunity systems to humans.

Murine infection models have been most widely used for *S. aureus* research. Similar to humans, mice can present with a diverse spectrum of diseases when infected with *S. aureus*, however, the bacterial dose required to produce a pathology is often extremely high and varies widely (H. K. Kim et al., 2014; Pollitt et al., 2018; Salgado-Pabón & Schlievert, 2014). Mouse models are used in a variety of *S. aureus* disease studies, some of which include sepsis (Cheng et al., 2010; Kuklin et al., 2006), endocarditis (Panizzi et al., 2011), pneumonia (Kneuper et al., 2014; Wardenburg & Schneewind, 2008), subcutaneous skin infection (Kugelberg et al., 2005) septic arthritis (Bremell et al., 1991) and intradermal infection/abscesses (Bunce et al., 1992). Within the landscape of staphylococcal T7SS research murine sepsis, pneumonia and skin models are have been used (Anderson et al., 2017; Burts et al., 2005, 2008; Dai et al., 2017; Ishii et al., 2014; Kneuper et al., 2014; Ohr et al., 2017; Y. Wang et al., 2016). However, it is important to note that mice do not serve as a natural host for *S. aureus* isolates. Human and bovine staphylococcal strains are well adapted to their hosts, with virulence factors that are often ineffective in mouse infection

models (H. K. Kim et al., 2014; Salgado-Pabón & Schlievert, 2014; Spaan et al., 2013).

1.8.2 *In vitro* infection models

The evaluation of staphylococcal infections in mouse models provide vital insight into virulence, however, findings are often not reproducible in human trials, especially when it comes to vaccine development (Salgado-Pabón & Schlievert, 2014). Lung and other organ anatomy and physiology, as well as the immune response, significantly differ between mice and men (Masopust et al., 2017) Reliable *in vitro* models closely resembling the physiological conditions of humans are required for the identification of novel vaccine components and to assess infection dynamics.

Organ-on-Chip-based assays provide accessibility to study pathogen-induced diseases in real time and at high resolution, they can open new avenues to uncover bacterial pathogenesis in a human-relevant environment.

Organ-on-Chip technology is based on the interdisciplinary science of microfluidics. Microfluidics involves the manipulation of microlitre volumes of fluids, in an artificially fabricated optically clear microsystem (Whitesides, 2006). The creation of a microfluidic chip involves the marriage of multiple disciplines in a series of fabrication methodologies during which polydimethylsiloxane (PDMS) microchannels are bonded to a glass slide. Microchannel applications extend from biosensors and cell culture to protein crystallization all carried out in under constant perfusion. Cell culture in microfluidic devices has become increasingly popular and has evolved into the whole field of science known as organs-on-chips (Bhatia & Ingber, 2014).

The fundamental aim of this kind of cell culture is to recreate host physiology with tissue-level complexity inside the microfluidic channel. This approach has made it possible to micro-fabricate models of blood vessels (Hasan et al., 2015) lung and airways (Benam et al., 2016; Schultze et al., 2010a), liver (Bhise et al.,

2016), brain (Dauth et al., 2017), gut (H. J. Kim et al., 2012; H. J. Kim & Ingber, 2013) kidney (K. J. Jang et al., 2013; Wilmer et al., 2016) and many more tissues. Static 2D and 3D *in vitro* cell culture environments can lack the richness required to successfully imitate *in vivo* states (Abbott, 2003). The microfluidic models can mimic essential physiological qualities such as constant nutrient supply, waste removal, introduction of immune cells, shear stress and maintenance of temperature and gas levels (Walker et al., 2004). Shear stress is a particular factor that is known to have a large effect on *S. aureus* adhesion to host factors (Herman-Bausier et al., 2018; Viela et al., 2019). Organ-on-chip technologies are thought to occupy the middle ground between simple *in vitro* experiments and animal models, providing a window to a more specific and predictive framework of infectious disease processes in humans (Baddal, 2019). A collection of practical advantages including small reagent costs, reduced consumption of reagents, reduced contamination risk and high throughput experimentation also make this an attractive research platform (Halldorsson et al., 2015).

Microfluidic organ mimics have excellent applications in investigating host-pathogen interactions, however this is still an under-exploited line of enquiry (Baddal, 2019; Baddal & Marrazzo, 2021). Gut-on-a-chip microfluidic culture was one of the first models used to better understand bacterial and viral infections. A group led by Professor Donald Ingber at the Wyss Institute, Harvard have been instrumental in the creation and use of organ-on-chip technology. They fabricated a two-channel gut-on-chip model that incorporated commensal microbes in contact with the human intestinal epithelial cells and used this to study the effect of the introduction of pathogenic enteroinvasive *E. coli* (EIEC) (H. J. Kim et al., 2016). Peripheral blood mononuclear cells (PBMCs) were even introduced into the lower capillary channel of the device to investigate the impact of the immune system on EIEC infection and epithelial disruption. They found previously unknown contributors to intestinal inflammation such as specific cytokines, mechanical motions and members of the gut microbiome (H. J. Kim et al., 2016). In similar models the damage of the human colonic epithelium induced by enterohemorrhagic *E. coli* (EHEC) infection (Tovaglieri et al.2019) and the

impact of intestinal mechanical forces on *Shigella* infection were studied (Grassart et al., 2019). Other infection models-on-chips, such as differentiated human villus intestinal epithelium, was used to demonstrate the response of these caco2 intestinal epithelial cells to a viral infection by the enterovirus Coxsackie virus B1 (Villenave et al., 2017). A microfluidic primary human hepatocyte system, or liver-on-chip, has been used to recapitulate all steps of hepatitis B virus infection and revealed important pathways for immune evasion (Ortega-Prieto et al.2018).

Complex lung-on-chip or closely related platforms have been around for more than 10 years (Schultze et al., 2010a) but it is only very recently that we have started to see a dramatic increase in their use in host-pathogen interaction studies. The Ingber group used their microfluidic small airway-on-chip (Benam et al., 2016) to investigate the impact of influenza viral infection of human airway (Si et al., 2019) and even for drug testing on COVID-19 (Si et al., 2020). Other groups have utilised lung-on-chip infection models to study bacterial infections such as *M. tuberculosis* (Thacker et al., 2020) and *S. aureus* (Deinhardt-Emmer et al., 2020). Deinhardt-Emmer et *al.* created a human *in vitro* alveolus model system composed of vascular and epithelial cell structures with cocultured macrophages resembling the human alveolus architecture and functions in order to detect the morphological and functional alterations attributed to infection as well as the spatiotemporal spreading of pathogens during pneumonia. The model involves the triple-cell co-culture of NCI-H441/NHBE epithelial, HUVEC endothelial and myeloid THP-1 cells to recreate a lung barrier model. The group found that *S. aureus* infections, in particular co-infections with influenza via the epithelium, induced a high inflammatory response and pathogen spread to the endothelium. Co-infection also lead to the disruption of the endothelial barrier but did not damage the integrity of the epithelium (Deinhardt-Emmer et al., 2020).

1.9 Project background and aims

Prior to this project the staphylococcal T7SS and its associated effector proteins were identified as virulence factors that contribute to severe disease and persistence in mouse models(Anderson et al., 2017; Burts et al., 2005, 2008; Ishii et al., 2014; Jäger et al., 2018). *In vitro* studies have strongly suggested the T7SS modulates programmed host cell death and immune response pathways (Cruciani et al., 2017; Dai et al., 2017; Korea et al., 2014), but we are missing a comprehensive understanding   of molecular interactions between T7SS proteins and specific host pathways. Due to the immunoregulatory characteristics of the T7SS and the known ability for *S. aureus* to overcome phagocyte antimicrobial factors and induce cell death (Moldovan & Fraunholz, 2019; Pidwill et al., 2021; Strobel et al., 2016), we decided to investigate the impact of the T7SS in macrophages. The T7SS has not been studied in the context of intracellular macrophage infections before. The contribution of T7SS to infection *in vivo* has thus far concentrated largely on sepsis or pneumonia models and lack investigations into its effect on local infection and bacterial dissemination. We therefore chose to study the effect of the T7SS using mouse skin abscess models. Although mouse models provide invaluable data for *S. aureus* host interactions, there can sometimes be a disconnect between mouse and human findings (Salgado-Pabón & Schlievert, 2014). For that reason, this project also involved the design, fabrication and characterisation of a microfluidic airway-blood vessel interface for the study of *S. aureus* and its T7SS with human cells under physiologically relevant conditions. Overall, the collection of this data will inform on an important virulence factor already incorporated into vaccine development as well as a possible novel target for antimicrobials (Mancini et al., 2016b; Torre et al., 2015). Specific aims for this project are as follows:

- To determine the effect of staphylococcal T7SS on macrophages during intracellular infection.
    - Use *in vitro* assays with human THP-1 macrophages to investigate the effect of the staphylococcal T7SS on intracellular bacterial

uptake and survival as well as to determine cytotoxic and immunoregulatory effects of T7SS on macrophages.

- Utilise Human THP-1 macrophages in time-lapse imaging to determine fates of individual cells infected with *S. aureus* and WT and T7SS deletion mutants.

- To investigate the host response pathways affected by T7SS effectors
  - Use *in vitro* assays to determine which host cell pathways are modulated by the presence of the T7SS proteins.

- To investigate the T7SS impact in murine skin infections.
  - Employ a murine intradermal skin infection model to determine the effect of the T7SS on bacterial survival and dissemination over time in murine skin.
  - Use tissue staining and immunohistochemistry to determine the T7SS effect on tissue disruption, abscess formation and macrophage recruitment in skin abscesses.

- To develop and optise a microfluidic blood-vessel-airway interface that enables the real time microscopic investigation of *S. aureus* WT and T7SS mutant infections of host cells.
  - Determine the optimal design of microfluidic channel for the culture of Human A549 epithelial cells and HUVEC endothelial cells under flow.
  - To optimise a microfluidic circuit and set-up for the investigation of *S aureus*- host interactions under a microscope.

2 Chapter 2: Methods

2.1 Bacterial strains and growth conditions

S. aureus WT USA300 LAC JE2 strain (BEI Resources (NARSA)) and three markerless, isogenic mutants, *ΔesxC, ΔessC* and *ΔesxC-D* carrying deletions of only *esxC*, or *essC* or 4 T7SS proteins *esxC*, *esxB*, *esaE* and *esxD* respectively were used during this project. Mutants were generated in house using allelic replacement as previously described (Bae & Schneewind, 2006; Korea et al., 2014). *ΔesxC-D* mutant was generated as part of this project as follows: 1-kb DNA fragments flanking the esx genes were amplified by polymerase chain reaction (PCR) using ExTaq enzyme (TaKaRa) and manufacturer's instructions (with primers 1 to 4 in Table 2.1). Forward and reverse primers incorporated the AttB1 and AttB2 sites required for homologous recombination. The resulting PCR fragments were gel-extracted (QIAquick gel Extraction, Qiagen) and underwent a Splicing by overlap extension (SOEing) PCR in which the overhanging fragments were ligated together. The ligated product was used for recombination with the pKOR1 *Escherichia coli/S. aureus* shuttle vector, plasmids are shown in Figure 2.1.

Table 2.1: Primers used to create Δ*esxC-D S. aureus* mutant.

ID	Prime name	Primer sequence
1	EsxD-downstream-Soeing-Fwd	AAATAGGAGGGAGGTATGTTGTGCATGACATGACAAAAGAT
2	AttB1-EsxC Up-Fwd	GGGGACAAGTTTGTACAAAAAAGCAGGCTGAGCTAACGCTATGAAAACACC
3	EsxC-upstream-Rev	AACATACCTCCCTCCTATTT
4	AttB2-EsxD-downstream-Rev	GGGGACCACTTTGTACAAGAAAGCTGGGTGTTACGAGATTGATTCAACACAC
5	EsxD-15-codons-SOEing-fwd	GAGGAGTAATGACGTTGAGTGGAAATATTGAGGGATAGGTGCATG
6	EsxD-15codons-rev	TCCACTCAACGTCATTACTCCTC
7	EsxD down-Fwd	GTGCATGACATGACAAAAGAT

8	AttB2-EsxD down-Rev	GGGGACCACTTTGTACAAGAAAGCTGGGTGTT ACGAGATTGATTCAAC
9	LacO fwd	GGAATTGTGAGCGGATAAC
10	T7 fwd	TAATACGACTCACTATAGGG
11	EssC-cPCR-fwd	CGACAGAACCAATGCCACAT

Two key components of the pKOR1 lambda recombination cassette are *attP* sites which recombine with attB sequences of DNA inserts and *ccdB*, which encodes an *E. coli* gyrase inhibitor protein for selection of non-recombinant plasmids. For recombination pKOR1 was incubated overnight at 25°C with the ligated DNA product in Tris- Ethylenediaminetetraacetic acid (TE) buffer (pH 8.0) and BP clonase II enzyme (Thermofisher). Ice cold pKOR1 was then mixed with competent E. coli strain DH5α and plated on pre-warmed Lysogeny broth (LB) agar (Sigma) with 100μg/mL ampicillin (Formedium) and incubated overnight at 37°C for plasmid uptake via heat shock. Competent *E. coli* DH5α were made using 3 washes with 0.5M Sucrose (Sigma) and incubation on ice for 30 mins. Colonies underwent colony PCR with GoTaq enzyme (Promega) (primers 2 and 8 in Table 2.1) to confirm presence of plasmid, the other part was incubated in LB ampicillin 100 μg/mL (Formedium). Plasmid purification was carried out (QIAprep Spin Miniprep Kit, Qiagen) and sequences confirmed by sanger sequencing (GATC Biotech), using primers 10 and 7 in Table 2.1.

pKOR1 with confirmed ΔesxC-esxD insert were transferred via electroporation to electrocompetent *S. aureus* RN4220 (a restriction minus and methylation positive strain). Electrocompetent RN4220 *S. aureus* were made using 3 washes with 0.5M Sucrose and incubation on ice for 30 mins. Electroporation was carried out (BioRad gene pulse Xcell) under the following conditions, 100 Ω, 2.5 kV, 25 μF with 0.1 cm cuvette. The bacteria were recovered in TSB and incubated at 30 °C with shaking for 1hr then spread on a tryptic soy agar (TSA) plate with 10 ug/mL of chloramphenicol (chlor-10) (Formedium) for overnight incubation at
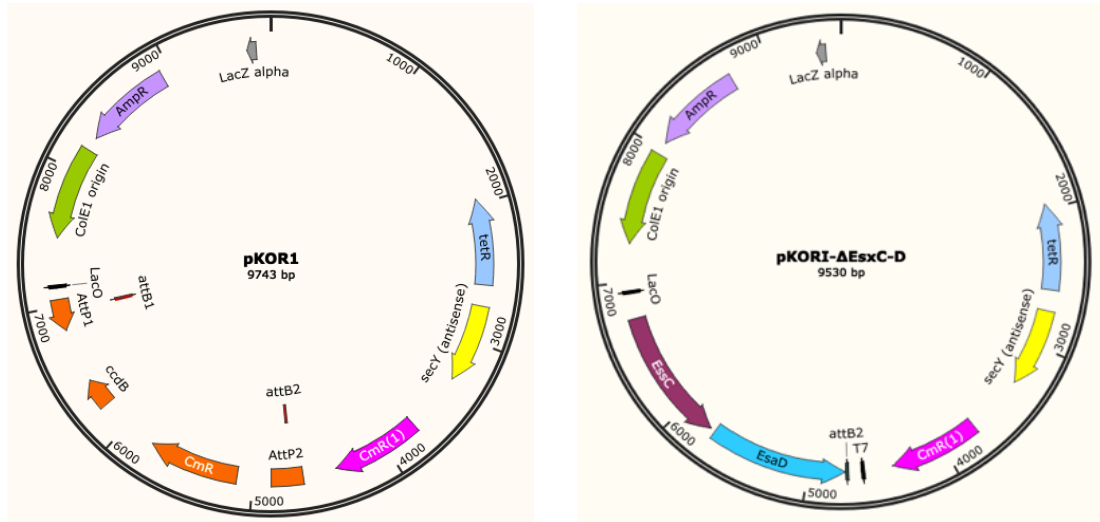
Figure 2.1: Plasmid maps for pKOR1 and Δ*esxC-D* pKOR1.

pKOR1 shuttle vector used in the cloning methods for *S. aureus* gene knockout of *esxC, esxB, esaE* and *esxD* (*esxC-D*). Including *repF* (replication gene of pE194ts), c*mr* (chloramphenicol acetyltransferase resistance), antisense *secY570* (N-terminal 570 nucleotides of secY including ribosome binding site) under the control of a Pxyl/tetO promoter with and the lambda recombination cassette (Gateway Technology, Invitrogen) which consists of *att* recombination sites and *ccdB*, a gene encoding for an *E. coli* gyrase inhibitor protein to allow for the growth of *E. coli* with successful recombination plasmids only.

30 ˚C. Colony PCR with prior lysostaphin 5 µg/mL (Sigma) was carried out to confirm presence of the plasmid. The PKOR1 Δ*esxC-wsxD* plasmid extracted from RN4220 cultures and finally transferred via electroporation to electrocompetent USA300 JE2 strain of *S. aureus* as previously described for RN4220. Resulting transformed cells were spread on a TSA chl-10 plate overnight at 30 ˚C. The next day colonies were used to inoculate TSB (chl-10) and incubated again overnight.

Plasmid positive USA300 JE2 colonies were then grown in non-permissive conditions (42 ˚C chlor-10 TSB) to allow for integration of the plasmid into *S. aureus* chromosomal DNA as shown in Figure 2.2. This step was repeated with fresh TSB chl-10 to increase the yield of integrated cells. The resulting culture was streaked on TSA chl-10 plates and incubated overnight at 42 ˚C. TSB was inoculated with fast growing colonies and incubated at 30 ˚C overnight. To confirm the integration, chromosomal DNA was extracted from cells using GenElute bacterial genomic DNA kit (Sigma). PCR amplification of a 4.9kb section of chromosomal DNA and inserted plasmid was used to confirm upstream integration of the plasmid using primer 8 and 10 (Table 2.1) and Hot Start II Phire enzyme (Thermo Scientific). TSB cultures positive for integration were diluted with sterile water and spread on TSA anhydrotetracycline (100ng/mL) (Melford) for overnight incubation at 37 ˚C to promote of seY antisense expression and therefore plasmid excision. Colonies were streaked out on both TSA chlor-10 and TSA with no antibiotics to verify the lack of chloramphenicol resistance and therefore plasmid excision. Mutants were confirmed by PCR, using external primers targeting flanking regions and then sequencing (GATC Biotech). Full genome sequencing (carried out by Arnaud Kengmo Tchoupa) was used to confirm the strain did not contain nonsynonymous single nucleotide polymorphisms

For time-lapse imaging, a plasmid pJL94 carrying constitutively expressed yellow fluorescent protein (*yfp*) (obtained from Prof. Christiane Wolz, University of Tübingen) (Münzenmayer et al., 2016) was transferred into USA300 JE2 strains by Φ11 phage (obtained from Prof. Christiane Wolz) transduction. For

production of lysate *S. aureus* RN4220 containing pJL94 grown on TSA chlor-10 was mixed with phage buffer (1mM MgSO$_4$, 4mM CaCl$_2$, 50mM Tris pH 7.4, 5.9 g/L Nacl, 1g/L Gelatine) and 0.6% TSA top agar then poured onto TSA chlor-10 plates. Plates were incubated until clear (bacterial lawn is cleared), then top agar was scraped off in the presence of TSB medium, collected and melted at 55 ℃. The mixture was centrifuged at 5000g, 10 min, 4°C then filter sterilised (0.22 μm filter). For plasmid transduction, USA300 JE2, grown on TSA plates was mixed with phage buffer then divided into 5 aliquots. RN4220 lysates were added to aliquots as follows, 1 x 0.1μL, 1x + 1μl lysate, 1x + 10 μl lysate, 1x without lysate (control), then mixed and incubated for 10 min at 37°C. Phage top agar (casamino acid, yeast extract, NaCl, agar) was added to aliquots, then each were poured on TSA chlor-10 plates and incubated for 2 days at 37°C. Resulting colonies were repeatedly streaked on TSA chlor-10 (3 times) followed by repeat inoculations into TSB chlor-10 (3 times) to remove phages. Obtained transductants were verified by fluorescence microscopy.
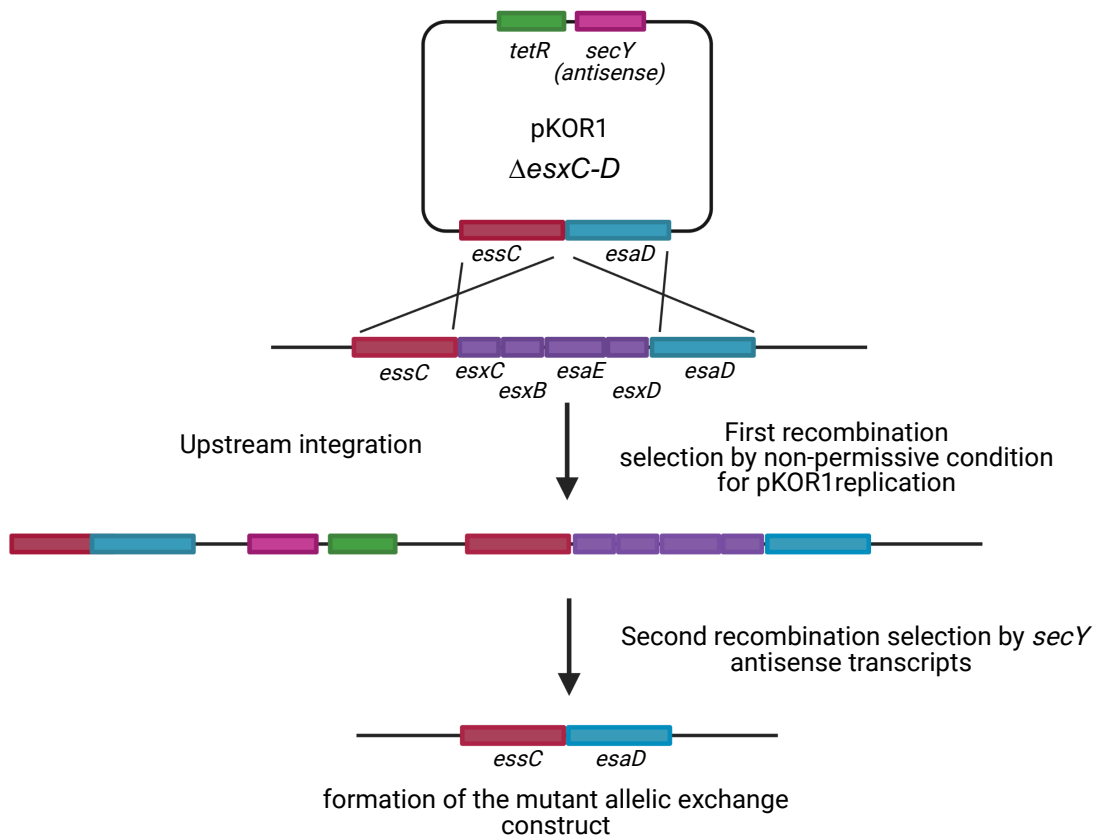
Figure 2.2: Formation of Δ*esxC-D* mutant by allelic replacement.

Gene knockout of *esxC*, *esxB*, *esaE* and *esxD* via homologous recombination. First homologous recombination event occurs between the DNA in the upstream regions or the downstream regions resulting in plasmid integration into the chromosome (upstream product shown). A second recombination event occurs resulting in the original allele being excised with the plasmid leaving the mutated allele in the chromosome.

2.2 Bacterial growth conditions

Bacteria were grown aerobically in Tryptic soy broth (TSB) (Sigma-Aldrich) shaking overnight at 37°C, cultures were refreshed in TSB the following day and grown to achieve an OD_{600} of 1.5 unless stated otherwise.

2.3 Haemolysis assays

Red blood cells (RBCs) (E & O Laboratories LTD) were collected by centrifuging whole sheep's blood at 500 g for 10 mins at 4°C followed by resuspension in Roswell Park Memorial Institute (RPMI) medium, this was repeated twice. Pellets were then resuspended in phosphate buffered saline (PBS) to achieve 4% RBCs. Bacterial strains were cultured as above to reach OD_{600} 1.5 or stationary phase (overnight cultures). Cultures were pelleted at 5000 rpm, supernatant was collected and filtered with 0.22 μm filter. RBCs and bacterial supernatant were added at a 1:1 ratio in 96-well plates. Control included RBCs plus PBS and lysed control was RBCs plus 2% triton in PBS. Plates were incubated shaking at 700 rpm at 37°C for 1 hr absorbance at wavelength 541 nm was measured with FLUOstar OMEGA plate reader (BMG LabTech).

2.4 Eukaryotic cell culture

The human monocytic cell line THP-1, obtained from Public Health England, were cultured in suspension in complete Roswell Park Memorial Institute (RPMI) growth medium, consisting of RPMI + 2mM L-glutamine (Gibco) supplemented with 10% fetal bovine serum (FBS) and 1% penicillin and streptomycin (Sigma) at 37°C and 5% CO_2 maintained at approximately 1×10^6 cells/mL. To initiate the differentiation of THP-1 monocytes into macrophages, cells were centrifuged at 1000 rpm for 5 mins and re-suspended to achieve a density of 2.5×10^5 cells/mL in complete RPMI with 100 ng/mL of phorbol 12-myristate 13-acetate, (PMA) (Sigma Aldrich). The cells were then seeded and incubated at 37°C and 5% CO_2 for 72 hrs. For further differentiation into inflammatory macrophages, cells were

incubated with complete RPMI supplemented with 50 ng/mL Interferon-γ (IFN-γ) (Gibco) for a further 24 hours after PMA treatment.

For microfluidic experiments human type II alveolar epithelial cells (A549), obtained from the American Type Culture Collection (ATCC), were cultured in Dulbecco's Modified Eagle Medium (DMEM) supplemented with 10% FBS. Immortalised Human umbilical vein endothelial cell line (HUVEC), generated by the Stewart group at St Andrew's University using puromycin selection (unpublished), were cultured in Endothelial cell growth medium (Promocell) supplemented with 0.2 µg/ml puromycin and growth medium Supplementpack (Promocell). No antibiotics were used 24 hours prior to experiments. Cells were seeded at 5 x 10^5 cells/mL in microfluidic channels.

2.5 Macrophage *S. aureus* challenge

Overnight *S. aureus* cultures were refreshed in TSB and grown to OD_{600} 1.5 as described above. Cultures were diluted in RPMI complete growth medium to 2.5 x 10^6 colony forming unit (CFU)/mL and added to macrophage cultures to achieve an MOI of 10 unless stated otherwise. After 1 or 2 hours of incubation at 37°C with 5 % CO_2, extracellular bacteria were killed by adding 20 µg/ml lysostaphin (Sigma-Aldrich) and 50 µg/mL of gentamicin (Melford) for 30 mins at 37°C. Cells were then washed twice with PBS and either immediately processed or refreshed with RPMI complete growth medium and incubated at 37°C with 5 % CO_2 for processing at indicated timepoints. For intracellular Infections with antibiotics over extended periods, after initial extracellular bacterial killing by gentamicin and lysostaphin as stated above, cells were washed twice with PBS and refreshed with complete RPMI medium supplemented with 5 µg/mL lysostaphin until specified timepoints.

2.6 CFU determination

Infection assays were carried out in 24-well plates (Falcon), Permanox plastic chamber slides (177437 Nunc Lab-Tek) or RS treated soda lime glass chamber

slides (154526, Nunc, Lab Tek II) as detailed in section 2.5 with MOI 10 unless otherwise specified. For infections with extended exposure to lysostaphin, at indicated timepoints infected THP-1 macrophages were washed twice with PBS and lysed with 1 mL cold sterile distilled water and vigorous pipetting. Lysates were serially diluted in PBS then plated on TSB agar (Sigma-Aldrich). The following day colonies were counted, and CFU/mL was calculated. For infection assays that were incubated with antibiotic-free RPMI, total bacteria present (intracellular and extracellular) was quantified by combining infected macrophage supernatants and cell lysates (collected as above), which was serial diluted in PBS and plated on TSB agar. The following day colonies were counted, and CFU/mL was calculated.

2.7 Time-lapse microscopy

Infection assays were carried out as above in 4 well chamber slides with RS treated Soda-lime glass (Nunc Lab-Tek) or Permanox plastic (Nunc Lab-Tek). After initial killing of extracellular bacteria with lysostaphin and gentamicin (section 2.5) macrophages were washed with PBS twice and refreshed with either complete RPMI or complete RPMI supplemented with 5 μg/mL lysostaphin for antibiotic containing experiments. Fluorescent and phase contrast images of infections were taken every 10 minutes of 3 fields per well from 1.5 hrs to 24 hrs post-infection using a Leica DMi8 widefield fluorescent microscope with CO_2 stage top incubator (Okolab). Time-lapse videos were used to quantify macrophage cellular morphologies. Morphologies of 100 macrophages per biological replicate were recorded at indicated times post infection. The morphological features included spindle shaped (elongated cell body and apical cytoplasmic extensions), fried egg shaped (enlarged ameboid cell body), rounded (small, round), pore-induced intracellular trap (PIT)-like morphology (Immobilised, swollen, characteristically round cell body, semi-permeable membrane, condensed organelles as detailed by Jorgensen et *al*. (2016) and apoptotic blebbing (immobilised shrunken cell body with characteristic protrusions and membrane blebbing, formation of apoptotic bodies). Where

molecular inhibitors were used activated THP-1 cells were pre-treated for 1 hour with 1mL of RPMI supplemented with either 10 μM necrosulfonamide (NSA) (Merck Millipore, Massachusetts, United States), a potent inhibitor of MLKL or 10 μM Z-VAD-FMK (Bio-Techne Ltd, Abingdon, UK), a pan-caspase inhibitor, before undergoing invasion assays as described above in chamber slides. Concentrations of NSA or Z-VAD-FMK were maintained in RPMI throughout the 24-hour infections. Time-lapse images were taken as described above.

For microscopy bacterial challenges were carried out in RS glass chamber slides (LabTek II) as in section 2.5 for 2 hrs at MOI 10 unless stated otherwise. After initial lysostaphin and gentamicin treatment infected cells were either processed or refreshed with complete RPMI media supplemented with 5μg/mL lysostaphin. For cell death positive cells, uninfected THP-1 macrophages were treated with 0.1mM staurosporine (Sigma) for 2 hours before processing. At indicated timepoints fixation was carried out with 4% paraformaldehyde (PFA) (Alfa Aesar) at room temperature for 15 mins. Macrophages were permeabilised using 1% saponin (Sigma) and 0.1% triton-X100 (ThermoFisher Scientific) in PBS for 20 minutes at room temperature. Cells were then blocked with 3% bovine serum albumin (BSA) for 30 minutes at room temperature. Slides were washed with 1% BSA in PBS in preparation for cell staining. For visualization of F-actin cells were stained with Phalloidin 650nm (Cell Signaling Technology) for 40 mins in the dark. For observation of intracellular bacteria, *S. aureus* membranes were stained with vancomycin-BODIPY for 30 mins in the dark (Invitrogen). Finally, for visualization of nuclei, DAPI (4',6-diamidino-2-phenylindole) anti-fade mounting medium (Cell Signaling Technology) was added to each well, sealed with a coverslip and incubated in the dark for 40mins. Images were acquired with PerkinElmer UltraVIEW Vox spinning disk confocal microscope and analysed using ImageJ. At least 48 images for each infection condition over 4 independent experiments were used for quantification.

2.8 Cytotoxicity quantification

Macrophage bacterial challenges with and without extended incubation of antibiotics were carried out in 96 well plates (falcon) at MOI 10 (section 2.5). Supernatants of infected and uninfected macrophages at indicated timepoints were used in CytoTox96 assays (Promega, USA) according to manufacturer's instructions to determine level of Lactose dehydrogenase (LDH) release. Maximum LDH release was determined by lysis of uninfected macrophages with the CytoTox96 kit lysis buffer (Promega). Optical density (OD_{490}) of each well was measured on a FLUOstarOmega Microplate reader and percent cytotoxicity was determined from 3 independent experiments. Percentage cytotoxicity was calculated with the following equation:

$$\text{Percent cytotoxicity} = 100 \times \frac{\text{Experimental LDH release (OD}_{490})}{\text{Maximum LDH release (OD}_{490})}$$

Cytotoxicity of infected macrophages was also determined by propidium iodide staining (PI). Infected cell cultures in black 96 well clear bottom plates (Greiner Bio-One LTD) were washed with PBS then incubated with PI (Sigma) at a concentration of 10 μg/mL for 15 mins at 37°C with 5 % CO_2. Fluorescence was quantified with FLUOstarOmega Microplate reader with excitation wavelength of 544 nm and an emission wavelength of 612 nm

2.9 Immunoblots

Infection assays were carried out with MOI 10 (section 2.5). Infected and non-infected THP-1 cells were lysed using Radioimmunoprecipitation assay buffer (RIPA) buffer (Thermo Scientific) containing 1X Halt protease and phosphatase single-use inhibitor cocktail (Thermo Scientific). Lysate protein concentration was determined by Pierce Detergent Compatible Bradford Assay (Thermofisher Scientific). Equal concentrations of protein were loaded and separated on 4%–15% Mini-PROTEAN TGX Protein Gels (Bio-Rad) then electrotransferred using Trans-Blot Turbo Transfer System (Bio-Rad) with Mini PDVF transfer packs (Bio-Rad). Blots were blocked with 5% BSA in TBST (Tris-buffered saline plus Tween20) for 1 hour at room temperature and immunodetection was performed

overnight at 4°C using rabbit anti-Cleaved GSDMD (c-GSDMD) (Asp275) (Cell Signaling), rabbit anti-GSDMD (L60) (Cell Signaling), rabbit anti-MLKL (D2I6N) (Cell Signaling), rabbit anti-Phosphorylated MLKL (p-MLKL) (Ser358) (cell signaling), rabbit anti-Caspase-3 (D3R6Y), mouse anti-Caspase-8 (1C12), mouse anti-β-actin (Sigma-Aldrich) antibodies. Blots were washed 3 times in 1 x TBST followed by 1 hr incubation at room temperature with anti-mouse IgG, HRP-linked Antibody (Cell Signalling) or anti-rabbit IgG, HRP-linked antibody (Cell Signalling). Immunoblots were developed with Pierce horseradish peroxidase (HRP) Western blot substrate (Thermo Scientific). Relative densitometry of bands was determined by ImageJ and normalised to β-actin loading controls. Blots were stripped for blocking and re-probing using Abcam mild stripping buffer (glycine, Sodium dodecyl sulfate, Tween20 and distilled water pH 2.2) followed by 2 washes in PBS and 2 washes in TBST.

2.10 Caspase-1 quantification

THP-1 macrophage challenges were carried out in 96 well white, opaque-walled solid bottom plates (Corning) with and without extended lysostaphin treatment as detailed in section 2.5. The CaspaseGlo-1 Inflammasome Assay (Promega) was used as manufacturer's instructions to quantify levels of caspase-1 in macrophage cultures at indicated timepoints. Inclusion of the proteasome inhibitor, MG-132, in the reagent eliminates nonspecific proteasome/caspase-mediated cleavage of the substrate, enabling sensitive detection of caspase-1 activity. Luminescence was measured using a FLUOstar OMEGA plate-reader.

2.11 ELISAs

Levels of human TNF-α and IL-1β were quantified from the supernatants of infected and non-infected macrophages from THP-1 supernatants using Human TNF-alpha DuoSet ELISA (DY210) or Human IL-1 beta/IL-1F2 DuoSet ELISA (DY201) (R&D Systems) following the manufacturer's instructions. Briefly, the capture antibody was diluted and used to coat 96-well microplate for incubation overnight at room temperature. The following day wells were washed, and plates

blocked. 100 μL of 1:5 (TNF-α) or 1:10 (IL-1β) diluted sample was added to wells and incubated for 2 hours at room temperature. Wells were washed and detection antibody was added for 2-hour incubation at room temperature. Streptavidin-HRP solution was added with 20-minute incubation period. The optical density of each well was measured using a FLUOstar OMEGA plate reader set to 450 nm and 570 nm. 570nm readings were subtracted from 540 nm readings and a third order polynomial least squares fit was used to interpolate concentrations on Prism (GraphPad).

2.12 Multiplex cytokine assays

For electrochemiluminescence studies, a custom U-Plex assay from Meso Scale Discovery (MSD), designed to measure Granulocyte-macrophage colony-stimulating factor (GM-CSF), IFN-β, IL-1β, IL-6, IL-8, IL-10, Monocyte chemoattractant protein 1 (MCP-1), Macrophage inflammatory protein-1α (MIP-1α), TNF-α and MIP-1β, was used to identify levels of these cytokine and chemokines in the supernatant of infected and non-infected THP-1 cells collected at 24 hrs post infection. MSD plates were analyzed on the MS2400 imager (MSD). Assay was performed according to the manufacturer's instructions with no dilution of THP-1 supernatants.

2.13 ROS detection

ROS detection was carried out with uninfected cells cultured on RS glass or Permanox plastic chamber slides (Nunc LabTek). Chemical hydrolysis of 2′,7′-Dichlorofluorescin diacetate was performed to acquire a final DCF-DA reagent yield of 50 μM. Briefly, 0.5 ml of 5 mM DCF (2,7-dichlorofluorescein) dissolved in 100% ethanol, was reacted with 2 ml of 0.1 N NaOH at room temperature for 30 min. The reaction was stopped using 7.5mL 10X PBS. THP-1 cells were washed with PBS followed by incubation with 20 μM DCF-DA for 30 mins. Cells were washed again then viewed under Leica DMi8 fluorescence microscope. Image quantification was carried out with Image J and normalised by cell number. A total of 34 images were quantified from 2 independent experiments.

2.14 Whole blood killing assay

Overnight *S. aureus* cultures were refreshed in TSB and grown to OD_{600} 1.5 as described in section 2.2. Cultures were pelleted and resuspended in PBS to achieve 2.5 x 10^8 CFU/mL. Samples of 1 mL fresh heparinised blood from a total of 6 wildtype ICR CD1 mice (over two separate days) were each split into 150 µL aliquots in Eppendorfs. 10 µL of bacterial inoculum was added to each aliquot of blood and incubated at 37°C rotating for 2 hr or 4 hrs. Inoculum achieved was approximately 2.5 x 10^6 CFU/mL. Blood was then serially diluted in PBS and plated on TSB agar, incubated overnight at 37°C and CFU/mL was calculated.

2.15 Murine skin abscess model

All animal procedures were evaluated by the Animal Welfare and Ethical Review Board of the University of Warwick (AWERB) and carried out in strict accordance with the Animals (1986) Scientific Procedures Act of the UK under the authority of Licence PCEC27E7D. Overnight cultures of *S. aureus* strains were refreshed with TSB and grown to OD_{600} 1.5 at 37°C shaking. Staphylococci were centrifuged, washed twice, and diluted in PBS to achieve a low dose of 1-2 x 10^7 or a high dose of 2.3-2.7 x 10^8 CFU/mL. Infection groups of 10 or 5 female 7-week-old BALB/c mice (Charles River Laboratories, UK) were injected on each flank with 50 µl of bacterial suspension (total of 1-2 x 10^6 for low dose or 2.3-2.7 x 10^7 CFU per mouse for high dose infections). On day 1 or 4 of the infection mice were euthanized by compressed CO_2 inhalation. Skin abscesses/skin at site of infection were removed along with the spleen and the left lobe of the liver. The left abscess, half the spleen and half the liver lobe of each mouse were homogenized in PBS using FastPrep-24 5G instrument (MP Biomedicals, USA), 4 m/s for 2 mins. Homogenates were diluted and plated on TSB agar for triplicate determination of CFU. For histology, right flank skin abscesses were fixed in 4% PFA.

2.16 Mouse tissue staining and immunohistochemistry

Mouse skin abscesses fixed in 4% PFA were sent to University of Manchester Core Histology Facility where they were paraffin embedded and sectioned at 5μm intervals. A selection of sections were stained with Hematoxylin and eosin (H&E) and digital scans were obtained. Other slices underwent immunohistochemical analysis for the detection of macrophages. Briefly, tissue sections were deparaffinated in xylene, 2 incubations 5 mins each, followed by rehydration using an ethanol gradient (absolute, 95%, 80%, 70%), 20 seconds each. Sections were washed in dH_2O and antigen retrieval was achieved by incubation with trypsin (VWR Life Science) at 37 °C in a humidified chamber. Sections were washed 2x in TBST for 5 mins then blocked with 5% Normal Goat serum (NGS) for 1 hour at room temp. Slices were incubated with rabbit anti-F4/80 primary antibody (Cell Signaling) diluted 1:600 in 5% NGS (Cell Signaling) overnight at 4°C. The following day slices were washed in TBS and incubated with goat anti rabbit alexa 488-conjugated secondary antibody (Thermofisher) at 1:500 in 5% NGS for 1 hr at room temperature. Slices were washed in TBST with slight agitation then viewed under Leica DMi8 fluorescent widefield microscope.

2.17 Photolithography for microfluidics

Master moulds of microfluidic devices were fabricated using photolithography during which SU-8 photoresist is deposited on a 4-inch round silicon wafer in shape of the microfluidic design. This creates a positive mould that can be used time and time again. As the channel design involves two main channels of one height and many interlinking channels at a smaller height, the photoresist was deposited in two layers. First the connecting channels layer is created. Photoresist (SU- 8 2025) was spin coated at 1000 rpm on the wafer to make a layer with height approximately 10 μm. The wafer is pre-baked for 2 minutes at 95 °C before the acetate sheet with printed microfluidic design was placed onto the wafer and exposed to UV light for 7 seconds. The acetate sheet was removed and the wafer underwent a post-bake at 95 °C for 2 mins.

A second coat of photoresist (SU-8 2035) to create the main channels was then spin coated at 2000 rpm on top to create a layer with height approximately 70 μm. The wafer was pre-baked at 95 °C for 7 mins. The acetate sheet with printed designs was carefully aligned with the previous layer of photoresist using a mask aligner (MJB3, Karl Suss), then exposed to UV light for 11 seconds before post-baking at 95 °C for 7 mins. Finally, the mask was developed with 2-methoxy-1 methylethyl acetate (MicroChem and a profilometer (Xp100 Stylus Surface Profiler, Ambios) was utilized to determine the height of the photoresist pattern deposited onto the silicon wafer.

2.18 Soft lithography for microfluidics

During Soft lithography Polydimethylsiloxane (PDMS) is poured onto the microfluidic master mould in order to create a negative replica, i.e. the channels appear to be etched into the PDMS. To do this a mixture of PDMS prepolymer and cross linker at a ratio of 9:1 was placed in a vacuum chamber to ensure all bubbles were removed. The PDMS mixture is then poured over the silicon master wafer to create a layer around 1 cm in thickness. The wafer is left to cure on a hot plate for 4 hours at 70 °C. Once set each individual PDMS microfluidic chip was cut out using a scalpel and fluid inlets and outlets were created using 1 mm biopsy punches. Assembly of the microfluidic device required a glass coverslip (24 x 60 mm^2), both coverslip and PDMS chip surfaces were irreversibly bonded by oxygen plasma treatment. The bond was reinforced by leaving the device on a hotplate at 95 °C for 10 minutes. Fluidic connections were established using microfluidic needles and 0.51 mm internal diameter polyethylene tubing (Tygon ND 100-80).

2.19 Microfluidic circuit and resistance determination

The microfluidic circuit consisted of an OB1 microfluidic pressure pump (Elveflow) connected to a reservoir bottle of DMEM + 1% FBS, tubing from the reservoir is connected to a microfluidic serpentine resistance chip followed by a

3-way Leuer valve that connects to the airway-blood vessel chip. All components were UV sterilized prior to use. The microfluidic circuit minus airway-blood vessel chip were primed with DMEM media using the microfluidic pump. When the circuit appears to have no bubbles and the flow is stable the airway-blood vessel interface device was added via the 3- valve. A liquid-to-liquid connection between tubing or valve and tubing was always made to minimise bubble formation.

To determine microfluidic circuit resistance with and without the serpentine resistor chip, the pressure (mbar) driven by the microfluidic pressure pump (Elveflow) was set to increase over 1 min until it reached the maximum pressure achievable. The corresponding increase in flow (µl/min) was recorded with a flow rate sensor (Elvelflow). This was repeated 3 times. For each replicate the pressure was plotted against flow rate and the gradient of each line, and therefore the resistance, was determined with Prism (Graphpad).

2.20 Measuring velocity profiles in the vertical plane

To prepare airway-blood vessel-on-a-chip channels for use with colloids, 0.15% BSA was syringed into the tubing and channels, left for 30 minutes then gently flushed through with distilled water. A concentration of 0.02% Fluoresbrite Carboxylate 1 µm Microsphere colloids (Polysciences Inc) in water were pumped the lung-on-a-chip at pressures 40 mbar and 20 mbar generated by the OB1 MK3 microfluidic pressure pump (Elveflow). An area in the centre of the width (y) and length (x) of the main channels was chosen to take short movies. Colloids travelling in the x direction of the channel over 11 different heights (z) were recorded using fluorescent imaging techniques with a Leica DMi8 microscope. The velocity of each colloid in the interrogation field was determined by using the well-established TrackMate ImageJ plugin (v. 3.5.3) for single particle tracking (Tinevez et al., 2017). When using TrackMate each colloid or "spot" is segmented in multiple frames and its trajectory or "track" is reconstructed by assigning it an identity over these frames. The link velocity (or velocity) is defined for a single

link between two spots (distance between the two spots divided by the time difference). The mean of the link velocity over all the links of one track I calculated. At least n=15 tracks were analysed for each height.

2.21 Microfluidic channel coating and cell seeding

Directly after microfluidic channel fabrication, channels were flushed with PBS followed by air and sterilized by exposure to UV light for 30 minutes. Channels were coated with 50 μg/mL human fibronectin (Sigma-Aldrich) and left at 37°C for 1 hr. Any unbound protein is removed with a PBS wash. Both A549 and HUVEC cell lines were routinely cultured in flasks until ~ 90 % confluent (as described in section 2.4). Cells were trypsinized (VWR Life Sciences), collected and re- suspended in DMEM before being seeded into the microfluidic channel at a density of 5 x 10^5. To seed the cells 1mL of cell containing media was syringed into the inlets of the channels via microfluidic needles and tubing. Any bubbles are then removed by pressurizing. To pressurize, sterile unfolded paperclips were inserted into the holes while the inlets remain attached to tubing and syringes blocked the channel outlets. More cell containing media mix was then pushed into the channels via syringe until resistance is felt. The syringes were pushed further every couple of minutes until the syringe will move no further. The device was then incubated overnight at 37°C and 5% CO_2 with syringes attached for cells to adhere.

2.22 Invasion assay in microfluidic chip

Bacteria were cultured as described in section 2.2. OD_{600} 1.5 cultures were diluted to achieve 2.5 x 10^6 CFU/mL in DMEM. 500 μL bacteria were syringed into the primed microfluidic circuit via a 3-way valve. Bacterial interactions with the airway-blood vessel interface were viewed under a DMi8 widefield microscope (Leica) in static conditions and time-lapse images were acquired.

2.23 Statistical analysis

All data were analysed using GraphPad Prism (MacOS version8.4.2). Pairwise statistical analysis was carried out by Man-Whitney U test and all other data were analysed using ANOVA and post-hoc Tukey's HSD tests where necessary or Kruskal-Wallis where specified in the text.

3 Chapter 3: The role of the *S. aureus* T7SS in macrophage infections

3.1 Introduction

The majority of experimental studies on the staphylococcal T7SS have focused on the molecular makeup of the secretion apparatus, genetic diversity, secreted components and structural interactions of associated proteins (Ahmed et al., 2018; Anderson et al., 2011, 2013; Jäger et al., 2016; Kneuper et al., 2014; Martin Zoltner et al., 2013). *In vitro* and *in vivo* studies have identified a toxin substrate of the staphylococcus T7SS that mediates intraspecies competition (Cao et al., 2016; Ulhuq et al., 2020). Importantly, *In vivo* studies have reviewed the impact of removing T7SS proteins on infection outcomes in mouse models, which has led to the identification of the staphylococcal T7SS as a virulence factor with immunogenicity characteristics (Anderson et al., 2011, 2017; Burts et al., 2005, 2008; Dai et al., 2017; Kneuper et al., 2014; Torre et al., 2015; Y. Wang et al., 2016; Zhang et al., 2015). Only three previous studies have focused on effects of the T7SS on hosts at a cellular level, consequently its molecular function during infection is still largely unclear (Cruciani et al., 2017; Dai et al., 2017; Korea et al., 2014).

At a host cell level the staphylococcal T7SS effector proteins (EsxA, EsxB or EsxX) have been implicated in the regulation of host cell death in epithelial cells, dendritic cells or neutrophils (Cruciani et al., 2017; Korea et al., 2014). Thus far, the impact of the *S. aureus* T7SS has not been studied in the context of intracellular macrophage infection, even though macrophages have been identified to be crucial for the defence against *S. aureus* (Pidwill et al., 2021). The contribution of macrophages to the uptake and clearance of *S. aureus* during the initial stages of infection in mice has earned them the label "gatekeepers" of infection (Boldock et al., 2018; McVicker et al., 2014; Pidwill et al., 2021; Pollitt et al., 2018). In response to this, *S. aureus* has evolved multiple mechanisms to survive within, manipulate and escape from macrophages (Pidwill et al., 2021). A

key area of investigation is the effect of *S. aureus* on the induction of programmed cell death pathways apoptosis, pyroptosis and necroptosis in macrophages (Missiakas & Winstel, 2021). Studying *S. aureus* induced activation of cell death pathways is vitally important to understanding infection dynamics because the kind of cell death that occurs is often attributed to the inflammatory nature of infection and ability for hosts to clear bacteria (Jorgensen et al., 2017; Kitur et al., 2016; Missiakas & Winstel, 2021).

In this chapter the effect of the staphylococcal T7SS on macrophage cell responses is assessed, with a focus on host cell death. Time-lapse microscopy along with other methods are utilised to examine morphologies and cell death pathway activation of individual macrophages in response to intracellular *S. aureus* WT JE2 and isogenic T7SS deletion mutant infections. The use of time-lapse microscopy offers invaluable data on these dynamic infections at both a single cell and population level resolution, which can be used in addition to traditional cell death analyses to provide a comprehensive overview of the effect of the T7SS.

3.2 Results

3.2.1 Construction of staphylococcal T7SS mutants

Investigations into the *S. aureus* T7SS on macrophage responses was carried out with the use of isogenic mutants lacking either a single T7SS secretion substrate, EsxC, multiple secretion substrates, EsxC, EsxB, EsaE and EsxD (EsxC-D), or the ATPase driving T7SS protein export, EssC, in the USA300 JE2 background. Δ*esxC* and Δ*essC* mutants were created previously in our lab (Kengmo Tchoupa et al., 2020) by allelic replacement as previously described (Bae & Schneewind, 2006). The Δ*esxC-D* mutant was generated during this project using the same technique, as described in Methods section 2.1, then confirmed by PCR and further confirmed by Sanger sequencing carried out by Arnaud Kengmo Tchoupa. The *S. aureus* T7SS mutants used in this project are detailed in Figure 3.1.
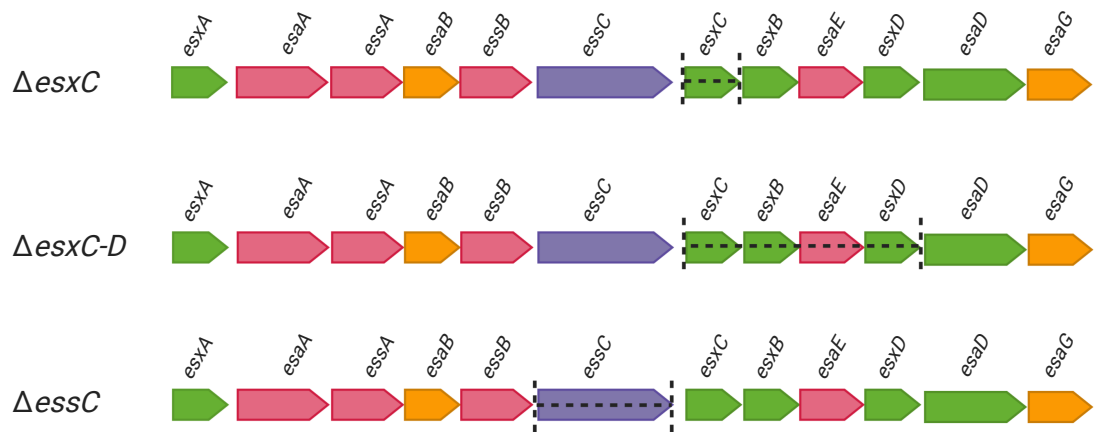
Figure 3.1: T7SS mutants in USA300 JE2 background.

Diagram shows the *ess* locus of deletion mutants *esx*C, Δ*esxC-D* and Δ*essC* in the USA300 JE2 *S. aureus* background. Δ*esx*C-D was generated during this project by allelic replacement. Locus is coloured according to the following categories: membrane-associated proteins (pink), FtsK/SpoIII ATPase (purple), secreted substrates (green), cytoplasmic proteins (orange).

3.2.2 Deletions of T7SS proteins does not impact *S. aureus* growth rate or haemolysis activity

The growth rate of *S. aureus* JE2 WT, *ΔesxC*, *ΔessC* and *ΔesxC-D* strains was measured in order to determine if the deletions had an effect on bacterial replication. Figure 3.2A shows the growth of *S. aureus* strains in TSB and RPMI cell culture media over a 9-hour period. WT and T7SS mutant strains did not differ in growth rate in either growth medium. Haemolysis activity was also assessed as an indicator for secretion of membrane damaging toxins that cause lysis of red blood cells. Figure 3.2B shows percentage of sheep blood cell lysis when incubated with filtered supernatants of exponential and stationary phase *S. aureus* cultures. Results suggest no differences in cytolysis effect between WT and T7SS mutant strains.

3.2.3 *S. aureus* is internalised by macrophages and uptake is not impacted by the T7SS.

To investigate the effect of the T7SS on *S. aureus* uptake by macrophages, a conventional antibiotic protection assay was employed (Easmon et al., 1978). THP-1 macrophages were incubated with *S. aureus* for 2 hrs followed by a 30 min treatment with lysostaphin and gentamicin then PBS washes, which successfully removed all extracellular bacteria, as confirmed by confocal microscopy. The quantification of viable intracellular bacteria was carried out by THP-1 lysis and CFU counting. Previous reports have suggested that macrophage-*S. aureus* interactions are dependent on MOI (Jubrail et al., 2016), therefore 3 different MOIs (2:1, 5:1 and 10:1) were used in macrophage bacterial challenges, but this did not show differences between WT and mutant infections (Figure 3.3A). In addition, similar uptake of WT and mutant *S. aureus* was observed when using RPMI with 1% FBS (instead of 10%), THP-1 monocytes lacking PMA activation, or macrophages pre-treated with PMA then IFN-γ, a potent macrophage activating cytokine which has been associated with increasing the ability for cells to phagocytose and kill intracellular *S. aureus* (Jubrail et al., 2016; Kubica et al., 2008) Figure 3.3B.

A

B
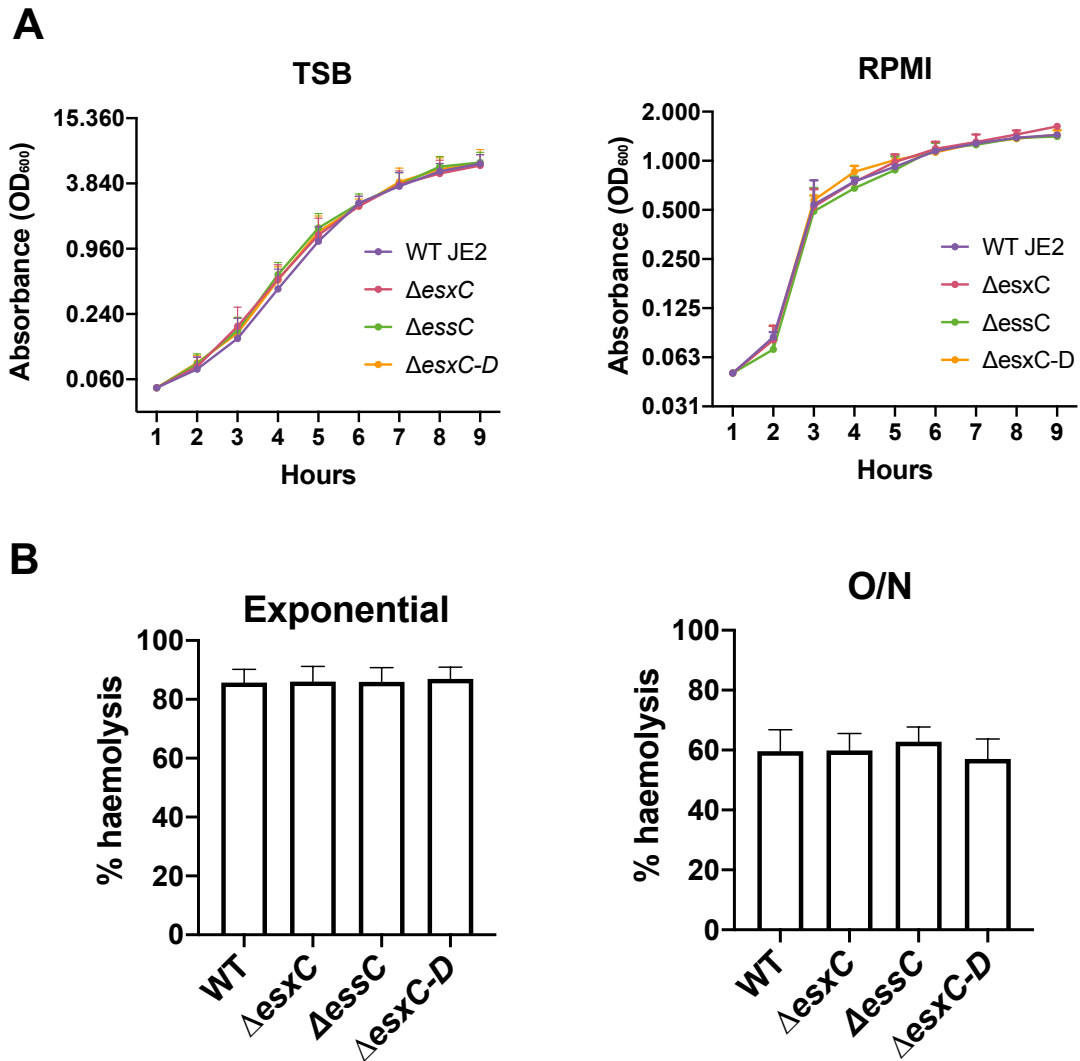
Figure 3.2: Growth rate and haemolysis activity of JE2 WT and T7SS mutant strains.

(A) Optical density (OD_{600}) readings of WT and mutant strains grown in TSB or RPMI shaking at 37°C were taken every hour; mean $\pm$ SD plotted on $\log_2$ graph, n=3. (B) Haemolysis caused by WT and T7SS strains when exponential culture supernatants or overnight (O/N) culture supernatants were incubated with sheep blood for 1 hr. % haemolysis was calculated from absorbance of blood with no treatment controls. Graphs show mean $\pm$ SD, n=3. Kruskal-Wallis shows no significant effect of genotype on homolysis of exponential (H_4 = 2.837 P= 0.417) or O/N (H_4= 7.707 P= 0.053) cultures.
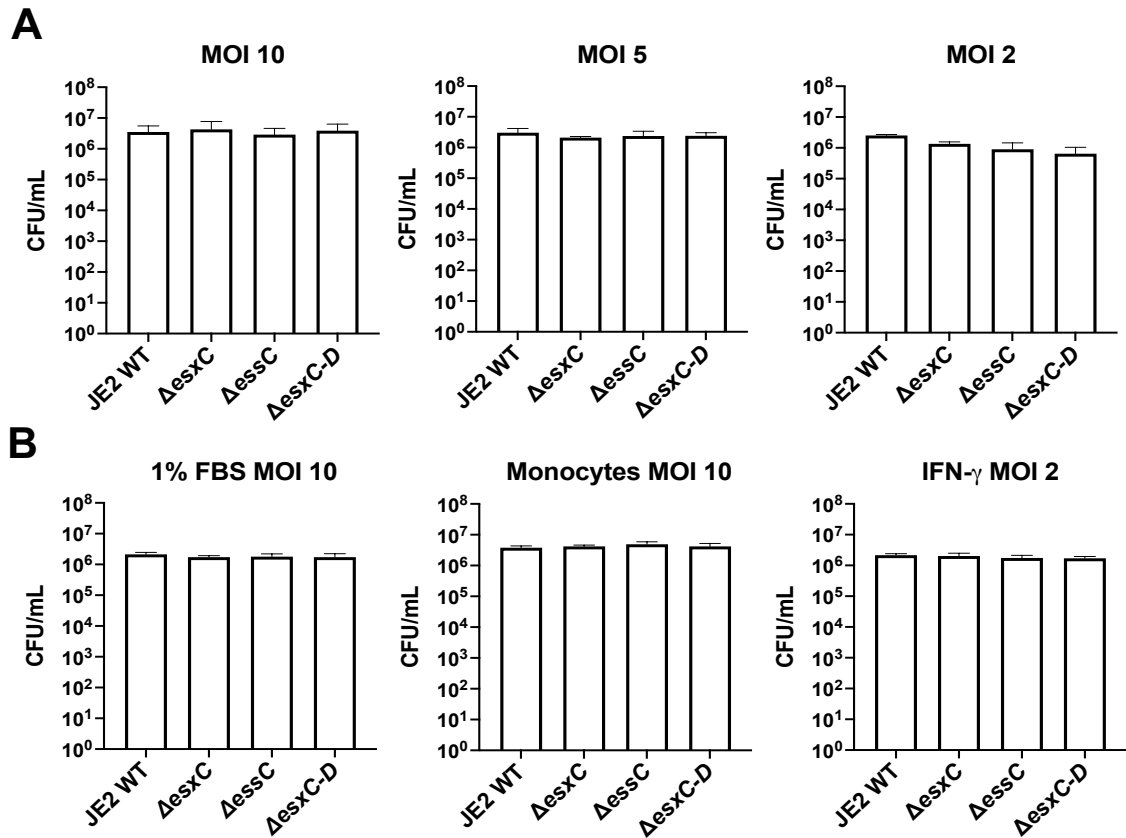
Figure 3.3: Macrophage internalisation of *S. aureus* WT and T7SS mutants. Invasion assays were carried out by incubating THP-1 cells with WT JE2 or Δ*esxC*, Δ*essC* or Δ*esxC-D* isogenic mutant strains for 2hrs, extracellular bacteria were killed, and THP-1 cells lysed for intracellular bacteria quantification by CFU counting. (A) Intracellular bacterial counts with three different multiplicity of infections (MOIs) bacteria:macrophages, 10:1, 5:1 and 2:1. (B) Intracellular bacterial counts collected with the following modifications to invasion assays: THP-1 macrophages with RPMI containing 1% FBS MOI 10, THP-1 monocytes without PMA treatment at MOI 10; THP-1 cells with PMA plus IFN-γ activation at MOI 2. All graphs show mean $\pm$ SD, at least *n*=3. One-way ANOVA showed no significant effect of genotype.

Infected THP-1 macrophages were studied in parallel using confocal microscopy, to confirm CFU data and assess percentage of cells infected. Figure 3.4A shows confocal images of THP-1 cells after 2 hours incubation with WT and T7SS mutants. In all cases macrophages appeared stretched out with spindle or fried egg morphologies and nuclei appeared similar to those of uninfected cells. No specific trends were observed in bacterial location inside macrophages. The number of infected cells was quantified and is presented as a percentage of total cells present in each field of view in Figure 3.4B. Percentages of cells infected were very high (88.5-91%) and similar between WT and mutants. Overall, this suggests no role of the T7SS in macrophage uptake of *S. aureus.*

3.2.4 The staphylococcal T7SS has no effect on bacterial persistence in macrophages

To investigate the effect of the T7SS on staphylococcal resistance to killing by THP-1 macrophages, the antibiotic protection assay was extended to further timepoints. After 2 hours of incubation with WT and T7SS mutants, extracellular bacteria were killed with gentamicin and lysostaphin, THP-1 cells were extensively washed and incubated for 6 or 24 hrs with RPMI medium containing a low concentration of lysostaphin. This stops extracellular replication of bacteria that have escaped from infected cells. Figure 3.5 shows viable intracellular bacterial counts from THP-1 macrophages lysed at 2 hrs, 6 hrs and 24 hrs post infection with a selection of MOIs and conditions as previously stated in section 3.2.3. In all cases viable intracellular bacteria numbers decreased over 24 hours, suggesting either macrophages killed a proportion of the intracellular *S. aureus* or bacteria escaped from macrophages over time, but no significant differences were seen when comparing CFU/mL between genotype and interactions between genotype *time.

Figure 3.4: THP-1 macrophages infected with *S. aureus* strains 2 hrs post infection.

(A) Representative confocal microscope images of uninfected macrophages and macrophages after incubation with *S. aureus* JE2 WT or isogenic T7SS mutant strains for 2 hrs followed by fixation with PFA. Intracellular bacteria were stained with vancomycin-BODIPY, shown in green, macrophage actin stained with phalloidin, shown in red, and nuclei stained with DAPI, shown in blue. (B) Number of THP-1 cells infected as a percentage of total cells in the field of view. mean $\pm$ SD is shown. Images were collected from 48 different fields of view from 3 independent experiments. ANOVA showed no significant effect of genotype ($F_{3,12}$=0.998 *P*=4.27).
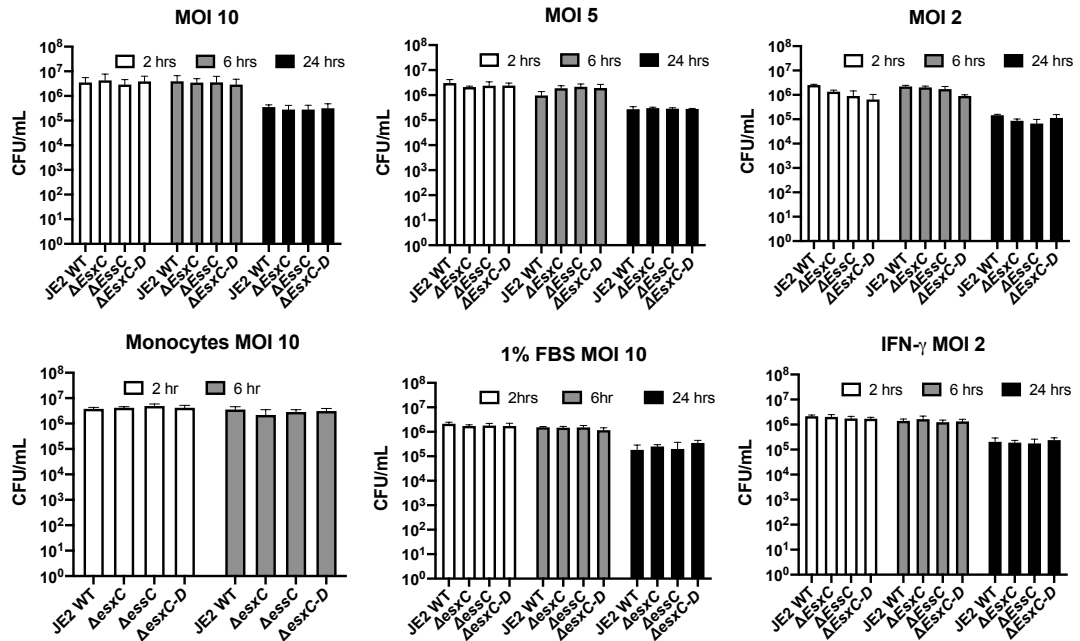
Figure 3.5: Intracellular persistence of *S. aureus* WT and T7SS mutants.

S. aureus challenges were carried out by incubating THP-1 cells with JE2 WT or Δ*esxC*, Δ*essC* or Δ*esxC-D* mutant strains for 2hrs. Extracellular bacteria were killed followed by PBS washes and incubation with RPMI media + 5 ug/ml lysostaphin. Cells were lysed at indicated timepoints for intracellular bacterial quantification by CFU counts. Graphs show intracellular bacterial counts with three different multiplicity of infections (MOIs), 10:1, 5:1 and 2:1 (bacteria:macrophages). Intracellular bacterial counts were also collected with the following modifications to invasion assays: THP-1 monocytes without PMA treatment at MOI 10; THP-1 cells with PMA plus IFN-γ activation at MOI 2 and THP-1 cells with RPMI containing 1% FBS instead of the standard 10% at MOI 10. All graphs show mean $\pm$ SD. *n*=3, data were analysed by two-way ANOVA for differences between genotype and time and interactions between genotype*time. Genotype had no significant effect on CFU/mL in all conditions (MOI 10 ($F_{3,87}$= 0.417 *P*=0.852), MOI 5 ($F_{3,24}$= 0.101 *P*=0.901), MOI 2 ($F_{3,24}$= 2.367 *P*=0.080), monocytes ($F_{3,16}$= 0.639 *P*=0.600), 1% FBS ($F_{6,24}$= 0.804 *P*=0.5038), IFN-γ ($F_{3,50}$= 2.388 *P*=0.080)). CFU/mL did vary significantly between time points in all cases but no significant interaction between genotype and time was found (MOI 10 ($F_{6,87}$=

0.417 P=0.866) MOI 5 ($F_{6,24}$= 1.793 P=0.1431) MOI 2 ($F_{6,24}$= 0.700 P=0.578), monocytes ($F_{3,16}$= 1.329 P=0.299), 1% FBS ($F_{2,24}$= 1.009 P-0.443) IFN- γ ($F_{6,50}$= 1.109 P=0.371)).

3.2.5 T7SS has an impact on macrophage morphology and cell number during intracellular infection

S. aureus infection of macrophages were visualised with confocal microscopy 24 hrs post infection. A large proportion of macrophages infected with WT appeared rounded with actin rearrangement and in some cases a condensed, degraded nucleus as compared to the uninfected control (Figure 3.6A). In contrast, the vast majority of T7SS mutant infected macrophages remained as spindle or fried egg morphologies. WT-infected cell morphology appeared similar to the uninfected THP-1 cells treated with staurosporine, a well-known inducer of caspase-dependent and independent cell death (Belmokhtar et al., 2001). Figure 3.6B shows macrophage count (per field of view) normalised to the average number of macrophages present in control uninfected wells. A striking difference was shown in number of macrophages remaining on the slide after 24 hours in the WT infections compared to all T7SS mutant infections. This could suggest increased cell death followed by either detachment due to washing during staining and/or clearance of WT infected macrophages via efferocytosis. Despite the difference in cell numbers, no difference in the percentage of macrophages with intracellular bacteria was observed at 24 hrs post infection (Figure 3.6C).

As microscopic analysis suggested a possible role for T7SS in promoting macrophage cell death, traditional cell death quantification assays were employed in an attempt to capture these differences. Lactose dehydrogenase (LDH) release assays and propidium iodide (PI) uptake assays both quantify cell death as a function of cell membrane integrity. Figure 3.7 shows quantification of cell cytotoxicity by both LDH release and PI uptake. At 8 and 24 hrs WT induced LDH release appeared slightly higher than all three T7SS mutant infections, however, this was not significant. PI assays also showed no significant differences in membrane damage induced by WT and T7SS mutants.
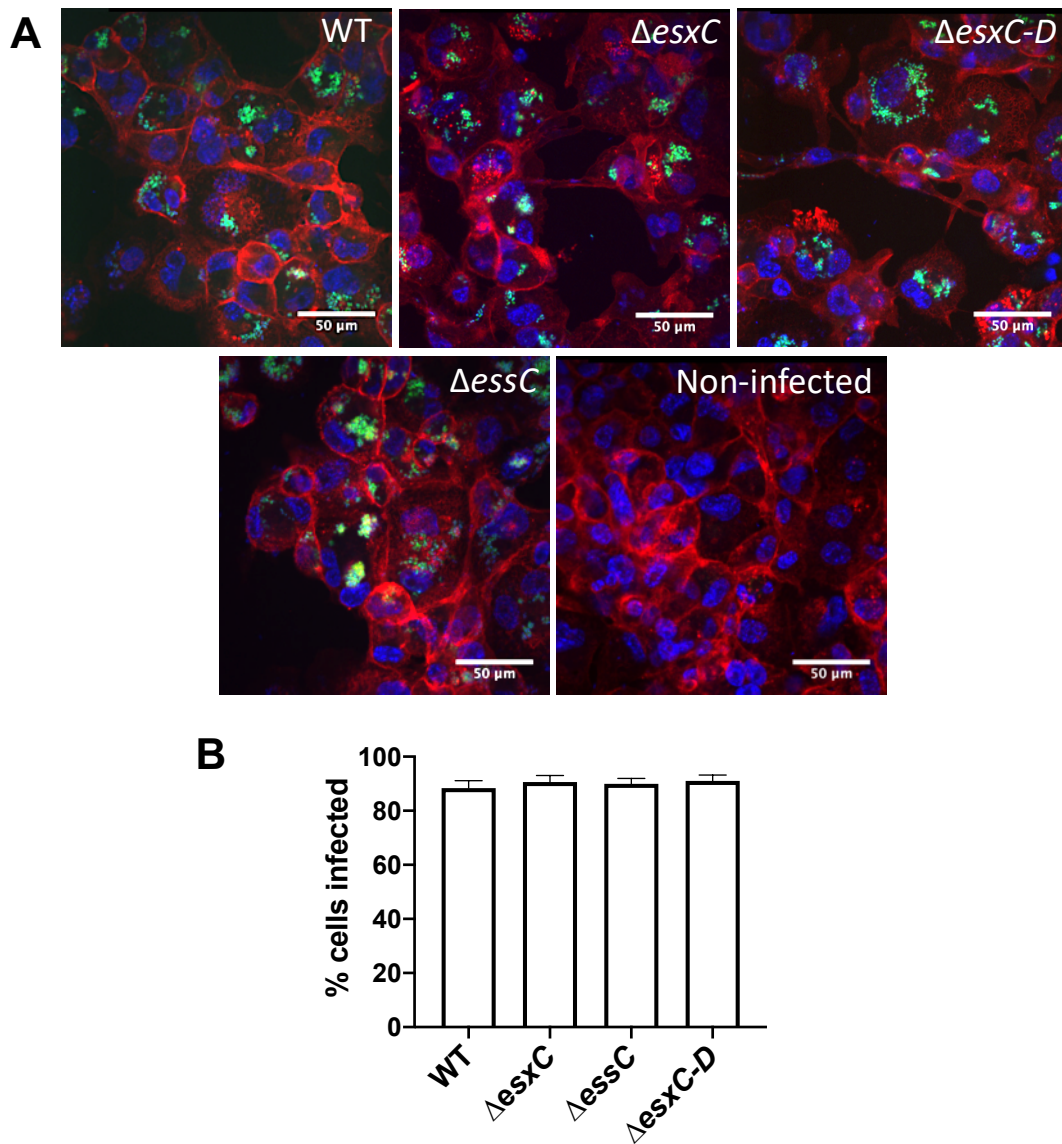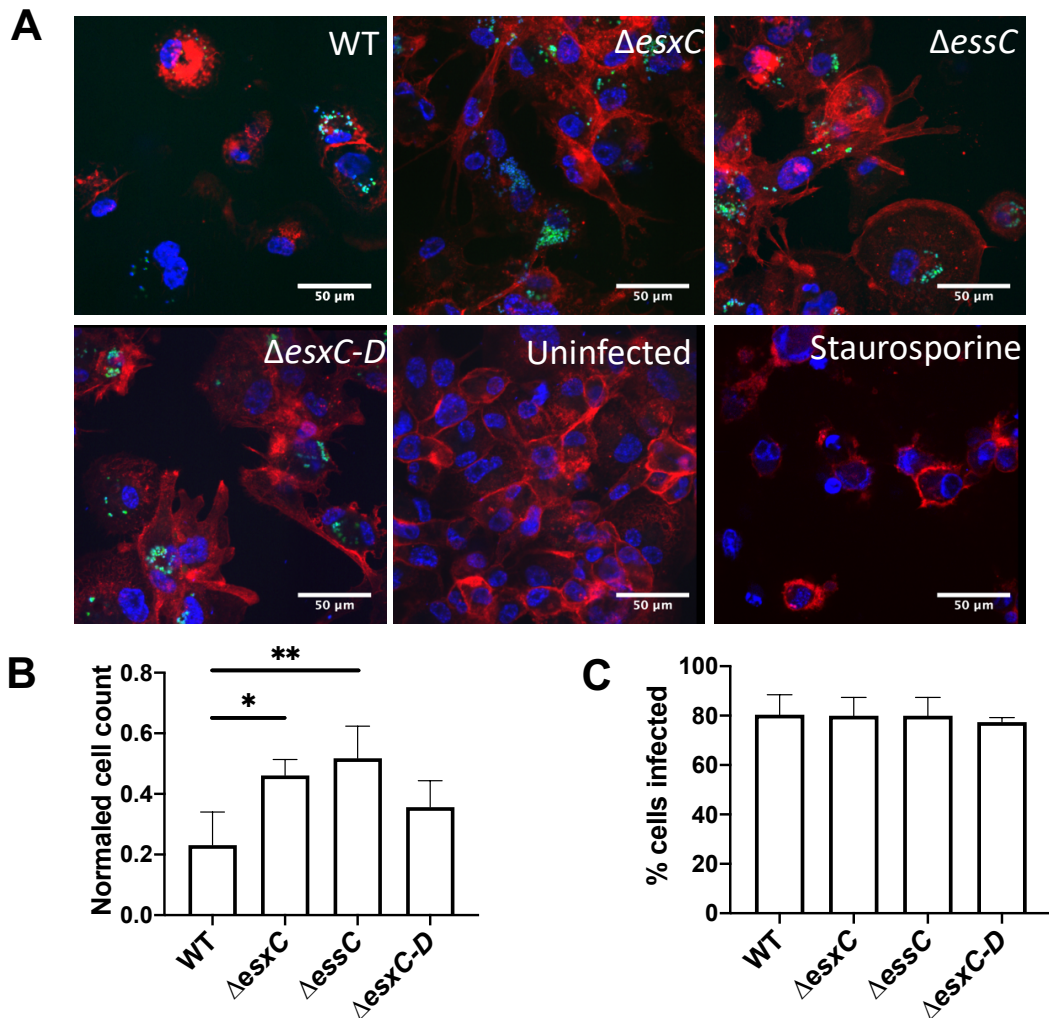
Figure 3.6: THP-1 Macrophages infected with *S. aureus* strains 24 hours post infection.

(A) Confocal microscope images of uninfected macrophages, and macrophages after incubation with *S. aureus* JE2 WT or T7SS mutant strains 24 hrs post infection. Images of uninfected cells treated with staurosporine, a potent inducer of cell death, are also shown. Intracellular bacteria were stained with vancomycin-BODIPY (green), macrophage actin stained with phalloidin (red) and macrophage nuclei stained with DAPI (blue). (B) THP-1 macrophage cell counts per image at 24hrs normalised by the average cell counts of uninfected cells per image. Images collected from 48 different images from 3 independent experiments, mean $\pm$ SD is shown. One-way ANOVA ($F_{3,12}$=7.553 *P*=0.0042) and Tukey's multiple comparisons test showed significant differences between WT and Δ*essC* **P*=0.004 and WT and ΔesxC* *P*=0.0184. (C) Number of THP-1 cells infected as a percentage of total cells in the microscope image. One-way ANOVA showed no significant differences ($F_{3,12}$=0.165 *P*=0.918)
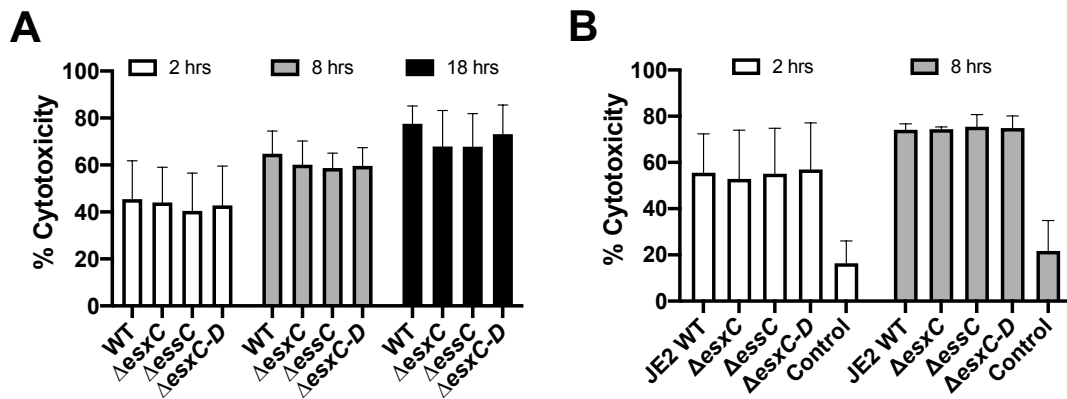
Figure 3.7: Cytotoxicity of macrophages infected with WT and T7SS mutants.

Invasion assays were carried out by incubating THP-1 cells with JE2 WT or isogenic $\Delta esxC$, $\Delta essC$ or $\Delta esxC\text{-}D$ mutant strains for 2hrs. Extracellular bacteria were then killed, THP-1 cells washed and refreshed with RPMI media + lysostaphin. (A) At indicated timepoints supernatant from infected THP-1 cells, uninfected THP-1 cells and lysed uninfected THP-1 cells were collected for quantification of lactose dehydrogenase (LDH) via a colorimetric assay. Percentage cytotoxicity was calculated from LDH release from lysed cells as detailed in Methods section 2.9. Two-way ANOVA showed no significant differences in cytotoxicity between strains ($F_{3,28}$=0.479 P=0.696), a significant difference between cytotoxicity over time ($F_{2,28}$=16.290 P<0.0001), but no significant interaction between strain and time ($F_{6,28}$=0.072 P=0.998). (B) Propidium iodide (PI) in PBS was incubated with infected THP-1 cells for 15 mins at stated timepoints. Cells were washed then fluorescence was measured at 600nm, % cytotoxicity was calculated from PI readings of lysed cells. Two-way ANOVA showed no significant differences in cytotoxicity between strains ($F_{3,16}$=0.029 P=0.993), a significant difference between cytotoxicity over time ($F_{1,16}$=11.600 P=0.0036), but no significant interaction between strain and time ($F_{3,16}$=0.021 P=0.996). All graphs show mean $\pm$ SD, n=3.

3.2.6 Macrophages infected with *S. aureus* are associated with heterogeneous cell morphologies and death-associated outcomes

Time-lapse microscopy of infections was chosen to clarify the effect of the T7SS on cell death and single cell responses to infection can be analysed in great detail over time. Bacterial challenges were carried out with YFP expressing *S. aureus* and THP-1 cells in plastic chamber slides. Time-lapses were recorded with an image taken every 10 mins over a 24-hr period. Initially assays were carried out with 1 hr bacterial challenge, followed by lysostaphin and gentamicin treatment, then incubation with antibiotic free media under the microscope. This enabled investigation into *S. aureus* escape. Later, the impact of altering culture conditions, including sustained lysostaphin treatment and macrophage culture on glass-based slides, instead of plastic, was evaluated and led to striking findings regarding infection dynamics.

When inside macrophages *S. aureus* is known to invoke multiple host inflammatory and cell death pathways (Kitur et al., 2015, 2016) and while induction of these pathways have been extensively studied, the downstream effect on cellular outcomes and bacterial fates are less well defined. It was clear from time-lapse microscopy that over 24-hrs individual JE2 WT infected THP-1 macrophages adopted different morphologies. Some macrophages took on a large spindle morphology with an elongated body and cytoplasmic extensions on their apical ends (Figure 3.8A). Other macrophages appeared as a fried egg or amoeboid shape with roundish cell bodies and often with numerous small cytoplasmic extensions (Figure 3.8B). Both of these morphologies are associated with activated states known as "M1" inflammatory or "M2" wound healing macrophages (Heinrich et al., 2017; McWhorter et al., 2013; Ploeger et al., 2013). A proportion of macrophages were very round in shape (Figure 3.8C), which can be attributed to both a "naïve" M0 macrophage state or the early stages of cell death (Heinrich et al., 2017; Taabazuing et al., 2017).

Throughout the 24-hr time-lapse macrophages underwent outcomes associated with cell death, during which cells demonstrated a loss in their ability to form membrane ruffles leaving a totally immobilized corpse or cell debris. Some underwent shrinking and blebbing then partitioned into membrane-bound bodies (Figure 3.8D), demonstrating the hallmarks of apoptosis as shown before with macrophages and *S. aureus* in live-microscopy (R. S. Flannagan et al., 2016). A much larger proportion of cells rapidly swelled to form a characteristically rounded immobilized corpse which is indicative of a pore-induced intracellular trap or PIT (Figure 3.8E). PITs are the result of inflammatory cell death such as pyroptosis or necroptosis and to our knowledge have not been directly associated with *S. aureus* before (Jorgensen, Zhang, et al., 2016; Jorgensen et al., 2017). Their formation causes a distinct change in cell mass distribution, as organelles dramatically condense and collect at one side of the cell during membrane swelling (Jorgensen, Zhang, et al., 2016). The PIT-like cell corpse remained adhered to the substratum often entrapping *S. aureus* within its semi-permeable membrane, at least for some time. *S. aureus* was able to rapidly replicate within the PIT-like structures then breach the PIT membrane to continue replication in the extracellular environment (Figure 3.8F). Some of these bacteria-filled PITs acted as the starting point for the formation of microcolonies, visible to the naked eye, which is discussed later.
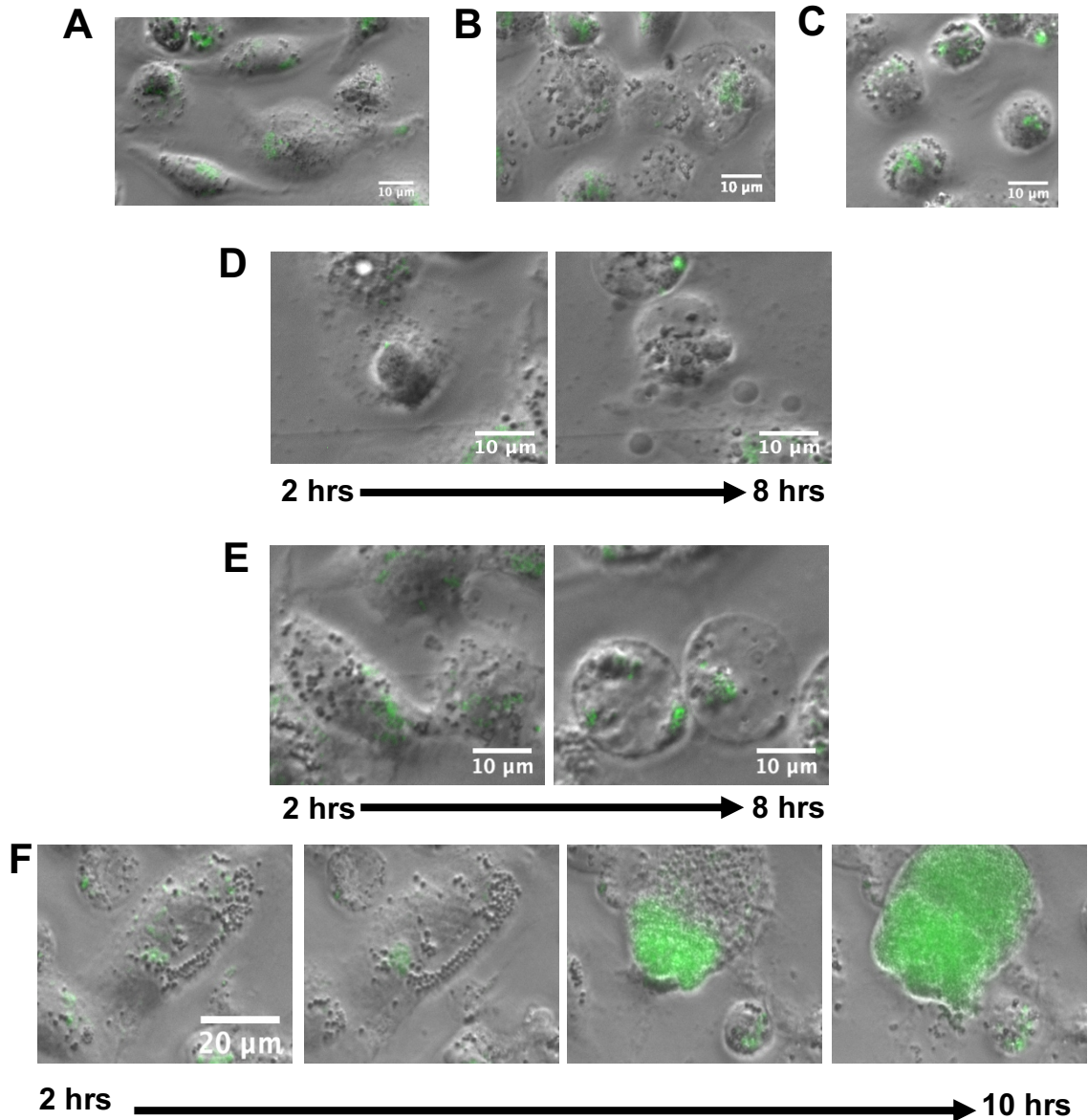
Figure 3.8: Morphologies of *S. aureus* WT infected macrophages.

Fluorescent microscope images of macrophages infected with YFP expressing WT *S. aureus* JE2 (green). Infected macrophages have heterogeneous morphologies such as (A) spindle shaped, (B) fried egg/pancake-like or (C) rounded. Infected macrophages also adopt cell death-associated morphologies over time including (D) cell shrinking with apoptotic-like bodies that detach from the cell and (E) the formation of classically round pore induced intracellular trap (PIT)-like structures. (F) Images show mass replication of *S. aureus* within a macrophage that adopts a PIT-like structure. By 10 hrs *S. aureus* escapes into the extracellular environment.

113

Figure 3.9A shows images of the typical heterogeneous population of macrophages observed during *S. aureus* WT infections and uninfected control experiments. The frequency of the different morphologies was quantified at different timepoints (Figure3.9B). By 6 hrs post infection the dominant proportion of infected macrophages (40.6 % $\pm$ 14.1%) had adopted a PIT-like structure which increased to 76.8% $\pm$ 20.2 by 10 hrs (Figure 3.9B), suggesting a significant number of macrophages were undergoing inflammatory cell death. A small percentage (7.7% $\pm$ 4.2%) were shrunken and apoptotic-like at 6 hrs and this only increased to (14.1 % $\pm$ 8.9%), suggesting apoptotic-like cell death was not a dominant form of death in this WT *S. aureus* infected THP-1 macrophage population. The rest of the infected macrophages were observed to be spindle/fried egg shaped (21.89 % $\pm$ 8.67 %) or rounded (29.9% $\pm$ 9.9) at 6 hrs but the presence of these morphologies decreased over time as cells took on PIT-like or apoptotic-like morphologies.

When time to cell death associated morphologies (PIT-like and apoptosis-like) for each cell are plotted over time in a violin plot, as shown in Figure 3.9C, an interesting multimodal distribution is observed. Individual cell death data is often represented in violin plots to asses population trends (Frenoy & Bonhoeffer, 2018; Gelles et al., 2019; Gelles & Chipuk, 2020). Multiple peaks could represent multiple waves of cell death with the earlier peaks likely caused by an intracellular stimulus whereas later cell death peaks could be the result of mass extracellular bacterial growth after bacterial escape, which usually occurred after 6 hrs.
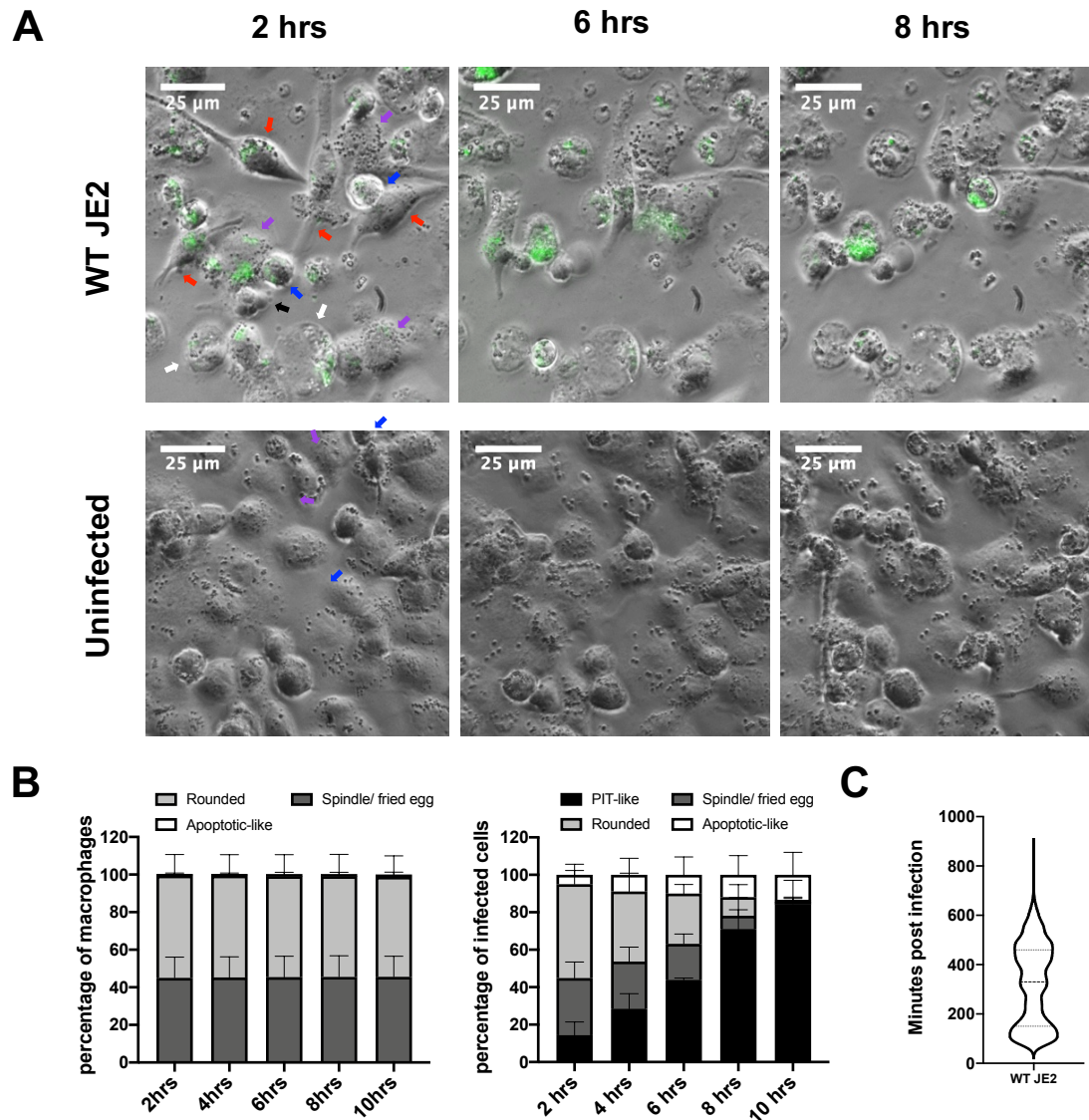
Figure 3.9: Macrophages infected with WT *S. aureus* are a heterogeneous population.

THP-1 macrophages were incubated with YFP expressing *S. aureus* JE2 WT at MOI 10:1 for 1 hr. Extracellular bacteria were killed with lysostaphin and gentamicin, then cells washed and refreshed with antibiotic-free medium. For time-lapse videos images were taken every 10 mins with a fluorescent widefield microscope. The morphologies of a total of 300 infected THP-1 macrophages were recorded over 3 indpendent time-lapse experiments. (A) Fluorescent widefield microscopy images of WT JE2 (green) infected or uninfected THP-1 macrophages at 2 hrs, 6 hrs or 8 hrs post infection. Arrows highlight examples of PIT-like (white),

apoptotic-like (black), rounded (blue), spindle (red) and fried egg (purple) morphologies at 2 hrs. (B) Macrophage morphology counts observed between 2 hrs and 10 hrs in either uninfected controls, shown as a percentage of total macrophages (left), or WT JE2 infected macrophages, shown as a percentage of total infected macrophages. Graphs show mean $\pm$SD, n=3. (C) Violin plot showing distribution of all macrophages that adopted a cell death-associated morphology (PIT-like or apoptosis-like structures) over the 24-hr time period. The median time of all experiments is represented as the middle horizontal dashed line with 75% and 25% quartiles above and below.

3.2.7 Staphylococcal T7SS proteins manipulate macrophage outcomes during infection

Comparative analyses of WT and T7SS mutant infections captured with time-lapse microscopy enabled the assessment of the effect of the staphylococcal T7SS on infected cell morphologies. Over 24 hrs 100% of WT or mutant infected cells assumed a PIT-like or apoptosis-like morphology, however Figure 3.10A shows the distribution of morphologies over 24-hrs was significantly modified in T7SS mutant infections. Comparisons showed a much larger proportion of WT infected macrophages take on an PIT-like or apoptosis-like morphologies ealry on in infection (between 2 hrs 30 and 7 hrs 40 mins), while these occur later in T7SS mutant infected macrophages. *S. aureus* Δ*essC* had the most significantly shifted spread of the bulk of data to between 7 hrs and 9 hrs 30 mins, which is clear in time-lapse images (Figure 3.10B).

Morphologies of cells were also recorded at discrete timepoints (Figure 3.10C). Levels of PITs observed at 4 and 6 hrs were higher in WT than Δ*essC* infections. Despite significant ANOVA results for the main effect of genotype for PITs and cells undergoing apoptosis, post hoc analysis did not show significant results (Figure 3.10C). Numbers of spindle/fried egg macrophages were significantly decreased in WT infections when compared to Δ*essC* at 6 hrs post infection suggesting a modified cell population. Levels of cells with a rounded morphology took on a similar trend, but this was not significant. Together these data suggest that the presence of the T7SS increased the number of macrophages that adopted death morphologies early on in infection.
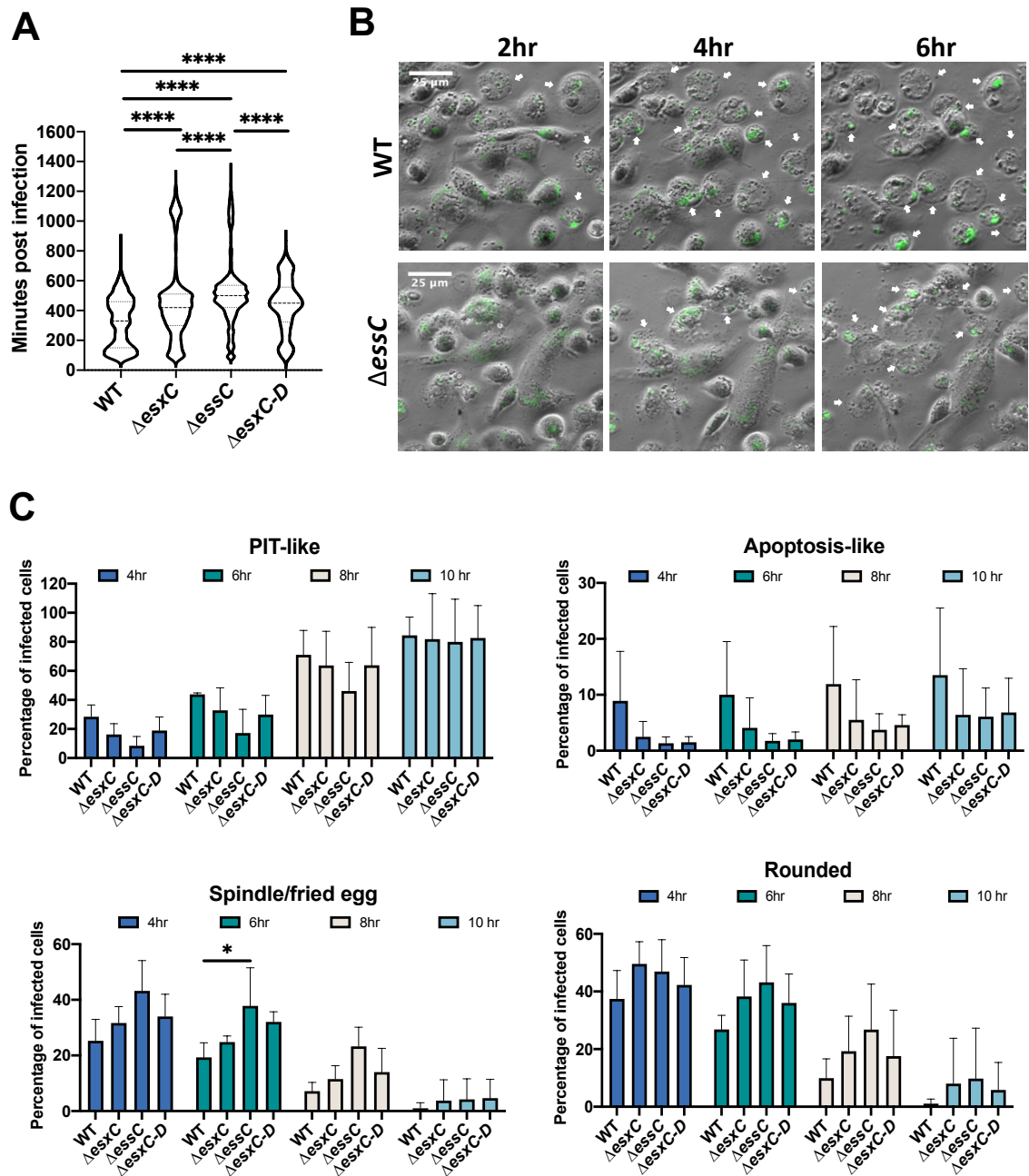
Figure 3.10: Staphylococcal T7SS decreases time taken for macrophages to adopt cell death-associated morphologies.

THP-1 macrophages were incubated with YFP expressing *S. aureus* JE2 WT or isogenic ΔesxC, Δ*essC*, Δ*esxC-D* mutant strains at MOI 10:1 for 1 hr. Extracellular bacteria were then killed, cells washed and refreshed with antibiotic-free media. Time-lapse videos of infected THP-1 cells were collected by taking images every 10 mins with a fluorescent widefield microscope. The morphologies of 300 infected THP-1 cells were assessed in each of 3 indpendent time-lapse

experiments (n=900). (A) Violin plot displays entire population distribution of time to macrophage PIT-structure formation and apoptosis morphology in 24 hr time-lapse experiments. Population statistics was carried out using Kruskal-Wallis rank test (H_4= 530.8 P<0.001) followed by Dunn's multiple comparison test (**** $P < 0.0001$, *** $P < 0.001$, ** $P < 0.01$) (B) Images of WT and $\Delta essC$ mutant *S. aureus* infections of THP-1 cells at indicated timepoints post infection. Bacteria are shown in green and white arrows represent cell-death associated PIT and apoptosis morphologies. (C) Percentage of infected macrophages with PIT-like, apoptosis-like, Spindle/fried egg or rounded morphologies at indicated timepoints post infection. All bar graphs show mean $\pm$ SD. For PIT-like cells ANOVA analysis revealed significant main effects of genotype ($F_{3,48}$=2.900 P=0.045) and time but no significant interaction between genotype and time ($F_{9,48}$=0.241 P=0.986). For apoptosis-like cells ANOVA analysis shows significant main effects of genotype ($F_{3,48}$=5.215 P=0.003) and but no significant main effects of time or interaction between genotype and time ($F_{9,48}$=0.021 P=0.999). For spindle/fried egg cells ANOVA analysis revealed significant main effects of genotype ($F_{3,48}$=10.65 P<0.0001) and significant main effect of time but no significant interaction between genotype and time ($F_{9,48}$=0.849 P=0.575). For rounded cells ANOVA analysis revealed significant main effects of genotype ($F_{3,48}$=3.603 P=0.0199) and significant main effect of time but no significant interaction between genotype and time ($F_{9,48}$=0.151 P=0.007) . Results of Tukey's multiple comparison tests are shown on graphs (* P<0.05).

3.2.8 T7SS has no effect on intracellular bacterial replication and outgrowth

During the formation of PITs, organelles and membrane bound vesicles condense and collect at one side of the cell (Jorgensen, Zhang, et al., 2016) which was visible during time-lapse microscopy in all *S. aureus* infections shown here. WT and T7SS mutant bacteria remained associated with this mass of dense organelles throughout macrophage PIT formation and appeared as tightly bound clumps of bacteria increasing in size over time as shown in Figure 3.11A. This may suggest *S. aureus* is replicating inside membrane bound vesicles, although no formal verification of this was carried out. It is not until after PIT formation that the *S. aureus* is released from the tightly bound clumps to fill the rounded PIT corpse or to disseminate away (Figure 3.11A). Here PITs were in many cases successful at restricting *S. aureus* WT and T7SS mutants' access to the extracellular environment, at least for some time. On very rare occasions PITs were efferocytosed by adjacent infected THP-1 macrophages as shown in Figure 3.11B., however, there were no differences between levels of efferocytosis events between WT and mutant infections. When a heavily infected PIT was efferocytosed by a secondary macrophage *S. aureus* escape from the PIT was stopped, but the large burden of bacteria eventually induced cell death in the secondary macrophage.

The total level of bacteria recovered from both inside and outside the macrophages at 1 hr, 8 hrs and 24 hrs post infection were not perturbed by deletion of T7SS proteins (Figure 3.12A). WT and mutant *S. aureus* had equal abilities to form numerous microcolonies on the macrophage monolayer (Figure 3.12B-C) These observations may indicate that the T7SS proteins EssC, EsxC, EsxD, EsxB and EsaE are not involved in ability of *S. aureus* to escape from the macrophage.

A

B
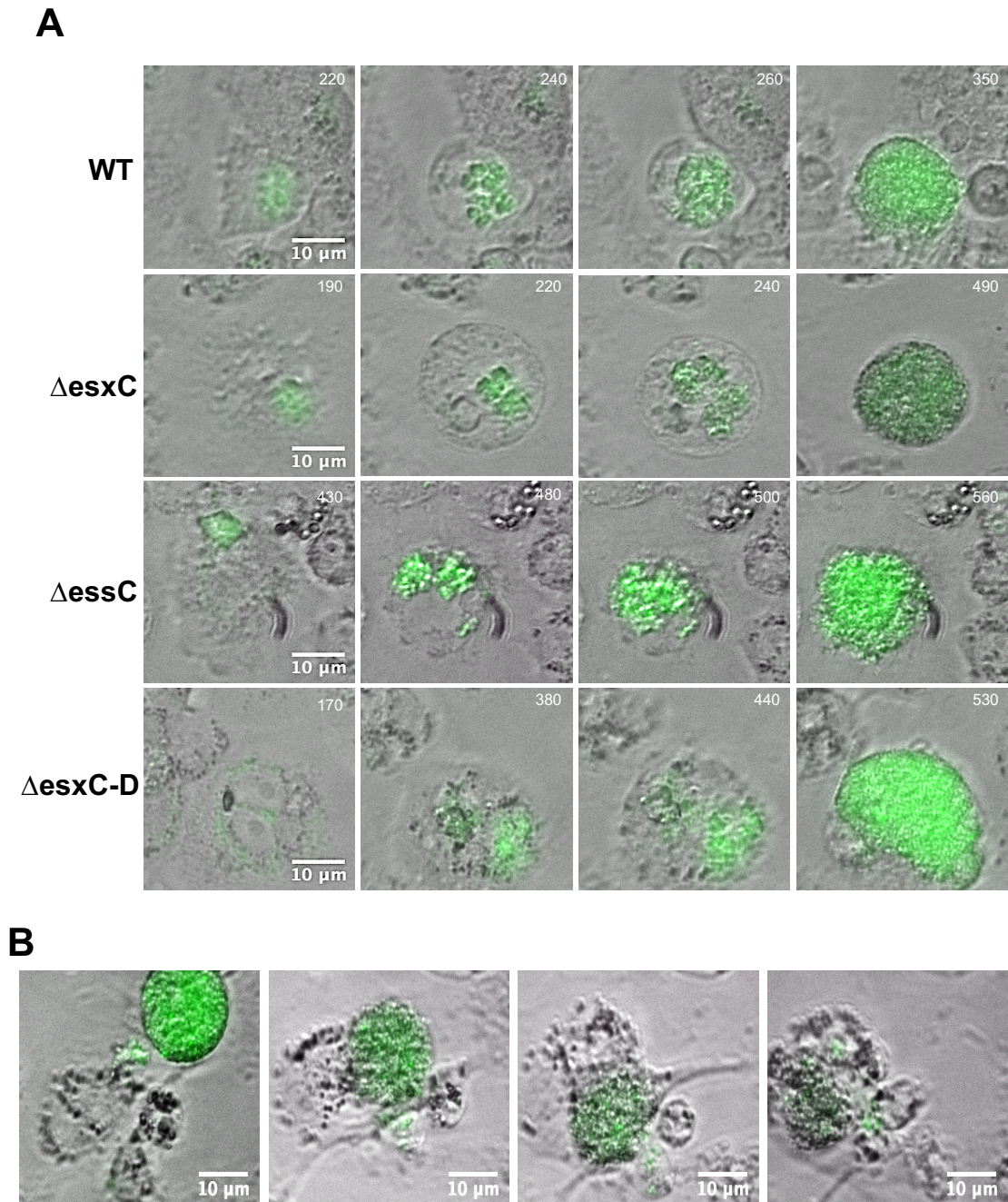
Figure 3.11: T7SS has no impact on the fates of *S. aureus in vitro*.

(A) Time-lapse images of YFP expressing WT, Δ*esxC*, Δ*essC* and Δ*esxC-D* infected THP-1 macrophages undergoing pore-induced intracellular trap (PIT) formation. Bacteria are able to replicate in and eventually escape from these PIT-like structures. Minutes post infection displayed in top right hand corner. (B) Time-lapse images of WT infected PIT structure efferocytosed by an adjacent THP-1 macrophaege.

A

B

C
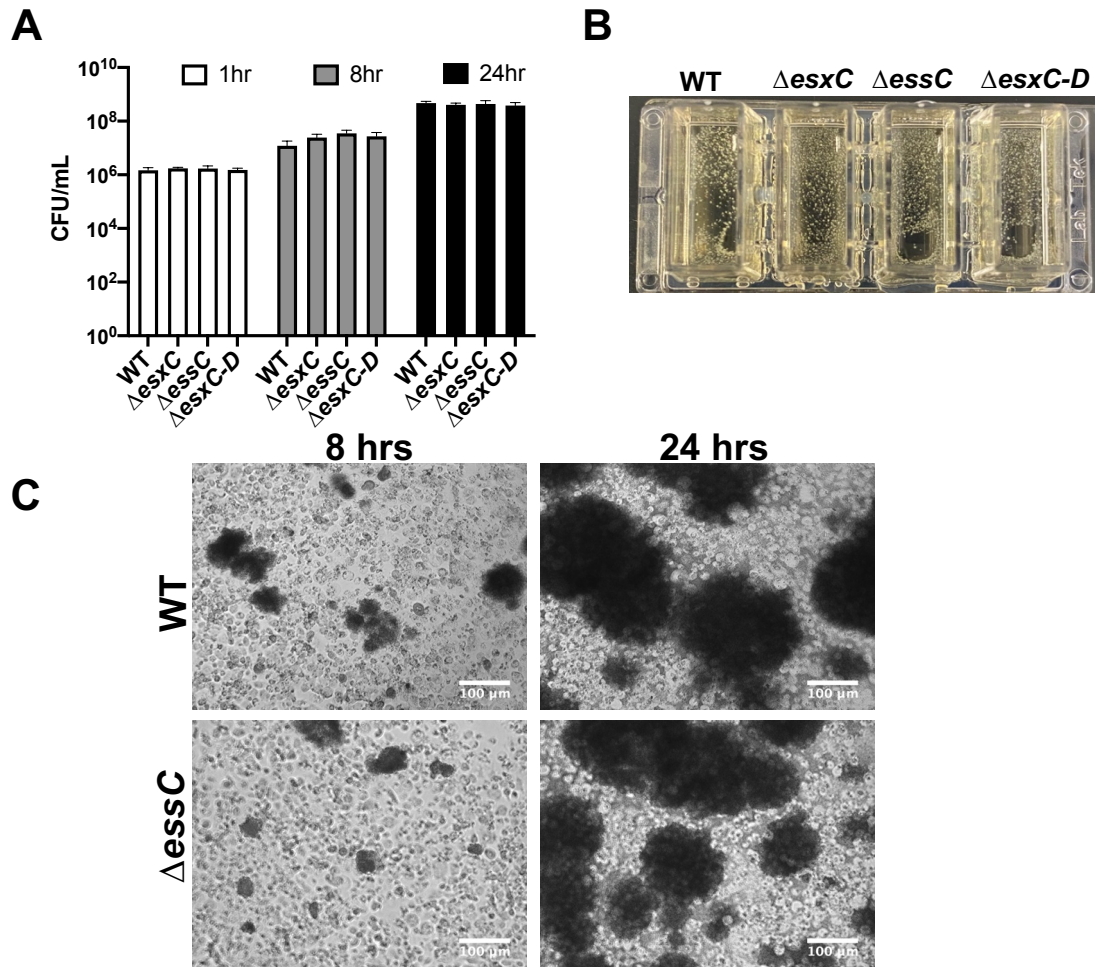
 Figure 3.12: The T7SS does not significantly impact staphylococcal escape and extracellular replication.

(A) THP-1 macrophages were incubated with *S. aureus* JE2 WT or isogenic Δ*esxC*, Δ*essC*, Δ*esxC-D* mutant strains at MOI 10:1 for 1 hr. Extracellular bacteria were killed then cells either lysed for intracellular bacterial number quantification by CFU counting at 1hr or refreshed with media for quantification of intracellular and extracellular bacteria by CFU counting at later timepoints. Two-way ANOVA analysis revealed no significant effect of genotype ($F_{3,36}$=0.4563 *P*=0.715) a signficant effect of time but no significant interaction between genotype and time ($F_{6,36}$=0.646 *P*=0.693) (B) Photo of microcolonies within wells after 24 hrs of infection. (C) Time-lapse images showing the bacterial outgrowth and formation of microcolonies during WT and Δ*essC* THP-1 macrophage infections at 8 hrs and 24 hrs post infection, *S. aureus* is visualised as phase dark cocci, x10 objective.

3.2.9 The staphylococcal T7SS increases the release of inflammatory cytokines by macrophages

Previous *in vivo* and *in vitro* studies have uncovered a role for the T7SS in modulation of inflammatory cytokine responses (Anderson et al., 2017; Cruciani et al., 2017; Ohr et al., 2017). The release of inflammatory cytokines, such as IL-1β and TNF-α, are tightly coupled with the activation of programmed cell death pathways (Cai et al., 2014; Miao et al., 2011). Therefore, the impact of the T7SS on macrophage release of both IL-1β and TNF-α into supernatant during infection was analysed. In accordance with the higher level of pyroptosis-associated PIT-like structures formed early on in WT infections, IL-1β was more strongly released by WT infected macrophages than those infected with the $\Delta essC$ mutant (Figure 3.13). A similar trend was observed with release of TNF-α at 4 hrs post infection with $\Delta essC$ defective in stimulating a response equal to that of the WT infections, however, differences were lost at 8 hrs (Figure 3.13). Collectively, this indicates that the deletion of the EssC transporter reduces the ability of *S. aureus* JE2 induce macrophage inflammatory cytokine production.
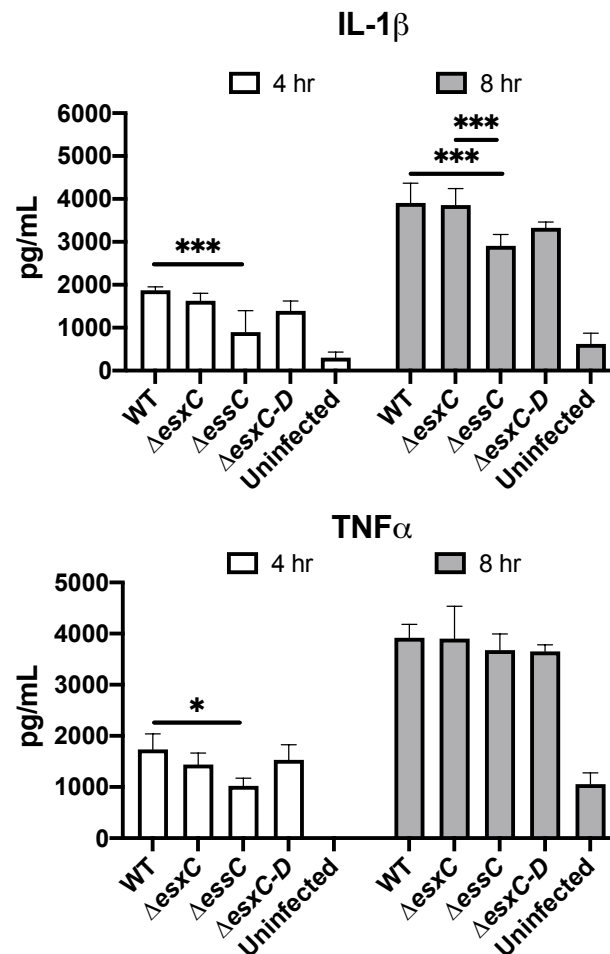
Figure 3.13: The staphylococcal T7SS induces the release of inflammatory cytokines.

Levels of TNF-α and IL-1β released into supernatant by THP-1 uninfected cells and THP-1 cells infected with WT JE2 or $\Delta esxC$, $\Delta essC$, $\Delta esxC$-D isogenic mutants quantified by ELISA. Graphs show mean $\pm$SD, n=5. Two-way ANOVA conducted on TNF-α data revealed significant main effect of genotype ($F_{3,32}$=3.765 P=0.020) and of time but not a significant interaction between genotype and time ($F_{3,32}$=1.488 P=0.236). Two-way ANOVA conducted on IL-1β data revealed significant main effect of genotype ($F_{3,32}$=19.79 P<0.0001) and of time but not a significant interaction between genotype and time ($F_{3,32}$=0.397 P=0.756), results of Tukey's multiple comparison tests are shown on graph (* P<0.05, ** P<0.01, ***P<0.001).

3.2.10 T7SS proteins promote necroptosis in macrophages

PITs are known to be the result of inflammatory cell death such as pyroptosis and necroptosis (Jorgensen, Zhang, et al., 2016). Necroptosis is a caspase-independent form of inflammatory cell death that requires the activation of RIPK1 and RIPK3 and is executed by MLKL (Guo et al., 2015). When the catalytic activity of the caspase-8–FLIP$_L$ complex is inhibited the formation of a stable necrosome including FADD, RIPK1 and RIPK3 can cause phosphorylation of MLKL which subsequently oligomerises to form pores in the plasma membrane (Dhuriya & Sharma, 2018; Oberst et al., 2011). In order to determine if necroptosis participated in *S. aureus* infections and to understand the role of the T7SS, infected THP-1 macrophage lysates were obtained and immunoblots for phosphorylated MLKL were carried out. Phosphorylated MLKL (p-MLKL) is a well-studied marker for necroptotic pathway execution (Dondelinger et al., 2014; L. Sun et al., 2012). Direct evidence was obtained to show necroptosis is occurring in *S. aureus* infected THP-1 cells by the presence of p-MLKL in lysates (Figure 3.14). The removal of EssC or secreted proteins EsxC, EsxD, EsxB and EsaE significantly decreased the levels of phosphorylated MLKL at 4 hours when compared to WT, while levels of MLKL remained similar. By 6 hours the level of phosphorylated MLKL was similar between WT and T7SS mutants but by 8 hrs Δ*essC* mutants were on average inducing higher expression and phosphorylation of MLKL than the WT and Δ*esxC-D* mutants. It must be noted that variations between infections were high at 8 hrs, replicate western blots are shown in appendix Figure S2.

A

B
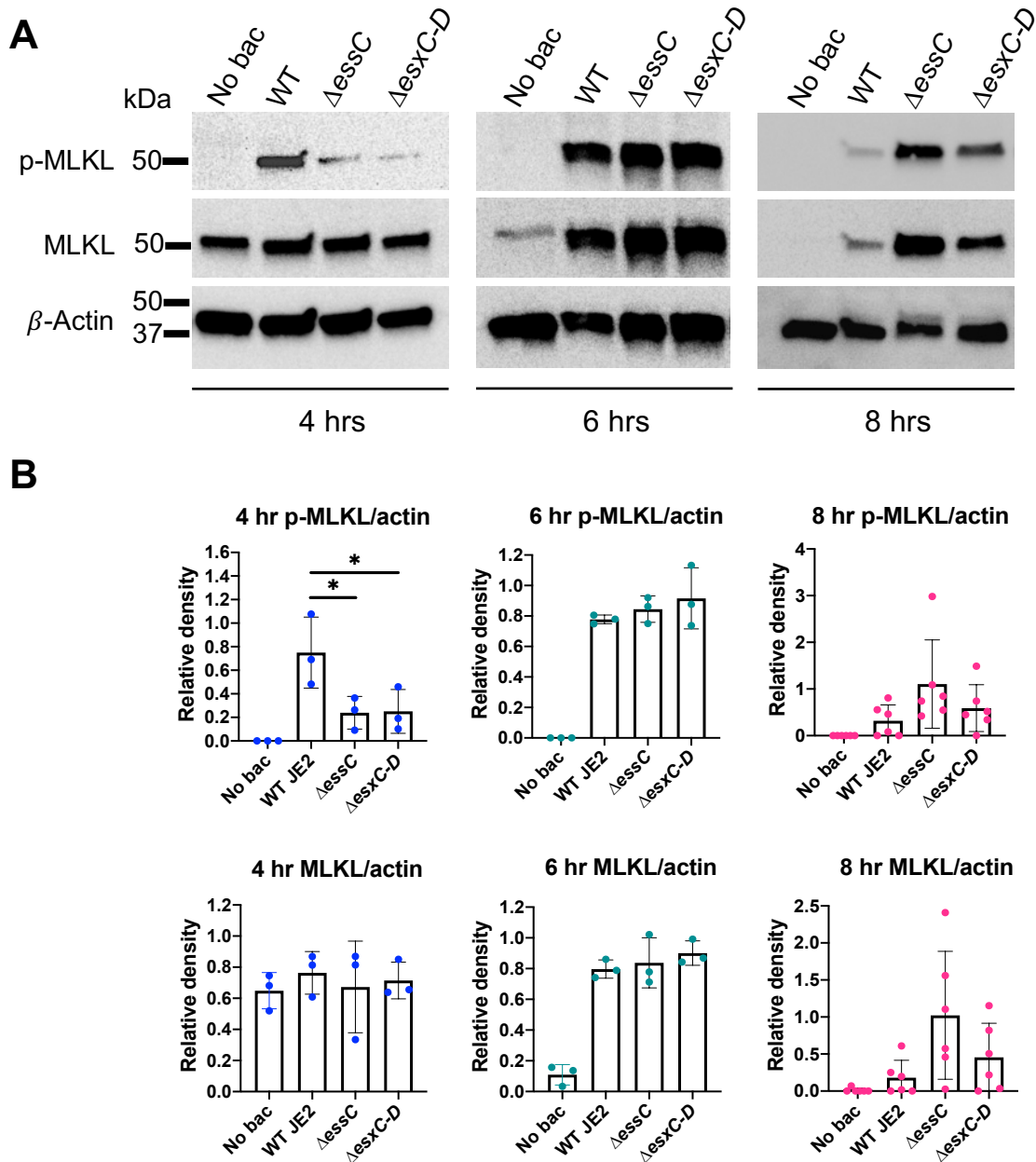
Figure 3.14: Staphylococcal T7SS proteins induce early necroptosis in macrophages.

(A) Representative western blots of phosphorylated MLKL (p-MLKL), MLKL and β-actin, from non-infected (no bac), WT and T7SS mutant infected THP-1 cells 4 hrs, 6hrs and 8 hrs post infection. (B) Graphs show mean relative density of western blot bands normalised to β-actin, each point represents a biological repeat. Also see Appendix Figure S2. One-way ANOVA revealed significant impact of genotype on levels of p-MLKL at 4 hrs only ($F_{3,8}=8.244$ $P=0.0079$). Results of Tukey's multiple comparison test are shown on graph (*$P<0.05$)

3.2.11 T7SS deletion mutants increase induction of *S. aureus* induced pyroptosis and necroptosis at later timepoints

Pyroptosis relies on the activation of inflammasomes (eg. NLRP3, NLRC4) which mediates the stimulation of caspase-1 (X. Liu et al., 2016; Shi et al., 2015). Caspase-1 activity processes pro-IL-1β and pro-IL-18 into active forms and cleaves gasdermin-D (GSDMD), the pore forming molecule required for cellular demise(Netea et al., 2010; Shi et al., 2015). The N-terminal GSDMD cleavage product assembles into large oligomeric rings that insert into and permeabilise the membrane to cause lytic cell death (X. Liu et al., 2016). We found that *S. aureus* induced the cleavage of GSDMD in THP-1 macrophages, providing evidence that in addition to necroptosis, pyroptosis is also executed among cells in this system (Figure 3.15). Similar levels of cleaved GSDMD are present in the lysates of THP-1 cells infected with WT and T7SS deletion mutants at 4 hrs post infection, while later at 6 and 8 hrs Δ*essC* infections on average stimulate more c-GSDMD than WT (Figure 3.15 A and B). Interestingly at 8 hrs macrophage responses to Δ*esxC-D* are highly variable between biological replicates, displaying behaviour similar to both WT and Δ*essC* mutant infected macrophages. GSDMD is cleaved by caspase-1 which itself is activated by formation of an inflammasome complex. Luminescence assays to detect caspase-1 activity during infections were carried out to determine if cleaved GSDMD levels correlated with inflammasome activation. Results indicated that caspase-1 activity, and therefore inflammasome activation, was not modulated by T7SS proteins at 6 hrs post infection (Figure 3.16).
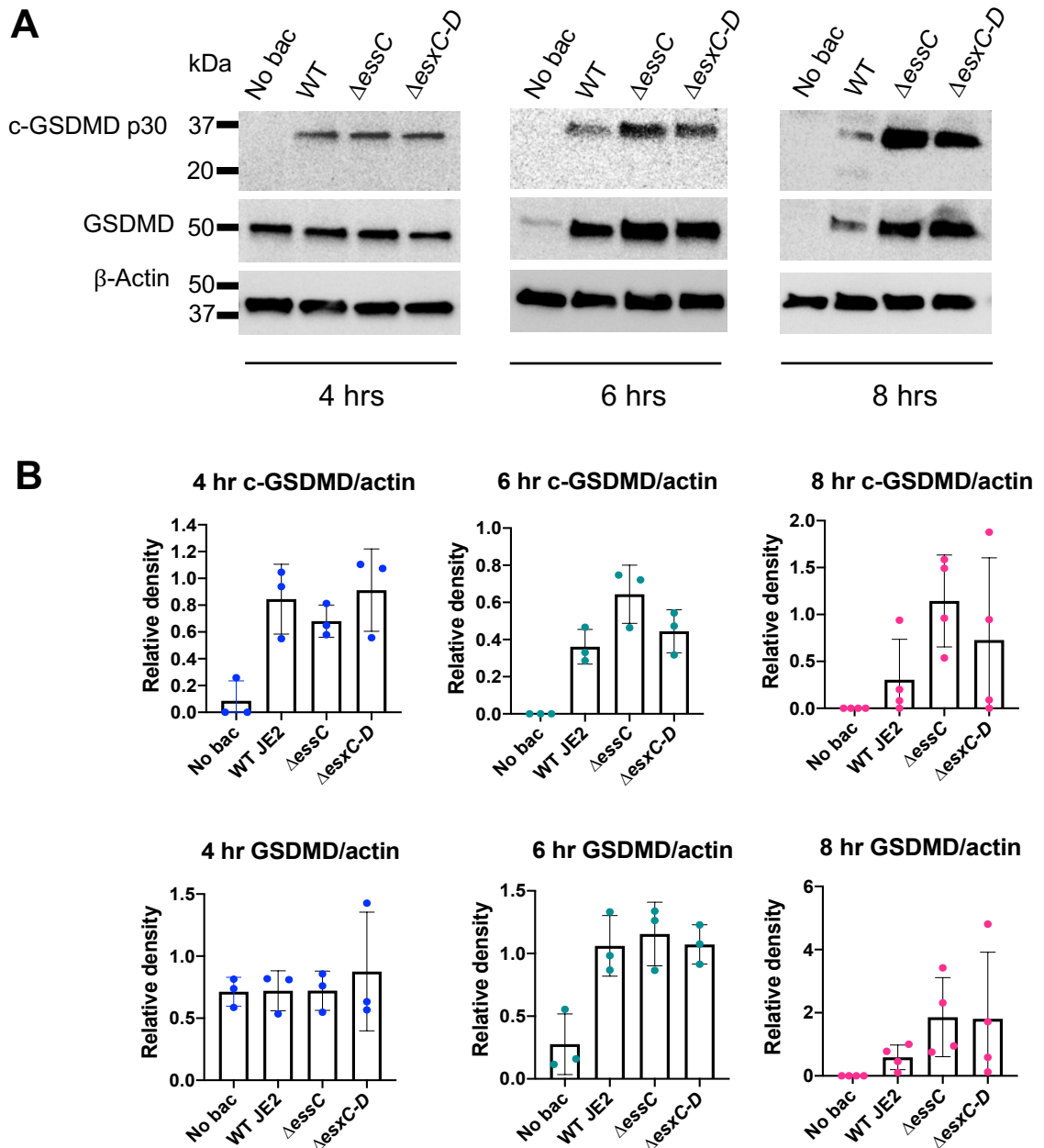
Figure 3.15: Deletion of T7SS proteins promotes late pyroptosis.

(A) Representative western blots of cleaved GSDMD (c-GSDMD), GSDMD and β-actin, from non-infected (no bac), WT and T7SS mutant infected THP-1 cells 4 hrs, 6hrs and 8 hrs post infection. (B) Graphs show mean relative density of western blot bands normalised to β-actin, each point represents a biological repeat. Also see Appendix Figure S3. One-way ANOVA showed no significant differences.
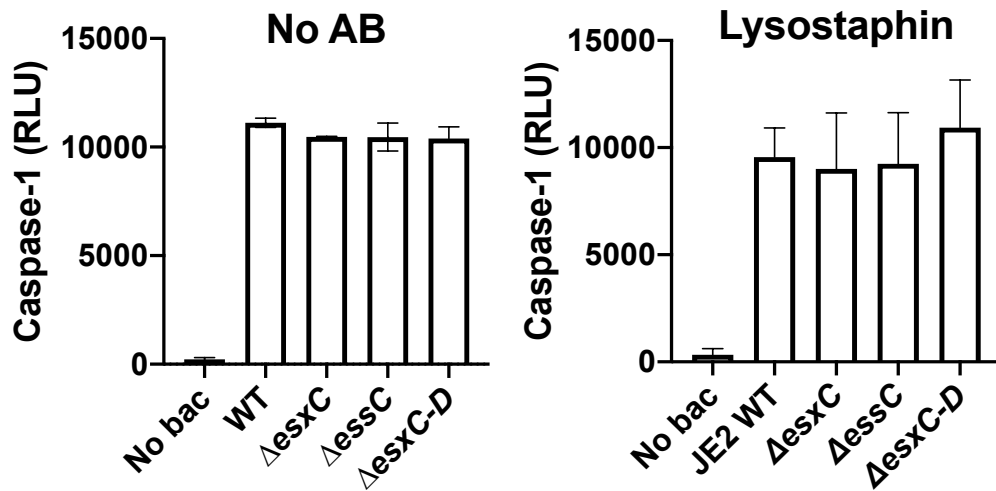
Figure 3.16: Caspase-1 activity is not modulated by staphylococcal T7SS in THP-1 macrophage infections.

Caspase-1 glo luminescence assays were used to quantify caspase-1 activity was quantified in THP-1 macrophages with no bacteria (no bac) or infected with WT or T7SS mutant *S. aureus* after 6 hrs of incubation either without the presence of antibiotics (no AB) or in the presence of 5 µg/mL of lysostaphin. Graphs show mean ±SD. One-way ANOVA showed no significant differences.

3.2.12 Execution of apoptosis is not detected in *S. aureus* WT and T7SS mutant macrophage infections

Time-lapse microscopy revealed a small number of infected macrophages underwent apoptosis-like membrane blebbing. During apoptosis pro-caspase-8 homodimerization induces auto-proteolysis and activation of caspase-8 which can go on to processes the executing caspases 3 and 7 as well as inhibit RIPK1 and RIPK3 of the necroptosis pathway (Taylor et al., 2008; Vanden Berghe et al., 2015). *S. aureus* induced the cleavage of caspase-8 during THP-1 infections (Figure 3.17A). Levels of cleaved caspase-8 subunits (p41/43 and p18) did not differ between WT and T7SS infections up to 6hrs post infection (Figure 3.17). At 8 hrs large variations in caspase-8 cleavage were found between biological replicates with no consistent result (Appendix Figure S4)

Downstream of caspase-8 apoptosis is carried out by activated caspase-3 and caspase-7. Caspase-8 cleaves pro-caspase-3/7 -8 into two smaller protease subunits to initiate their activity (Taylor et al., 2008). The cleaved caspase-3 subunits are absent in both WT and T7SS mutant macrophage infections at all timepoints suggesting apoptosis is not occurring in this population of infected THP-1 cells, or not occurring at high enough levels to be detected via Immunoblotting (Figure 3.17A and Appendix Figure s4).

A

B
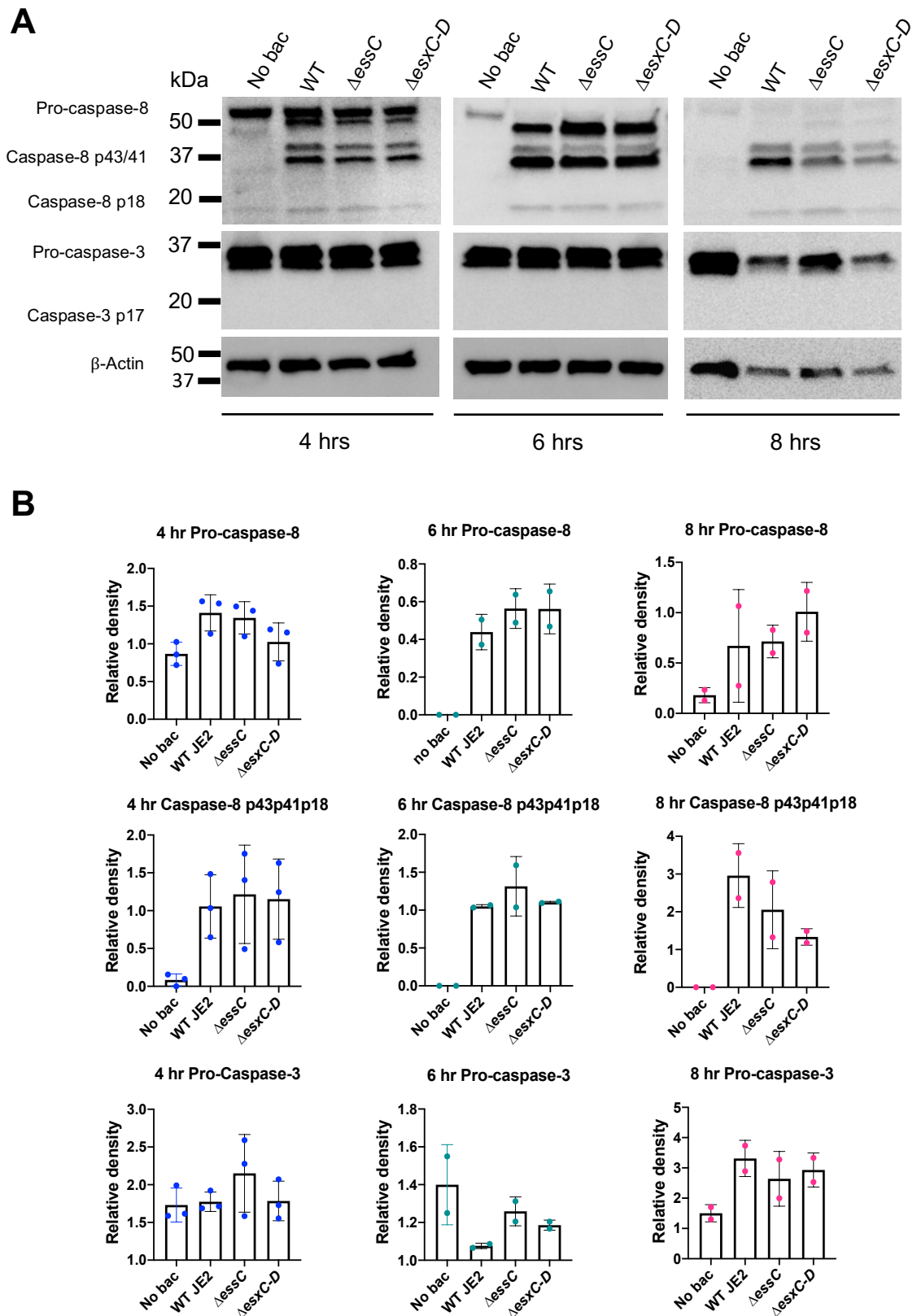
Figure 3.17: Apoptosis is not the dominant cell death pathway executed in *S. aureus* infection of THP-1 macrophages.

Western blots of pro-caspase-3 and pro-caspase-8 plus cleaved subunits from non-infected (no bac) or infected WT and T7SS mutant THP-1 infections at 4 hrs, 6hrs and 8 hrs post infection. (B) Mean relative density of western blot bands normalised to β- actin, each point represents a biological repeat, error bars represent SD. Also see Appendix Figure S4. One-way ANOVA revealed no significant results.

3.2.13 Antibiotics modifies the effect of the staphylococcal T7SS on cell death-associated outcomes but maintains similar cytokine responses.

So far in this chapter all time-lapse data describes THP-1 intracellular infections that have undergone an initial extracellular bacterial killing step followed by incubation with media that did not contain antibiotics. Many previous studies have however utilised a low concentration of antibiotics in the culture medium to isolate the intracellular effect of *S. aureus* over extended time periods (Cruciani et al., 2017; Fraunholz & Sinha, 2012; Gresham et al., 2000; Korea et al., 2014; Qazi et al., 2001). To investigate T7SS dependent trends in macrophage responses with antibiotics, time-lapse infection assays were carried out with 5 µg/mL lysostaphin in the culture medium after initial extracellular bacterial killing. Unlike previous conditions, prolonged lysostaphin treatment enabled a proportion of macrophages to survive the full 24 hr experiment. In WT infections 42.78 % $\pm$ 11.7 % of macrophages retained membrane ruffling/cell motility after 24 hrs, and similar proportions were found in T7SS mutant infections (Figure 3.18A). As perhaps expected, due to the lack of emerging viable bacteria from macrophages, the distribution of cells that adopted PIT-like and apoptosis morphologies in WT infections over 24 hours no longer had multiple peaks (Figure 3.18B). Instead, a major peak of cell death occurred before 4 hrs and little occurred after 6 hrs.

The presence of lysostaphin also dramatically changed the distribution of PIT-like and apoptosis morphology occurrence in T7SS mutant infections over 24 hrs (Figure 3.18C). Peaks occurred earlier than in infections with no antibiotics (Figure 3.18C and Figure 3.10A), suggesting that antibiotics modifies macrophage responses to intracellular *S. aureus*. Importantly, differences between WT and strains lacking T7SS proteins were still evident. PIT-like structure formation and apoptosis were more spread out over the 24-hr time period for mutants. Again, this is most apparent with the Δ*essC* mutant, descriptive statistics of distributions are detailed in Table3.1.

Table 3.1: Descriptive statistics of the distribution of PIT-like structures and apoptosis over 24 hrs.

	Time post infection (hrs:mins)							
	No antibiotics				Lysostaphin			
	WT	ΔesxC	ΔessC	ΔesxC-D	WT	ΔesxC	ΔessC	ΔesxC-D
Mean	05:22	07:42	08:41	07:15	04:58	06:46	08:29	05:52
25% Percentile	02:30	05:00	07:00	5:22	02:20	03:50	03:50	02:50
Median	05:30	07:00	08:20	07:30	03:30	05:50	07:20	04:50
75% Percentile	07:40	08:30	09:30	09:17	06:17	08:40	11:50	07:30

At discrete timepoints both PIT-like structure formation and apoptosis were higher in WT infections compared to Δ*esxC* and Δ*essC* mutants, as seen in no antibiotic conditions, notably however, WT remained higher than Δ*esxC* and Δ*essC* for longer periods of time in lysostaphin than antibiotic-free conditions (Figure 3.18D). the inverse was observed with cells that appeared rounded with a significant difference at 10 hrs (Figure 3.18D).

The effect of lysostaphin on macrophages' ability to produce inflammatory cytokines during WT and mutant infections was also examined. Levels of both IL-1β and TNF-α were high in WT infections compared to mutants, producing a similar trend to antibiotic-free conditions (Figure 3.19 and Figure 3.13). Antibiotics accentuated the difference between WT and mutants' ability to invoke a cytokine response at 8 hrs post infection. This conforms that lysostaphin does not mask T7SS induced macrophage inflammatory response but may even promote responses at later timepoints. The absence of extracellular bacteria at 24 hrs post infection in lysostaphin conditions made it possible to examine the presence of cytokines and chemokines at this later timepoint. Levels of IFN-β, IL-10, IL-6, GM-CSF, IL-1β, TNF-α, MCP-1, MIP-1α and MIP-1β in the supernatant of infected macrophages at 24 hrs were not significantly different between WT and all T7SS mutants (Appendix Figure S1).
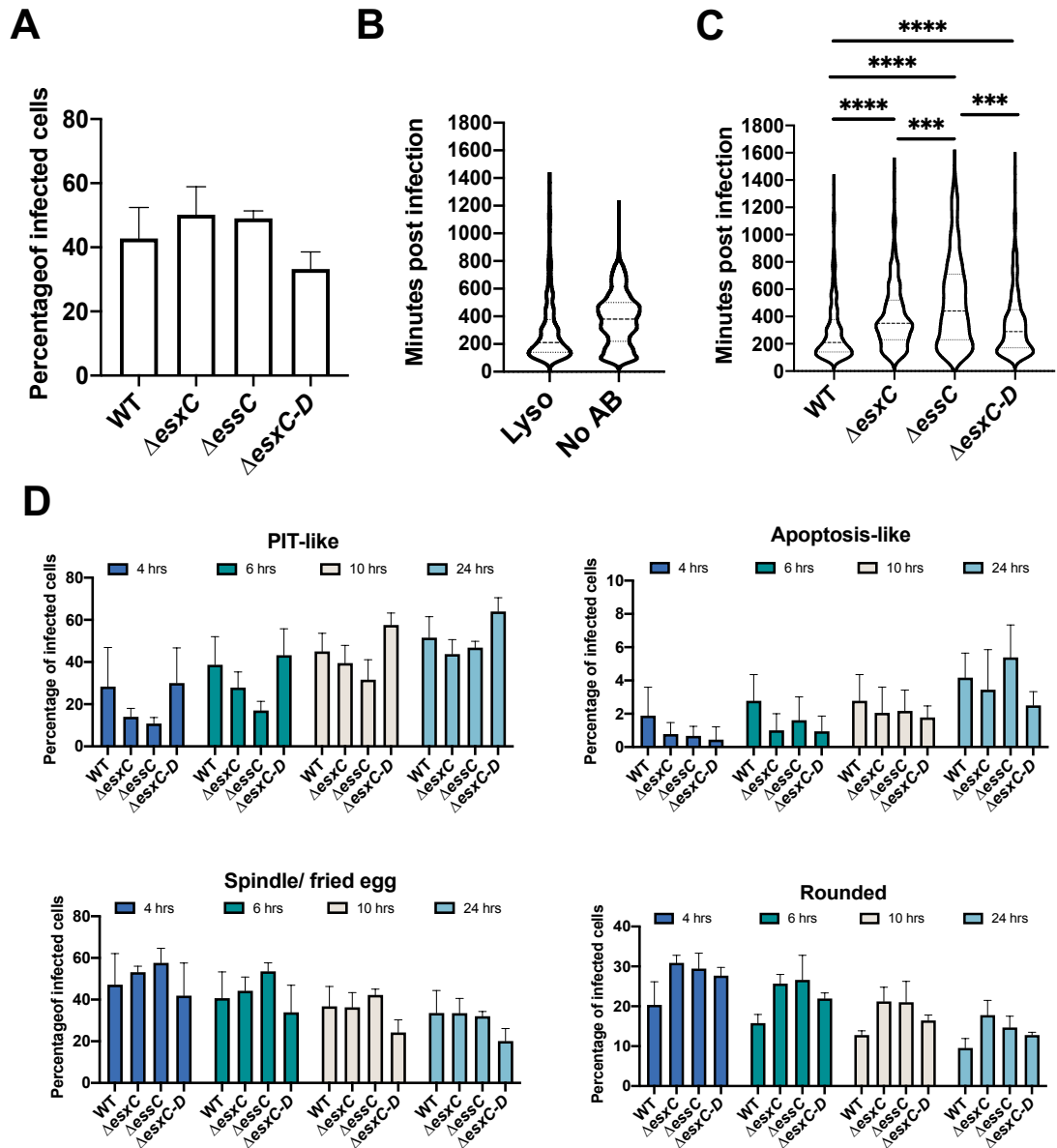
Figure 3.18: The effect of lysostaphin on WT and T7SS mutant *S. aureus* infection dynamics

THP-1 macrophages were incubated with YFT expressing *S. aureus* JE2 WT or isogenic ΔesxC, Δ*essC*, Δ*esxC-D* mutant strains at MOI 10:1 for 1 hr incubation, extracellular bacteria were killed then cells refreshed with media containing 5 μg/mL lysostaphin to stop baterial outgrowth. Time-lapse videos of infected THP-1 cells were collected by taking images every 10 mins with a fluorescent widefield microscope. Morphologies of a total of 300 infected THP-1 macrophages were recorded over 3 indpendent time-lapse experiments, n=900.

(A) Percentage of infected cells that retain membrane ruffling after 24 hours of infection, graph shows mean $\pm$ SD. (B) Violin plot displays distribution of time to PIT-structure and apoptosis morphologies from the entire population of macrophages in 24 hr time-lapse experiments with lysostaphin (lyso) as described above and without antibitotics (no AB) as described in figure 3.12. (C) Violin plot to show distribution of cell-death associated outcomes of THP-1 cells in WT and T7ss mutants over 24 hrs. Population statistics was carried out using Kruskal-Wallis rank test (H_4= 181.6 P<0.0001) followed by Dunn's multiple comparison test shown on graphs (**** $P < 0.0001$, ***$P < 0.001$, ** $P < 0.01$). (D) Percentage of infected macrophages with PIT-like, apoptosis-like spindle/fried egg or rounded morphologies at indicated time points post infection. All bar graphs show mean $\pm$ SD. A two-way ANOVA showed a significant main effect of genotype on PIT-like cells ($F_{3,32}$=12.30 P=<0.0001) and of time but no significant interaction between genotype and time, Tukey's multiple comparison test showed no significant results. No other main significant effects of genotype or significant interactions between time and genotype were found for other cell morphologies.
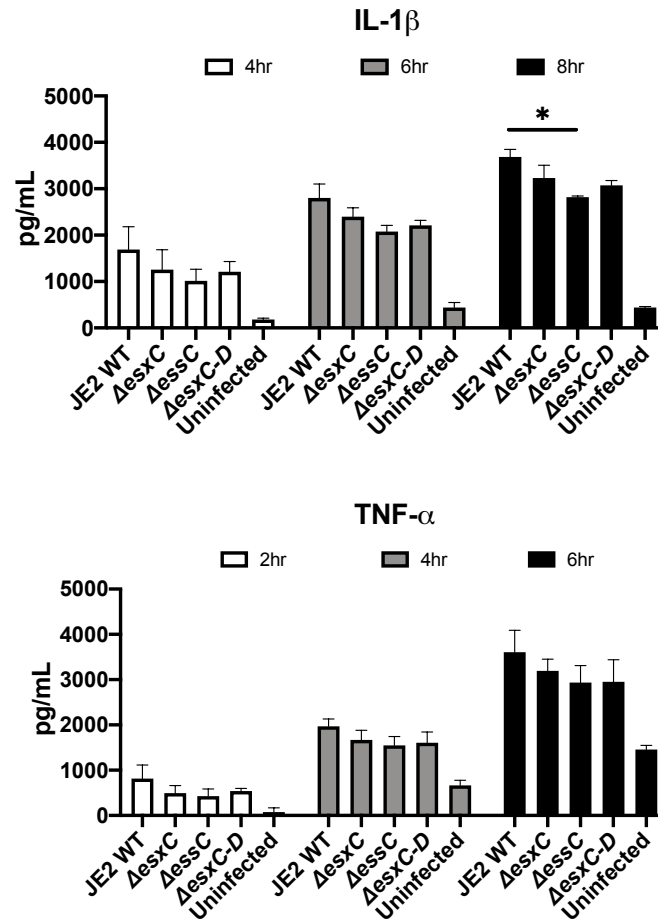
Figure 3.19: Lysostaphin has little effect on the T7SS-associated release of inflammatory cytokines.

Levels of TNF-α and IL-1β released into supernatant by THP-1 uninfected cells and THP-1 cells infected with WT JE2 or $\Delta esxC$, $\Delta essC$, $\Delta esxC$-D isogenic mutants. Incubations post extracellular killing included 5 µg/mL lysostaphin. Supernatant level of cytokines quantified by ELISA Graphs show mean ±SD, n=3. For TNF-α a two-way ANOVA revealed a significant main effect of genotype ($F_{3,24}$=5.251 P= 0.0063) and a main effect of time but no significant interaction between time and genotype ($F_{6,24}$=0.308 P=0.927). For IL-1β a two-way ANOVA revealed a significant main effect of genotype ($F_{3,24}$=13.77 P<0.001) and a main effect of time but no significant interaction between time and genotype ($F_{6,24}$=0.1186 P=0.993). Results of a Tukey's multiple comparison test are shown on graphs (* P< 0.05).

3.2.14 Macrophage culture surface impacts the responses to *S. aureus* in a T7SS dependent manner.

It is well known that THP-1 cells are sensitive to many stimuli (Aldo et al., 2013; Chanput et al., 2014). When THP-1 macrophages were cultured on Lab-Tek II RS treated Soda lime glass rather than on Lab-Tek Nunclon Delta treated Permanox plastic, there were stark differences in infection dynamics. Firstly, at 8 hrs, levels of total *S. aureus* (intracellular and extracellular) were decreased compared to 1 hr CFU counts, whereas an increase in total bacteria was seen at this time in plastic conditions (Figure 3.20A and 3.12A). This suggests some clearance of bacteria by macrophages cultured on glass but not plastic. Later at 24 hrs, total WT bacteria levels on glass were approximately 100-fold less than those seen on plastic surfaces (Figure 3.20B), this was made obvious to the eye by a lack of microcolony formation in these conditions (Figure 3.20D). The stark difference in WT bacterial levels on glass and plastic was not mirrored in T7SS mutant infections. Total Δ*essC* Δ*esxC-D* and Δ*esxC* CFU on glass were similar to those counted from plastic cultures, making them around 100-fold higher than WT CFU when cultured on glass (Figure 3.20A and E). Consequently, mutant infections produced more microcolonies than WT in glass chamber slides but these microcolonies were less frequent and larger than those on plastic. (Figure 3.20C-E).
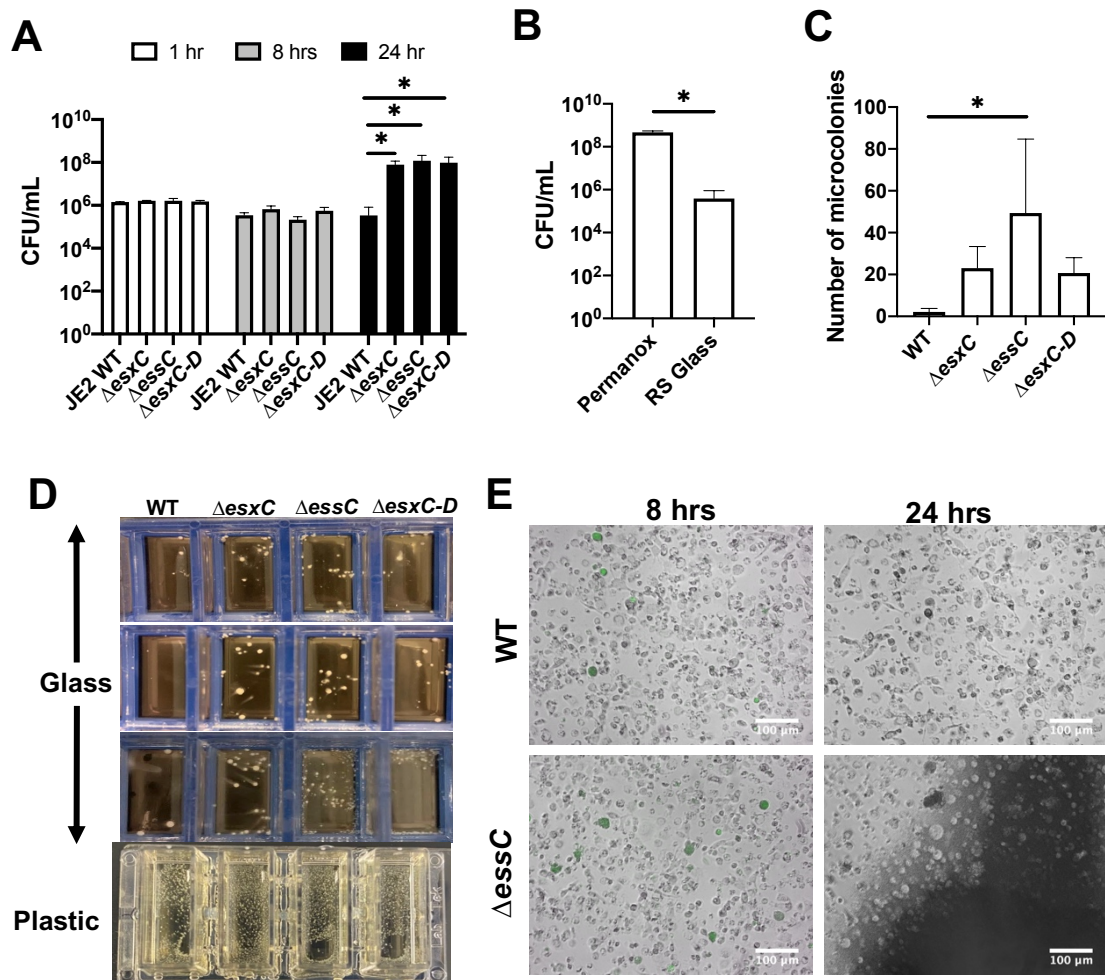
Figure 3.20: Culture surface dramatically effects the ability for THP-1 macrophages to contain *S. aureus* infections.

THP-1 macrophages cultured on RS treated glass chamber slideswere incubated with YFP expressing *S. aureus* JE2 WT or isogenic ΔesxC, Δ*essC*, Δ*esxC-D* mutant strains at MOI 10:1 for 1 hr, extracellular bacteria were then killed, cells washed and refreshed with RPMI media. (A) Total *S. aureus* CFU counts from WT and T7SS mutant infections of THP-1 cells on RS treated glass at indicated timepoints, n=3. Statistics was carried out using Kruskal-Wallis rank test for each time point. At 24 hrs analysis showed a significant difference between CFU/mL of genotypes (H_4=13.06 *P*= 0.004), results of a Dunn's multiple comparison test is shown on the graph (* *P* < 0.05). No other statistically significant results were found. (B) Total (intracellular and extracellular) *S. aureus* CFU counts from WT infections of THP-1 cells on RS treated glass and Permanox plastic at 24 hours post infection, n=3. Results of Mann-Whitney test

(U=0 P= 0.015) shown on graph (*P<0.05). (C) Microcolony counts from THP-1 cell infections with WT and T7SS mutant on RS treated glass at 24 hours post infection n=3. Analysis of data with Kruskal-Wallis test showed significant effect of genotype (H_4=7.721 P=0.022), results of Dunn's multiple comparison test is shown on graph (*P<0.05). (D) Images of infection assays carried out on RS treated glass or Permanox plastic chamber slides after 24 hrs of infection, microcolonies are visible to the eye (yellow colonies). (E) Microscope images of THP-1 macrophages infected with WT or Δ$essC$ JE2 *S. aureus* at 8 hours and 24hrs post infection. Mass extracellular replication of bacteria is observed in Δ$essC$ infections by 24 hrs. All bar graphs show mean ±SD.

Time-lapse assessment of cell morphologies on glass revealed that a large proportion of WT infected cells remained viable over 24 hrs, as membrane ruffling/motility was evident, whereas this was not the case in T7SS mutant infections (Figure 3.21A). WT infected macrophage populations displayed high efferocytosis activity, which resulted in uptake of a number of cell corpses/cell debris (Figure 3.21B). The efferocytosis of cell corpses by neighbouring macrophages was rarely observed in macrophage infections carried out on plastic, with and without antibiotics. Overall T7SS mutant infections produced more PIT-like structures in macrophages over 24 hrs (Figure 3.21E), however PIT formation and apoptosis occurred slightly later in in these infections compared to WT (Figure 3.21C and Table 3.2). Quantification of cell morphologies linked with activation/polarisation states (spindle/fried egg and rounded) showed mutant infections on average had lower levels of spindle/fried egg-shaped macrophages at 24 hrs post infection but did not differ from WT infection with regards to levels of rounded cells (Figure 3.21 E and F), this can be clearly seen in time-lapse images (Figure 3.21D).

Table 3.2: Descriptive statistics of distribution of PIT-like morphology or apoptosis events over 24 hrs on glass chamber slides.

	Time post infection (hrs:mins)			
	WT	ΔesxC	ΔessC	ΔesxC-D
Mean	03:14	04:37	05:58	06:06
25% Percentile	01:30	01:50	0:1:30	0:1:30
Median	01:30	02:00	02:05	02:30
75% Percentile	02:30	05:00	09:40	09:45
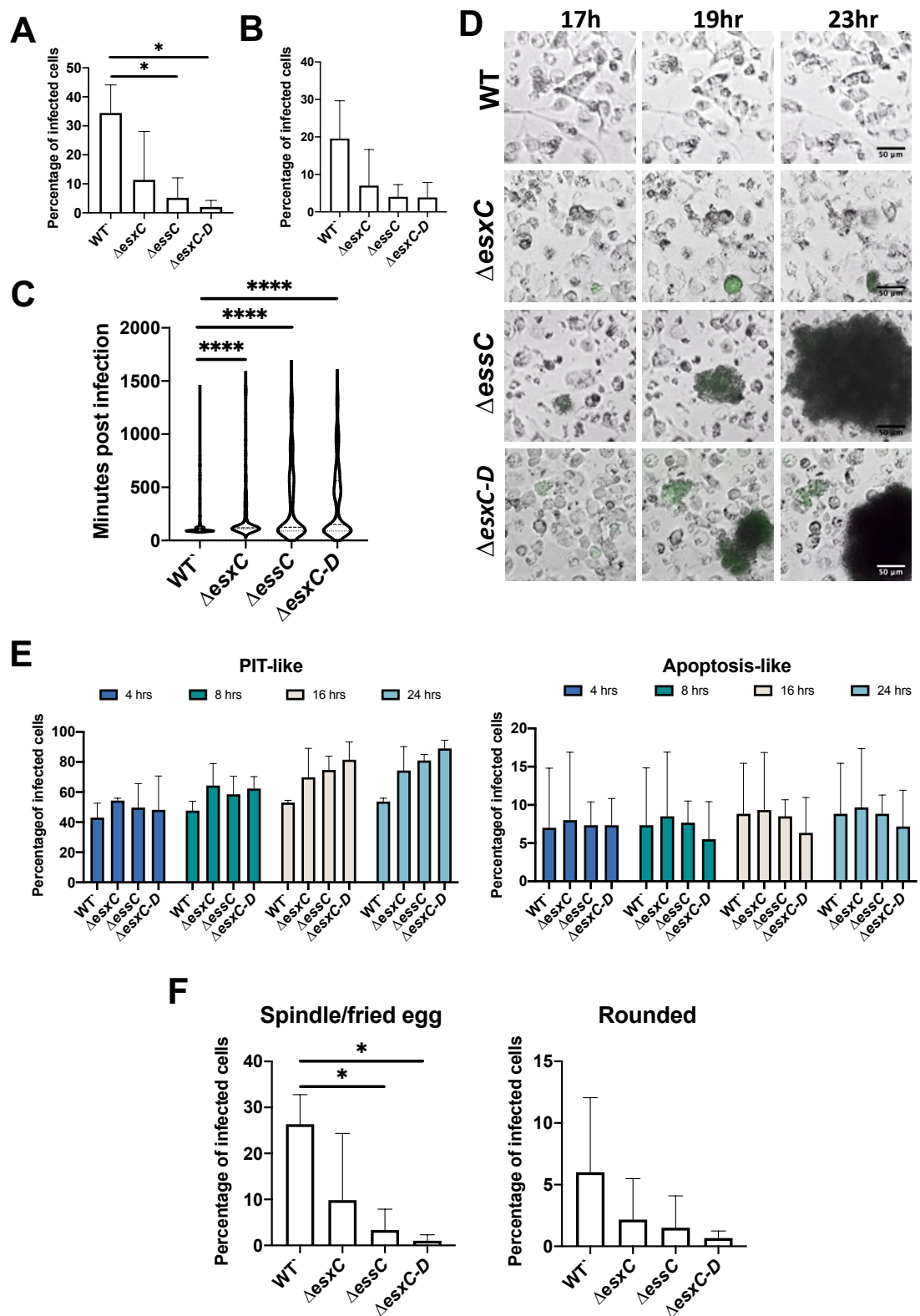
Figure 3.21: The culture surface changes macrophage response to *S. aureus* in a T7SS dependent manner.

Invasion assays carried out on RS treated glass chamber slides with THP-1 cells and *S. aureus* WT JE2 and T7SS isogenic mutants at MOI 10. A total of 200 cells for each of 3 independent experiments were assessed, n=600. (A) Percentage of infected macrophages that retain membrane ruffling at 24 hrs post infection. One-way ANOVA shows significant effect of genotype ($F_{3,8}$=6.078 *P*=0.0185), results of Tukey's multiple comparison test are shown on graph (**P*<0.05). (B) Percentage of infected macrophages observed to carry out efferocytosis of cell debris/cell corpses over 24 hr time-lapse experiments one-way ANOVA shows no significant results ($F_{3,8}$=3.006 *P*=0.094).   (C) Violin plot represents distribution of cell death-associated outcomes of THP-1 cells over 24 hrs of all collected data over 3 independent experiments. Population statistics was carried out using Kruskal-Wallis rank test (H_4=64.32 *P*<0.001) followed by Dunn's multiple comparison test, results are shown on graph (*****P*<0.0001). (D) Time-lapse images of WT Δ*esxC*, Δ*essC* and Δ*esxC-D* (green) infections of THP-1 cells. (E) Percentage of infected macrophages with PIT-like or apoptosis-like, morphologies at 4 hrs, 8hrs, 16 hrs and 24 hrs post infection. Two-way ANOVA reveals no significant effect of genotype or time. (F) Percentage of infected cells that exhibited a spindle/fried egg morphology 24 hrs post infection. ANOVA showed significant effect of genotype ($F_{3,8}$ =5.715 *P*=0.0218), results of Tukey's multiple comparison test are shown on graphs (**P*<0.05).   (G) Percentage of infected cells that exhibited a rounded morphology 24 hrs post infection. ANOVA revealed no significant results ($F_{3,8}$=1.216 *P*=0.365). All bar graphs show mean $\pm$ SD.

To assess the involvement of MLKL in the macrophage response to staphylococcal T7SS proteins, necrosulfonamide (NSA), a pharmacological inhibitor of MLKL was added to cells during infection in glass chamber slides. The analysis of one independent experiment showed that the inhibition of MLKL in WT infections dramatically increased the formation of microcolonies compared to untreated WT infections, making the infection outcome similar to that of untreated mutant infections (Appendix Figure S2 A and B). In addition, MLKL inhibition caused a distribution of cell death that was similar to that seen in plastic. The population of Δ*essC* mutant infected macrophages underwent a delayed cell death when compared to WT and Δ*esxC* which was not previously seen in glass (Appendix Figure S2 D). This trend was reflected in the percentage of cells undergoing PIT formation (Appendix Figure S2 E).

The use of a pan-caspase inhibitor, Z-VAD-FMK during infection in glass chamber slides induced no change in microcolony formation from the untreated infection outcomes observed for WT or mutants (Appendix Figure S2 A and C). The distribution of cell death over time in WT and mutant infections were also similar, while the onset of PITs appeared to be higher in WT at earlier timepoints (Appendix Figure S2 D and E).

These interesting observations flagged up a number of questions. Firstly, what happens during infections on glass to cause such a dramatic difference in macrophage restriction of WT bacterial replication compared to plastic? Secondly, why is this dependent on the presence of the T7SS proteins? In an attempt to investigate this, cell morphologies and the ROS production of uninfected macrophages cultured on glass and plastic were assessed. A higher level of spindle and fried egg-shaped cells were observed in macrophage populations on glass than plastic, as shown in Figure 3.22A and B, implying RS washed glass may act to heighten activation of macrophages. ROS can provide details on cell state as production can be attributed to both inflammatory activation and stress (Forman & Torres, 2001). Figure 3.22C shows intracellular ROS production by uninfected THP-1 cells with the use of DCF-DA staining. DCF-

DA can diffuse into cells, cellular ROS oxidises DCF-DA creating fluorescent DCF, which can be viewed under a microscope. DCF fluorescence intensity and quantification of fluorescence area suggests THP-1 macrophages cultured on plastic has increased ROS production than those cultured on glass (Figure 3.22D). Together this indicates a difference in macrophage behaviour depending on culture surface.
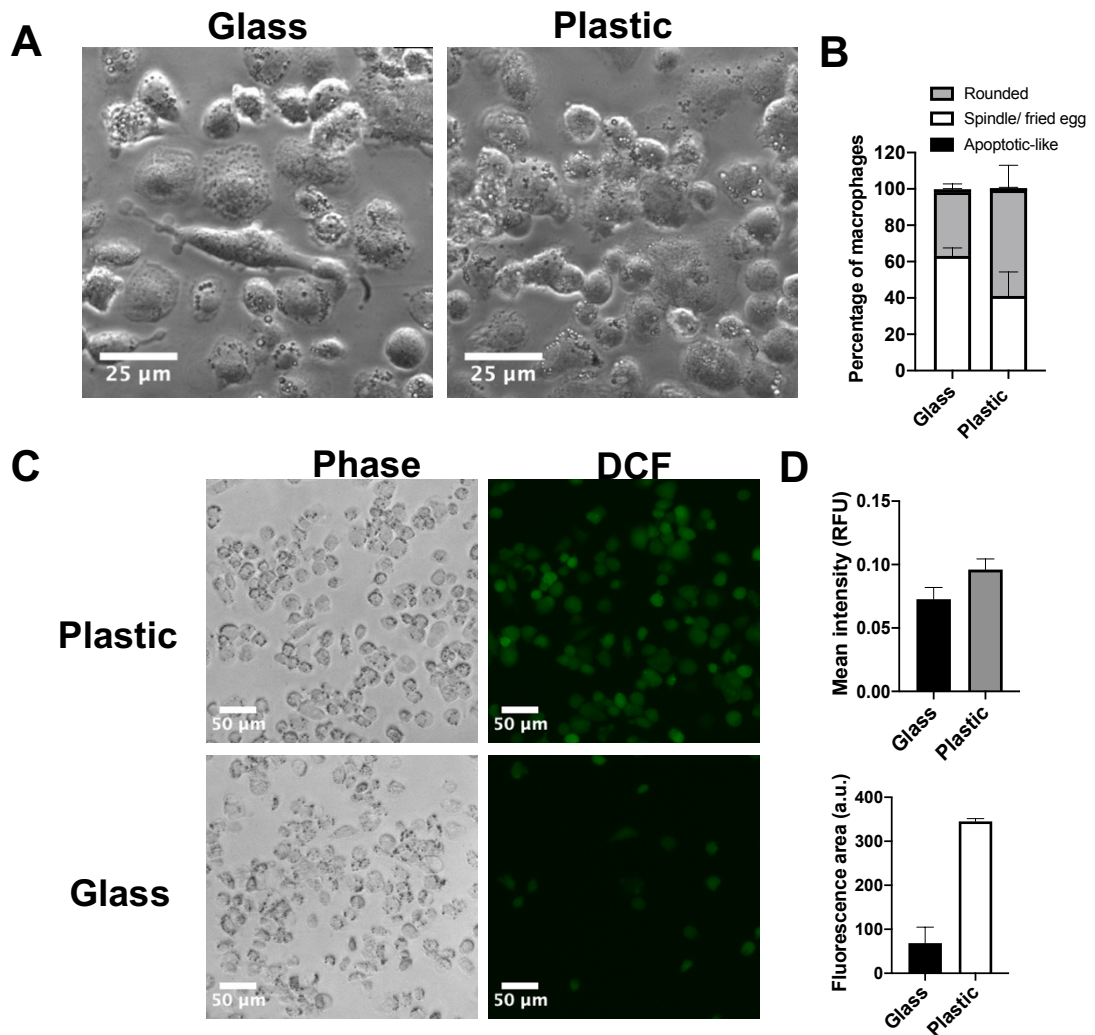
Figure 3.22: Macrophage culture on RS washed glass verses Permanox plastic.

(A) Phase contrast images of uninfected THP-1 macrophages on soda-lime RS washed glass or Permanox plastic chamber slides. (B) Percentage of uninfected THP-1 macrophages that have a spindle/fried egg, rounded or apoptotic-like cell morphology after 6 hrs of time-lapse video capture, n=3 (C) Images show uninfected THP-1 macrophages cultured on glass or plastic after incubation with DCF-DA for 15 mins. DCF-DA diffuses into cell and is oxidised by ROS to become fluorescent DCF. Fluorescence generated is proportional to the amount of oxidised DCF-DA. (D) Mean intensity of DCF fluorescence normalised by cell number (top) and area of fluorescence pixels normalised by cell number (bottom), n=2. All graphs show mean± SD.

3.3 Discussion

The capacity of *S. aureus* to kill cells such as macrophages through promotion of cell death pathways has been well studied (Fraunholz & Sinha, 2012; Pidwill et al., 2021), however, details of staphylococcal modulation of these pathways, particularly during intracellular infections, and resulting fates of host cells and bacteria are ill-defined (Fraunholz & Sinha, 2012). The aim of this chapter was to clarify our understanding of intracellular *S. aureus* interaction with macrophages, specifically, the impact of the staphylococcal T7SS proteins, which have been identified as virulence factors involved in manipulating cell death in other cell types (Cruciani et al., 2017; Dai et al., 2017; Korea et al., 2014).

A large proportion of results in this chapter were generated from time-lapse microscopy. Time-lapse videos of THP-1 infections with fluorescent *S. aureus* strains offered a more precise view of host cell morphologies and death during infection, as well as the emergence of staphylococci from individual macrophages. This is one of only a handful of studies that have used live-microscopy to study *S. aureus* induced host cell death (R. S. Flannagan et al., 2016; Kobayashi et al., 2010; Stelzner, Hertlein, et al., 2020; Stelzner, Winkler, et al., 2020; Yao et al., 2020). The analysis of videos generated here was carried out with manual annotation as it remains the most accurate reproducible form of analysis (Vicar et al., 2020) . In 2020, Vicar et al. published the first quantitative phase imaging (QPI) tool able to distinguish between the lytic and non-lytic types of cell death according to their end-point features and subtle changes in cell mass distribution. Unfortunately, micrographs still only have a 76% accuracy in detecting cell death when compared with manual annotation (Khmaladze et al., 2012; Pavillon et al., 2010, 2012; Vicar et al., 2020).

Baseline time-lapse analyses revealed a heterogeneous population of WT *S. aureus* infected macrophages over 24 hrs, including cell morphologies associated with highly activated states and cell death. The majority of infected macrophages adopted inflammatory cell death-associated pore induced intracellular trap

(PIT)-like structures over a 24-hr period. A much smaller proportion became apoptotic-like with a blebbing and shrinking morphology. PITs are an outcome of pyroptosis or necroptosis recently shown to be induced by the intracellular pathogen *Salmonella enterica* serovar Typhimurium in bone marrow derived macrophages (Jorgensen, Zhang, et al., 2016; Jorgensen et al., 2017; Jorgensen & Miao, 2015). To our knowledge this is the first time *S. aureus* has been directly linked to the onset of PIT structures. The escape of *S. aureus* into the extracellular environment was often physically limited, at least for some time, by the PIT membrane that balloons due to osmotic lysis. PITs are known to entrap viable bacteria and are conceptually similar to neutrophil extracellular traps (NETs) or macrophage extracellular traps (METs) that also form in response to *S. aureus* (Bhattacharya et al., 2018; Hoppenbrouwers et al., 2018; Shen et al., 2016)*.* PITs however confine bacteria that occupy an intracellular niche rather than extracellular pathogens (Jorgensen, Zhang, et al., 2016). Although PITs have not been shown to kill intracellular bacteria themselves, secondary phagocytes, for example, neutrophils, can efferocytose the corpse and effectively kill the bacteria residing within (Jorgensen, Zhang, et al., 2016). On rare occasions *S. aureus* filled PITs were observed to be efferocytosed by adjacent infected macrophages, and this activity was pronounced in glass chamber slide experiments where macrophages appeared to better cope with WT infections. PITs therefore have the potential to limit *S. aureus* dissemination if other viable phagocytes can clear them before bacteria disassociate (Jorgensen et al., 2017).

Within the WT infected macrophage population, individual cells adopted a PIT-like structure or apoptosis morphology at different times over 24-hrs, resulting in a multi-peak distribution of cell death. The initial large peak, around 2 hrs post infection, is attributed to intracellular activation of cell death as virtually no bacteria were in the extracellular environment at this point. The later peak is more likely linked to the increasing number of replicating bacteria escaping from host cells that produce high concentrations of pore-forming toxins (Alonzo & Torres, 2014; DuMont et al., 2013). Published investigations into *S. aureus*-host cell interactions often overlook the rate of cell death or time to cell death, a factor

that is hard to measure with methods based on endpoint or single time point analyses.

S. aureus is well known to activate apoptosis, pyroptosis and necroptosis pathways in macrophages (R. S. Flannagan et al., 2016; Kitur et al., 2015, 2016; Melehani et al., 2015; X. Wang et al., 2020; Wong Fok Lung et al., 2020; Yao et al., 2020). Two studies utilise live microscopy of infected macrophages (R. S. Flannagan et al., 2016; Yao et al., 2020). Flannagan et al. (2016) report quintessential apoptotic and necrotic cell death morphologies, importantly these infections were carried out with RAW murine macrophages and M-CSF-derived human macrophages. Yao et al (2020) captured lytic cell death under live microscopy characterised by bubbles protruding from THP-1 macrophages, which is consistent with the formation of inflammatory cell death pores on the membrane. The researchers suggest this resulted from pyroptotic cell death, although their investigations did not rule out the activation of the necroptotic pathway, which is known to exhibit similar morphologies (Dondelinger et al., 2014; Frank & Vince, 2019; Jorgensen, Zhang, et al., 2016; Shi et al., 2015). They also do not allude to the formation of PITs during lytic cell death, despite the presence of a small number of PIT-like structures entrapping bacteria in their published videos. An explanation for contrasting results could be the use of different *S. aureus* strains, unfortunately Yao et al. (2020) do not report the strain used. In addition, they activate THP-1 cells prior to infection by treatment of with IFN-γ and LPS (Yao et al., 2020), which was not employed in this project. Perhaps when macrophages are primed for efficient bacterial killing, PIT formation is less likely to happen.

The *M. tuberculosis* (Mtb) T7SS has also been linked to the onset of pyroptosis, necroptosis and apoptosis in primary monocytes and macrophages (Aguilo et al., 2013; Beckwith et al., 2020; Danilchanka et al., 2014; Pajuelo et al., 2018; J. Sun et al., 2015). Similar to our findings, Mtb ESX-1-associated cell death resulted in apoptotic bodies and swollen cell corpses captured during live-cell imaging (Beckwith et al., 2020). Some Mtb bacilli were lost into the medium immediately

after pyroptosis while the rest were trapped in the pyroptotic cells which were efferocytosed by neighbouring cells (Beckwith et al., 2020). Mtb studies also suggest T7SS factors have a temporal effect on cell death, with ESX-1 causing the onset of apoptosis or pyroptosis early on in macrophage infections (Aguilo et al., 2013; Aguiló et al., 2013; Beckwith et al., 2020).

With baseline macrophage infection dynamics established for WT JE2 *S. aureus*, T7SS mutant strains were assessed for differences in their interactions with macrophages. Colony count data and confocal imaging from antibiotic protection assays showed that macrophage uptake of *ΔesxC, ΔessC and ΔesxC-D* was similar to WT infections, which is consistent with previous T7SS focused studies (Cruciani et al., 2017; Dai et al., 2017; Korea et al., 2014). Despite this, time-lapse microscopy revealed differences in the time taken for mutant strains to initiate cell death-associated PIT-like structures and apoptosis morphologies. The early peak of these events induced in WT infections was absent with Δ*essC,* and considerably reduced with Δ*esxC* and Δ*esxC-D* infections. Notably T7SS mutants were not defective at causing cell death but peaks were shifted to later timepoints. This resulted in a population of mutant infected macrophages composed of more spindle/fried egg cells and rounded cells, morphologies associated with various degrees of cell activation early on in infection (De La Rosa et al., 2015; Heinrich et al., 2017; McWhorter et al., 2013). The majority of mutant infected macrophages eventually formed PIT-like corpses that entrapped *S. aureus* for some time, before escaping and forming microcolonies in a similar manner to WT.

To uncover which cell death pathways were responsible for the demise of macrophages during *S. aureus* infections we probed for the activation of key proteins in the necroptosis, pyroptosis and apoptosis pathways. Immunoblots showed that cleaved GSDMD and phosphorylated MLKL, two proteins sufficient and required for the execution of pyroptosis and necroptosis respectively (Dondelinger et al., 2014; Shi et al., 2015), are present in the population of WT infected macrophages. This along with the high numbers of PIT structures

observed in time-lapse microscopy suggests that pyroptosis and necroptosis are the main contributing cell death pathways during *S. aureus* infection of THP-1 cells. At early timepoints both Δ*essC* and Δ*esxC-D* mutants were unable to induce phosphorylated MLKL levels comparable to that of the WT, implicating secreted proteins EsxC, EsxB, EsxD, EsxA and EsaE as potential candidates for necroptosis stimulation in macrophages. Later during infection, Δ*essC* infections exhibited on average higher levels of c-GSDMD and p-MLKL than WT infections. In addition, the Δ*esxC-D* mutant induced an intermediate necroptotic and pyroptotic response, sometimes behaving like WT infections and other times like Δ*essC* infections. This could suggest that secreted protein EsxA, which is still present in Δ*esxC-D* mutants, has variable effects on cell death if it is not accompanied by one or more of the other secreted proteins (EsxC, EsxD, EsaE or EsxB). EsxC is a prime candidate for imposing a joint effect with EsxA , as together they have been shown to form heterodimers as well as and homodimers (Anderson et al., 2013). EsxC may itself be directly involved in secretion or be part of the secretion apparatus because it has been shown to reside in cell membrane and cell wall fractions of *S. aureus* (Anderson et al., 2013, 2017; Bobrovskyy et al., 2018; Cao et al., 2016; Kengmo Tchoupa et al., 2020).

Activation of the apoptotic pathway was also shown in all infections by the presence of cleaved caspase-8; however, this did not result in cleavage of caspase-3, implying apoptosis execution was not occurring at detectable levels in WT or mutant infections. In line with this, researchers have previously reported *S. aureus* engagement with all three of these cell death pathways in BMDMs and keratinocytes (Kitur et al., 2016). The same study showed that pyroptosis and necroptosis, but not apoptosis, were involved in cytotoxicity. A surprisingly large number of published reports on *S. aureus* infection fail to consider the contribution of more than one death pathway to cellular demise within a population or even within a single cell. Host cell death pathways are interweaved with multiple points of crosstalk, proving that cell death is a carefully regulated process which is guarded from foreign manipulation (Jorgensen et al., 2017; S. Kang et al., 2015; T. B. Kang et al., 2013; Kitur et al., 2016). The cross-talk between

151

necroptosis and pyroptosis suggests that both GSDMD and MLKL pores can occur at the same time (Conos et al., 2017; Evavold et al., 2018).

T7SS mutants were not defective at causing necroptosis in macrophages, but the promotion of this pathway appeared to occur later on in mutant infections. This provides evidence to suggest multiple staphylococcal factors contribute to the onset of necroptosis in macrophages. *S. aureus* toxins have also been implicated in the onset of necroptosis. In line with our findings, *S. aureus* mutants lacking *agr, hla , psm(α/β/hld), lukAB, pvl (lukSF), lukGH* have demonstrated a reduced capacity to induce necroptosis/necrotic cell death in live *S. aureus* assays, however, the deletion of these toxins does not completely eradicate cytotoxicity (Kitur et al., 2015; Kobayashi et al., 2010; Melehani et al., 2015; Pang et al., 2010; Ventura et al., 2010). It is quite possible that the promotion of necroptosis observed at later time-points in T7SS mutant infections was due to *Staphylococcus* toxin production.

We also carried out preliminary investigations with pharmacological inhibitors that target MLKL and results further solidified the notion that necroptosis is heavily involved in the T7SS induced cell death and the overall outcome of infection. The inhibition of caspases had little to no effect on the formation of microcolonies or distribution of cells death in WT and mutant infections on glass, suggesting caspases are not differentially activated by the T7SS. It should be noted that data was only collected from one independent experiment carried out on glass. Unfortunately, due to time restrictions infections were not carried out with pharmacological inhibitors on plastic.

Necroptosis is often observed as a backup cell death defence mechanism triggered when apoptosis is hindered, such as during pathogen infection (Brault & Oberst, 2017), Inhibition of caspase-8 protease activity is a main factor in the onset of lethal necroptotic signalling (Fritsch et al., 2019). Caspase-8 analysis here does not show any obvious signs of a T7SS effect on caspase-8 cleavage/activation at any timepoint. Perhaps individual cell analysis would

identify a subset of 'necroptosis ready' cells in which caspase-8 activity is low, effectively priming them for RIPK3-activation (Kearney & Martin, 2017). T7SS proteins may inhibit capase-8 activity by upregulating its binding partners such as cFLIP (Oberst et al., 2011). An intriguing hypothesis is the idea that host cells have evolved other 'trap doors' to induce necroptosis activation other than caspase-8 (Brault & Oberst, 2017). Previous T7SS studies in the USA300 background have implicated EsxA in delaying apoptosis in epithelial and dendritic cells, although, researchers did not shown activation of specific apoptosis pathway markers. It is very possible that the T7SS proteins have different effects in different host cell types. One hypothesis involves EsxA and other T7SS proteins targeting components of the apoptosis pathway, which macrophages may be able to rapidly detect, resulting in the onset of necroptosis. Meanwhile in epithelial cells EsxA manipulation may not trigger necroptosis and so *S. aureus* is successful at delaying cell death though apoptosis inhibition.

The *Mycobacterium tuberculosis* T7SS proteins have also been associated with inducing both caspase-independent cell death and pyroptosis in macrophages (Abdallah M. Abdallah et al., 2011; Beckwith et al., 2020; Pajuelo et al., 2018; J. Sun et al., 2015). Furthermore, Mtb has been shown to change the macrophage intracellular signalling landscape by upregulating MLKL, TNFR1, and ZBP1, whilst downregulating cIAP1, which established a strong pro-necroptotic milieu (Stutz et al., 2018). Mtb may additionally employ ESX-3 effector proteins to increase necroptosis or pyroptosis downstream of MLKL as EsxG and EsxH have been shown to directly interfere in recruitment of ESCRT proteins to membrane damage sites, thereby reducing membrane repair (Mehra et al., 2013; Portal-Celhay et al., 2016). The interference with membrane repair may be a characteristic retained by the staphylococcal T7SS because secreted proteins EsxA and EsxB have some homology with an ESCRT-III component named CHMP4B (Cruciani et al., 2017).

Necroptosis promotion by the staphylococcal T7SS could be though direct or indirectly interference with the necroptosis pathway. Many bacterial pathogens

are known to directly target cell death machinery for their own advantage, and often lead to a fine-tuned regulation of bacterial escape from host cells (Ashida et al., 2011). The bacterial gut pathogen, EPEC, utilises a type III secretion system to translocate NleB1 and NleF into host cells to inhibit caspase activation and subsequent apoptosis during infection (Pearson et al., 2013; Pollock et al., 2017). EPEC also delivers EspF and Map to host cells, which target the mitochondria and stimulate cell death by disrupting the mitochondrial membrane potential (Nougayrède & Donnenberg, 2004; Ramachandran et al., 2020). *Salmonella* Typhimurium induces apoptosis in gastrointestinal epithelial cells, which could limit inflammation during bacterial penetration of the gut (Wemyss & Pearson, 2019). But this action is dependent on host cell as during infection of macrophages *S.* Typhimurium induces pyroptosis, which activates host immunity. Crucially, the timing of macrophage pyroptosis seems to be spatiotemporally modulated by effectors translocated by SPI-1 and SP-2 type III secretion systems. By delaying macrophage pyroptosis, *S.* Typhimurium can replicate in a protected niche and use the cell to facilitate pathogenesis (Wemyss & Pearson, 2019). *Shigella* can even hijack host cell death crosstalk. The OspC1 effector protein blocks caspase-8 apoptosis and the host backup necroptotic cell death pathway is counteracted with OspD3, a protease that degrades RIPK1 and RIPK3 (Ashida et al., 2020). Cytoprotective signalling appears to be dominant during early bacterial replication within epithelial cells but at later stages is overwhelmed by pro-cell death signalling promoted by *Shigella*, thereby allowing the bacteria to escape and transit toward the lumen (Carneiro et al., 2009; Mattock & Blocker, 2017)

The type of cell death carried out during infection can play a crucial role in the resolution of *S. aureus* infections (Pidwill et al., 2021). Pyroptosis is well known to function as a proinflammatory death pathway as inflammasome activation and GSDMD pore formation function to release of IL-1β and IL-18 (Shi et al., 2015). The consequences of necroptosis are far more convoluted, some say this is a result of its origin as an inflammatory pathway and subsequent evolution into a death signalling pathway (Brault & Oberst, 2017). The complex contribution of

necroptosis signalling to the outcome of *S. aureus* infections has been outlined in a number of different studies. Researchers show that pharmacological and genetic perturbation of MLKL, RIPK1, or RIPK3 can clearly protect human and murine macrophages as well as neutrophils from USA300 and its secreted toxins (González-Juarbe et al., 2015; Greenlee-Wacker et al., 2014; Kitur et al., 2015; Kobayashi et al., 2010). Furthermore, genetic perturbation of RIPK3 in mice can clearly improve outcomes during experimental *S. aureus* skin, sepsis and lung infection (Kitur et al., 2015, 2016). Lack of RIPK3 correlated with limited production of IL-1β, activation of apoptosis, and accumulation of anti-inflammatory alveolar macrophages in the lung, which afforded protection from *S. aureus*-induced inflammatory damage. In contrast mouse infections with MLKL deletions demonstrated increased *S. aureus* persistence and increased lethality compared to WT, despite promotion of phagocyte recruitment and cytokine production (Kitur et al., 2016). Overall, execution of necroptosis during *S. aureus* infections is an essential component of the host response necessary to limit harmful inflammation (Kitur et al., 2016; Missiakas & Winstel, 2021). These previous studies bare many resemblances to results shown here as early necroptosis signalling correlated with increased cellular demise and cytokine production. In addition this project shows that promotion of necroptosis is correlated with increased PIT formation which is a host response known to improve clearance of bacteria (Jorgensen, Zhang, et al., 2016; Jorgensen & Miao, 2015).

The staphylococcal T7SS stimulation of the necroptotic pathway could be viewed as both a strategy to confer a bacterial advantage over host, or a strategy employed by the host to overcome infection. *S. aureus* is not an obligate intracellular pathogen, making cell death a less valuable option for host defence. Indeed, *S. aureus* can cause cell death in immune cells to successfully evade the host response (Heyman et al., 2013). Subverting cell signalling to necroptosis and elimination of key immune cells may result in premature termination of the cytokine responses such as IL-1β (Kearney & Martin, 2017). However, Both RIPK3 and MLKL have shown to trigger NLRP3-caspase-1-mediated IL-1β

maturation and secretion, proving necroptosis can be highly inflammatory (Conos et al., 2017; Gutierrez et al., 2017; Lawlor et al., 2015). In this chapter we demonstrated that T7SS proteins conferred *S. aureus* the ability to invoke a more potent and sustained IL-1β and TNF-α inflammatory cytokine response in macrophages. The immunogenicity characteristic of T7SS have also been well documented in murine models (Anderson et al., 2017; Ohr et al., 2017). Here, increased IL-1β release in WT infections compared to mutants was not reflected in caspase-1 activity, which introduces the possibility of the involvement of other IL-1β processing molecules, such as caspase-4 and -5 (Viganò et al., 2015).

In contrast to data presented here, Cruciani et *al.* (2017) reports an immunoregulatory effect of the T7SS proteins, as the deletion of secreted protein EsxB caused USA300 to promote the release of inflammatory IL-12, TNF- α, IL-6, and IL-1β by dendritic cells. Deletion of the single EsxB protein was not tested here but the Δ*esxC-D* mutant lacks EsxB along with other secreted proteins. Contrasting results highlights possible cell specific responses and may suggest individual or synergistic roles for T7SS proteins in immune response modulation. The roles of specific proteins in the onset of cell death and cytokine stimulation shown here are unclear. Complexity to this system is further increased by the possibility of T7SS effector proteins interactions (EsxA-EsxC, EsxB-EsxD) (Anderson et al., 2013).

In the context of general host-bacteria research we see that this chapter has highlighted multiple points of discussion with regard to commonly used methodologies and culture techniques. Traditional cytotoxicity assays failed to detect the same level of differences in cell death between WT and T7SS infections as time-lapse microscopy. Assays that identify cell death based on membrane integrity are perhaps not the most suitable method for bacterial infections because *S. aureus* can produce pore-forming toxins at sublytic concentrations making leukocytes leaky, irrespective of the effect of the T7SS (Alonzo & Torres, 2013). In addition, it has recently come to light that pore formation during necroptosis and pyroptosis can be repaired by ESCRT proteins leading to

downstream negative regulation of cell death (Gong et al., 2017; Rühl et al., 2018). Hence, the measure of cellular content leakage may not produce a true representation of cell death. Commonly used methods for apoptosis and lytic cell death detection tend to be focused on typical biochemical parameters such as visualization of phosphatidylserine exposure, DNA fragmentation and loss of plasma membrane integrity (L. Galluzzi et al., 2009; Lorenzo Galluzzi et al., 2018). Nevertheless, almost all these methods are based on colourimetric, fluorometric or endpoint visualization of the analysed parameter and can be categorized as indirect assays prone to producing misleading results (Cummings & Schnellmann, 2004; Vicar et al., 2020). It is important to use a combination of cell death detection methods as is presented in this chapter (Lorenzo Galluzzi et al., 2018).

For more than 20 years antibiotic gentamicin and lysostaphin protection assays have been the most widely used method to study intracellular *S. aureus* over extended periods of time (Fraunholz & Sinha, 2012; Gresham et al., 2000; Qazi et al., 2001). These assays rely on the ability of antibiotics to effectively kill all extracellular and membrane-bound bacteria and assume that the antibiotics used are unable to penetrate eukaryotic cell membranes to kill intracellular bacteria (Elsinghorst, 1994; J. H. Kim et al., 2019). As the T7SS modulation of host cell responses has been linked with bacteria residing in the intracellular niche (Cruciani et al., 2017; Korea et al., 2014), time-lapse experiments were also performed with lysostaphin to inhibit the extracellular growth of *S. aureus* over extended periods of time. Increased macrophage survival, motility and efferocytosis were observed in comparison to infections carried out without antibiotics. The significant differences observed between WT and T7SS with regard to early PIT onset and IL-1β and TNF-α response in antibiotic-free media were dampened in antibiotic conditions and overall distributions of cell death were dramatically changed. This suggests the presence of antibiotics changes infection dynamics in a way that masks the full intracellular effects of the T7SS.

Many publications have reported possible nonspecific killing of intracellular bacteria, modified infection dynamics and decreased eukaryotic cell death during extended gentamicin and lysostaphin protection assays (Drevets et al., 1994; R. S. Flannagan et al., 2016; J. H. Kim et al., 2019; Klein et al., 2006; Menashe et al., 2008; VanCleave et al., 2017). Phagocytes such as macrophages are highly pinocytic and continuously consume their fluid phase environment. Antibiotics in close proximity to phagocytes can be internalised and delivered to intracellular bacteria as demonstrated by Flannagan et al. (2016).

Macrophages are highly sensitive to cell culture conditions, which can play a major role in polarization (Aldo et al., 2013; Rostam et al., 2016). Time-lapse experiments revealed that THP-1 macrophage responses to *S. aureus* infections were drastically modified when cultured in RS washed glass chamber slides rather than Permanox plastic. WT infections of macrophages on glass surfaces resulted in little to no microcolony formation, whereas mutant infections on glass produced large microcolonies with CFU counts similar to those obtained from infections on plastic. The combination of glass culture surface and the presence of the full staphylococcal T7SS appeared to increase the macrophages' ability to limit *S. aureus* escape and extracellular replication. Individual infected macrophages responded to intracellular WT *S. aureus* in two distinct ways, either by early cell death or by retaining high motility and efferocytosis activity throughout the 24-hr experiment. When *esxC, essC or esxC-D* were removed from *S. aureus*, macrophages more consistently responded to infection with cell death leading to more bacteria escaping to the extracellular milieu.

Glass has been shown to cause more extensive cell differentiation during mesenchymal stem cell and C2C12 myoblast cultures than Permanox plastic (Ho et al., 2006; Murray et al., 2016). This has been attributed to the notable hydrophilic characteristics of glass and hydrophobic nature of Permanox (Murray et al., 2016). Macrophages have been observed to polarize towards an "M1-like" phenotype on hydrophilic surfaces and towards "M2-like" phenotypes on hydrophobic surfaces (Rostam et al., 2016). Here we show non-infected THP-

1 cells cultured on glass and plastic had distinct ROS profiles and differences in morphological features, but they cannot be defined to specific polarization states without further investigation. Macrophage polarization can be categorized into "M1" inflammatory or "M2" wound healing states dependent on macrophage stimulation, although, these are outdated labels that limit the description of macrophages (Martinez & Gordon, 2014). The presence of macrophages with specific polarization states are known to impact abscess formation in response to *S. aureus* dermal mouse infection and can influence pro- or anti- inflammatory responses (Asai et al., 2010; Werz et al., 2018). Increased ROS production found in macrophages grown on plastic may suggest a more stressed cell with a predisposition towards cell death (Forman & Torres, 2001), but could equally represent a population more polarized towards an M1 inflammatory state (Tan et al., 2016).

Collectively, results from this chapter provide evidence for T7SS mediated induction of early necroptosis in macrophages resulting in increased PIT formation. Specific interactions between T7SS proteins and host proteins remain unknown and so it is still unclear if manipulation of cell death is a primary or secondary impact of the T7SS. The consequence of delayed cell death is not immediately obvious during these *in vitro* experiments as *S. aureus* escape and microcolony formation over 24 hrs is comparable between WT and mutants. This is a prime example of the limits of *in vitro* investigations. Without observing *S. aureus* infection in the context of the 3D tissue structure with multiple cell types and complex immune system, it is difficult to understand whether the T7SS proteins confer an advantage to the host or enables *S. aureus* to exploit this pathway to combat macrophages. The next chapter focuses on the influence of the *S. aureus* T7SS in the context of the more complex whole organism by utilising murine skin infection models.

4 Chapter 4: Role of the staphylococcal T7SS in infection *in vivo*

4.1 Introduction

Mouse models of infection have consistently identified the staphylococcal T7SS as a virulence factor. In pneumonia models and nasal colonisation assays T7SS machinery in RN6390, COL and Newman strains was required to support nasal colonization and increased mortality (Ishii et al., 2014; Kneuper et al., 2014). In intravenous bacteraemia models, deletion or disruption of several staphylococcal T7SS proteins, both secreted and membrane associated (EsxA, EsxB, EsxC, EsaD, EsaE, EssB), caused infections with reduced bacterial load and less abscess formation in kidneys (Anderson et al., 2011, 2017; Burts et al., 2005, 2008; Dai et al., 2017; Lopez et al., 2017; Y. Wang et al., 2016). Only one research group has employed a skin abscess model for the investigation of T7SS factors and this was carried out with mutants in the ST398 background, a prominent Chinese strain (Dai et al., 2017; Y. Wang et al., 2016). They showed deletion of EssB and EsxX caused smaller skin abscesses, less infiltration of inflammatory cells and decreased skin tissue destruction when compared to WT.

Staphylococcal infections in humans can occur at sites where there is a breach in skin barrier function e.g. wound or surgical site infections or without apparent breaches, for example at hair follicles (folliculitis) or superficial lesions (impetigo) (Tong et al., 2015). MRSA strains of the USA300 lineage are the cause of the vast majority of community-acquired skin infections in the United States and so are often investigated in murine skin models (H. K. Kim et al., 2014; Talan et al., 2011). Here we utilize a mouse skin abscess model for the investigation of the impact of WT USA300 JE2 and isogenic mutant strains Δ*essC*, Δ*esxC-D* on bacterial colonization, dissemination, abscess formation and macrophage recruitment.

4.2 Results

4.2.1 Role of T7SS in *S. aureus* survival in whole mouse blood

Human blood serum and fatty acids, which are found extensively in blood, are both potent stimulators of the staphylococcal T7SS expression (Burts et al., 2008; Lopez et al., 2017). *S. aureus* can regularly escape local infection sites and disseminate via the bloodstream which can lead to sepsis. In addition, whole blood is a rich source of leukocytes including monocytes, therefore, the survival and replication of *S. aureus* WT and T7SS mutant strains were assessed in whole murine blood. Whole blood aliquots taken from a total of 6 wildtype ICR CD1 mice were incubated with approx. 3.5 x 10^6 CFU/mL of WT JE2, Δ*essC* or Δ*esxC-D S. aureus*, bacterial counts were enumerated at 2 hrs and 4 hrs and are shown in figure 4.1. No differences were seen between WT and T7SS mutants' ability to survive or replicate in murine blood. When compared to inoculums bacteria levels initially lowered at 2 hrs, followed by a approx. 200-fold increase by 4 hrs in all cases.
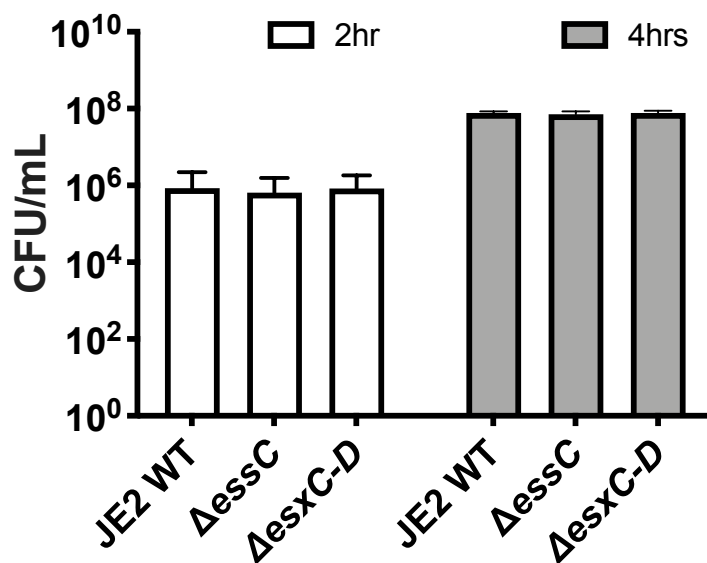
Figure 4.1: EssC and EsxC-D proteins do not impact *S. aureus* survival in whole mouse blood.

Aliquots of fresh heparinised blood from a total of 6 wildtype ICR CD1 mice were incubated with rotation with approx. 3.5×10^6 CFU/mL of WT JE2, $\Delta essC$ or $\Delta esxC\text{-}D$. After 2 hr or 4 hrs bacterial numbers were enumerated by CFU counting.

4.2.2 Role of T7SS in a skin infection model

A murine skin abscess model involves a localised infection which can be visually monitored over time due to the formation of skin lesions. The localised skin infection also enables monitoring of immune cells recruitment, local immunostimulatory effects and dissemination which is a suitable extension of the *in vitro* work shown earlier in this project. The effect of low-dose (10^6 CFU) and a high-dose (10^7 CFU) inoculums of *S. aureus* were investigated in skin abscess models using WT JE2, Δ*esxC-D* and Δ*essC* strains. Two different doses were used in order to optimise this model for use with USA300 JE2 and isogenic T7SS strains, doses were chosen from preliminary data collected using this model.

4.2.3 Low dose infections

For low-dose infections cohorts of (n=10) BALB/c mice were intradermally injected on both flanks with 2.5-3 x 10^6 CFU of either *S. aureus* WT or T7SS mutant strains. Four days after challenge, mice were euthanized and the average load of *S. aureus* per gram of skin abscess, liver and spleen tissue was determined. Surprisingly, both mutant strains were more successful than the WT at establishing a skin tissue infection over the 4 days with the Δ*essC* mutant having a significantly higher CFU count (Figure 4.2). Furthermore, bacteria from liver and spleen tissue were recovered in more mice infected with Δ*essC* and Δ*esxC-D* mutant strains than WT and at higher CFUs (Figure 4.2).
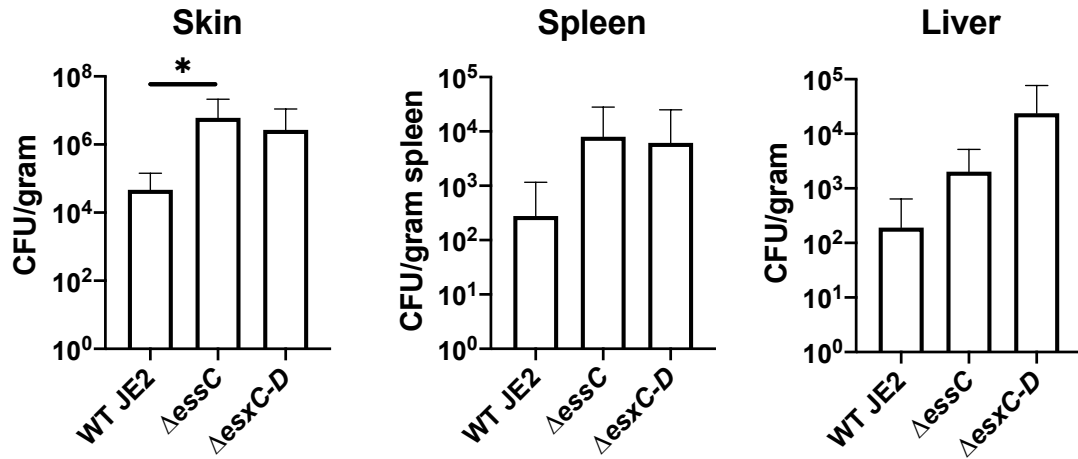
Figure 4.2: T7SS proteins decrease *S. aureus* colonisation and recovery from distal sites during low dose skin infection models. For low-dose skin-abscess model, mice (n=10/group) were infected on both flanks with a total of 10^6 CFU of WT, $\Delta essC$ or $\Delta esxC$-D mutants. After 4 days, bacteria were enumerated in the skin, spleen and liver by colony counts. Graph shows mean$\pm$ SD, statistical analysis was carried out using a Kruskal-Wallis test for skin (H_3=6.325, P=0.0423), spleen (H_3=4.545, P=0.103) and liver H_3=2.068, P=0.356). Results of Dunn's multiple-comparison test is shown on graph (* P < 0.05).
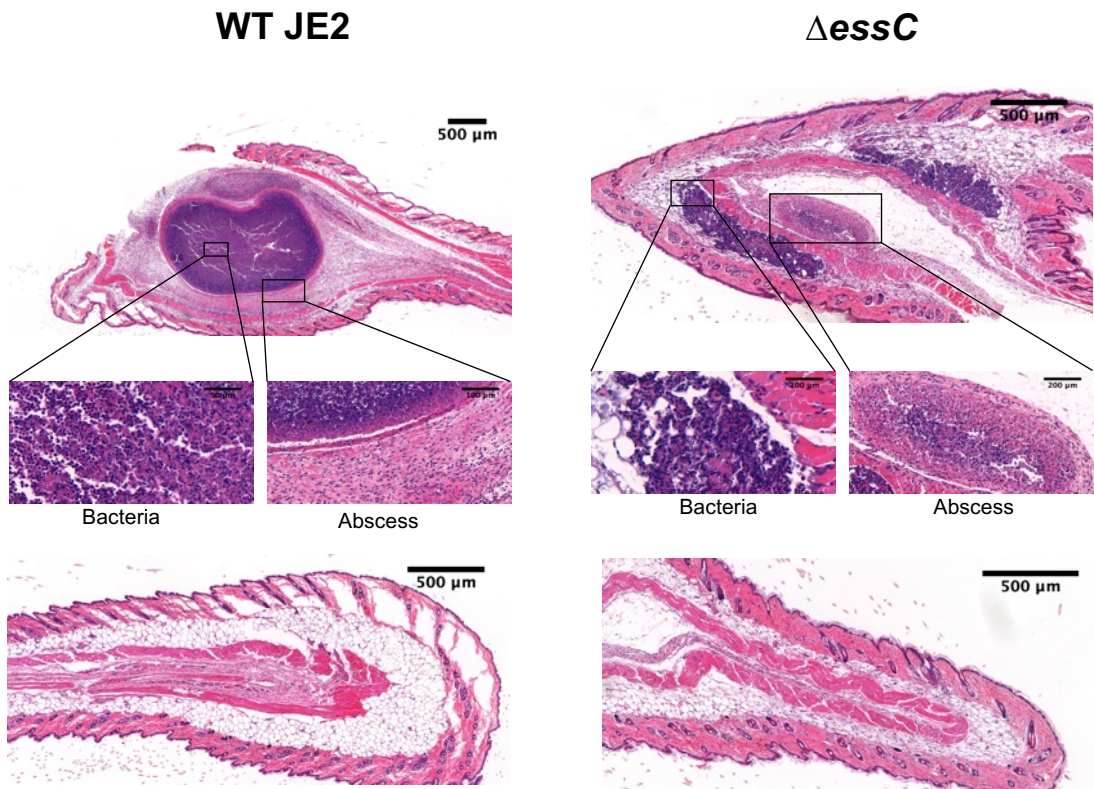
Figure 4.3: Possible role for T7SS in abscess formation.

For low-dose skin-abscess model mice (cohorts of n=10) were infected on both flanks with a total of 10^6 CFU of WT, $\Delta essC$ or $\Delta esxC\text{-}D$ mutants. After 4 days tissue from site of infection was excised, fixed in PFA, embedded, sectioned at 5μm intervals then stained with hematoxylin and eosin (H&E). Top images show WT bacteria encased in mature abscess and $\Delta essC$ not encased in an abscess, zoomed in images show accumulation of bacteria and fibrous abscess walls. Bottom images show representative images of tissue in which bacteria had largely been cleared. n=3/group, two images per group shown.

No visible necrotic lesions were seen on the skin of WT and T7SS infected mice after 4 days of infection. Skin tissue from the flanks of WT and Δ*essC* infected mice was sectioned and stained with hematoxylin and eosin (H & E) (Manchester Histology Facility, Faculty of Biology, Medicine and Health). This revealed high variance in the ability of mice to clear bacteria in both WT and mutant infections. Of 3 skin sections per group that underwent histological staining only 1 from each infection group had visible bacterial infection after 4 days. In these tissue samples WT *S. aureus* was observed to be encased within a large mature abscess while in the case of Δ*essC*, masses of bacteria did not appear to be encased in a fibrous capsule and were located in more than one area of the tissue (Figure 4.3).

4.2.4 High dose infections: dose-specific effects of T7SS

For high-dose infections, BALB/c mice (n=5/group) were intradermally injected on both flanks as previously with 2.3-2.75 x 10⁷ CFU. Due to the significant decline in health, mice were euthanized after 1 day. In contrast to the low-dose infection, mice infected with the WT strain showed notably higher CFU counts in skin abscess, spleen and liver compared to the T7SS mutant strains (Figure 4.4A). Mice infected with the T7SS mutant strains produced necrotic skin lesions whereas WT infections did not (Figure 4.5A). A 1-day low dose skin infection with BALB/c mice (n=5) was also performed to enable direct comparison with the 1-day high dose infection, which confirmed a lower number of CFU for WT-infected mice as seen in the 4-day infections, although the differences in CFU in the spleen and liver were not significant (Figure 4.4B).

Histological staining of WT and Δ*essC* mutant high-dose 1-day infected skin indicate a more severe infection in the case of the WT which aligns well with the bacterial CFU obtained from skin. The WT infected mice produced much more substantial abscesses than Δ*essC* as indicated by increased cell infiltration and increased deposition of fibrous material in the vicinity of the bacterial infection, the Δ*essC* mutant *S. aureus* were also concentrated to smaller areas (Figure 4.5B). Cell recruitment to the infection site is likely immune cells such as neutrophils, which is indicative of early abscess formation (Kobayashi et al., 2015).

4.2.5 Macrophage recruitment

Immunohistochemical analysis of a small number of thin-sectioned tissue was used to assess the abundance of anti-F4/80-positive macrophages at the site of *S. aureus* high-dose infection in the skin. Preliminary data suggests that when compared to skin infected by WT *S. aureus*, the Δ*essC* mutant displayed increased infiltration of macrophages across skin sections (Figure 4.6A). Macrophages were also recruited to the infection site by WT but to a lesser extent. Both infections caused the formation of macrophage clumps (figure 4.6B). Thus, the Δ*essC* mutation not only affects the establishment of *S. aureus* infection at high doses but may also impact the ability of staphylococci to manipulate cellular recruitment.

A

B
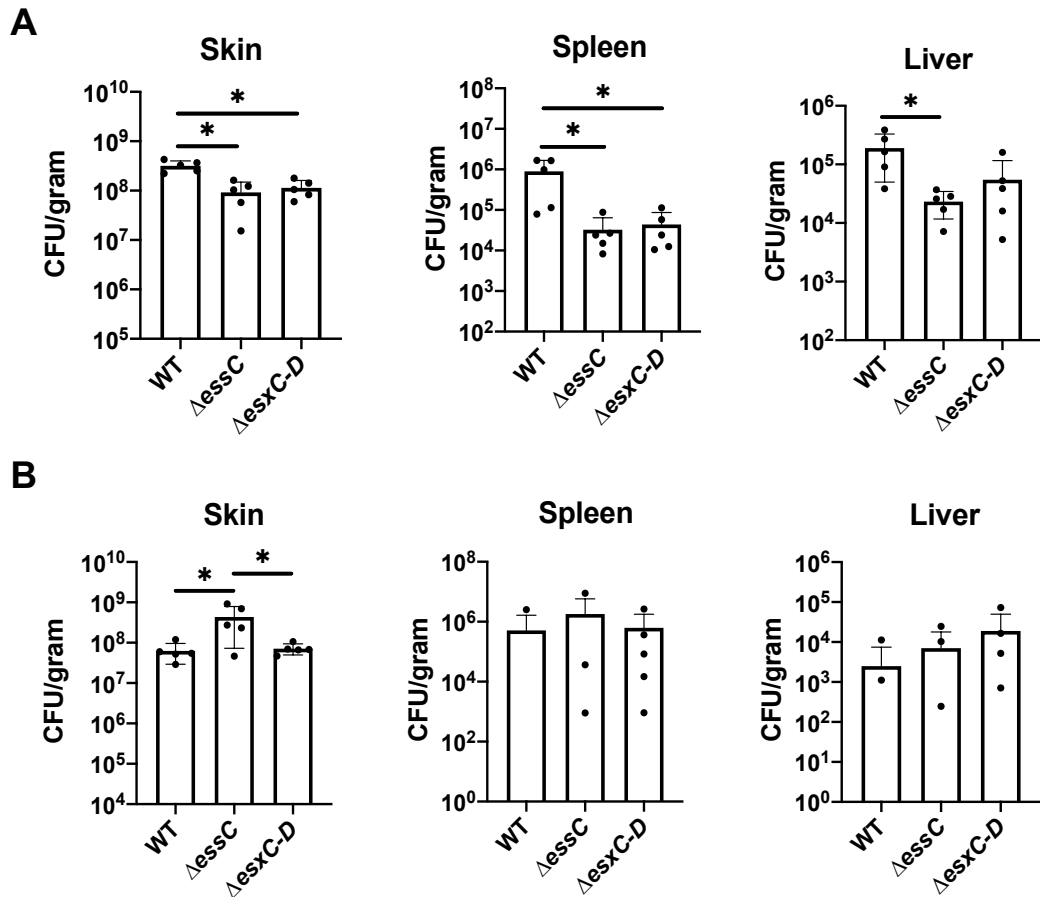
Figure 4.4: Dose specific effect of *S. aureus* T7SS mutants in skin abscess models.

Skin-abscess model mice (cohorts of n=5) were infected on both flanks with a high dose or low dose of WT, Δ*essC* or Δ*esxC-D* mutants. After 1-day bacteria were enumerated in the skin, spleen and liver by colony formation. (A) CFU counts from high dose (10^7) mouse infections. Graphs show mean± SD. Statistical analysis was carried out using a Kruskal-Wallis test for skin (H_3=9.620, *P=0.0018*), spleen (H_3=7.940, *P*=0.011) and liver (H_3=7.22, *P*=0.019). Dunn's multiple-comparison test results are shown on the graph (* P < 0.05). (B) CFU counts from low dose (10^6 CFU) mouse infections. Graphs show mean± SD. Statistical analysis was carried out using a Kruskal-Wallis test for skin (H_3=4.340, *P*=0.0251), spleen (H_3=3.904, *P*=0.142) and liver (H_3=1.744, *P*=0.452. Dunn's multiple-comparison test results are shown on graph (* P < 0.05).
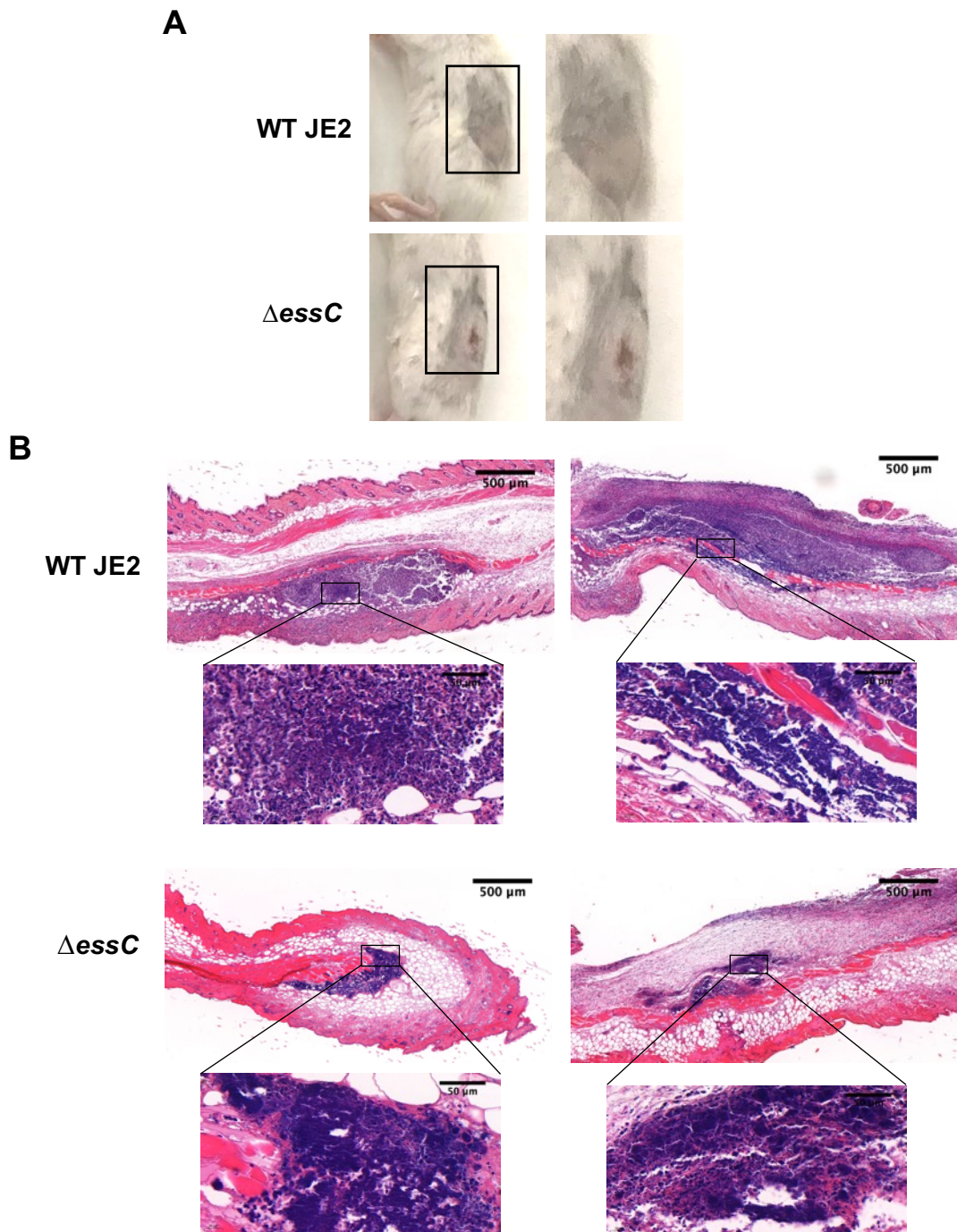
Figure 4.5: T7SS increases cell recruitment to infection site.

(A) Representative images of mouse skin at site of injection of high-dose infections showing visible necrotic lesions (B) Mouse skin at site of infection from high-dose 1-day infections were fixed in PFA, embedded, sectioned at 5µm intervals then stained with hematoxylin and eosin (H&E) to visualise nuclei (purple) and extracellular matrix/cytoplasm (pink). Zoomed in images show accumulation of bacteria, 2 biological replicates shown, n=3.

169
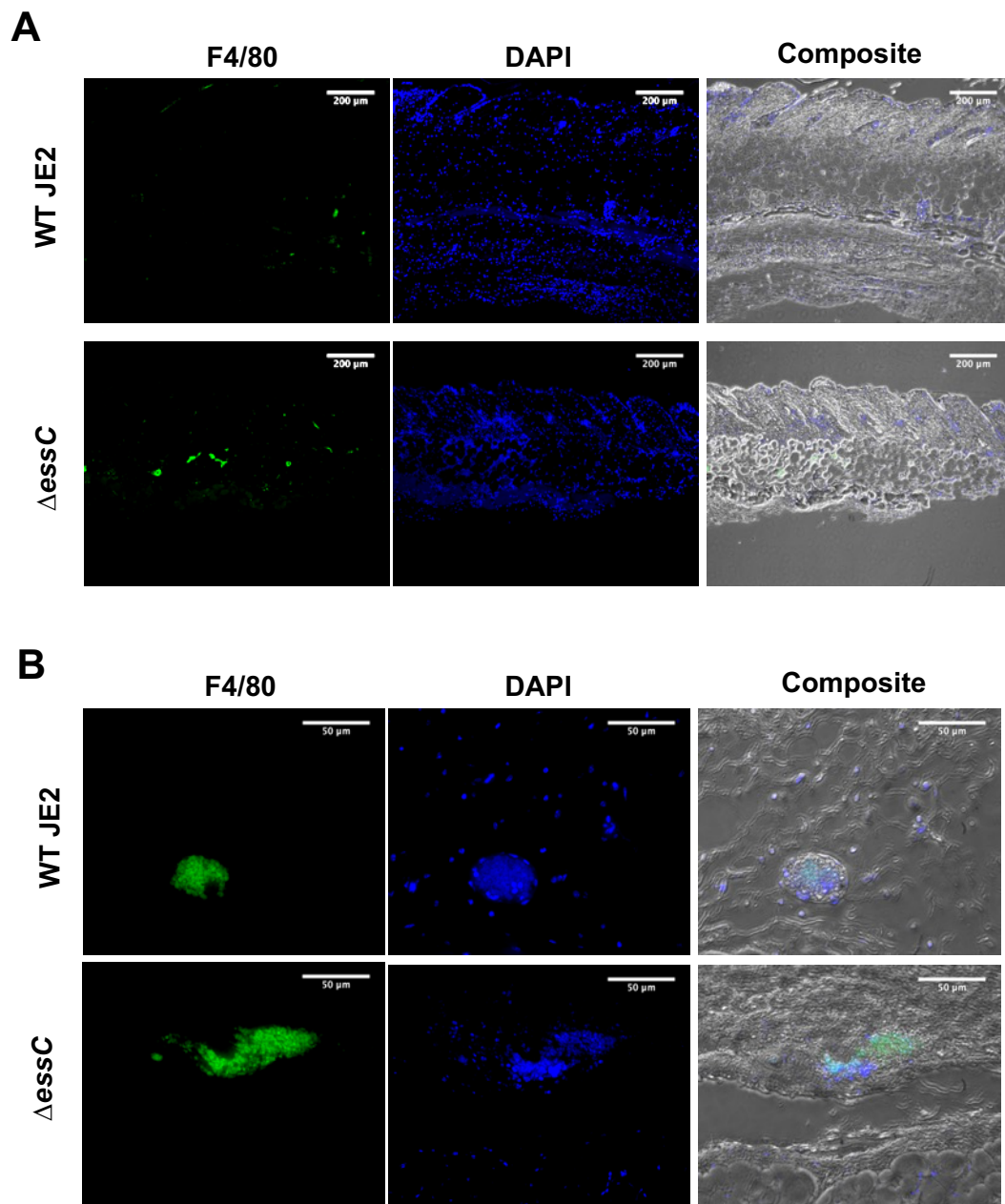
Figure 4.6: Staphylococcal T7SS may suppress macrophage infiltration into mouse skin.

(A) Mouse skin abscesses from high-dose 1-day infection were fixed in PFA, embedded, sectioned at 5µm intervals then incubated with F4/80 antibody, a macrophage-specific marker (green) then DAPI (blue). Magnification x 10, n=2. (B) Images of F4/80 positive cell clumps in sectioned tissue magnification x 40.

4.3 Discussion

A murine skin abscess model provides a localised infection site in which to investigate bacterial colonisation, monitor infection progression, determine bacterial spread and observe localised host responses. *S. aureus* is a prominent cause of SSTIs therefore this was a well-suited model to evaluate the effect of T7SS proteins on staphylococcal infection. Surprisingly this model has only been employed by one group in staphylococcal T7SS studies which investigated the EsxX and EssB proteins of the emerging Chinese *S.aureus* ST398 isolate in a high dose (10^7 CFU/mL) skin infection (Dai et al., 2017; Y. Wang et al., 2016). Researchers found strains lacking these proteins induced visible abscess that were significantly smaller than those caused by the WT. In pneumonia models with high inoculums of 10^8 CFU, knockout of the entire 12 gene *ess* loci or just the *essC* transporter in strains RN6390, COL or Newman significantly decreased bacterial colonisation and virulence (Ishii et al., 2014; Kneuper et al., 2014). Similarly, in bacteraemia models (10^6- 10^9 CFU) strains lacking EsxA, EsxB, EsxC, EsxH, EsaE, (EssE), EsaD (EssD) and EssB displayed defects in *S. aureus* virulence (Anderson et al., 2011, 2017; Burts et al., 2005, 2008; Dai et al., 2017; Lopez et al., 2017; Ohr et al., 2017; Y. Wang et al., 2016).

Here studies with high and low doses were carried out to optimise the skin abscess model. In high-dose models where CFU matches previous T7SS associated skin abscess studies, the presence of the T7SS proteins significantly increased the survival and spread of *S. aureus* in the skin compared to strains lacking EssC and EsxC-D (EsxC, EsxB, EsxD, EsaE). Previous T7SS focused skin abscess models did not report enumeration of bacteria but did show through histological examination that Δ*esxX* and Δ*essB* infections had decreased infiltration of immune cells and skin tissue destruction compared to WT which is in line with the histological examination presented here (Dai et al., 2017; Y. Wang et al., 2016). Interestingly, in the project formation of visible necrotic lesions occurred only during T7SS mutant high-dose infections and not in the WT. Earlier studies investigating the effect of *S. aureus* induced cell death in a mouse skin

model show significantly larger necrotic regions forming on mice that lacked *MLKL*, a key element of the necroptotic signalling pathway (Kitur et al., 2016). The same study shows MLKL -/- infected mice recruited more macrophages and PMNs to the primary skin lesion (Kitur et al., 2016), our preliminary immunohistochemistry examination showed increased macrophage infiltration across Δ*essC* infected tissue and Anderson et al. (2017) also report a T7SS mutant strain (Δe*ssE* USA300) caused an abundant infiltration of macrophages within kidneys while WT attracted macrophages strictly around the kidney abscesses during intravenous infections. Together could support the notion that T7SS dependent promotion of necroptosis, as observed during *in vitro* macrophage studies, may have a substantial effect on the outcome of real infection.

In stark contrast to high-dose skin abscess infections, low-dose infections demonstrated that the presence of the T7SS was detrimental to the survival of *S. aureus* in the skin compared to strains lacking EssC and EsxC-D (EsxC, EsxB, EsxD, EsaE) and over 4 days T7SS mutants were more successful at spreading to distal sites. This may be due to T7SS elicited host responses as WT was encased in a quintessential abscess with fibrous capsule after 4 days of infection while Δ*essC* *S. aureus* was not. It is vital that histological staining of more biological replicates and control tissue is completed to conclude but high-dose 1-day experiments also showed possible defects in T7SS ability to promote early abscess characteristics such as dramatic recruitment of host cells, likely leukocytes, to the infection site leukocytes (Kobayashi et al., 2015). This is consistent with decreased abscess formation observed in kidneys and skin of mice infected with T7SS protein deletion mutants as compared to WT (Anderson et al., 2011, 2017; Burts et al., 2005, 2008; Ohr et al., 2017).

Abscesses are known to be a defensive host response to staphylococcal invasion, without fibrin deposits and abscess formation healthy tissues are less well shielded from the disseminating microbe although bacterial replication may still continue within the abscess (Cheng et al., 2011). Host IL-1β release has been shown to be essential for host abscess formation in mice since adoptive transfer

of IL-1β expressing neutrophils was sufficient to restore impaired abscess formation in *S. aureus*-infected IL-1β- deficient mice (Cho et al., 2012). In chapter 3 results from *in vitro* assays showed Δ*essC S. aureus* infection of macrophages conferred decreased IL-1β response and earlier work reported a similar diminished IL-1β profile in serum of mice infected with Δ*essE* (Anderson et al., 2017). This dampened pro-inflammatory signalling may contribute to the reduced abscess response. Furthermore, a lack of abscess formation may explain the observed increase spread of ΔessC and Δ*esxC-D* to distal host tissue.

To confirm dose specific effects, low-dose infections were also carried out for 1-day. A heightened success in colonisation of skin was seen once again with the Δ*essC* mutant. Unlike 4-day experiments however, levels of Δ*esxC-D* mutant in the skin was similar to WT. This is consistent with *in vitro* data in that the Δ*esxC-D* mutant behaved in some regards like the WT and in others like the Δ*essC* mutant, suggesting unique functions or effects of individual T7SS proteins during infection.

Inoculums of similar CFU to those used in low dose infections here were employed in T7SS focused studies only in invasive models using strain Newman (Burts et al., 2005, 2008). All other models utilized in T7SS studies, including skin abscess, pneumonia and bacteraemia use typically high inoculums (Anderson et al., 2013; Ishii et al., 2014; Kneuper et al., 2014; Lopez et al., 2017; Ohr et al., 2017). Mouse models typically require a high inoculum dose (10^7-10^9) of *S. aureus* to ensure infection is reliably established (H. K. Kim et al., 2014; Salgado-Pabón & Schlievert, 2014). It is highly improbable that such large doses are mirrored in human infection situations, consequently, high dose models are less physiologically relevant. Subcutaneous injection of a relatively large inoculum is known to prevent the identification of virulence factors acting at early stages of disease such as adherence to skin structures and invasion across epidermal layers (H. K. Kim et al., 2014). Despite the caveats the importance of high dose models for discovery of basic disease parameters still stands but the relative

merits of the available models should be considered before relying on them to make useful conclusions.

During initial stages of *in vivo* infection *S. aureus* undergoes a population bottleneck, from which only a few bacteria can go on to establish abscesses (Boldock et al., 2018; McVicker et al., 2014; Pollitt et al., 2018). The bottleneck has been attributed to macrophages and neutrophils but is overcome when high inoculums are administered, suggesting these immune cells have simply been overwhelmed, leading to less bacterial uptake by host cells and consequently more extracellular bacteria (Boldock et al., 2018; Pollitt et al., 2018). It was further shown that a CFU inoculum of 10^5 *S. aureus* supplemented with peptidoglycan can augment *S. aureus* infection in the same way a typical high inoculum can (Boldock et al., 2018), suggesting that past a certain bacterial number peptidoglycan of *S. aureus* is the main cause of pathophysiology observed in mouse models. High-dose models may therefore mask or change the effect of the T7SS, which is shown to be involved in disrupting host responses after *S. aureus* internalisation by host cells, including macrophages as shown here (Cruciani et al., 2017; Korea et al., 2014).

High densities of extracellular bacteria have the potential form biofilms and previous work has indicated that increased biofilm formation may mask the effect of the T7SS in pneumonia models. Kneuper et al. (2014) revealed that the strain SA113, which is able to form more robust biofilms due to a mutation in *agr*, showed no difference in nasal colonisation upon deletion of the full *ess* locus but Δ*ess* mutants in the background RN6390 and COL had significantly decreased colonisation compared to their corresponding WT strain. Furthermore, work in our lab recently showed that planktonic T7SS mutants are more sensitive to unsaturated fatty acids (Kengmo Tchoupa et al., 2020), which are abundant in skin. This may explain why in high-dose infections, where more bacteria likely remain extracellular and exposed to fatty acids, T7SS mutants survive less well as compared to WT.

Overall, this chapter demonstrates that T7SS imposes a significant effect on *S. aureus* colonisation of the skin and bacterial spread to other tissues, which changes according to inoculum dose, although, high-dose studies which may overwhelm the function of macrophages and neutrophils in initial colonisation, should be interpreted with caution.

5 Chapter:5 The design and characterisation of a microfluidic infection model

5.1 Introduction

Mouse models have led to important advancements in our understanding of host-*S. aureus* interactions, as well as to the identification of key virulence factors and potential treatment strategies for *S. aureus* infections, however many treatments developed through mouse models fail to show efficacy in human clinical trials, particularly vaccine trials (Salgado-Pabón & Schlievert, 2014). Several factors could contribute to the disconnect between mouse and human infection outcomes, for example the high infectious dose required for mouse studies, differences in the constitution and function of the immune system of mice and humans, species-specific staphylococcal toxins and immune evasion molecules; as well as species-specific staphylococcal adhesins and nutrient acquisition systems (Mrochen et al., 2020).

An artificial model that can mimic the physiology and pathophysiology of the human organs and tissues is pivotal to better understand *S. aureus* interactions within our body and can accelerate the process of vaccine development. An emerging platform which has the potential to bridge this gap is organ-on-a-chip technology (Baddal, 2019). The concept of an organ-on-a-chip was pioneered by the Wyss institute where devices were fabricated to simulate human organ-level functions and disease using one or many microfluidic channels (Schultze et al., 2010a). Human cells can be compartmentalizing into microchambers and dynamically perfused to continuously supply nutrients and remove waste and intends to emulate an authentic biological response of cells. Consequently, organ-on-a-chip devices containing human cells can remain stable for many weeks allowing for long term studies (Schultze et al., 2010a; Zamprogno et al., 2021). Microfluidic platforms can be interfaced with various microscopic, flow cytometry, genomic and proteomic techniques to investigate a broad range of

molecular and cellular events. This approach has made it possible to micro-fabricate models of blood vessels (Hasan et al., 2015) lung and airways (Benam et al., 2016; Huh et al., 2010), liver (Bhise et al., 2016), brain (Dauth et al., 2017), gut (Kim et al., 2013, 2012) and kidney (Jang et al., 2013k ; Wilmer et al., 2016) among other tissues. A number of these models have been employed in the study of host-pathogen interactions (Baddal & Marrazzo, 2021) some are detailed in Figure 5.1, but this is a grossly underused platform for bacterial focused studies, with only a handful of organ-on-a-chip models reported with the use of *S. aureus* (Deinhardt-Emmer et al., 2020; J. J. Kim et al., 2019; Pappelbaum et al., 2013). *S. aureus* is a predominant cause of chronic respiratory infections that require hospitalisations (Tong et al., 2015) but chronic infections in mouse models are challenging to establish and alternative models are required (H. K. Kim et al., 2014; Salgado-Pabón & Schlievert, 2014) In an attempt to provide an alternative study platform to investigate the effects of T7SS in chronic *S. aureus* infection an airway-blood vessel-on-chip was designed, fabricated and tested for its suitability.
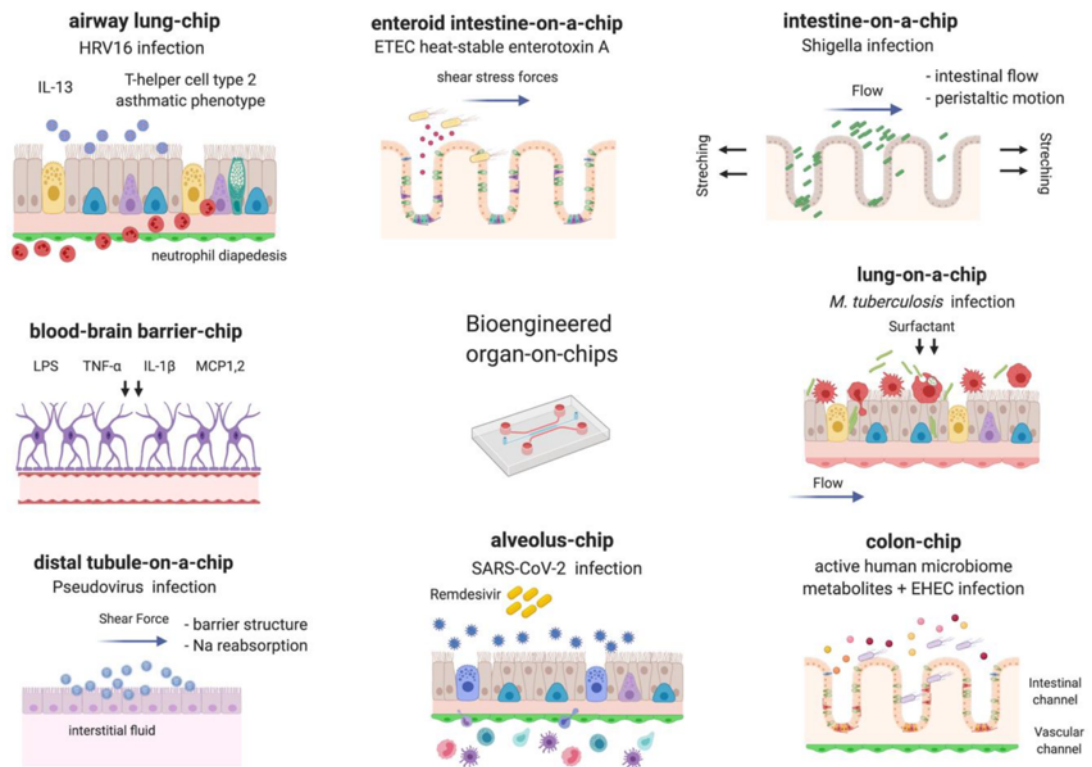
Figure 5.1: **Examples of microfluidic organ-on-chip platforms used in host-pathogen interaction studies.**

Image from Baddal, 2020.

Some of the most important features of organ-on-chips is the replication of a physiologically realistic ratio of cell mass from one tissue to another and the ability to apply flow rate that generate shear stress (Ergir et al., 2018). Shear stress is the mechanical force induced by the friction of liquid against the apical cell membrane (White & Frangos, 2007). *In vivo*, several adherent cell types are exposed to mechanical shear stress such as endothelial and epithelial cells and this drag force works on commensal and pathogenic microorganisms (Galbraith et al., 1998; J. W. Kim et al., 2017; Soyer & Duménil, 2011). Within this project, the design, fabrication and characterisation of a microfluidic airway-blood vessel interface was carried out with the intension of using this to investigate gain insight on the effect of shear stress on *S. aureus*-host interactions, specifically adhesion, invasion and bacterial spread. In this chapter, a combination of governing equations of microfluidics and experimental measurements are used to assess the suitability of an organ-on-a-chip design, robustness of device, fluid behaviour, suitable fluid flow rates/shear stress and identifies areas for design improvement.

5.2 Results

5.2.1 Design and fabrication of a microfluidic airway-blood vessel model

In contrast to previous lung-on-chip devices that include stacked microfluidics channels my design incorporated two main channels for cell culture side-by-side, with connecting channels between them essentially creating a porous wall that allows for cell interactions between monolayers as shown in Figure 5.2. It was designed such that HUVEC endothelial cells would reside in one channel and A549 lung epithelial cells in the other, overall, it represents an airway-blood vessel tissue interface. The intended use of the model is to investigate dynamic host pathogen interactions by introducing *S. aureus* and *S. aureus* T7SS mutants via liquid flow followed by tracking of bacterial- host cell infections with live phase contrast and fluorescent microscopy. The design has the potential to be made more complex with the addition of immune cells and 3D extracellular matrix-like scaffolding.

Similar to other organ-on-a-chip devices, PDMS was chosen as the material for fabrication of the airway- blood-vessel interface. PDMS has good biocompatibility, gas permeability, low auto-fluorescence, optical transparency and can be easily prototyped, (McDonald & Whitesides, 2002). To obtain the desired features of the microfluidic channels by casting onto PDMS, the reverse of the features, also known as the negative mould, was made through a process called photolithography. Photolithography refers to the transfer of patterns through a mask onto a photosensitive chemical, called photoresist, as it sits on a silicon wafer. Designs for the channels were drafted with a vector-based software and negatively printed on acetate sheets such that chip designs were transparent and the rest of the sheet was opaque. Several different designs of the channels, as detailed in Table 5.1. and Figure 5.3A, were included to examine which dimensions were achievable with photolithography and which provided a good model for cell culture.

Each main channel had a circular inlet to introduce fluid flow via tubing and an outlet to remove fluid flow via tubing, both with a diameter of 2 mm. The width and length for the main channel, 500 μm and 70 μm, were chosen by incorporating knowledge of bronchiole physiology (J. W. Kim et al., 2017) and prior knowledge from other lab members on successful growth of cells in microfluidic devices. The height:width ratio of 1: 6.66 also satisfied microfluidic device design guidelines set out by Lake *et al.* (2015) which suggest acceptable aspect ratios (height:width) between 1: 10 < x < 4: 1. Any PDMS channel made less than 1:10 will likely to sag in the middle, any channel greater than 4:1 is unstable and prone to collapse (Figure 5.3B). In addition, during photolithography photoresist features may fuse if they are too close together. The major concern was finding the correct and achievable dimensions for connecting channels as these need to be very small to maintain cell monolayers and have minimal effect on fluid flow, while also enabling cell-cell interactions. The width of the connecting channels was on the cusp of the resolution achievable with the acetate sheet during photolithography (5μm), so robustness of the resulting photoresist masks and eventually the PDMS chips were rigorously evaluated.
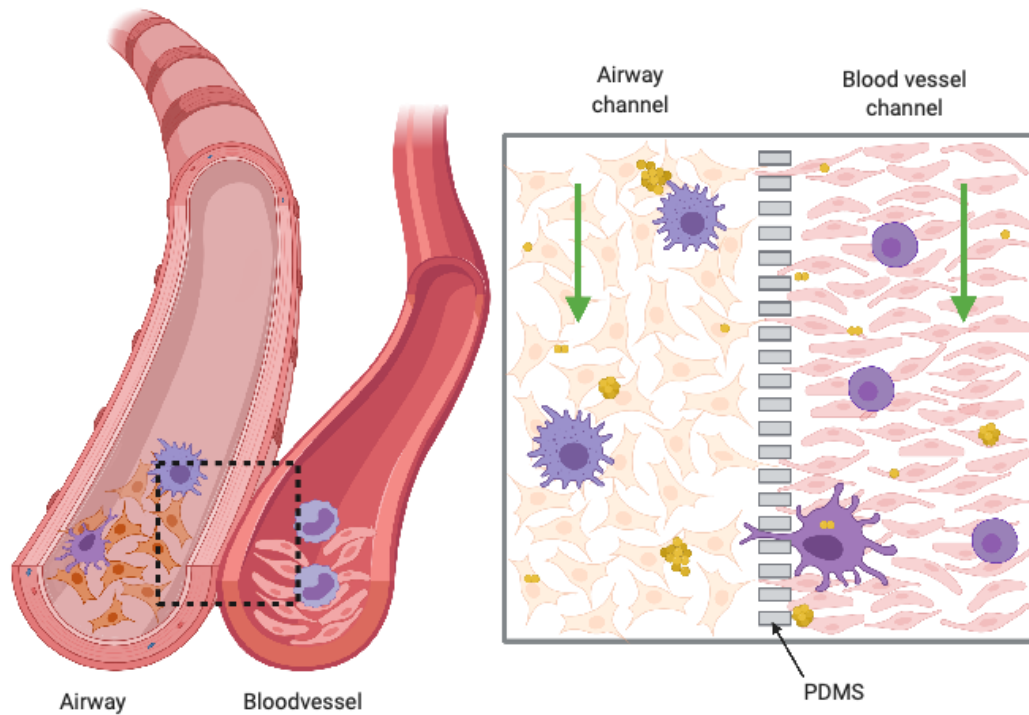
Figure 5.2: Schematic of microfluidic airway-blood vessel-on-chip. The airway-blood vessel interface diagram shown on the left is modelled on the right as two adjacent and connected microfluidic channels. Epithelial and endothelial cells occupy the Polydimethylsiloxane (PDMS) main channels which are connected via smaller PDMS channels that essentially form a porous wall. Host cells are able to interact through connecting PDMS channels while maintaining distinct monolayers. *S. aureus* (yellow) can be flowed into the model as well as immune cells such as macrophages (purple). Green arrow show direction of media flow. Host-pathogen interactions and infection dynamics can be captured with live phase contrast and fluorescent microscopy.
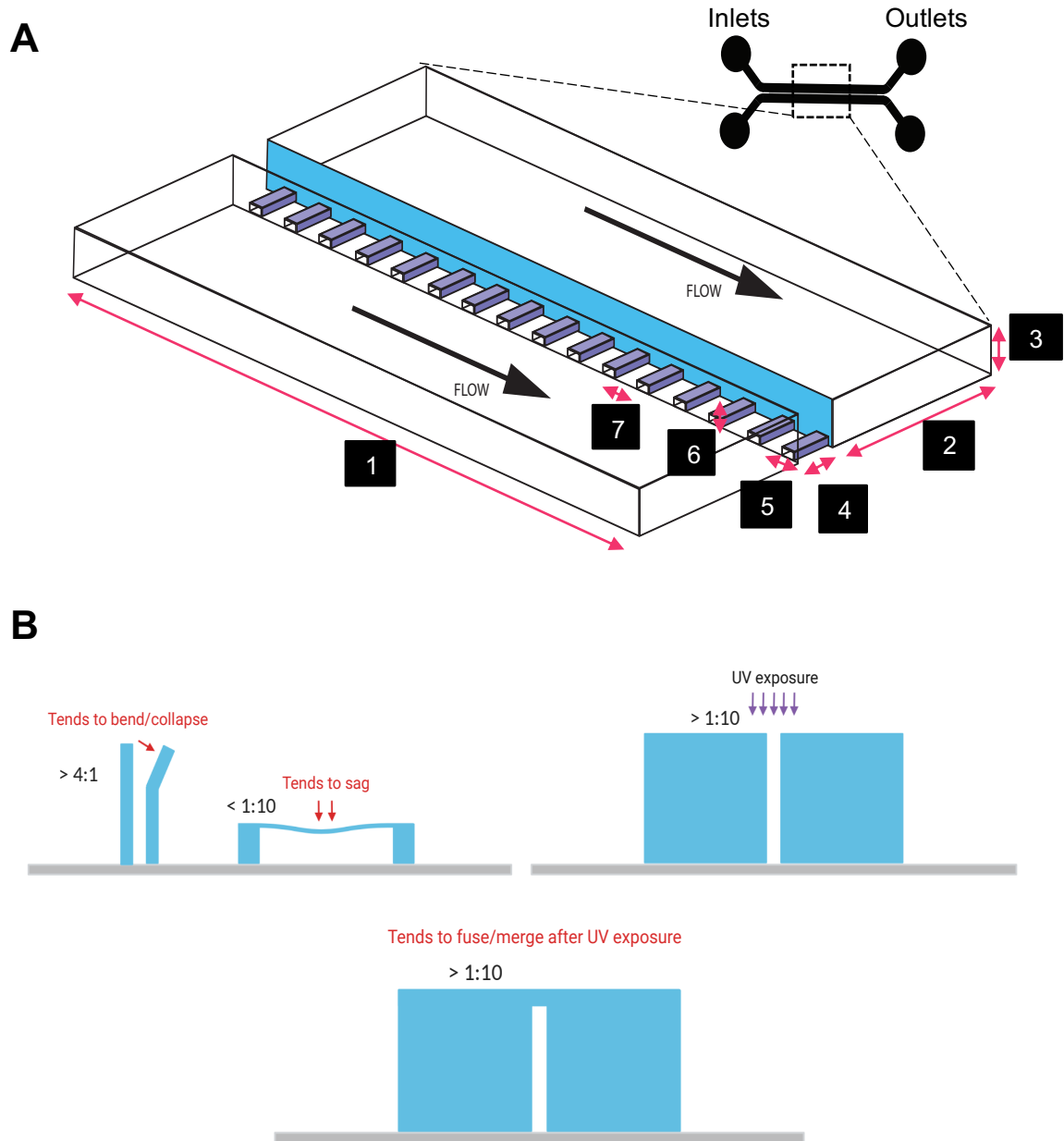
Figure 5.3: Airway-blood vessel-on-a-chip design and 3D schematic.

(A) An airway-blood vessel-on-chip design which was printed on acetate sheets and zoomed in 3D schematic of resulting PDMS chip. Numbers correspond to dimensions listed in Table 6.1. 1=Length of main channel; 2=Width of main channel; 3=Height of main channel; 4=Length of connecting channel; 5=Width of connecting channel; 6=Height of connecting channel; 7=Space between connecting channels. (B)   PDMS design considerations. Ideal aspect ratios (height:width) are 1: 10 < x < 4: 1. Figure based on Lake et *al.* 2015.

Table 5.1: Dimensions for different airway-blood-vessel-on-chip designs.

Design ID	Main channels			Connecting channels			
	Length [mm]	Width [µm]	Height [µm]	Length [µm]	Width [µm]	Height [µm]	Space between [µm]
A1	11	500	70	50	5	~10	10
A2	11	500	70	50	5	~10	20
A3	11	500	70	50	5	~10	40
A4	11	500	70	50	8	~10	40
A5	11	500	70	50	8	~10	20
B1	11	500	70	30	5	~10	10
B2	11	500	70	30	5	~10	20
B3	11	500	70	30	5	~10	40
B4	11	500	70	30	8	~10	40
B5	11	500	70	30	8	~10	20

The photolithography method used to create the airway-blood-vessel-on-a-chip is illustrated in Figure 5.4. As connecting and main channels were designed to be two different heights, designs for each were printed onto different acetate sheet masks. The first acetate mask was used in conjunction with photolithography methods to create photoresist positive moulds of the smaller connecting channels then the second mask was aligned on top and used to create positive photoresist moulds of the main channels either side of the connecting channels. Alignment of the second acetate sheet proved to be difficult and often failed due to limitations of microscope stage movement sensitivity (Figure 5.5A), therefore alignment guides had to be included on acetate sheets in the second round of designs. Optimisation of photoresist UV exposure was required as high level of cross-linking created stress on the resist which was relieved by deforming the SU-8 photoresist layer (Figure 5.4B).
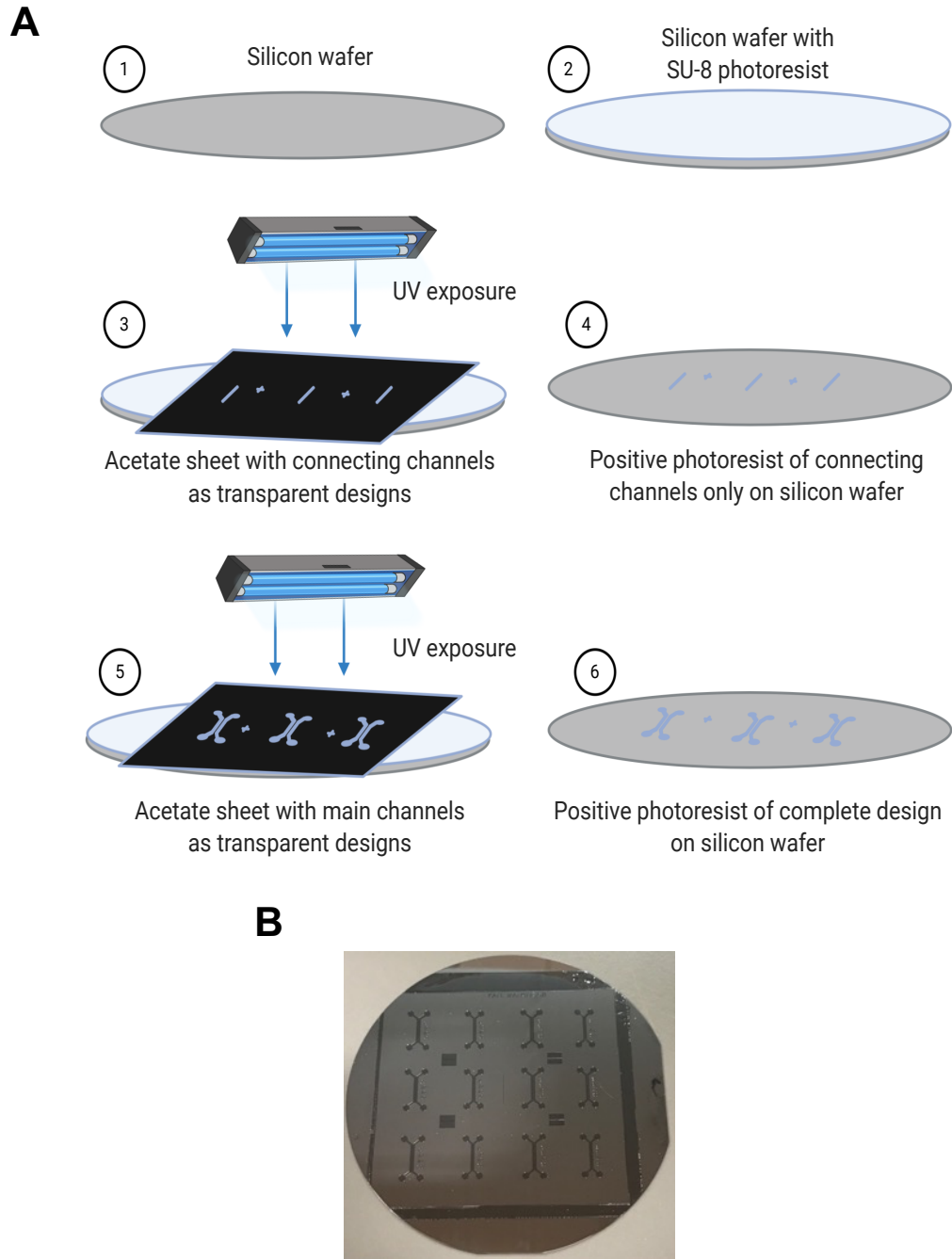
Figure 5.4: Fabrication of the airway-blood vessel microfluidic channel master mould using photolithography.

(A) Photolithography method to make the master mould. (1) A silicon wafer is cleaned and (2) SU-8 photoresist is spin coated on top to make a layer with a height ~ 10 μm. (3) After baking, an opaque acetate sheet with transparent drawings of connecting channels is placed on top of the photoresist and exposed to UV light. Photoresist UV dependent cross-linking occurs only in transparent

areas. (4) Non-cross-linked photoresist is washed away leaving the hardened photoresist in the shape of the connecting channels. (5) Another layer of photoresist is spun on top to make a layer of height 70 μm, photoresist is baked and an acetate sheet with transparent main channel designs is placed on top and aligned. UV exposure occurs again. (5) Non-cross-linked photoresist is washed away leaving the complete positive master mould for the microfluidic channels. (B) Final photoresist moulds on silicon wafer each with different connecting channel dimensions.

When alignment was successful positive moulds of main channels, inlets and outlets had high-quality well-defined side profiles (Figure 5.5D and E). Connecting channels with a width of 8 μm or 10 μm appeared to be robust however 5 μm width channels collapsed and fused (Figure 5.5C). Designs with larger spaces between each connecting channel (20 μm and 40 μm) were well defined but 10 μm spacing caused collapsed photoresist.

PDMS channels created from the master mould designs A5 and B5 provided distinct and robust channel profiles (Figure 5.5D and E). Soft lithography-based methods were then used to mould PDMS to the photoresist positive features. Resulting PDMS chips were bonded to glass slides via oxygen plasma treatment which forms an irreversible seal by a covalent siloxane (Si-O-Si) bond. This resulted in tightly sealed channels which enabled water to flow from inlet to outlet without leakage (Figure 5.5F). The PDMS channels made from design B5 offered a structure that more resembled the desired porous wall due to the shorter length of connecting channels, i.e., the space between main channels, therefore the B5 master mould was carried forward and used to create PDMS chips for circuit resistance determination and velocity profile experiments as detailed in the next sections.
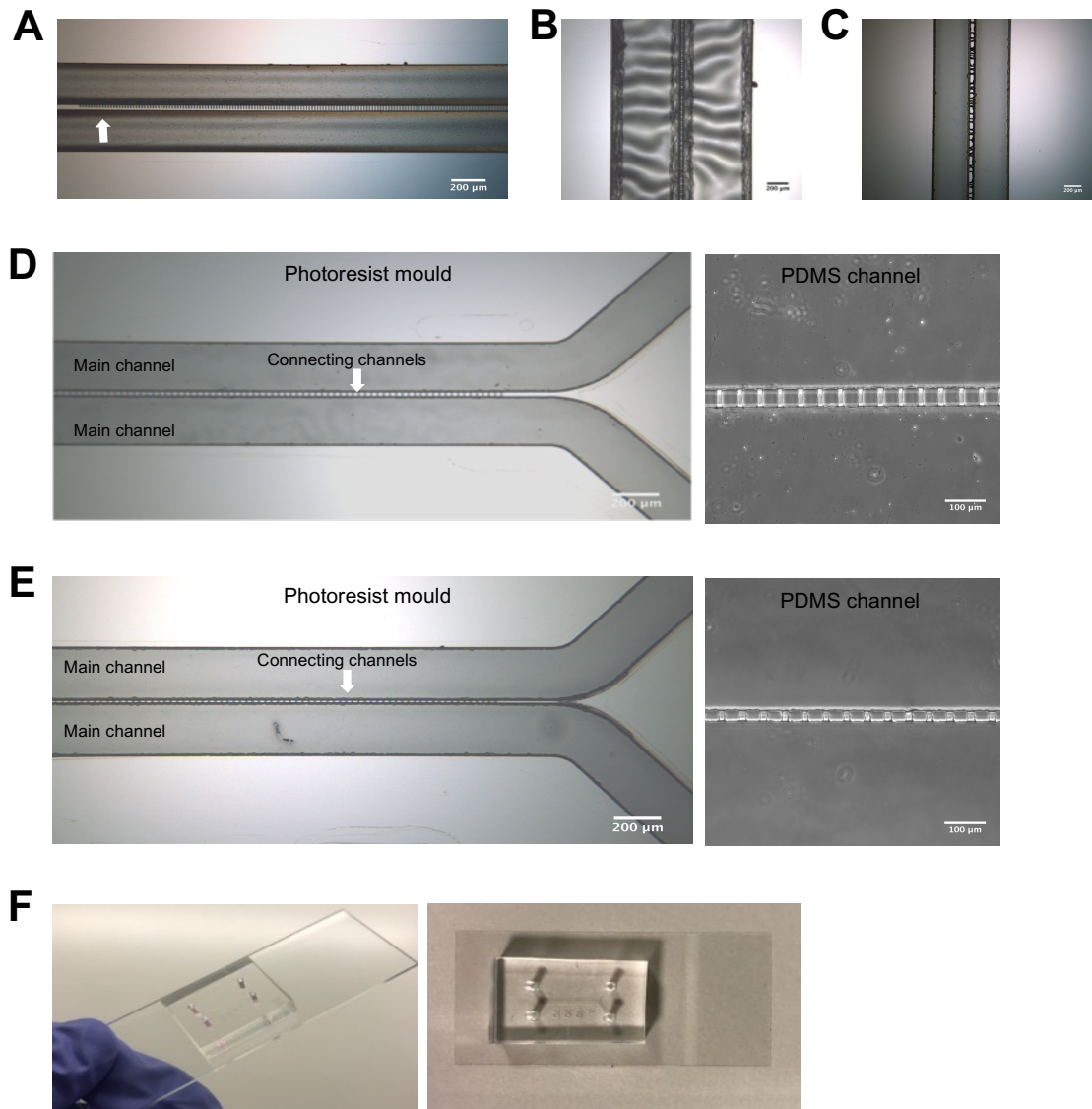
Figure 5.5: Photoresist master moulds and resulting PDMS airway-blood vessel-on-a-chip.

(A) Microscope image of photoresist mould on silicon wafer, white arrow shows misalignment of main and connecting channels. (B) Photoresist mould overexposed with UV. (C) Photoresist mould with collapsed connecting channels (D) Microscope image of photoresist mould A5 including connecting channels 50 μm in length and resulting PDMS channels from the mould. (E) Photoresist mould B5 with connecting channels 50 μm in length channels and resulting PDMS channels. (F) PDMS airway-blood-vessel-on-chip mounted on glass microscope slide.

188

5.2.2 Optimising circuit resistance

The physics of microfluidics is a branch of fluid dynamics in which we consider fluids that are confined in structures of micrometre scales. Microscale fluid flow behaviour is governed by a set of equations known as the Navier-Stokes equations (Bruus, 2014). A key parameter in the Navier-Stokes equations is the Reynolds number. The Reynolds number is a dimensionless ratio of inertial forces ($\rho V L$) and dynamic viscous forces (η) that is expressed as

$$R_e = \frac{\rho V L}{\eta} \qquad (1)$$

The mechanical response of fluid to pressure forces depends on the relative magnitude of the inertial response to the viscous response, so the Reynolds number is a useful characterization of any flow obtained (Bruus, 2014). In microfluidic devices viscous forces are highly significant therefore the Reynolds number is low and flow is laminar flow (Grigoriev, 2011). According to the Navier-Stokes equations a Poiseuille flow is achieved when a pressure-driven steady-state laminar flow occurs through a long straight microchannel (Bruus, 2014). For this type of flow, the volumetric flow rate (Q) is directly related to the pressure drop (or driving pressure) ΔP and resistance (R) in the equation

$$Q = \frac{\Delta P}{R} \qquad (2)$$

Resistance causes both the flow rate and pressure to drop making it a very important component in generating a steady low flow rate. The hydraulic resistance (R) for a channel with a rectangular cross-section is a function of the geometry of the microchannel and the dynamic viscosity of the fluid (η) which can be calculated with the following approximation equation,

$$R = \frac{12\eta L}{h^3 w} \qquad (3)$$

where *L, h* and *w* are the length, height and width of the microchannel respectively (Bruus 2011). Organ-on-chips are notorious for creating very low resistance in a circuit as their wide dimensions are designed to be compatible with cell culture. If required resistance in the form of serpentine channels or specialised resistance tubing can be added into the circuit. When adding multiple in-line channels that each exert resistance in one circuit the total resistance created can be calculated using the following in-parallel rule

$$\frac{1}{R_{Total}} = \frac{1}{R_1} + \frac{1}{R_2} \tag{4}$$

To begin a simple microfluidic circuit was assembled to include the following fundamental components: a microfluidic pressure pump, a reservoir of fresh media, a microfluidic channel and a reservoir for waste media all connected with minimal lengths of 0.02-inch internal diameter tubing (Figure 5.6A). The hydraulic resistance exerted by this simple circuit, without added resistance, was theoretically calculated using equation 3 and 4 and measured experimentally. Results are displayed in Table 6.2. Resistance was evaluated experimentally by recording pressure increase and corresponding flow rates. When pressure is plotted against flow rate (Figure 5.6C) the slope of the trend line gives the measure of resistance as described by equation 2.

As expected, the basic microfluidic circuit with only the airway-blood-vessel-on-a-chip channel created very little resistance resulting in inconsistently high flow rates in which small incremental increases could not be achieved (Figure 5.6C). A resistance microfluidic chip in the form of a long thin serpentine channel, with dimensions (20 µm) and width (300 µm) but long length (70 mm) as shown in Figure 5.6B, was incorporated into the circuit. Table 5.2 and Figure 5.6B show how this channel dramatically increased resistance due to its small height and enabled a more continuous flow increase over time.
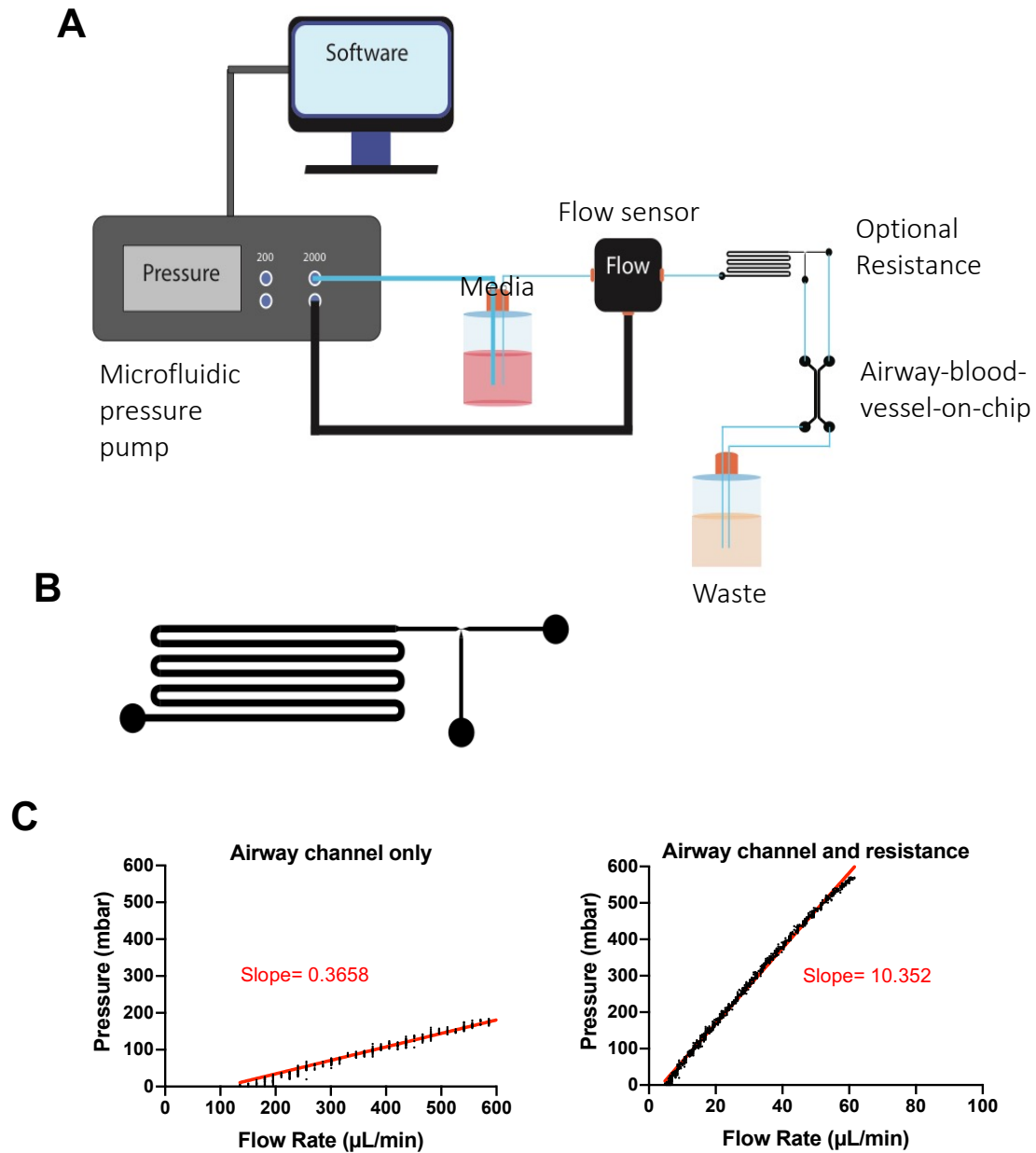
Figure 5.6: Optimising resistance in the microfluidic circuit.

(A) Schematic of microfluidic circuit with optional resistance incorporated before the airway-blood vessel channel. (B) Schematic of serpentine channel used to create resistance, approximate dimensions are height 20 μm, width 300μm and length 70 mm. (C) Example of pressure and flow rate measured in a microfluidic circuit with airway-blood-vessel-on-a-chip only or airway-blood-vessel-on-a-chip plus resistance chip, trend line and corresponding slope are shown in red, n=3, one representative experiment shown.

Table 5.2: Theoretical and experimental measurements of the resistance in microfluidic circuits.

	Resistance mbar/(ul/min)	
	Airway-on-chip only	Resistance channel + airway-on--chip
Theoretical	0.15	7.81
Measured	0.37 ± 0.04	10.63 ± 0.42

Theoretical pressures required for the initiation of specific flow rates in the airway-blood vessel channels with and without the resistance chip were calculated and are shown in Table 6.3. In circuits with just the airway-blood vessel channel flow rates listed in this table could not be achieved experimentally due to limitations of the pressure pump, however when resistance was added desired flow rates were achieved with the predicted pressures. Importantly the resistance chip also increased the range of pressures that can be utilized to achieve steady flow rates by approximately 25-fold (Table 6.3). This stopped the occurrence of large jumps in flow rate and inconsistent readings (Figure 5.6C).

Table 5.3 Pressure required to achieve specific flow rates in the microfluidic circuit with and without resistance. Calculated using slopes from pressure verses flow rate plots (Table6.2).

Flow rate (μL/min)	Pressure (mbar)	
	Airway-blood-vessel-on-chip only	Resistance channel + airway-blood-vessel-on-chip only
5	1.85	51.8
10	3.7	103.6
20	7.4	207.2
40	14.8	425.2
Range	12.95	321

5.2.3 Experimental velocity profiles of vertical plane

In a Poiseuille flow the basic velocity distribution across the channel varies parabolically across the shortest dimension of the channel, commonly the height of the microchannel (Bruus, 2015). Figure 5.7A demonstrates Poiseuille flow in microfluidic channels. The distribution of the average velocity across the channel width, or as the device is viewed from above, is largely unchanged, except for regions near the walls where no-slip boundary conditions are employed (Bruus, 2015). Velocity profiles are important to characterise and understand how cells, bacteria or molecules will move when flowed through the channel. The experimental determination of velocity profiles was required here as the airway-blood-vessel channels had small holes in their walls which may disrupt the characteristic Poiseuille parabolic velocity profiles.

Velocity can be measured in this circuit by recording objects flowing through the channel over time, here spherical fluorescent colloids with a diameter of 1 μm, similar to the dimensions of *S. aureus* were used. Colloids travelling in the *x* direction or length of the channel over 11 different heights (*z*) were recorded using fluorescent imaging techniques. The velocity of the colloids in the interrogation field was determined using single particle tracking software, when plotted velocities formed the characteristic parabolic shape, suggesting the holes are too small to disrupt laminar flow (Figure 5.7B).

A
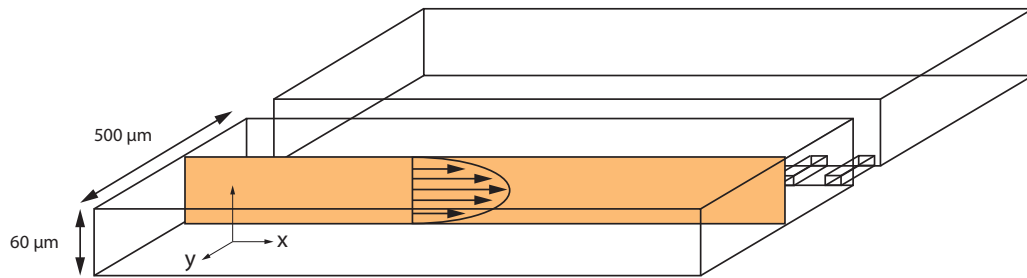
B
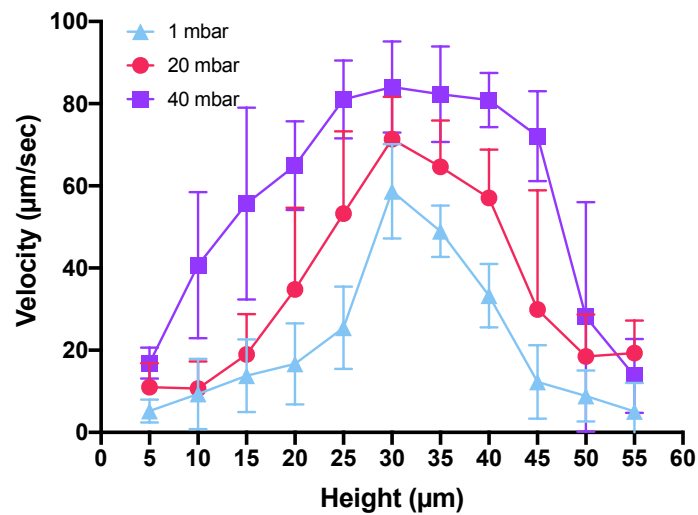
Figure 5.7: Velocities across the height of the airway-blood vessel-on-a-chip are distributed parabolically.

(A) Schematic of the parabolic flow across the z direction in a microfluidic channel. (B) Velocities of 1 µm colloids flowing through the airway-on-a-chip circuit with a serpentine resistor channel at different channel heights. Colloid particle velocities were tracked using TrackMate ImageJ plugin. Graph shows average velocities $\pm$ SD, n=3.

5.2.4 Host cell responses to microfluidic flow

The fundamental aim of an organ-on-a-chip is to culture host cells or tissue interfaces in a way that represents a realistic functional unit of an organ. In order to prepare the PDMS airway-blood-vessel chip to be a receptacle for cell culture the PDMS chip, mounted on a glass slide and connective microfluidic tubing were UV treated for sterilization followed by coating with fibronectin. A549 lung epithelial cells and/or human umbilical vein endothelial cells (HUVECs) were flowed into the fibronectin primed channels using a syringe and left in static conditions to adhere and replicate over-night Figure 5.8A. For initial characterisation and optimisation of cell culture in channels a simplified model was used with only lung epithelial cells seeded into both channels. Under low flow conditions (20µL/mL) epithelial cell bodies remained in the channel they were initially seeded in, but apical cellular extensions protruded into connecting channels Figure 5.8B.

In Poiseuille flow, an estimation of shear stress (σ) exerted on microfluidic walls, or cell monolayers, by fluid flow can be generated using the following equation

$$\sigma \ = \ \frac{6Q\eta}{wh^2} \qquad (5)$$

Where Q represents volumetric flow rate, η is dynamic viscosity (estimated to be 0.001 Pa.s) and w and h are the width and height of the microchannel (Berg, 2018). Table 6.4 shows shear stress generated by different flow rates within the airway-blood-vessel-on-chip channels. Physiological wall shear stress levels range between 5-80 dyne/cm^2 in pulmonary blood vessels (M. Li et al., 2009) and approximately 0.5–3 in airways at rest breathing (Sidhaye et al., 2008) which are achievable with the dimensions and flow rates generated in the airway-blood vessel-on-a-chip.
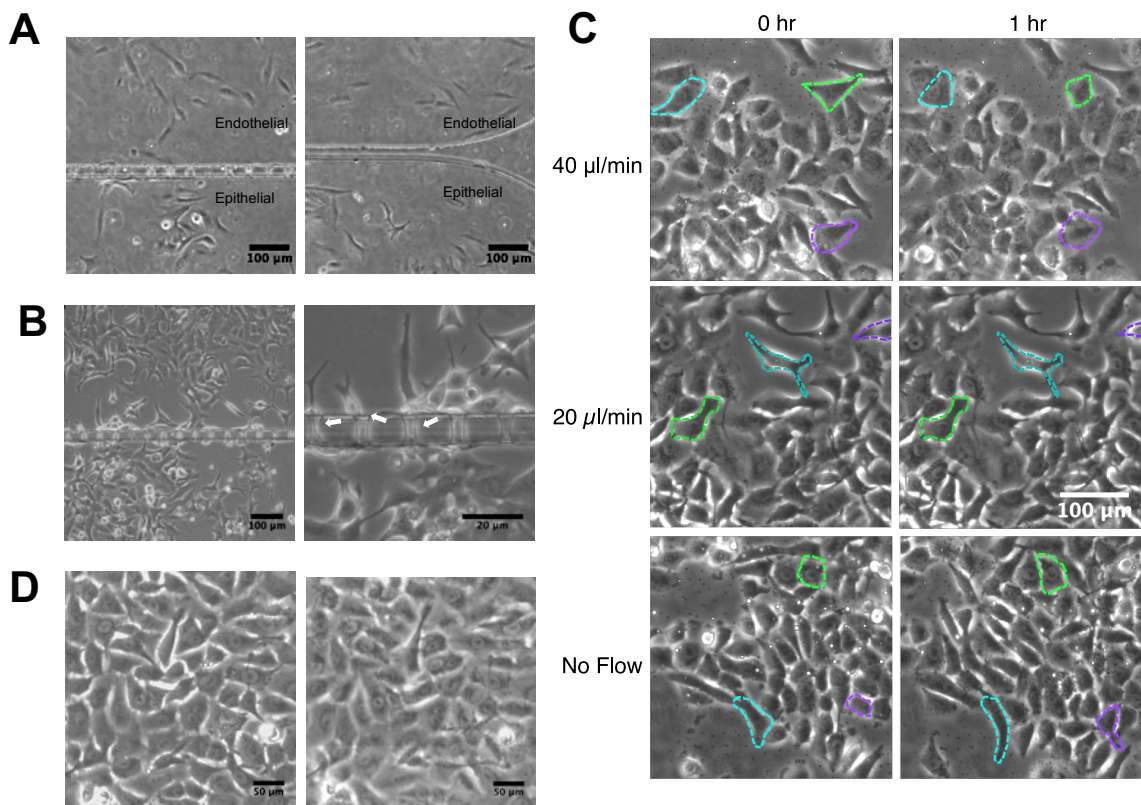
Figure 5.8: Host cells cultured in airway-blood vessel-on-a-chip.

(A) Phase contrast images of HUVEC endothelial and A549 lung epithelial cells adhering to PDMS channels after initial seeding. (B) A549 cells cultured in parallel airway-on-a-chip channels under 20µL/min DMEM perfusion. Arrows on zoomed in image show cells extending through connecting PDMS channels. (C) Representative images of A549 lung epithelial cells exposed to no flow, 20 µL/min or 40 µL/min flow rates for 1 hour. Coloured lines highlight cell shape before and after flow. (D) Confluent A549 monolayer cultured in the airway-on-a-chip channel exposed 20 µL/min for 1 hour (left) and 6 hours (right).

Table 5.4 Shear stress exerted on walls in the airway-blood-vessel-on-chip channels. Calculations used equation 5 and the dimensions of the channel.

Flow Rate (µL/min)	Shear Stress (dyne/cm²)
1	0.410
5	2.041
10	4.082
20	8.163
40	16.327
100	40.816
200	81.63

A number of biomarkers and visual cues are used in research to determine how cells react to shear stresses, the most common being cell shape the state of the cytoskeleton (Helmke et al., 2001; Verma et al., 2012; Yoon et al., 2001). The effect of different flow rates and corresponding shear stress on cells seeded in microfluidic channels was experimentally evaluated to determine a reasonable and physiologically comparable flow rate that also maintains monolayer integrity. At a media perfusion rate of 300 µL/min epithelial cells began detaching from the channels but at lower rates more subtle changes occurred. A simple way to monitor subtle cell responses is phase-contrast imaging. Cell morphological changes were evaluated qualitatively by pixel correlation analysis of images taken before and after different flow rates. A correlation index of 1 would indicate that an image at time zero and subsequently at 1 hour are identical (Table 6.5).

Table 5.5: Correlation index generated between images of A549 epithelial cells before and after 1 hr of media perfusion at indicated flow rates or static culture. Mean $\pm$SD shown, results from 5 pairs of images.

	Flow rate (µL/min)		
	0	20	40
Correlation index	0.302 ± 0.08	0.904 ± 0.01	0.594 ± 0.09

Figure 5.8D shows images of epithelial cells before and after exposure to a flow of media of for 1 hour. Images generated under no perfusion before and after 1 hour had a low correlation index, cells extended and changed shape over time. At 20 µl/min flow a high correlation index was determined and little morphological change was observed. At 40 µl/min perfusion rate the correlation index decreased with evidence of cell shrinkage and rounding throughout the 1-hour of flow. Over 6 hrs of flow rates of 20 µL/min epithelial cells appeared to close gaps between each other creating a tighter monolayer (Figure 5.8D).

5.2.5 Issues encountered and updated designs

Cell seeding and initiation of flow in microfluidic channels were coupled with two fundamental issues that made it difficult to achieve consistent monolayers cells and often led to abandoned experiments. During cell seeding in static conditions cells got trapped and clumped at inlets and even when seeded at low densities. These large clumps would then detach when flow was initiated, then travel thought the channel causing significant disruption to cells in the monolayer.

Spontaneous bubble formation in the microfluidic circuit was an issue over long periods of flow. Without intervention bubbles would migrate to the channel and strip cells from the fibronectin coated glass slide (Figure 5.8A and B). Bubbles were thought to initiate in and get displaced from media reservoirs and/or from valves in the circuit which may not be airtight. Three-way valves were incorporated into the tubing before the air-way chip as a method for introducing

bacteria via a syringe into the circuit. Unfortunately, valves have dead space which, if not completely filled with fluid, can be the source of bubbles.

In light of these fundamental issues with the airway-blood-vessel-on-chip set up bacterial infection experiments under flow were not achieved with my design, although, infections under static conditions were successful and showed adherence of small *S. aureus* clumps to epithelial cells (Figure 5.9C). Major changes must be made to the design of the channels and circuit equipment used to progress this platform further. A new design of microfluidic chip is shown in Figure 5.9D. It incorporates inlets specifically for cell seeding. Once cells are seeded these inlets can be closed off and fluid initiated through a different inlet with the idea that this will decrease cell clump displacement. With regard to reducing the likelihood of bubble formation new airtight media reservoirs should be incorporated and valves removed. Without valves *S. aureus* must be introduced into the flow circuit in a different way. One such proposed method is the injection of *S. aureus* directly into microfluidic tubing followed by rapid and localised heat treatment to seal micro holes. Commercially available bubble traps may also be incorporated into the circuit (Skolimowski et al., 2012).
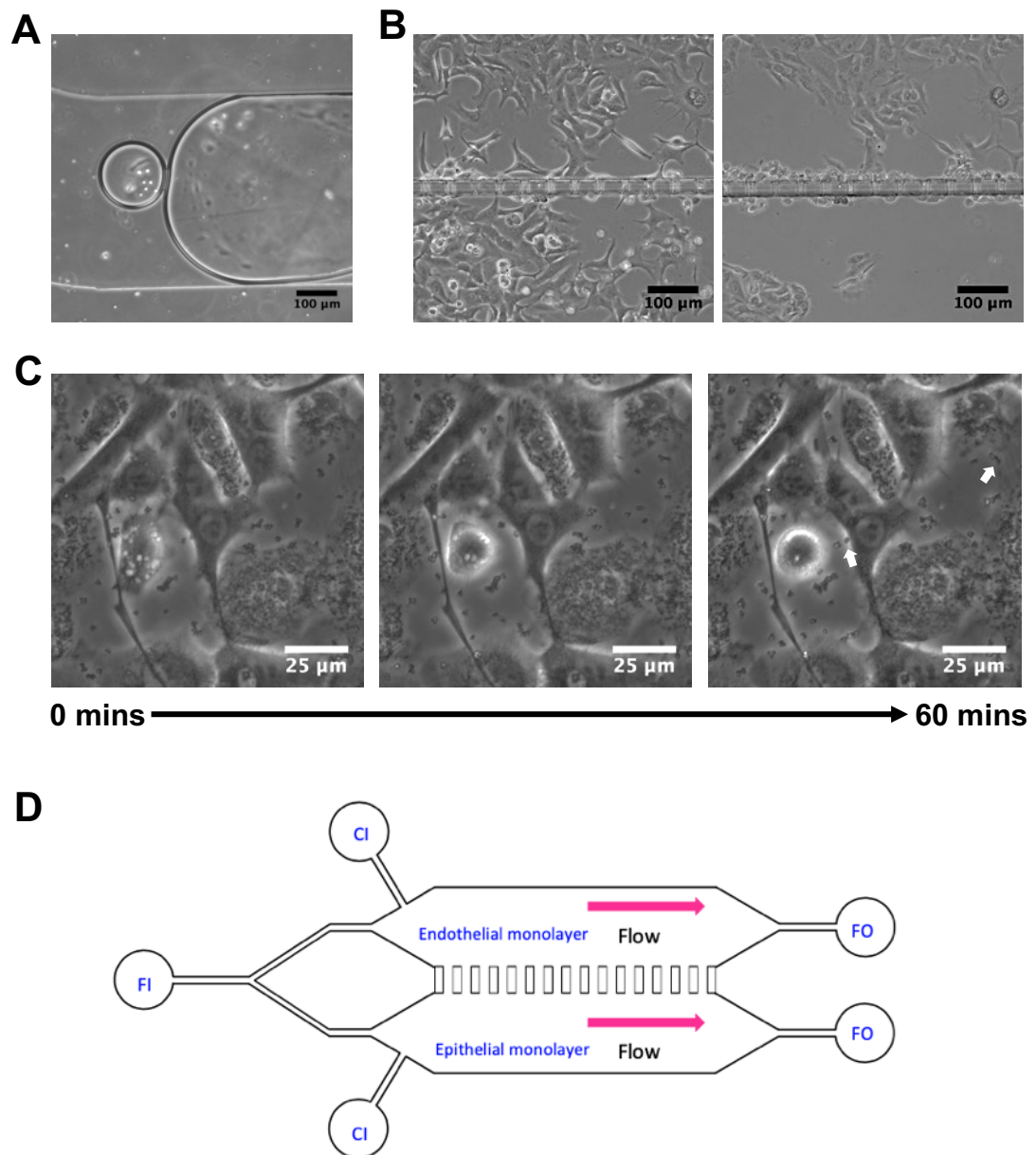
Figure 5.9: Limitations of current microfluidic circuit and new microfluidic chip design.

(A) Image of bubble formation in microfluidic channel. (B) Images of epithelial cells before (left) and after (right) initiation of flow in microfluidic airway-blood-vessel-on-chip. (C) Static *S. aureus* USA300 JE2 infection of epithelial cells imaged over 1 hour. Arrows indicated *S. aureus* that has adhered to host cells. (D) Newly proposed design of microfluidic airway-blood vessel interface. FI indicates flow inlet, CI indicates cell inlets for seeding only and FO indicates flow outlets.

5.3 Discussion

Microfluidic organ-on-chip technology is bridging the gap between *in vitro* conventional experimental models and human pathophysiology while providing alternatives for animal models. Organ-on-a-chip technology is an underused tool in the study of host bacterial interactions. During this project a microfluidic airway-blood-vessel-on-chip model was fabricated, characterised and evaluated for use in *S. aureus* infections of endothelial and epithelial cells under live microscopy. The microfluidic chip created here offered a novel design for tissue-tissue interactions that consisted of adjacent channels separated by a porous wall while previous microfluidic lung models incorporate tissue–tissue interfaces within stacked microfluidic channels making microscope analysis very difficult (Benam et al., 2016; Deinhardt-Emmer et al., 2020; Schultze et al., 2010b; Zamprogno et al., 2021). The aim was to create a simple microfluidic model which upgrades *in vitro* host-pathogen interaction studies by adding physiologically relevant levels of shear stress. The design can be adapted later down the line to incorporate further physiological variables such as 3D architecture or airflow. Some more established microfluidic labs have created stacked lung-on-a-chip models that incorporate air-liquid interfaces as well as multiple sections of human airways which have concentrated on biochemical outputs but their stacked design does not lend itself well to live-cell microscopy (Huh, 2015; Skolimowski et al., 2012).

Looking further afield organ-on-chip platforms have helped to identify a role for pulmonary surfactants in the removal of virulence-associated lipids from the cell surface of *M. tuberculosis*, thereby attenuating bacterial intracellular growth in macrophages (Stallings et al., 2020). Intestine-on-chip models have been used to identify pathogenic mechanisms of *Shigella Flexner* and enterotoxigenic *Escherichia coli* (ETEC) that exploit intestine architecture and/or luminal flow to maximize infectivity (Grassart et al., 2019; Sunuwar et al., 2019). At the Wyss institute a microfluidic airway-chip was even employed in an effort to repurpose FDA-approved drugs as therapeutics against SARS-CoV-2. The model helped to

identify amodiaquine and toremifene as potential entry inhibitors for SARS-CoV-2 in the model (Si et al., 2020). Microfluidics has some fantastic potential which has been made clear by its identification as next-generation technology for studying host-pathogen interactions (Baddal, 2019).

The intended use of this microfluidic chip was to investigate mechanical aspects of staphylococcal infection dynamics and host responses under physiological relevant shear stress conditions. Particular research interests include the effect of shear stress on adhesion and invasion of individual bacterial cells or bacterial clumps, the impact of shear stress on bacterial clearance and the spatiotemporal aspects of bacterial spread. All these questions can also be investigated in the context of the T7SS with use of deletion mutants. Although some previous studies have incorporated shear stress into *in vitro* investigations of *S. aureus* adhesion these studies often use isolated specific host cell components or use flow chambers with dimensions that create unrealistic cell masses (Claes et al., 2014; Herman-Bausier et al., 2018; Reddy & Ross, 2001; Viela et al., 2019; Zheng Jian Li et al., 2000)*.* Through the use of atomic force microscopy, Herman-Bausier et al. (2018) found that the adhesion of ClfA to host fibrinogen is regulated by mechanical tension. The bond between ClfA and immobilized fibrinogen is weak (approx. 0.1 nN) at low tensile force, but is dramatically enhanced (approx. 1.5 nN) by mechanical tension, suggesting bacterial attachment could be promoted under high physiological shear stress (Herman-Bausier et al., 2018). The same group also used showed the glycoprotein von Willebrand factor (vWF) binds to the *S. aureus* SpA via a force-sensitive mechanism (Viela et al., 2019). They hypothesise that elongation of vWF may lead to the exposure of a high-affinity SpA-binding site to which *S. aureus* can firmly attach (Viela et al., 2019). Both these studies point out the importance of including shear stress in studies on bacterial adhesion and invasion.

Only a handful of microfluidic studies have investigated *S. aureus*-host cell interactions (Deinhardt-Emmer et al., 2020; Pappelbaum et al., 2013; Viela et al., 2019). Microfluidic blood-vessel-like chambers modelling endocarditis demonstrated that *S. aureus* ultralarge von Willebrand factor (ULVWF)

contributes to luminal adherence of *S aureus* under high shear stress (Pappelbaum et al., 2013). A co-inflection of *S. aureus* after primary influenza virus infection in an alveolus-on-a-chip showed initial epithelial infection led to high inflammatory responses that spread to the endothelium and although the integrity of the epithelium was not compromised significant endothelial cell damage occurred (Deinhardt-Emmer et al., 2020). Due to time constraints and lack of access to equipment the airway-blood-vessel-on-chip and microfluidic circuit detailed here did not undergo the design modifications required to create a consistent and reliable platform for host-pathogen interaction investigations. The photolithography stage of fabrication takes place in a clean room, this is a major limiting factor for microfluidics in general as it can be difficult to gain access to such a facility and in many cases expert training is required. Steps are being made towards developing fabrication techniques that do not rely on access to a clean room (Challa et al., 2017). Despite this, value was found in channel characterisation which highlighted areas of strength and limitations that can be incorporated into new designs for the microfluidic vascular-lung interface. Fabrication methods resulted in robust and consistent wide dual chamber chips which were sterile and well suited for endothelial and epithelial cell culture (Tehranirokh et al., 2013; Young & Beebe, 2010).

Low levels of resistance generated by the airway-blood-vessel-on-chip in a microfluidic circuit was rectified with the incorporation of a serpentine channel. The added resistance increased the range of pressures that could be utilized to achieve steady flow rates and therefore impart physiological levels of shear stress (M. Li et al., 2009; Tehranirokh et al., 2013). Flow rates could be successfully increased or decreased in small increments which did not disrupt cell monolayers in the channel. Flow rates can be made even more reproducible by replacing the in-line serpentine chip with commercially available resistor tubing that exerts the experimentally evaluated level of resistance. This will both be cost and time effective.

Fluid behavioural studies defined the velocity profiles across the channels z plane to be parabolic despite the presence of a series of small holes in the channel walls. This suggested that the porous walls of the main channels were not perturbing laminar flow and caused minimal mixing of fluid as you would expect at a bronchiole-blood vessel interface. The presence of regular and predictable laminar flow streams enables exceptional spatial and temporal control and understanding of how objects move through the channel (Bruus, 2014). Where the modelling of fluid behaviour has been published for other lung-on-a-chip devices velocity profiles prove to be far more complex with fluid being driven from the lower channel across the porous membrane into the top channel (Shrestha et al., 2019). These contrasting results were likely due to the positioning of channels and the size of pores between channels.

Investigations into the effect of specific flow rates and shear stress on cell adhesion and morphological features suggests that a flow rate of around 20 µL/min, which generated a shear stress of 8.16 dyne/cm2 initiated the formation of a tight monolayer without cell rounding which is consistent with previous studies (Deinhardt-Emmer et al., 2020; Mahto et al., 2014). When a shear stress of 16.33 dyn/cm^2 (40µL/mL) was applied detrimental effects to cell morphology was observed as seen before with A549 epithelial cells (Mahto et al., 2014). It has been shown that low to moderate shear stresses (<15 dyn/cm^2) can be tolerated by a number of epithelial cells in terms of cytoskeletal damage (Verma et al., 2012; Yoon et al., 2001), but most notably by endothelial cells (Helmke et al., 2001). The incorporation of sensors into the channels such as transepithelial/endothelial electrical resistance (TEER), a valuable method for assaying *in vitro* barrier tissue integrity at different flow rates, and would enable more in depth analysis of barrier integrity during bacterial infections (Tavana et al., 2011).

Major issues in this microfluidic set up, such as bubble and cell clump formation, made the success rate of setting up microfluidic experiments very low. These issues can be addressed by adding features to the device to aid cell seeding and

incorporating bubble trapping technology into the circuit (Zheng et al., 2010). Overall, this effort to create a microfluidic airway-blood vessel interface or an 'infection on a chip' provided valuable insight into desirable and valuable features that are required to create a consistent and accurate platform to investigate host-pathogen interactions. New designs and ideas have been proposed for the progression of this device and should be used to develop this technology.

6   Chapter 6: Final discussion

Staphylococcus aureus is an extremely successful pathogen and underpinning its infectious proficiency is its ability to manipulate and evade the immune system with its many virulence factors (Thammavongsa et al., 2015). The staphylococcal T7SS has previously been identified as a virulence factor (Anderson et al., 2017; Burts et al., 2005, 2008) and in addition to this, a small number of cellular infection studies determined a potential role for the T7SS in the regulation of host cell death and immune responses (Cruciani et al., 2017; Dai et al., 2017; Korea et al., 2014). This project aimed to understand the role of the T7SS in host infections with a focus on macrophages, a key immune cell in the clearance of staphylococcal infections (Pidwill et al., 2021). The capacity for *S. aureus* to induce cell death in immune cells such as macrophages through the extracellular secretion of toxins has been well characterised, (Alonzo & Torres, 2014; DuMont et al., 2013; Melehani et al., 2015) but the onset of cell death via intracellular means is less well defined. The T7SS proteins are prime candidates for the manipulation of host responses and so were investigated using WT and isogenic T7SS deletion mutants in *in vitro* and *in vivo* infections.

First, baseline infection dynamics were established with WT *S. aureus* and macrophages which revealed notable findings. Time-lapse microscopy showed the primary outcome for *S. aureus* infections in macrophages was the formation of a pore-induced intracellular trap (PIT)-like structures, a phenomenon only recently characterised as the end result of lytic cell death including necroptosis and pyroptosis in phagocytes (Jorgensen, Zhang, et al., 2016). In chapter 3, it was confirmed through immunoblotting that the majority of cell death that occurred throughout *S. aureus* macrophage infections was the result of pyroptosis and necroptosis, but not apoptosis, which is consistent with other studies that also probed all three pathways in *S. aureus* infections (Kitur et al., 2015, 2016). The link between *S. aureus* and the onset of PITs has not been directly linked prior to this study, although, some indication of pyroptotic corpses have been mentioned (Yao et al., 2020). PITs entrap viable bacteria within the cellular debris of the

necroptotic or pyroptotic cell corpse, which was observed in *S. aureus* macrophage infections, furthermore PITs are known to be efferocytosed by professional phagocytes (Jorgensen, Lopez, et al., 2016; Jorgensen, Zhang, et al., 2016), which was evident to some extent. Further investigations based on visualisation of swollen organelle debris and loss of soluble proteins through the permeabilised membrane should be carried out to conform the PIT-like structures are the same as those previously described (Jorgensen, Zhang, et al., 2016).

Time-lapse microscopy of macrophages infected with mutant *S. aureus* strains, Δ*essC*, Δ*esxC* and Δ*esxC-D* revealed that WT JE2 *S. aureus* induced an early peak of cell death, characterised by early onset of PIT-like structures or occasional apoptosis morphologies, which was almost absent in Δ*essC* infections and greatly reduced in the case of Δ*esxC* and Δ*esxC-D.* T7SS mutants were not defective in causing macrophage PIT-like structures or apoptosis events, but perhaps delayed (as indicated by a shift of peaks to later time points) during infection. Cell death occurring at later timepoints could be the result of staphylococcal pore forming toxins such as Hla or LukAB(Kitur et al., 2015; Ventura et al., 2010). The early peak in PIT formation in WT infections was attributed to enhanced necroptosis activation as significantly higher MLKL was phosphorylated than in WT than Δ*essC* infections at 4 hrs, meanwhile other pathways did not show differential activation. It is yet to be determined if the T7SS interacts directly with the components of necroptosis or if necroptosis activation is the result of T7SS involvement in disrupting related pathways. In parallel to this, analysis of macrophage supernatant revealed the presence of T7SS proteins, especially EssC, conferred an increase in the release of proinflammatory cytokines IL-1β and TNF-α suggesting the T7SS components elicit an inflammatory response in macrophages. Together the seemingly subtle effects of the T7SS *in vitro* may be exacerbated *in vivo* or under different culture conditions, as shown by the lack of microcolony formation by WT when macrophages are infected on a glass surface.

This is the first time the staphylococcal T7SS has been associated with the activation of the necroptotic pathway, a pathway that has previously been reported to be induced by *S. aureus* during intracellular infection of macrophages and other host cells (Kitur et al., 2015, 2016; Tam et al., 2020; Wong Fok Lung et al., 2020). Mycobacterial T7SSs, ESX-1 and ESX-5, have been linked on multiple occasions to the induction of a necrotic cell death however whether this is programmed necrosis, i.e. necroptosis has not been fully established (Abdallah M. Abdallah et al., 2011; Dallenga et al., 2017; K.-W. Wong, 2017). Mtb studies have linked ESX-1 with the indirect promotion of necroptosis due to its phagosome escape function (Pajuelo et al., 2018; J. Sun et al., 2015) Furthermore, an ESX-3 effector protein has the ability to inhibit downstream repair of necroptotic pores, perhaps hinting at some conservation in functional roles of the T7SS between pathogens (Gong et al., 2017; Mehra et al., 2013; Portal-Celhay et al., 2016). Necroptosis is thought to be activated as a "trap-door" mechanism by the host, when the apoptotic pathway is compromised, so that the cell can still die (Brault & Oberst, 2017). This has been shown to occur in EPEC and *Shigella* infections due to their type-III secretion system substrate interaction with caspases, but these pathogens also possess virulence factors that induce cell death (Ashida et al., 2011; Pearson et al., 2013; Pollock et al., 2017). During *in vivo* infection, necroptosis has been shown to be hugely important in influencing the outcome of *S. aureus* disease, with its presence causing reduced inflammatory responses and better outcomes for mice in models of skin infection and sepsis (Kitur et al., 2015, 2016). Here we suggest the T7SS may be a strong contributing factor to the type of cell death that occurs in the infection of highly important immune cells.

With the use of a mouse skin abscess model, it was shown that the deletion of T7SS proteins EssC or EsxC, EsxD, EsxB and EsaE had a significant effect on *S. aureus* skin colonisation and bacterial spread to other tissues, however this effect changed according to the inoculum dose. While high-dose inoculums showed ΔessC and ΔesxC-D cause a less substantial infection than WT, which is consistent with other studies of T7SS factors during high-dose skin, pneumonia and

bacteraemia infections (Anderson et al., 2017; Burts et al., 2005, 2008; Dai et al., 2017; Ishii et al., 2014; Kneuper et al., 2014; Lopez et al., 2017; Ohr et al., 2017; Y. Wang et al., 2016), we propose that caution should be taken when interpreting these results. High-dose inoculums in many different models appear to bypass the natural bacterial population bottleneck which is caused by macrophages and neutrophils during infection establishment, although we must also consider that outcomes could be dependent on local immune responses (Boldock et al., 2018; McVicker et al., 2014; Pollitt et al., 2018). High bacterial numbers may simply overload the immune system which could mask the intracellular effects of the T7SS. In low-dose skin infections models, which have not been previously employed for investigations with T7SS mutants, Δ*essC* and Δ*esxC-D* mutants produced a more substantial infection than WT, raising the possibility that the T7SS may limit *S. aureus* success in skin infections under certain conditions.

The combination of previously published data, and data collected in this project led to the proposal of a working hypothesis which is illustrated in Figure 6.1 and described here. Upon invasion of *S. aureus* into skin tissue, at a low-dose ($\leq 10^6$ CFU)*,* resident macrophages are one of the first immune cell types that internalise *S. aureus* (Cheng et al., 2011; R. Flannagan et al., 2015)*.* While inside macrophages *S. aureus* replicates and the T7SS proteins promote the activation of necroptosis through direct or indirect interactions with pathway components. *S. aureus* also induces pyroptosis including the release of inflammatory cytokines such as IL-1β which is exacerbated by the presence of the T7SS either as a consequence of crosstalk form necroptosis and/or through a separate mechanism. Infected macrophages undergo rapid lytic necroptosis and PIT formation. *S. aureus* replication then further occurs within PITs and in some cases the bacteria may escape into the extracellular environment. However, if secondary phagocytes such as neutrophils are rapidly recruited to the area by high levels of cytokines such as IL-1β and IL-18, PITs may be cleared and a substantial abscess response promoted, which limits bacteria spreading to distal sites (Jorgensen, Lopez, et al., 2016). If PIT formation and high cytokine release does not occur rapidly, as in the case of Δ*essC* infections, neutrophil recruitment and clearance of bacteria may be

less effective, leading to high bacterial numbers, reduced abscess response and more bacterial spread. These events are likely dependent on the local immune response and bacterial load. In a high dose infection context where bacterial numbers overwhelm macrophages, *S. aureus* may survive better in the abscess environment that they induce. Esx proteins of *Mycobacterium marinum* have previously been shown to stimulate a cytokine response that causes macrophage recruitment and granuloma formation resulting in better bacteria survival (Davis & Ramakrishnan, 2009; Volkman et al., 2004).

Overall, this data brings into question whether the T7SS is always beneficial for the pathogen. The T7SS may of course have a different impact on severity of infection depending on the *S. aureus* strain used and the host cell type and/or tissue being infected. The immunostimulatory effects of the T7SS makes these proteins good candidates for a much-needed *S. aureus* vaccine. EsxA and EsxB effector proteins are were trialled as part of the GSK S 4C-Staph vaccine even though specific impacts on host cells are unknown (Mancini et al., 2016b; Torre et al., 2015). Our study has aided in shedding light on the role of the T7SS proteins while inside key immune cells and may provide useful information on why these proteins should, or should not, be incorporated into a *S. aureus* vaccine.
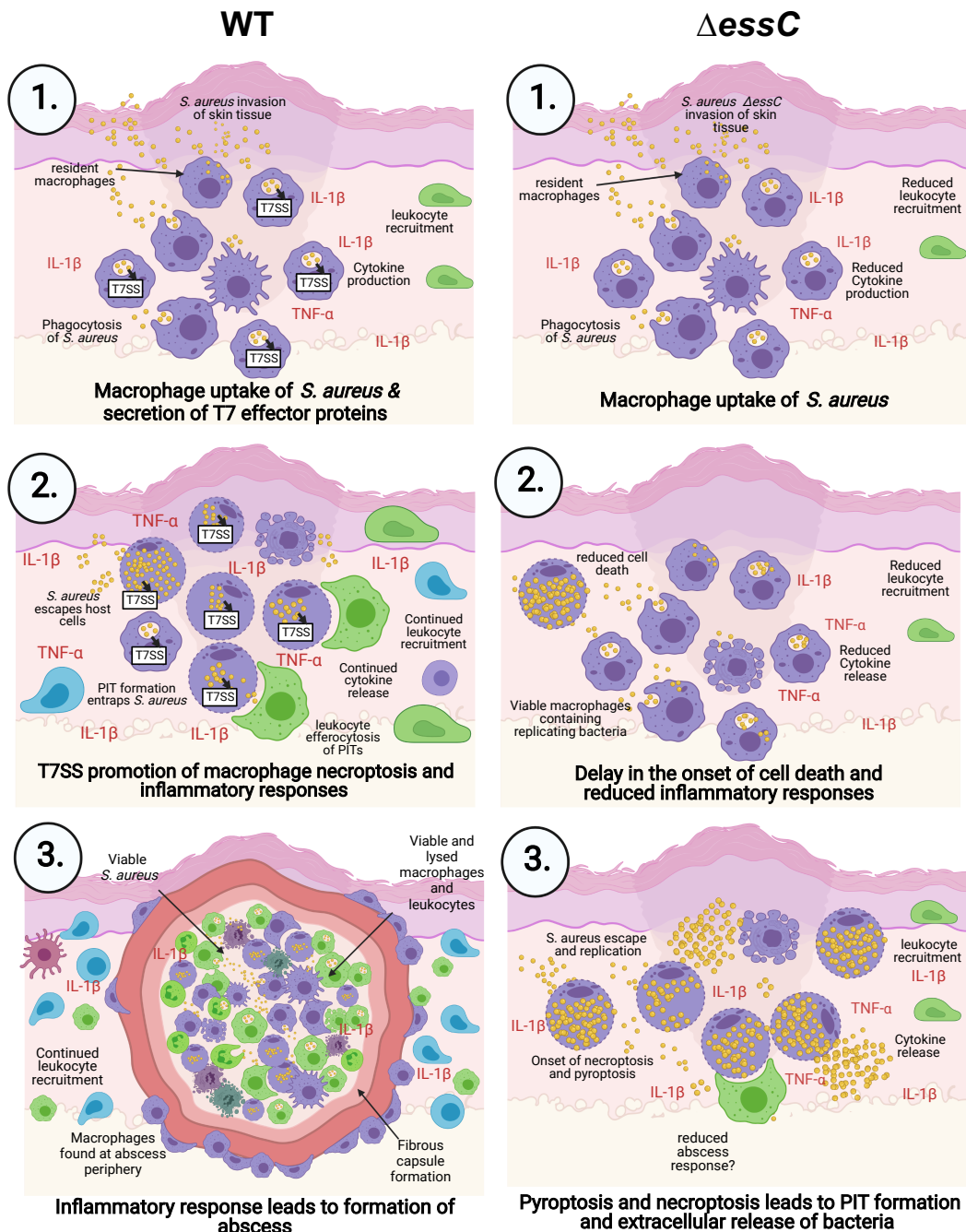
Figure 6.1 Working hypothesis for the role of T7SS in skin infection.

WT *S. aureus* infections (left)**:** 1. WT *S. aureus* breaches the epithelial layer of skin and resident macrophages phagocytose the bacteria and produce a strong inflammatory cytokine response 2. *S. aureus* T7SS proteins promote macrophage necroptosis causing rapid pore-induced intracellular trap (PIT) formation, in which bacteria replicate. Inflammatory cytokine response continues to recruit leukocytes, such as neutrophils, which work to efferocytose infected PITs and

clear extracellular bacteria. 3. *S. aureus* infection is contained by abscess formation with macrophages and fibrous material surrounding a core containing dead and viable leukocytes and *S. aureus.* For ΔessC *S. aureus* infections (right) 1. Macrophages phagocytose invading bacteria. 2. Replicating bacteria persist in viable macrophages and cause less early cell death and cytokine release than WT resulting in reduced leukocyte recruitment. 3. *S. aureus* induces pyroptosis and necroptosis in macrophages via a method other than T7SS proteins (possibly toxins). Replicating Δ*essC S. aureus* escapes into the extracellular environment and abscess response may be reduced.

Aside from what has already been discussed, this project has brought to light some other interesting points. Firstly, the use of time-lapse microscopy showed us the importance of using a combination of methods to assess cell death, and to not depend on final endpoint population-based assays as accurate read-outs for cell death during infection. Time-lapse microscopy of macrophage infections with and without extended exposure to lysostaphin revealed antibiotics dramatically shifted the distribution of macrophage death over time. Trends in levels of PIT formation remained the same with the incorporation of antibiotics but variance increased, and significance level was lost during early infection periods. Overall, the use of lysostaphin/gentamicin assays over extended periods of time was concluded to be detrimental for the analysis of the effect of the T7SS. This recommendation is mirrored in other publications regarding the study of *S. aureus* infection dynamics (R. S. Flannagan et al., 2016; Horn et al., 2017)

The use of both glass and plastic chamber slides during investigations flagged up the effect different culture surfaces have on *S. aureus* infections. Culturing macrophages on glass instead of plastic led to very different findings: there was a dramatic increase in the clearance of WT *S. aureus* from host cells, which led to almost no microcolony formation. Interestingly, the culture surface had much less of an effect on T7SS mutant infections as Δ*essC, esxC-D* and Δ*esxC* strains were able to escape from macrophages and form microcolonies on both glass and plastic chamber slides. Assessment of macrophage morphology and ROS production on glass and plastic did not provide a clear reason for this contrast but macrophage activation state, which could be altered by culture surface (Rostam et al., 2016), may be a reasonable explanation, and could suggest the state of the macrophage can alter how it responds to the staphylococcal T7SS.

Finally, this project identified the need for a suitable new model that overcomes issues with murine infection models such as differences in human and mouse susceptibility to *S. aureus* virulence factors and dose issues (H. K. Kim et al., 2014; Salgado-Pabón & Schlievert, 2014). Many publications also highlight this need, especially in the effort to create vaccinations for *S. aureus* (Salgado-Pabón &

Schlievert, 2014). Microfluidics has been identified as emerging technology that could elevate *in vitro* infection studies (Baddal & Marrazzo, 2021). Therefore, the design, fabrication and characterisation of a microfluidic organ-on-a-chip platform was carried out, from scratch, in this project. The device created, although not fully optimised, showed real potential for providing a platform to microscopically monitor the effect of the T7SS on chronic *S. aureus* infections at an airway-blood vessel-like interface, while incorporating physiological factors such as shear stress.

6.1 Study limitations

The major limitations of this study include the lack of confirmation of phenotypes in primary macrophages. Although THP-1 macrophages are generally considered to be a very good model to estimate modulation of monocyte and macrophage activities (Chanput et al., 2014), when compared to primary monocytes, THP-1 cells express low levels of CD14 and exhibit slightly different cytokine expression patterns following stimulation with bacterial factors (Schildberger et al., 2013). This project fully intended to incorporate the use of PBMCs isolated from human whole blood but due to various COVID restrictions this became unrealistic. Another limitation of this study is the lack of complementation of mutant strains. Data collected in this lab from investigations with a complemented single Esx protein deletion suggested complex complementation effects likely due to interactions between different effector proteins(Anderson et al., 2013). Antibiotics required for the episomal complementation may also disrupt infection dynamics.

6.2 Future directions

During my PhD I established and optimised a time-lapse assay and quantification system which has facilitated further microscopic analyses of *S. aureus* infected cell populations, including but not limited to, *S. aureus* infections with the molecular inhibitors of death pathways/cytokines and *S. aureus* infections of multiple other host cell types. I was able to offer key information and advice to

colleagues regarding the impact of cell culture surface and antibiotics on results and consistency of results. My data led to a decision within the lab group that only plastic chamber slides will be used during future analyses. This decision was made in order to be consistent with biochemical assays that are conducted in plastic wells and to ensure the assay is a transferrable across labs. I was also able to provide the designs and methods for optimisation of a microfluidic device to microscopically study *S. aureus* infection for future colleagues.

The following experiments could be used in the future to confirm and expand on the results of this study. Firstly, T7SS effects should be on cell death in primary peripheral blood mononuclear cells (PBMCs) and could even be extended to other cell types such as neutrophils or epithelial cells. Similar time-lapse microscopy experiments with fluorescent bacteria and western blot analysis of activated cell death pathways should be completed to ensure the T7SS effect on necroptosis and PIT formation is not limited to THP-1 cells.

Appropriate complementation strains should be generated to confirm phenotypes in macrophages. Further mutants lacking single (EsxA, EsxB and EsxD), or multiple effectors (EsxA-EsxB, EsxA-EsxC, EsxA-EsxD) could also be tested for bacterial survival by intracellular and total bacterial counts over time, and corresponding macrophage phenotypes using time-lapse microscopy assays as compared to the WT. The incorporation of more deletion mutants may tease out the important proteins for activation of necroptosis or could implicate an interdependence between T7SS proteins. Much of the *in vitro* work here was carried out with a single MOI. The MOI was specifically chosen as it resulted in a high percentage of macrophages infected with similar numbers of bacteria, however, MOIs can have a large impact on a phagocyte's ability to overcome infection (Jubrail et al., 2016; Schwartz et al., 2009). Lowering the MOI, and therefore creating a more natural infection environment with both infected and non-infected macrophages, and in combination with time-lapse microscopy could lead to a more relevant insight into the role of T7SS in infection outcomes, especially the effect of PITs and possible efferocytosis.

To more specifically determine the effect of T7SS on necroptosis, other proteins in the pathway, such as RIPK1 and RIPK3 should be probed for activation using Western blot analysis. This will aid in deciphering whether the T7SS specifically targets components of the necroptotic pathway or if it causes the activation of the whole pathway through other means. Commonly used inhibitors of MLKL, such as necrosulfonamide (NSA) or inhibitors of RIPK1 such as necrostatin (Nec-1) can also be used to confirm T7SS effects on this pathway. However, caution must be taken when using inhibitors as off-target activities have been noted (Rathkey et al., 2018; Takahashi et al., 2012) and host intrinsic cross-guarding of cell death pathways can make interpretation complex.

Most importantly the data presented here indicate T7SS modulation of cell death pathways but we do not yet understand which host proteins they interact with. Bio-ID, a mass spectrometry-based method used to probe for protein-protein interactors can be employed (Roux et al., 2018). Bio-ID is based on the ability of a promiscuous biotin ligase (BirA) to biotinylate proteins in close vicinity to bait proteins. Esx secreted proteins conjugated to BirA can transfected into host cells and binding partners assessed using this method. T7SS co-localisation with identified proteins can be confirmed with confocal analysis of infections with fluorescently tagged proteins and infections can be carried out host proteins knocked down using specific siRNAs.

Current *in vivo* findings can be strengthened with the histological staining and examination of more replicates of infected skin tissue as well as the immunohistochemical probing for the presence of macrophages, neutrophils, cytokines and *S. aureus* in skin slices. Tissue homogenates were saved and could be analysed by ELISA for levels of inflammatory cytokines such as IL-1β which will aid in understandning the overall impact of T7SS on infection dynamics and outcomes.

This project may have indicated that activation status of macrophages, due to culture surface, could further impact the effect of T7SS by decreasing the amount of bacteria released into the extracellular environment. This could be investigated by pre-activating of macrophages with specfic cytokines such as IFN-γ, IL-4 or IL-13 prior to infection under time-lapse microscopy or by probing for M1 or M2 associated markers such as chemokine receptors CCR2 and CX3CR1 (Italiani & Boraschi, 2014).

Another interesting add on to this work woul be analysis of *S. aureus* Esx protein expression during intracellular infection, which has not been previously been carried out. Dual RNA-seq of *S. aureus* and macrophages during infection could consolidate the link between Esx protein expression and upregulation of host cell death pathways and other host response pathways.

7 Bibliography

Abbott, A. (2003). Biology's new dimension. *Nature*, *424*(6951), 870–872.

Abd El-Fatah, R. M., Mesbah, N. M., Abo-Elmatty, D. M., & Aly, K. A. (2018). The C-terminus of the ESAT6-like secretion system virulence factor EsxC mediates divalent cation-dependent homodimerization. *Toxicon*.

Abdallah, A. M. ... Bitter, W. (2008). The ESX-5 Secretion System of Mycobacterium marinum Modulates the Macrophage Response. *Journal of Immunology (Baltimore, Md. : 1950)*, *181*, 7166–7175.

Abdallah, Abdallah M. ... Peters, P. J. (2011). Mycobacterial Secretion Systems ESX-1 and ESX-5 Play Distinct Roles in Host Cell Death and Inflammasome Activation. *The Journal of Immunology*, *187*(9), 4744–4753.

Abdallah, Abdallah M. ... Bitter, W. (2009). PPE and PE-PGRS proteins of Mycobacterium marinum are transported via the type VII secretion system ESX-5. *Molecular Microbiology*, *73*(3), 329–340.

Agerer, F., Michel, A., Ohlsen, K., & Hauck, C. R. (2003). Integrin-mediated Invasion of Staphylococcus aureus into Human Cells Requires Src Family Protein-tyrosine Kinases. *Journal of Biological Chemistry*, *278*(43), 42524–42531.

Aguilo, J. I. ... Martin, C. (2013). ESX-1-induced apoptosis is involved in cell-to-cell spread of Mycobacterium tuberculosis. *Cellular Microbiology*, *15*(12), 1994–2005.

Aguiló, N., Marinova, D., Martín, C., & Pardo, J. (2013). ESX-1-induced apoptosis during mycobacterial infection: To be or not to be, that is the question. *Frontiers in Cellular and Infection Microbiology*, *3*(88).

Ahmed, M. M., Aboshanab, K. M., Ragab, Y. M., Missiakas, D. M., & Aly, K. A. (2018). The transmembrane domain of the Staphylococcus aureus ESAT-6 component EssB mediates interaction with the integral membrane protein EsaA, facilitating partially regulated secretion in a heterologous host. *Archives of Microbiology*, *200*(7), 1075–1086.

Aldo, P. B., Craveiro, V., Guller, S., & Mor, G. (2013). Effect of culture conditions on the phenotype of THP-1 monocyte cell line. *American Journal of Reproductive Immunology*, *70*(1), 80–86.

Alonzo, F., & Torres, V. J. (2013). Bacterial Survival Amidst an Immune Onslaught: The Contribution of the Staphylococcus aureus Leukotoxins. *PLoS Pathogens*, *9*(2).

Alonzo, F., & Torres, V. J. (2014). The Bicomponent Pore-Forming Leucocidins of Staphylococcus aureus. *Microbiology and Molecular Biology Reviews*, *78*(2), 199–230.

Amarante-Mendes, G. P. … Bortoluci, K. R. (2018). Pattern recognition receptors and the host cell death molecular machinery. *Frontiers in Immunology*, *9*(2379).

Anderson, M., Aly, K. A., Chen, Y. H., & Missiakas, D. (2013). Secretion of atypical protein substrates by the ESAT-6 Secretion System of Staphylococcus aureus. *Molecular Microbiology*, *90*(4), 734–743.

Anderson, M., Chen, Y. H., Butler, E. K., & Missiakas, D. M. (2011). EsaD, a secretion factor for the Ess pathway in Staphylococcus aureus. *Journal of Bacteriology*, *193*(7), 1583–1589.

Anderson, M. … Missiakas, D. (2017). EssE promotes Staphylococcus aureus ESS dependent protein secretion to modify host immune responses during infection. *Journal of Bacteriology*, *199*(1).

Asai, A. … Suzuki, F. (2010). Pathogenic role of macrophages in intradermal infection of methicillin-resistant Staphylococcus aureus in thermally injured mice. *Infection and Immunity*, *78*(10), 4311–4319.

Ashida, H. … Sasakawa, C. (2011). Cell death and infection: A double-edged sword for host and pathogen survival. *Journal of Cell Biology*, *195*(6), 931–942.

Ashida, H., Sasakawa, C., & Suzuki, T. (2020). A unique bacterial tactic to circumvent the cell death crosstalk induced by blockade of caspase-8. *The EMBO Journal*, *39*(17).

Askarian, F. … Johannessen, M. (2014). A staphylococcus aureus TIR domain protein virulence factor blocks TLR2-mediated NF-κB signaling. *Journal of Innate Immunity*, *6*(4), 485–498.

Askarian, F., Wagner, T., Johannessen, M., & Nizet, V. (2018). Staphylococcus aureus modulation of innate immune responses through Toll-like (TLR), (NOD)-like (NLR) and C-type lectin (CLR) receptors. *FEMS Microbiology*

Reviews, *42*(5), 656–671.

Ates, L. S. … Houben, E. N. G. (2015). Essential Role of the ESX-5 Secretion System in Outer Membrane Permeability of Pathogenic Mycobacteria. *PLoS Genetics*, *11*(5), e1005190.

Ates, L. S. … Bitter, W. (2016). The ESX-5 System of Pathogenic Mycobacteria Is Involved In Capsule Integrity and Virulence through Its Substrate PPE10. *PLoS Pathogens*, *12*(6).

Baddal, B. (2019). Next-generation technologies for studying host-pathogen interactions: a focus on dual transcriptomics, CRISPR/Cas9 screening and organs-on-chips. *Pathogens and Disease*, *77*(6), 60.

Baddal, B., & Marrazzo, P. (2021). Refining host-pathogen interactions: Organ-on-chip side of the coin. *Pathogens*, *10*(2), 1–13.

Bae, T., & Schneewind, O. (2006). Allelic replacement in Staphylococcus aureus with inducible counter-selection. *Plasmid*, *55*(1), 58–63.

Bagnoli, F. … Grandi, G. (2015). Vaccine composition formulated with a novel TLR7-dependent adjuvant induces high and broad protection against Staphylococcus aureus. *PNAS*, *112*(12), 3680–3685.

Bantel, H. … Jänicke, R. U. (2001). α-is a mediator of Staphylococcus aureus-induced cell death and activates caspases via the intrinsic death pathway independently of death receptor signaling. *The Journal of Cell Biology*, *155*(4), 637–647.

Baptista, C., Barreto, H. C., & São-José, C. (2013). High Levels of DegU-P Activate an Esat-6-Like Secretion System in Bacillus subtilis. *PLoS ONE*, *8*(7), e67840.

Baran, J. … Pryjma, J. (1996). Apoptosis of monocytes and prolonged survival of granulocytes as a result of phagocytosis of bacteria. *Infection and Immunity*, *64*(10), 4242–4248.

Baran, J. … Pryjma, J. (2001). Fas (CD95)-fas ligand interactions are responsible for monocyte apoptosis occurring as a result of phagocytosis and killing of Staphylococcus aureus. *Infection and Immunity*, *69*(3), 1287–1297.

Barber, M. (1961). Methicillin-resistant staphylococci. *Journal of Clinical Pathology*, *14*, 385–393.

Bayles, K. W. ... Trumble, W. R. (1998). Intracellular Staphylococcus aureus escapes the endosome and induces apoptosis in epithelial cells. *Infection and Immunity*, *66*(1), 336–342.

Beckwith, K. S. ... Flo, T. H. (2020). Plasma membrane damage causes NLRP3 activation and pyroptosis during Mycobacterium tuberculosis infection. *Nature Communications*, *11*(1).

Behar, S. M., Divangahi, M., & Remold, H. G. (2010). Evasion of innate immunity by mycobacterium tuberculosis: Is death an exit strategy? *Nature Reviews Microbiology*, *8*(9), 668–674.

Belmokhtar, C. A., Hillion, J., & Ségal-Bendirdjian, E. (2001). Staurosporine induces apoptosis through both caspase-dependent and caspase-independent mechanisms. *Oncogene*, *20*(26), 3354–3362.

Benam, K. H. ... Ingber, D. E. (2016). Small airway-on-a-chip enables analysis of human lung inflammation and drug responses in vitro. *Nature Methods*, *13*(2), 151–157.

Bera, A., Herbert, S., Jakob, A., Vollmer, W., & Götz, F. (2005). Why are pathogenic staphylococci so lysozyme resistant? The peptidoglycan O-acetyltransferase OatA is the major determinant for lysozyme resistance of Staphylococcus aureus. *Molecular Microbiology*, *55*(3), 778–787.

Berg, H. C. (2018). Random Walks in Biology. In *Random Walks in Biology* (Extended). Princeton University Press.

Berube, B. J., & Wardenburg, J. B. (2013). Staphylococcus aureus α-toxin: Nearly a century of intrigue. *Toxins*, *5*(6), 1140–1166.

Bewley, M. A. ... Dockrell, D. H. (2011). A cardinal role for cathepsin D in co-ordinating the host-mediated apoptosis of macrophages and killing of pneumococci. *PLoS Pathogens*, *7*(1), e1001262.

Bhakdi, S., & Tranum-Jensen, J. (1991). Alpha-toxin of Staphylococcus aureus. *Microbiological Reviews*, *55*(4), 733–751.

Bhatia, S. N., & Ingber, D. E. (2014). Microfluidic organs-on-chips. *Nature Biotechnology*, *32*(8), 760–772.

Bhattacharya, M. ... Wozniak, D. J. (2018). Staphylococcus aureus biofilms release leukocidins to elicit extracellular trap formation and evade neutrophil-

mediated killing. *Proceedings of the National Academy of Sciences of the United States of America*, *115*(28), 7416–7421.

Bhise, N. S. … Khademhosseini, A. (2016). A liver-on-a-chip platform with bioprinted hepatic spheroids. *Biofabrication*, *8*(1), 014101.

Birmingham, C. L., Higgins, D. E., & Brumell, J. H. (2008). Avoiding death by autophagy: Interactions of Listeria monocytogenes with the macrophage autophagy system. *Autophagy*, *4*(3), 368–371.

Biswas, L. … Götz, F. (2009). Role of the twin-arginine translocation pathway in Staphylococcus. *Journal of Bacteriology*, *191*(19), 5921–5929.

Blanchet, C., Jouvion, G., Fitting, C., Cavaillon, J. M., & Adib-Conquy, M. (2014). Protective or deleterious role of scavenger receptors SR-A and CD36 on host resistance to Staphylococcus aureus depends on the site of infection. *PLoS ONE*, *9*(1), e87927.

Blander, J. M., & Medzhitov, R. (2004). Regulation of Phagosome Maturation by Signals from Toll-Like Receptors. *Science*, *304*(5673), 1014–1018.

Blättner, S. … Fraunholz, M. J. (2016). Staphylococcus aureus Exploits a Non-ribosomal Cyclic Dipeptide to Modulate Survival within Epithelial Cells and Phagocytes. *PLoS Pathogens*, *12*(9), 1–23.

Bobrovskyy, M., Willing, S. E., Schneewind, O., & Missiakas, D. (2018). EssH peptidoglycan hydrolase enables staphylococcus aureus type VII secretion across the bacterial cell wall envelope. *Journal of Bacteriology*, *200*(20), 1–15.

Bode, L. G. M. … Vos, M. C. (2010). Preventing surgical-site infections in nasal carriers of Staphylococcus aureus. *New England Journal of Medicine*, *362*(1), 9–17.

Boldock, E. … Foster, S. J. (2018). Human skin commensals augment Staphylococcus aureus pathogenesis. *Nature Microbiology*, *3*(8), 881–890.

Brandt, S. L., Putnam, N. E., Cassat, J. E., & Serezani, C. H. (2018). Innate Immunity to Staphylococcus aureus : Evolving Paradigms in Soft Tissue and Invasive Infections . *The Journal of Immunology*, *200*(12), 3871–3880.

Brault, M., & Oberst, A. (2017). Controlled detonation: Evolution of necroptosis in pathogen defense. *Immunology and Cell Biology*, *95*(2), 131–136.

Bravo-Santano, N. … Letek, M. (2018). Intracellular Staphylococcus aureus Modulates Host Central Carbon Metabolism To Activate Autophagy . *MSphere*, *3*(4), e00374-18.

Bremell, T., Lange, S., Yacoub, A., Ryden, C., & Tarkowski, A. (1991). Experimental Staphylococcus aureus arthritis in mice. *Infection and Immunity*, *59*(8), 2615–2623.

Brown, A. F., Leech, J. M., Rogers, T. R., & McLoughlin, R. M. (2014). Staphylococcus aureus colonization: Modulation of host immune response and impact on human vaccine design. *Frontiers in Immunology*, *4*, 1–20.

Bruus, H. (2014). Microscale Acoustofluidics. *Microscale Acoustofluidics*, 1–28.

Buchan, K. D., Foster, S. J., & Renshaw, S. A. (2019). Staphylococcus aureus: Setting its sights on the human innate immune system. *Microbiology*, *165*(4), 367–385.

Bunce, C., Wheeler, L., Reed, G., Musser, J., & Barg, N. (1992). Murine model of cutaneous infection with gram-positive cocci. *Infection and Immunity*, *60*(7), 2636–2640.

Bur, S., Preissner, K. T., Herrmann, M., & Bischoff, M. (2013). The staphylococcus aureus extracellular adherence protein promotes bacterial internalization by keratinocytes independent of fibronectin-binding proteins. *Journal of Investigative Dermatology*, *133*(8), 2004–2012.

Burts, M. L., DeDent, A. C., & Missiakas, D. M. (2008). EsaC substrate for the ESAT-6 secretion pathway and its role in persistent infections of Staphylococcus aureus. *Molecular Microbiology*, *69*(3), 736–746.

Burts, M. L., Williams, W. A., DeBord, K., & Missiakas, D. M. (2005). EsxA and EsxB are secreted by an ESAT-6-like system that is required for the pathogenesis of Staphylococcus aureus infections. *Proceedings of the National Academy of Sciences of the United States of America*, *102*(4), 1169–1174.

Cai, Z. … Liu, Z. G. (2014). Plasma membrane translocation of trimerized MLKL protein is required for TNF-induced necroptosis. *Nature Cell Biology*, *16*(1), 55–65.

Callahan, B. … Derbyshire, K. M. (2010). Conservation of structure and protein-

protein interactions mediated by the secreted mycobacterial proteins EsxA, EsxB, and EspA. *Journal of Bacteriology*, *192*(1), 326–335.

Cao, Z., Casabona, M. G., Kneuper, H., Chalmers, J. D., & Palmer, T. (2016). The type VII secretion system of Staphylococcus aureus secretes a nuclease toxin that targets competitor bacteria. *Nature Microbiology*, *2*(1), 1–11.

Carneiro, L. A. M. … Girardin, S. E. (2009). Shigella Induces Mitochondrial Dysfunction and Cell Death in Nonmyleoid Cells. *Cell Host and Microbe*, *5*(2), 123–136.

Carty, M. … Bowie, A. G. (2019). Cell Survival and Cytokine Release after Inflammasome Activation Is Regulated by the Toll-IL-1R Protein SARM. *Immunity*, *50*(6), 1412-1424.e6.

Casabona, M. G., Buchanan, G., … Palmer, T. (2017). Functional analysis of the EsaB component of the staphylococcus aureus type VII secretion system. *Microbiology (United Kingdom)*, *163*(12), 1851–1863.

Casabona, M. G., Kneuper, H., … Palmer, T. (2017). Haem-iron plays a key role in the regulation of the ess/type VII secretion system of staphylococcus aureus RN6390. *Microbiology*, *163*(12), 1839–1850.

Challa, P. K., Kartanas, T., Charmet, J., & Knowles, T. P. J. (2017). Microfluidic devices fabricated using fast wafer-scale LED-lithography patterning. *Biomicrofluidics*, *11*(1), 014113.

Chambers, H. F., & Deleo, F. R. (2009). Waves of resistance: Staphylococcus aureus in the antibiotic era. *Nature Reviews. Microbiology*, *7*(9), 629–641.

Chanput, W., Mes, J. J., & Wichers, H. J. (2014). THP-1 cell line: An in vitro cell model for immune modulation approach. *International Immunopharmacology*, *23*(1), 37–45.

Chen, Y. H., Anderson, M., Hendrickx, A. P., & Missiakas, D. (2012). Characterization of EssB, a protein required for secretion of ESAT-6 like proteins in Staphylococcus aureus. *BMC Microbiology*, *12*(Figure 1), 1–11.

Cheng, A. G., DeDent, A. C., Schneewind, O., & Missiakas, D. (2011). A play in four acts: Staphylococcus aureus abscess formation. *Trends in Microbiology*, *19*(5), 225–232.

Cheng, A. G. … Missiakas, D. M. (2009). Genetic requirements for Staphylococcus

aureus abscess formation and persistence in host tissues. *FASEB Journal*, *23*(10), 3393–3404.

Cheng, A. G. ... Schneewind, O. (2010). Contribution of coagulases towards Staphylococcus aureus disease and protective immunity. *PLoS Pathogens*, *6*(8), 19–20.

Cheung, G. Y. C., Joo, H. S., Chatterjee, S. S., & Otto, M. (2014). Phenol-soluble modulins - critical determinants of staphylococcal virulence. *FEMS Microbiology Reviews*, *38*(4), 698–719.

Chi, C. Y. ... Lin, C. F. (2014). Panton-valentine leukocidin facilitates the escape of staphylococcus aureus from human keratinocyte endosomes and induces apoptosis. *Journal of Infectious Diseases*, *209*(2), 224–235.

Cho, J. S. ... Miller, L. S. (2012). Neutrophil-derived IL-1β Is Sufficient for Abscess Formation in Immunity against Staphylococcus aureus in Mice. *PLoS Pathogens*, *8*(11), 1003047.

Claes, J. ... Verhamme, P. (2014). Adhesion of Staphylococcus aureus to the vessel wall under flow is mediated by von Willebrand factor - Binding protein. *Blood*, *124*(10), 1669–1676.

Clark, R. R. ... Gray, T. A. (2018). Direct cell–cell contact activates SigM to express the ESX-4 secretion system in Mycobacterium smegmatis. *Proceedings of the National Academy of Sciences of the United States of America*, *115*(28), E6595–E6603.

Clarke, S. R., & Foster, S. J. (2006). Surface Adhesins of Staphylococcus aureus. *Advances in Microbial Physiology*, *12*, 484–488.

Clauditz, A., Resch, A., Wieland, K. P., Peschel, A., & Götz, F. (2006). Staphyloxanthin plays a role in the fitness of Staphylococcus aureus and its ability to cope with oxidative stress. *Infection and Immunity*, *74*(8), 4950–4953.

Conos, S. A. ... Vince, J. E. (2017). Active MLKL triggers the NLRP3 inflammasome in a cell-intrinsic manner. *Proceedings of the National Academy of Sciences of the United States of America*, *114*(6), E961–E969.

Cosgrove, K. ... Foster, S. J. (2007). Catalase (KatA) and alkyl hydroperoxide reductase (AhpC) have compensatory roles in peroxide stress resistance

and are required for survival, persistence, and nasal colonization in Staphylococcus aureus. *Journal of Bacteriology*, *189*(3), 1025–1035.

Craven, R. R. … Duncan, J. A. (2009). Staphylococcus aureus α-hemolysin activates the NLRP3-inflammasome in human and mouse monocytic cells. *PLoS ONE*, *4*(10), e7446.

Creech, C. B., Al-Zubeidi, D. N., & Fritz, S. A. (2015). Prevention of Recurrent Staphylococcal Skin Infections. *Infectious Disease Clinics of North America*, *29*(3), 429–464.

Cruciani, M. … Coccia, E. M. (2017). Staphylococcus aureus Esx Factors Control Human Dendritic Cell Functions Conditioning Th1 / Th17 Response. *Frontiers in Cellular and Infection Microbiology*, *7Cruciani,*(July), 1–13.

Cummings, B. S., & Schnellmann, R. G. (2004). Measurement of Cell Death in Mammalian Cells. *Current Protocols in Pharmacology*, *25*(1).

Dai, Y. … Li, M. (2017). A novel ESAT-6 secretion system-secreted protein EsxX of community-associated Staphylococcus aureus Lineage ST398 contributes to immune evasion and virulence. *Frontiers in Microbiology*, *8*(MAY), 1–13.

Dallenga, T. … Schaible, U. E. (2017). M. tuberculosis-Induced Necrosis of Infected Neutrophils Promotes Bacterial Growth Following Phagocytosis by Macrophages. *Cell Host and Microbe*, *22*(4), 519-530.e3.

Danilchanka, O. … Niederweis, M. (2014). An outer membrane channel protein of Mycobacterium tuberculosis with exotoxin activity. *Proceedings of the National Academy of Sciences of the United States of America*, *111*(18), 6750–6755.

Das, S. … Fraunholz, M. J. (2016). Natural mutations in a Staphylococcus aureus virulence regulator attenuate cytotoxicity but permit bacteremia and abscess formation. *Proceedings of the National Academy of Sciences of the United States of America*, *113*(22), E3101–E3110.

Dauth, S. … Parker, K. K. (2017). Neurons derived from different brain regions are inherently different in vitro: A novel multiregional brain-on-a-chip. *Journal of Neurophysiology*, *117*(3), 1320–1341.

Davis, J. M., & Ramakrishnan, L. (2009). The Role of the Granuloma in Expansion and Dissemination of Early Tuberculous Infection. *Cell*, *136*(1), 37–49.

De La Rosa, J. M. R., Tirella, A., & Tirelli, N. (2015). Characterisation of THP-1 macrophages as an in vitro model for CD44-targeted Therapies. *Biotech, Biomaterials and Biomedical: TechConnect Briefs*, *3*, 86–89.

Deinhardt-Emmer, S. … Mosig, A. S. (2020). Co-infection with Staphylococcus aureus after primary influenza virus infection leads to damage of the endothelium in a human alveolus-on-a-chip model. *Biofabrication*, *12*(2).

Desvaux, M. … Henderson, I. R. (2005). Genomic analysis of the protein secretion systems in Clostridium acetobutylicum ATCC 824. *Biochimica et Biophysica Acta - Molecular Cell Research*, *1745*(2), 223–253.

Dhuriya, Y. K., & Sharma, D. (2018). Necroptosis: A regulated inflammatory mode of cell death. *Journal of Neuroinflammation*, *15*(1), 199.

Diekema, D. J. … Doern, G. V. (2014). Continued Emergence of USA300 Methicillin-Resistant Staphylococcus aureus in the United States: Results from a Nationwide Surveillance Study . *Infection Control & Hospital Epidemiology*, *35*(3), 285–292.

Dikic, I., & Elazar, Z. (2018). Mechanism and medical implications of mammalian autophagy. *Nature Reviews Molecular Cell Biology*, *19*(6), 349–364.

Dondelinger, Y. … Vandenabeele, P. (2014). MLKL Compromises Plasma Membrane Integrity by Binding to Phosphatidylinositol Phosphates. *Cell Reports*, *7*(4), 971–981.

Dortet, L. … Cossart, P. (2011). Recruitment of the major vault protein by inlk: A listeria monocytogenes strategy to avoid autophagy. *PLoS Pathogens*, *7*, e1002168.

Dossett, J., Kronvall, G., Williams, R. J., & Quie, P. (1969). Antiphagocytic effects of staphylococfcal protein A. *J Immunol*, *103*, 1405–1410.

Drevets, D. A., Canono, B. P., Leenen, P. J. M., & Campbell, P. A. (1994). Gentamicin kills intracellular Listeria monocytogenes. *Infection and Immunity*, *62*(6), 2222–2228.

Dumas, E. … Sapriel, G. (2016). Mycobacterial pan-genome analysis suggests important role of plasmids in the radiation of type VII secretion systems. *Genome Biology and Evolution*, *8*(2), 387–402.

DuMont, A. L. … Torres, V. J. (2013). Staphylococcus aureus elaborates leukocidin

AB to mediate escape from within human neutrophils. *Infection and Immunity*, *81*(5), 1830–1841.

Easmon, C. S. F., Lanyon, H., & Cole, P. J. (1978). Use of lysostaphin to remove cell-adherent staphylococci during in vitro assays of phagocyte function. *British Journal of Experimental Pathology*, *59*(4), 381–385.

Edwards, A. M., Potter, U., Meenan, N. A. G., Potts, J. R., & Massey, R. C. (2011). Staphylococcus aureus keratinocyte invasion is dependent upon multiple high-affinity fibronectin-binding repeats within FnBPA. *PLoS ONE*, *6*(4), 18899.

Edwards, A. M., Potts, J. R., Josefsson, E., & Massey, R. C. (2010). Staphylococcus aureus host cell invasion and virulence in sepsis is facilitated by the multiple repeats within FnBPA. *PLoS Pathogens*, *6*(6).

Elsinghorst, E. A. (1994). Measurement of invasion by gentamicin resistance. *Methods in Enzymology*, *236*(C), 405–420.

Enright, M. C. … Spratt, B. G. (2002). The evolutionary history of methicillin-resistant Staphylococcus aureus (MRSA). *Proceedings of the National Academy of Sciences of the United States of America*, *99*(11), 7687–7692.

Ergir, E., Bachmann, B., Redl, H., Forte, G., & Ertl, P. (2018). Small force, big impact: Next generation organ-on-a-chip systems incorporating biomechanical cues. *Frontiers in Physiology*, *9*(OCT).

Esen, M. … Gulbins, E. (2001). Mechanisms of Staphylococcus aureus induced apoptosis of human endothelial cells. *Apoptosis*, *6*(6), 431–439.

Essmann, F. … Jänicke, R. U. (2003). Staphylococcus aureus α-toxin-induced cell death: Predominant necrosis despite apoptotic caspase activation. *Cell Death and Differentiation*, *10*(11), 1260–1272.

Evavold, C. L. … Kagan, J. C. (2018). The Pore-Forming Protein Gasdermin D Regulates Interleukin-1 Secretion from Living Macrophages. *Immunity*, *48*(1), 35-44.e6.

Fang, L., Wu, H. M., Ding, P. S., & Liu, R. Y. (2014). TLR2 mediates phagocytosis and autophagy through JNK signaling pathway in Staphylococcus aureus-stimulated RAW264.7 cells. *Cellular Signalling*, *26*(4), 806–814.

Feuerstein, R., Seidl, M., Prinz, M., & Henneke, P. (2015). MyD88 in Macrophages

Is Critical for Abscess Resolution in Staphylococcal Skin Infection. *The Journal of Immunology*, *194*(6), 2735–2745.

Flannagan, R., Heit, B., & Heinrichs, D. (2015). Antimicrobial Mechanisms of Macrophages and the Immune Evasion Strategies of Staphylococcus aureus. *Pathogens*, *4*(4), 826–868.

Flannagan, R. S., Cosío, G., & Grinstein, S. (2009). Antimicrobial mechanisms of phagocytes and bacterial evasion strategies. *Nature Reviews Microbiology*, *7*(5), 355–366.

Flannagan, R. S., Heit, B., & Heinrichs, D. E. (2016). Intracellular replication of Staphylococcus aureus in mature phagolysosomes in macrophages precedes host cell death, and bacterial escape and dissemination. *Cellular Microbiology*, *18*(4), 514–535.

Flannagan, R. S., Kuiack, R. C., McGavin, M. J., & Heinrichs, D. E. (2018). Staphylococcus aureus uses the GraXRS regulatory system to sense and adapt to the acidified phagolysosome in macrophages. *MBio*, *9*(4), 1–20.

Flieger, A., Frischknecht, F., Häcker, G., Hornef, M. W., & Pradel, G. (2018). Pathways of host cell exit by intracellular pathogens. *Microbial Cell*, *5*(12), 525–544.

Forman, H. J., & Torres, M. (2001). Redox signaling in macrophages. *Molecular Aspects of Medicine*, *22*(4–5), 189–216.

Foster, T. J. (2005). Immune evasion by staphylococci. *Nature Reviews Microbiology*, *3*(12), 948–958.

Foster, T. J., Geoghegan, J. A., Ganesh, V. K., & Höök, M. (2014). Adhesion, invasion and evasion: The many functions of the surface proteins of Staphylococcus aureus. *Nature Reviews Microbiology*, *12*(1), 49–62.

Fournier, B., & Philpott, D. J. (2005). Recognition of Staphylococcus aureus by the innate immune system. *Clinical Microbiology Reviews*, *18*(3), 521–540.

Fowler, T. … Höök, M. (2000). Cellular invasion by Staphylococcus aureus involves a fibronectin bridge between the bacterial fibronectic-binding MSCRAMMs and host cell β1 integrins. *European Journal of Cell Biology*, *79*(10), 672–679.

Frank, D., & Vince, J. E. (2019). Pyroptosis versus necroptosis: similarities,

differences, and crosstalk. *Cell Death and Differentiation*, *26*(1), 99–114.

Fraunholz, M., & Sinha, B. (2012). Intracellular Staphylococcus aureus: live-in and let die. *Frontiers in Cellular and Infection Microbiology*, *2*, 43.

Frenoy, A., & Bonhoeffer, S. (2018). Death and population dynamics affect mutation rate estimates and evolvability under stress in bacteria. *PLoS Biology*, *16*(5).

Fritsch, M. … Kashkar, H. (2019). Caspase-8 is the molecular switch for apoptosis, necroptosis and pyroptosis. *Nature*, *575*(7784), 683–687.

Fritz, S. A. … Hunstad, D. A. (2013). A serologic correlate of protective immunity against community-onset staphylococcus aureus infection. *Clinical Infectious Diseases*, *56*(11), 1554–1561.

Galbraith, G. G., Skalak, R., & Chien, S. (1998). Shear stress induces spatial reorganization of the endothelial cell cytoskeleton. *Cell Motility and the Cytoskeleton*, *40*(4), 317–330.

Galluzzi, L. … Kroemer, G. (2009). Guidelines for the use and interpretation of assays for monitoring cell death in higher eukaryotes. *Cell Death and Differentiation*, *16*(8), 1093–1107.

Galluzzi, Lorenzo … Kroemer, G. (2018). Molecular mechanisms of cell death: Recommendations of the Nomenclature Committee on Cell Death 2018. *Cell Death and Differentiation*, *25*(3), 486–541.

Gelles, J. D., & Chipuk, J. E. (2020). High-Throughput Cell Death Assays with Single-Cell and Population-Level Analyses Using Real-Time Kinetic Labeling (SPARKL). *STAR Protocols*, *1*(1), 100034.

Gelles, J. D. … Chipuk, J. E. (2019). Single-Cell and Population-Level Analyses Using Real-Time Kinetic Labeling Couples Proliferation and Cell Death Mechanisms. *Developmental Cell*, *51*(2), 277-291.e4.

Genestier, A. L. … Genestier, L. (2005). Staphylococcus aureus Panton-Valentine leukocidin directly targets mitochondria and induces Bax-independent apoptosis of human neutrophils. *Journal of Clinical Investigation*, *115*(11), 3117–3127.

Gey Van Pittius, N. C. … Beyers, A. D. (2001). The ESAT-6 gene cluster of Mycobacterium tuberculosis and other high G+C Gram-positive bacteria.

Genome Biology, *2*(10), RESEARCH0044.

Giersing, B. K., Dastgheyb, S. S., Modjarrad, K., & Moorthy, V. (2016). Status of vaccine research and development of vaccines for Staphylococcus aureus. *Vaccine*, *34*(26), 2962–2966.

Giese, B. … Fraunholz, M. J. (2009). Staphylococcal alpha-toxin is not sufficient to mediate escape from phagolysosomes in upper-airway epithelial cells. *Infection and Immunity*, *77*(9), 3611–3625.

Giese, B. … Fraunholz, M. J. (2011). Expression of δ-toxin by Staphylococcus aureus mediates escape from phago-endosomes of human epithelial and endothelial cells in the presence of β-toxin. *Cellular Microbiology*, *13*(2), 316–329.

Glenny, A. T., & Stevens, M. F. (1935). Staphylococcus toxins and antitoxins. *The Journal of Pathology and Bacteriology*, *40*(2), 201–210.

Gómez, M. I. … Prince, A. (2004). Staphylococcus aureus protein A induces airway epithelial inflammatory responses by activating TNFR1. *Nature Medicine*, *10*(8), 842–848.

Gong, Y. N. … Green, D. R. (2017). ESCRT-III Acts Downstream of MLKL to Regulate Necroptotic Cell Death and Its Consequences. *Cell*, *169*(2), 286-300.e16.

González-Juarbe, N. … Orihuela, C. J. (2015). Pore-Forming Toxins Induce Macrophage Necroptosis during Acute Bacterial Pneumonia. *PLoS Pathogens*, *11*(12).

Goodyear, C. S., & Silverman, G. J. (2003). Death by a B cell superantigen: In vivo VH-targeted apoptotic supraclonal B cell deletion by a staphylococcal toxin. *Journal of Experimental Medicine*, *197*(9), 1125–1139.

Graille, M. … Silverman, G. J. (2000). Crystal structure of a Staphylococcus aureus protein a domain complexed with the Fab fragment of a human IgM antibody: Structural basis for recognition of B-cell receptors and superantigen activity. *Proceedings of the National Academy of Sciences of the United States of America*, *97*(10), 5399–5404.

Grassart, A. … Sauvonnet, N. (2019). Bioengineered Human Organ-on-Chip Reveals Intestinal Microenvironment and Mechanical Forces Impacting Shigella Infection. *Cell Host and Microbe*, *26*(3), 435-444.e4.

Gray, T. A. … Derbyshire, K. M. (2016). Intercellular communication and conjugation are mediated by ESX secretion systems in mycobacteria. *Science*, *354*(6310), 347–350.

Green, E. R., & Mecsas, J. (2016). Bacterial Secretion Systems: An Overview. *Microbiology Spectrum*, *4*(1).

Greenlee-Wacker, M. C., Kremserová, S., & Nauseef, W. M. (2017). Lysis of human neutrophils by community-associated methicillin-resistant Staphylococcus aureus. *Blood*, *129*(24), 3237–3244.

Greenlee-Wacker, M. C. … Nauseef, W. M. (2014). Phagocytosis of Staphylococcus aureus by Human Neutrophils Prevents Macrophage Efferocytosis and Induces Programmed Necrosis . *The Journal of Immunology*, *192*(10), 4709–4717.

Gresham, H. D. … Lindberg, F. P. (2000). Survival of Staphylococcus aureus Inside Neutrophils Contributes to Infection . *The Journal of Immunology*, *164*(7), 3713–3722.

Grigoriev, R. O. (2011). Transport and Mixing in Laminar Flows: From Microfluidics to Oceanic Currents. In *Transport and Mixing in Laminar Flows: From Microfluidics to Oceanic Currents*.

Gröschel, M. I., Sayes, F., Simeone, R., Majlessi, L., & Brosch, R. (2016). ESX secretion systems: Mycobacterial evolution to counter host immunity. *Nature Reviews Microbiology*, *14*(11), 677–691.

Grosz, M. … Fraunholz, M. (2014). Cytoplasmic replication of Staphylococcus aureus upon phagosomal escape triggered by phenol-soluble modulin α. *Cellular Microbiology*, *16*(4), 451–465.

Guo, H., Callaway, J. B., & Ting, J. P. Y. (2015). Inflammasomes: Mechanism of action, role in disease, and therapeutics. *Nature Medicine*, *21*(7), 677–687.

Gutierrez, K. D. … Oberst, A. (2017). MLKL Activation Triggers NLRP3-Mediated Processing and Release of IL-1β Independently of Gasdermin-D. *The Journal of Immunology*, *198*(5), 2156–2164.

Halldorsson, S., Lucumi, E., Gómez-Sjöberg, R., & Fleming, R. M. T. (2015). Advantages and challenges of microfluidic cell culture in polydimethylsiloxane devices. *Biosensors and Bioelectronics*, *63*, 218–231.

Hanzelmann, D. ... Peschel, A. (2016). Toll-like receptor 2 activation depends on lipopeptide shedding by bacterial surfactants. *Nature Communications*, *7*.

Harkins, C. P. ... Holden, M. T. G. (2017). Methicillin-resistant Staphylococcus aureus emerged long before the introduction of methicillin into clinical practice. *Genome Biology*, *18*(1).

Hasan, A., Paul, A., Memic, A., & Khademhosseini, A. (2015). A multilayered microfluidic blood vessel-like structure. *Biomedical Microdevices*, *17*(5), 88.

Haslinger-Löffler, B. ... Sinha, B. (2006). Staphylococcus aureus induces caspase-independent cell death in human peritoneal mesothelial cells. *Kidney International*, *70*(6), 1089–1098.

Haslinger-Löffler, Bettina ... Sinha, B. (2005). Multiple virulence factors are required for Staphylococcus aureus-induced apoptosis in endothelial cells. *Cellular Microbiology*, *7*(8), 1087–1097.

Haslinger, B., Strangfeld, K., Peters, G., Schulze-Osthoff, K., & Sinha, B. (2003). Staphylococcus aureus α-toxin induces apoptosis in peripheral blood mononuclear cells: Role of endogenous tumour necrosis factor-α and the mitochondrial death pathway. *Cellular Microbiology*, *5*(10), 729–741.

Haugwitz, U. ... Husmann, M. (2006). Pore-forming Staphylococcus aureus α-toxin triggers epidermal growth factor receptor-dependent proliferation. *Cellular Microbiology*, *8*(10), 1591–1600.

Hayward, A. ... Johnson, A. M. (2008). Increasing hospitalizations and general practice prescriptions for community-onset staphylococcal disease, England. *Emerging Infectious Diseases*, *14*(5), 720–726.

Heinrich, F. ... Spitzbarth, I. (2017). Morphologic, phenotypic, and transcriptomic characterization of classically and alternatively activated canine blood-derived macrophages in vitro. *PLoS ONE*, *12*(8), 1–33.

Helmke, B. P., Thakker, D. B., Goldman, R. D., & Davies, P. F. (2001). Spatiotemporal analysis of flow-induced intermediate filament displacement in living endothelial cells. *Biophysical Journal*, *80*(1), 184–194.

Herman-Bausier, P. ... Dufrêne, Y. F. (2018). Staphylococcus aureus clumping

factor A is a force-sensitive molecular switch that activates bacterial adhesion. *Proceedings of the National Academy of Sciences of the United States of America*, *115*(21), 5564–5569.

Heyman, J. ... De Veylder, L. (2013). ERF115 controls root quiescent center cell division and stem cell replenishment. *Science*, *342*(6160), 860–863.

Ho, M., Yu, D., Davidsion, M. C., & Silva, G. A. (2006). Comparison of standard surface chemistries for culturing mesenchymal stem cells prior to neural differentiation. *Biomaterials*, *27*(24), 4333–4339.

Hoebe, K. ... Beutler, B. (2005). CD36 is a sensor of diacylglycerides. *Nature*, *433*(7025), 523–527.

Holzinger, D. ... Loffler, B. (2012). Staphylococcus aureus Panton-Valentine leukocidin induces an inflammatory response in human phagocytes via the NLRP3 inflammasome. *Journal of Leukocyte Biology*, *92*(5), 1069–1081.

Hoppenbrouwers, T. ... van Neck, J. W. (2018). Staphylococcal protein a is a key factor in neutrophil extracellular traps formation. *Frontiers in Immunology*, *9*(FEB), 1.

Horn, J., Stelzner, K., Rudel, T., & Fraunholz, M. (2017). Inside job: Staphylococcus aureus host-pathogen interactions. *International Journal of Medical Microbiology*, *July*, 0–1.

Horsburgh, M. J. ... Foster, S. J. (2002). δb modulates virulence determinant expression and stress resistance: Characterization of a functional rsbU strain derived from Staphylococcus aureus 8325-4. *Journal of Bacteriology*, *184*(19), 5457–5467.

Houben, E. N. G., Korotkov, K. V., & Bitter, W. (2014). Take five - Type VII secretion systems of Mycobacteria. *Biochimica et Biophysica Acta - Molecular Cell Research*, *1843*(8), 1707–1716.

Hruz, P. ... Eckmann, L. (2009). NOD2 contributes to cutaneous defense against Staphylococcus aureus through α-toxin-dependent innate immune activation. *Proceedings of the National Academy of Sciences of the United States of America*, *106*(31), 12873–12878.

Huang, H. ... Cohen, S. H. (2006). Comparisons of community-associated methicillin-resistant Staphylococcus aureus (MRSA) and hospital-

associated MSRA infections in Sacramento, California. *Journal of Clinical Microbiology*, *44*(7), 2423–2427.

Huh, D. (2015). A Human Breathing Lung-on-a-Chip. *Ann Am Thorac Soc*, *12*, 42–44.

Humphreys, H. … Garau, J. (2016). Staphylococcus aureus and surgical site infections: benefits of screening and decolonization before surgery. *Journal of Hospital Infection*, *94*(3), 295–304.

Huppert, L. A. … Burton, B. M. (2014). The ESX system in Bacillus subtilis mediates protein secretion. *PLoS ONE*, *9*(5), e96267.

Hybiske, K., & Stephens, R. S. (2008). Exit strategies of intracellular pathogens. *Nature Reviews Microbiology*, *6*(2), 99–110.

Ishii, K. … Sekimizu, K. (2014). Induction of virulence gene expression in Staphylococcus aureus by pulmonary surfactant. *Infection and Immunity*, *82*(4), 1500–1510.

Italiani, P., & Boraschi, D. (2014). From monocytes to M1/M2 macrophages: Phenotypical *vs*. functional differentiation. *Frontiers in Immunology*, *5*(OCT), 1–22.

Iwaki, D. … Kuroki, Y. (2002). The extracellular toll-like receptor 2 domain directly binds peptidoglycan derived from Staphylococcus aureus. *Journal of Biological Chemistry*, *277*(27), 24315–24320.

Jäger, F., Kneuper, H., & Palmer, T. (2018). EssC is a specificity determinant for Staphylococcus aureus type VII secretion. *Microbiology*.

Jäger, F., Zoltner, M., Kneuper, H., Hunter, W. N., & Palmer, T. (2016). Membrane interactions and self-association of components of the Ess/Type VII secretion system of Staphylococcus aureus. *FEBS Letters*.

Jang, K. J. … Ingber, D. E. (2013). Human kidney proximal tubule-on-a-chip for drug transport and nephrotoxicity assessment. *Integrative Biology (United Kingdom)*, *5*(9), 1119–1129.

Jang, S. B., Kwon, A. R., Son, W. S., Park, S. J., & Lee, B. J. (2009). Crystal structure of hypothetical protein HP0062 (O24902-HELPY) from helicobacter pylori at 1.65 Å resolution. *Journal of Biochemistry*, *146*(4), 535–540.

Jarry, T. M., & Cheung, A. L. (2006). Staphylococcus aureus escapes more

efficiently from the phagosome of a cystic fibrosis bronchial epithelial cell line than from its normal counterpart. *Infection and Immunity*, *74*(5), 2568–2577.

Jarry, T. M., Memmi, G., & Cheung, A. L. (2008). The expression of alpha-haemolysin is required for Staphylococcus aureus phagosomal escape after internalization in CFT-1 cells. *Cellular Microbiology*, *10*(9), 1801–1814.

Jenul, C., & Horswill, A. R. (2019). Regulation of Staphylococcus aureus Virulence. *Microbiology Spectrum*, *7*(2).

Johnson, A. P. … Duckworth, G. (2012). Mandatory surveillance of methicillin-resistant Staphylococcus aureus (MRSA) bacteraemia in England: The first 10 years. *Journal of Antimicrobial Chemotherapy*, *67*(4), 802–809.

Johnson, A. P., Pearson, A., & Duckworth, G. (2005). Surveillance and epidemiology of MRSA bacteraemia in the UK. *Journal of Antimicrobial Chemotherapy*, *56*(3), 455–462.

Jonsson, K., Signas, C., Muller, H., & Lindberg, M. (1991). Two different genes encode fibronectin binding proteins in Staphylococcus aureus. *European Journal of Biochemistry*, *202*, 1041–1048.

Joo, H. S., Cheung, G. Y. C., & Otto, M. (2011). Antimicrobial activity of community-associated methicillin-resistant Staphylococcus aureus is caused by phenol-soluble modulin derivatives. *Journal of Biological Chemistry*, *286*(11), 8933–8940.

Jorgensen, I., Lopez, J. P., Laufer, S. A., & Miao, E. A. (2016). IL-1β, IL-18, and eicosanoids promote neutrophil recruitment to pore-induced intracellular traps following pyroptosis. *European Journal of Immunology*, *46*(12), 2761–2766.

Jorgensen, I., & Miao, E. A. (2015). Pyroptotic cell death defends against intracellular pathogens. *Immunological Reviews*, *265*(1), 130–142.

Jorgensen, I., Rayamajhi, M., & Miao, E. A. (2017). Programmed cell death as a defence against infection. *Nature Reviews Immunology*, *17*(3), 151–164.

Jorgensen, I., Zhang, Y., Krantz, B. A., & Miao, E. A. (2016). Pyroptosis triggers pore-induced intracellular traps (PITs) that capture bacteria and lead to their clearance by efferocytosis. *Journal of Experimental Medicine*, *213*(10),

2113–2128.

Josse, J., Laurent, F., & Diot, A. (2017). Staphylococcal adhesion and host cell invasion: Fibronectin-binding and other mechanisms. *Frontiers in Microbiology*, *8*(DEC), 2433.

Jubrail, J. … Dockrell, D. H. (2016). Inability to sustain intraphagolysosomal killing of Staphylococcus aureus predisposes to bacterial persistence in macrophages. *Cellular Microbiology*, *18*(1), 80–96.

Kahl, B. C. … Cheung, A. L. (2000). Staphylococcus aureus RN6390 replicates and induces apoptosis in a pulmonary epithelial cell line. *Infection and Immunity*, *68*(9), 5385–5392.

Kahl, Barbara C., Becker, K., & Löffler, B. (2016). Clinical significance and pathogenesis of staphylococcal small colony variants in persistent infections. *Clinical Microbiology Reviews*, *29*(2), 401–427.

Kang, S. … Alnemri, E. S. (2015). Caspase-8 scaffolding function and MLKL regulate NLRP3 inflammasome activation downstream of TLR3. *Nature Communications*, *6*.

Kang, T. B., Yang, S. H., Toth, B., Kovalenko, A., & Wallach, D. (2013). Caspase-8 Blocks Kinase RIPK3-Mediated Activation of the NLRP3 Inflammasome. *Immunity*, *38*(1), 27–40.

Karavolos, M. H., Horsburgh, M., Ingham, E., & Foster, S. J. (2003). Role and regulation of the superoxide dismutases of Staphylococcus aureus. *Microbiology*, *149*(10), 2749–2758.

Kashem, S., Haniffa, M., & Kaplan, D. (2017). Antigen-Presenting Cells in the Skin. *Annual Review of Immunology*, *35*, 469–499.

Kazakova, S. V … Dodson, D. (2005). A Clone of Methicillin-Resistant Staphylococcus aureus among Professional Football Players. *N Engl J Med*, *352*, 468–475. www.nejm.org

Kearney, C. J., & Martin, S. J. (2017). An Inflammatory Perspective on Necroptosis. *Molecular Cell*, *65*(6), 965–973.

Kebaier, C. … Duncan, J. A. (2012). Staphylococcus aureus α-hemolysin mediates virulence in a murine model of severe pneumonia through activation of the NLRP3 inflammasome. *Journal of Infectious Diseases*, *205*(5), 807–817.

Kengmo Tchoupa, A. … Unnikrishnan, M. (2020). The type VII secretion system protects Staphylococcus aureus against antimicrobial host fatty acids. *Scientific Reports*, *10*(1), 1–16.

Kennedy, A. D. … DeLeo, F. R. (2010). Targeting of alpha-hemolysin by active or passive immunization decreases severity of USA300 skin infection in a mouse model. *Journal of Infectious Diseases*, *202*(7), 1050–1058.

Khmaladze, A. … Chen, Z. (2012). Cell volume changes during apoptosis monitored in real time using digital holographic microscopy. *Journal of Structural Biology*, *178*(3), 270–278.

Kiedrowski, M. R., & Horswill, A. R. (2011). New approaches for treating staphylococcal biofilm infections. *Annals of the New York Academy of Sciences*, *1241*(1), 104–121.

Kim, H. J., Huh, D., Hamilton, G., & Ingber, D. E. (2012). Human gut-on-a-chip inhabited by microbial flora that experiences intestinal peristalsis-like motions and flow. *Lab on a Chip*, *12*(12), 2165–2174.

Kim, H. J., & Ingber, D. E. (2013). Gut-on-a-Chip microenvironment induces human intestinal cells to undergo villus differentiation. *Integrative Biology (United Kingdom)*, *5*(9), 1130–1140.

Kim, H. J., Li, H., Collins, J. J., & Ingber, D. E. (2016). Contributions of microbiome and mechanical deformation to intestinal bacterial overgrowth and inflammation in a human gut-on-a-chip. *Proceedings of the National Academy of Sciences of the United States of America*, *113*(1), E7–E15.

Kim, H. K., Missiakas, D., & Schneewind, O. (2014). Mouse models for infectious diseases caused by Staphylococcus aureus. *Journal of Immunological Methods*, *410*, 88–99.

Kim, J. H., Chaurasia, A. K., Batool, N., Ko, K. S., & Kima, K. K. (2019). Alternative enzyme protection assay to overcome the drawbacks of the gentamicin protection assay for measuring entry and intracellular survival of Staphylococci. *Infection and Immunity*, *87*(5).

Kim, J. J. … Raff, A. B. (2019). A microscale, full-thickness, human skin on a chip assay simulating neutrophil responses to skin infection and antibiotic treatments. *Lab on a Chip*, *19*(18), 3094–3103.

Kim, J. W., Heise, R. L., Reynolds, A. M., & Pidaparti, R. M. (2017). Aging effects on airflow dynamics and lung function in human bronchioles. *PLoS ONE*, *12*(8).

Kitur, K. ... Prince, A. (2015). Toxin-Induced Necroptosis Is a Major Mechanism of Staphylococcus aureus Lung Damage. *PLoS Pathogens*, *11*(4), 1004820.

Kitur, K. ... Prince, A. (2016). Necroptosis Promotes Staphylococcus aureus Clearance by Inhibiting Excessive Inflammatory Signaling. *Cell Reports*, *16*(8), 2219–2230.

Klein, M., Krönke, M., & Krut, O. (2006). Expression of lysostaphin in HeLa cells protects from host cell killing by intracellular Staphylococcus aureus. *Medical Microbiology and Immunology*, *195*(3), 159–163.

Klevens, R. M. ... Fridkin, S. K. (2007). Invasive methicillin-resistant Staphylococcus aureus infections in the United States. *Journal of the American Medical Association*, *298*(15), 1763–1771.

Kneuper, H. ... Palmer, T. (2014). Heterogeneity in ess transcriptional organization and variable contribution of the Ess/Type VII protein secretion system to virulence across closely related Staphylocccus aureus strains. *Molecular Microbiology*, *93*(5), 928–943.

Ko, Y. P. ... Rooijakkers, S. H. M. (2013). Phagocytosis Escape by a Staphylococcus aureus Protein That Connects Complement and Coagulation Proteins at the Bacterial Surface. *PLoS Pathogens*, *9*(12), 1–13.

Kobayashi, S. D. ... DeLeo, F. R. (2010). Rapid neutrophil destruction following phagocytosis of Staphylococcus aureus. *Journal of Innate Immunity*, *2*(6), 560–575.

Kobayashi, S. D., Malachowa, N., & Deleo, F. R. (2015). Pathogenesis of Staphylococcus aureus abscesses. *American Journal of Pathology*, *185*(6), 1518–1527.

Kobayashi, S. D. ... DeLeo, F. R. (2011). Comparative analysis of USA300 virulence determinants in a rabbit model of skin and soft tissue infection. *Journal of Infectious Diseases*, *204*(6), 937–941.

Kolata, J. ... Bröker, B. M. (2011). Distinctive patterns in the human antibody response to Staphylococcus aureus bacteremia in carriers and non-

carriers. *Proteomics*, *11*(19), 3914–3927.

Korea, C. G. … Unnikrishnan, M. (2014). Staphylococcal Esx proteins modulate apoptosis and release of intracellular Staphylococcus aureus during infection in epithelial cells. *Infection and Immunity*, *82*(10), 4144–4153.

Koymans, K. J. … Medina, E. (2017). The TLR2 Antagonist Staphylococcal Superantigen-Like Protein 3 Acts as a Virulence Factor to Promote Bacterial Pathogenicity in vivo. *Journal of Innate Immunity*, *9*(6), 561–573.

Koziel, J. … Potempa, J. (2013). The role of Mcl-1 in S. aureus -induced cytoprotection of infected macrophages. *Mediators of Inflammation*, *2013*, 12.

Koziel, J. … Potempa, J. (2009). Phagocytosis of Staphylococcus aureus by macrophages exerts cytoprotective effects manifested by the upregulation of antiapoptotic factors. *PLoS ONE*, *4*(4).

Kretschmer, D. … Peschel, A. (2010). Human formyl peptide receptor 2 senses highly pathogenic Staphylococcus aureus. *Cell Host and Microbe*, *7*(6), 463–473.

Krismer, B., Weidenmaier, C., Zipperer, A., & Peschel, A. (2017). The commensal lifestyle of Staphylococcus aureus and its interactions with the nasal microbiota. *Nature Reviews Microbiology*, *15*(11), 675–687.

Krut, O., Utermöhlen, O., Schlossherr, X., & Krönke, M. (2003). Strain-specific association of cytotoxic activity and virulence of clinical Staphylococcus aureus isolates. *Infection and Immunity*, *71*(5), 2716–2723.

Kubica, M. … Potempa, J. (2008). A potential new pathway for Staphylococcus aureus dissemination: The silent survival of S. aureus phagocytosed by human monocyte-derived macrophages. *PLoS ONE*, *3*(1), e1409.

Kugelberg, E. … Hughes, D. (2005). Establishment of a superficial skin infection model in mice by using Staphylococcus aureus and Streptococcus pyogenes. *Antimicrobial Agents and Chemotherapy*, *49*(8), 3435–3441.

Kuklin, N. A. … Anderson, A. S. (2006). A novel Staphylococcus aureus vaccine: Iron surface determinant B induces rapid antibody responses in rhesus macaques and specific increased survival in a murine S. aureus sepsis model. *Infection and Immunity*, *74*(4), 2215–2223.

Lacey, K. A., Geoghegan, J. A., & McLoughlin, R. M. (2016). The role of staphylococcus aureus virulence factors in skin infection and their potential as vaccine antigens. *Pathogens*, *5*(1).

Lacey, K. A., Mulcahy, M. E., Towell, A. M., Geoghegan, J. A., & McLoughlin, R. M. (2019). Clumping factor B is an important virulence factor during Staphylococcus aureus skin infection and a promising vaccine target. *PLoS Pathogens*, *15*(4).

Lacoma, A. … Bengoechea, J. A. (2017). Investigating intracellular persistence of Staphylococcus aureus within a murine alveolar macrophage cell line. *Virulence*, *8*(8), 1761–1775.

Laencina, L. … Girard-Misguich, F. (2018). Identification of genes required for Mycobacterium abscessus growth in vivo with a prominent role of the ESX-4 locus. *Proceedings of the National Academy of Sciences of the United States of America*, *115*(5), E1002–E1011.

Lâm, T. T. … Sinha, B. (2010). Phagolysosomal integrity is generally maintained after Staphylococcus aureus invasion of nonprofessional phagocytes but is modulated by strain 6850. *Infection and Immunity*, *78*(8), 3392–3393.

Lamkanfi, M., & Dixit, V. M. (2010). Manipulation of host cell death pathways during microbial infections. *Cell Host and Microbe*, *8*(1), 44–54.

Laupland, K. B., Ross, T., & Gregson, D. B. (2008). Staphylococcus aureus Bloodstream Infections: Risk Factors, Outcomes, and the Influence of Methicillin Resistance in Calgary, Canada, 2000–2006 . *The Journal of Infectious Diseases*, *198*(3), 336–343.

Lawlor, K. E. … Vince, J. E. (2015). RIPK3 promotes cell death and NLRP3 inflammasome activation in the absence of MLKL. *Nature Communications*, *6*.

Lehar, S. M. … Mariathasan, S. (2015). Novel antibody-antibiotic conjugate eliminates intracellular S. aureus. *Nature*, *527*(7578), 323–328.

Letek, M. … Vázquez-Boland, J. A. (2010). The genome of a pathogenic Rhodococcus: Cooptive virulence underpinned by key gene acquisitions. *PLoS Genetics*, *6*(9), e1001145.

Leung, K. Y., & Finlay, B. B. (1991). Intracellular replication is essential for the

virulence of Salmonella typhimurium. *PNAS*, *88*(24), 11470–11474.

Lewis, K. N. … Sherman, D. R. (2003). Deletion of RD1 from Mycobacterium tuberculosis mimics bacille Calmette-Guérin attenuation. *Journal of Infectious Diseases*, *187*(1), 117–123.

Li, M., Stenmark, K. R., Shandas, R., & Tan, W. (2009). Effects of pathological flow on pulmonary artery endothelial production of vasoactive mediators and growth factors. *Journal of Vascular Research*, *46*(6), 561–571.

Li, Z., Peres, A. G., Damian, A. C., & Madrenas, J. (2015). Immunomodulation and disease tolerance to Staphylococcus aureus. *Pathogens*, *4*(4), 793–815.

Lieberman, J., Wu, H., & Kagan, J. C. (2019). Gasdermin D activity in inflammation and host defense. *Science Immunology*, *4*(39).

Lindmark, R., Thorén-Tolling, K., & Sjöquist, J. (1983). Binding of immunoglobulins to protein A and immunoglobulin levels in mammalian sera. *Journal of Immunological Methods*, *62*(1), 1–13.

Liu, C., & Chambers, H. F. (2003). Staphylococcus aureus with heterogeneous resistance to vancomycin: Epidemiology, clinical significance, and critical assessment of diagnostic methods. *Antimicrobial Agents and Chemotherapy*, *47*(10), 3040–3045.

Liu, X. … Lieberman, J. (2016). Inflammasome-activated gasdermin D causes pyroptosis by forming membrane pores. *Nature*, *535*(7610), 153–158.

Lopez de Armentia, M. M. L., Gauron, M. C., & Colombo, M. I. (2017). Staphylococcus aureus alpha-toxin induces the formation of dynamic tubules labeled with LC3 within host cells in a Rab7 and rab1b-dependent manner. *Frontiers in Cellular and Infection Microbiology*, *7*(OCT), 431.

Lopez, M. S. … Brown, E. J. (2017). Host-derived fatty acids activate type VII secretion in Staphylococcus aureus. *Proceedings of the National Academy of Sciences of the United States of America*, *114*(42), 11223–11228.

Lowy, F D. (1998). Staphylococcus aureus infections. *The New England Journal of Medicine*, *339*, 520–532.

Lowy, Franklin D., Fant, J., Higgins, L. L., Ogawa, S. K., & Hatcher, V. B. (1988). Staphylococcus aureus-human endothelial cell interactions. *Journal of Ultrastructure Research and Molecular Structure Research*, *98*(2), 137–146.

Mahto, S. K., Tenenbaum-Katan, J., Greenblum, A., Rothen-Rutishauser, B., & Sznitman, J. (2014). Microfluidic shear stress-regulated surfactant secretion in alveolar epithelial type II cells in vitro. *American Journal of Physiology - Lung Cellular and Molecular Physiology*, *306*(7), 672–683.

Mancini, F. … Bertholet, S. (2016a). One dose of staphylococcus aureus 4C-staph vaccine formulated with a novel TLR7-dependent adjuvant rapidly protects mice through antibodies, effector CD4+ T Cells, and IL-17A. *PLoS ONE*, *11*(1), e0147767.

Mancini, F. … Bertholet, S. (2016b). One dose of staphylococcus aureus 4C-staph vaccine formulated with a novel TLR7-dependent adjuvant rapidly protects mice through antibodies, effector CD4+ T Cells, and IL-17A. *PLoS ONE*, *11*(1).

Martinez, F. O., & Gordon, S. (2014). The M1 and M2 paradigm of macrophage activation: Time for reassessment. *F1000Prime Reports*, *6*.

Masopust, D., Sivula, C. P., & Jameson, S. C. (2017). Of Mice, Dirty Mice, and Men: Using Mice To Understand Human Immunology. *The Journal of Immunology*, *199*(2), 383–388.

Matejuk, A. (2018). Skin Immunity. *Archivum Immunologiae et Therapiae Experimentalis*, *66*(1), 45–54.

Mattock, E., & Blocker, A. J. (2017). How do the virulence factors of shigella work together to cause disease? *Frontiers in Cellular and Infection Microbiology*, *7*, 1–24.

McDonald, J. C., & Whitesides, G. M. (2002). Poly(dimethylsiloxane) as a material for fabricating microfluidic devices. *Accounts of Chemical Research*, *35*(7), 491–499.

McGuinness, W. A., Malachowa, N., & DeLeo, F. R. (2017). Vancomycin resistance in Staphylococcus aureus. *Yale Journal of Biology and Medicine*, *90*(2), 269–281.

McNeil, J. C., & Fritz, S. A. (2019). Prevention Strategies for Recurrent Community-Associated Staphylococcus aureus Skin and Soft Tissue Infections. *Current Infectious Disease Reports*, *21*(4), 12.

McVicker, G. … Foster, S. J. (2014). Clonal Expansion during Staphylococcus

aureus Infection Dynamics Reveals the Effect of Antibiotic Intervention. *PLoS Pathogens*, *10*(2).

McWhorter, F. Y., Wang, T., Nguyen, P., Chung, T., & Liu, W. F. (2013). Modulation of macrophage phenotype by cell shape. *Proceedings of the National Academy of Sciences of the United States of America*, *110*(43), 17253–17258.

Mehra, A. … Philips, J. A. (2013). Mycobacterium tuberculosis Type VII Secreted Effector EsxH Targets Host ESCRT to Impair Trafficking. *PLoS Pathogens*, *9*(10).

Melehani, J. H., & Duncan, J. A. (2016). Inflammasome activation can mediate tissue-specific pathogenesis or protection in Staphylococcus aureus infection. *Current Topics in Microbiology and Immunology*, *397*, 257–282.

Melehani, J. H., James, D. B. A., DuMont, A. L., Torres, V. J., & Duncan, J. A. (2015). Staphylococcus aureus Leukocidin A/B (LukAB) Kills Human Monocytes via Host NLRP3 and ASC when Extracellular, but Not Intracellular. *PLoS Pathogens*, *11*(6), 2–25.

Menashe, O., Kaganskaya, E., Baasov, T., & Yaron, S. (2008). Aminoglycosides affect intracellular Salmonella enterica serovars typhimurium and virchow. *Antimicrobial Agents and Chemotherapy*, *52*(3), 920–926.

Mendum, T. A., Wu, H., Kierzek, A. M., & Stewart, G. R. (2015). Lipid metabolism and type VII secretion systems dominate the genome scale virulence profile of Mycobacterium tuberculosis in human dendritic cells. *BMC Genomics*, *16*(1).

Menzies, B. E., & Kernodle, D. S. (1996). Passive immunization with antiserum to a nontoxic alpha-toxin mutant from Staphylococcus aureus is protective in a murine model. *Infection and Immunity*, *64*(5), 1839–1841.

Menzies, B. E., & Kourteva, I. (1998). Internalization of Staphylococcus aureus by endothelial cells induces apoptosis. *Infection and Immunity*, *66*(12), 5994–5998.

Menzies, B. E., & Kourteva, I. (2000). Staphylococcus aureus aplha-toxin induces apoptosis in endothelial cells. *FEMS Immunology & Medical Microbiology*, *29*(1), 39–45.

Mestre, M. B., Fader, C. M., Sola, C., & Colombo, M. I. (2010). α-hemolysin is

required for the activation of the autophagic pathway in Staphylococcus aureus-infected cells. *Autophagy*, *6*(1), 110–125.

Miao, E. A., Rajan, J. V., & Aderem, A. (2011). Caspase-1-induced pyroptotic cell death. *Immunological Reviews*, *243*(1), 206–214.

Mielich-Süss, B. … Lopez, D. (2017). Flotillin scaffold activity contributes to type VII secretion system assembly in Staphylococcus aureus. *PLoS Pathogens*, *13*(11), e1006728.

Mietrach, N., Damián-Aparicio, D., Süß, B.-M., Lopez, D., & Geibel, S. (2020). Substrate interaction with the EssC coupling protein of the Type VIIb secretion system. *Journal of Bacteriology*.

Mihaila, L. … Branger, C. (2010). Probable intrafamily transmission of a highly virulent CTX-M-3-producing Escherichia coli belonging to the emerging phylogenetic subgroup D2 O102-ST405 clone. *Journal of Antimicrobial Chemotherapy*, *65*(7), 1537–1539.

Miller, L. S. … Modlin, R. L. (2006). MyD88 mediates neutrophil recruitment initiated by IL-1R but not TLR2 activation in immunity against Staphylococcus aureus. *Immunity*, *24*(1), 79–91.

Mishra, B. B. … Anes, E. (2010). Mycobacterium tuberculosis protein ESAT-6 is a potent activator of the NLRP3/ASC inflammasome. *Cellular Microbiology*, *12*(8), 1046–1063.

Missiakas, D., & Winstel, V. (2021). Selective Host Cell Death by Staphylococcus aureus: A Strategy for Bacterial Persistence. *Frontiers in Immunology*, *11*, 1–15.

Mittal, E. … Phillips, J. (2018). Mycobacterium tuberculosis Type VII Secretion System Effectors Differentially Impact the ESCRT Endomembrane Damage Response. *MBio*, *9*, 1–10.

Moldovan, A., & Fraunholz, M. J. (2019). In or out: Phagosomal escape of Staphylococcus aureus. *Cellular Microbiology*, *21*(3), 1–9.

Montgomery, C. P. … Daum, R. S. (2008). Comparison of virulence in community-associated methicillin-resistant staphylococcus aureus pulsotypes USA300 and USA400 in a rat model of pneumonia. *Journal of Infectious Diseases*, *198*(4), 561–570.

Moormeier, D. E., & Bayles, K. W. (2017). Staphylococcus aureus biofilm: a complex developmental organism. *Molecular Microbiology*, *104*(3), 365–376.

Moretti, J., & Blander, J. M. (2014). Insights into phagocytosis-coupled activation of pattern recognition receptors and inflammasomes. *Current Opinion in Immunology*, *26*(1), 100–110.

Mrochen, D. M., Fernandes de Oliveira, L. M., Raafat, D., & Holtfreter, S. (2020). Staphylococcus aureus host tropism and its implications for murine infection models. *International Journal of Molecular Sciences*, *21*(19), 1–35.

Mulcahy, M. E. … McLoughlin, R. M. (2012). Nasal Colonisation by Staphylococcus aureus Depends upon Clumping Factor B Binding to the Squamous Epithelial Cell Envelope Protein Loricrin. *PLoS Pathogens*, *8*(12).

Mulcahy, M. E. … McLoughlin, R. M. (2020). Manipulation of Autophagy and Apoptosis Facilitates Intracellular Survival of Staphylococcus aureus in Human Neutrophils. *Frontiers in Immunology*, *11*(November), 1–14.

Muñoz-Planillo, R., Franchi, L., Miller, L. S., & Núñez, G. (2009). A Critical Role for Hemolysins and Bacterial Lipoproteins in Staphylococcus aureus -Induced Activation of the Nlrp3 Inflammasome . *The Journal of Immunology*, *183*(6), 3942–3948.

Münzenmayer, L. … Wolz, C. (2016). Influence of Sae-regulated and Agr-regulated factors on the escape of Staphylococcus aureus from human macrophages. *Cellular Microbiology*, *18*(8), 1172–1183.

Murray, L. M., Nock, V., Evans, J. J., & Alkaisi, M. M. (2016). The use of substrate materials and topography to modify growth patterns and rates of differentiation of muscle cells. *Journal of Biomedical Materials Research - Part A*, *104*(7), 1638–1645.

Naber, C. K. (2009). Staphylococcus aureus Bacteremia: Epidemiology, Pathophysiology, and Management Strategies . *Clinical Infectious Diseases*, *48*(s4), S231–S237.

Nakayama, M. … Ogasawara, K. (2012). Inhibitory Receptor Paired Ig-like Receptor B Is Exploited by Staphylococcus aureus for Virulence . *The Journal of Immunology*, *189*(12), 5903–5911.

Nakayama, M. … Aderem, A. (2007). Paired Ig-Like Receptors Bind to Bacteria and Shape TLR-Mediated Cytokine Production. *The Journal of Immunology*, *178*(7), 4250–4259.

Natale, P., Brüser, T., & Driessen, A. J. M. (2008). Sec- and Tat-mediated protein secretion across the bacterial cytoplasmic membrane-Distinct translocases and mechanisms. *Biochimica et Biophysica Acta - Biomembranes*.

Netea, M. G. … Joosten, L. A. B. (2010). IL-1β processing in host defense: Beyond the inflammasomes. *PLoS Pathogens*, *6*(2), 1000661.

Neumann, Y. … Schmitz, I. (2016). Intracellular Staphylococcus aureus eludes selective autophagy by activating a host cell kinase. *Autophagy*, *12*(11), 2069–2084.

Nougayrède, J. P., & Donnenberg, M. S. (2004). Enteropathogenic Escherichia coli EspF is targeted to mitochondria and is required to initiate the mitochondrial death pathway. *Cellular Microbiology*, *6*(11), 1097–1111.

Nygaard, T. K. … Voyich, J. M. (2012). Alpha-toxin induces programmed cell death of human T cells, B cells, and monocytes during USA300 infection. *PLoS ONE*, *7*(5), 36532.

O'Keeffe, K. M. … McLoughlin, R. M. (2015). Manipulation of autophagy in phagocytes facilitates Staphylococcus aureus bloodstream infection. *Infection and Immunity*, *83*(9), 3445–3457.

Oberst, A. … Green, D. R. (2011). Catalytic activity of the caspase-8-FLIP L complex inhibits RIPK3-dependent necrosis. *Nature*, *471*(7338), 363–368.

Ohr, R. J., Anderson, M., Shi, M., & Schneewind, O. (2017). EssD, a Nuclease Effector of the Staphylococcus aureus ESS Pathway. *Journal of Bacteriology*, *199*(1), e005258-16.

Olaniyi, R., Pozzi, C., Grimaldi, L., & Bagnoli, F. (2017). Staphylococcus aureus-associated skin and soft tissue infections: Anatomical localization, epidemiology, therapy and potential prophylaxis. *Current Topics in Microbiology and Immunology*, *409*, 199–227.

Oliveira, D., Borges, A., & Simões, M. (2018). Staphylococcus aureus toxins and their molecular activity in infectious diseases. *Toxins*, *10*(6).

Otto, M. (2018). Staphylococcal Biofilms. *Microbiology Spectrum*, *6*(4), 699–711.

Page, R., & Peti, W. (2016). Toxin-antitoxin systems in bacterial growth arrest and persistence. *Nature Chemical Biology*, *12*(4), 208–214.

Pajuelo, D. … Niederweis, M. (2018). NAD+ Depletion Triggers Macrophage Necroptosis, a Cell Death Pathway Exploited by Mycobacterium tuberculosis. *Cell Reports*, *24*(2), 429–440.

Pallen, M. J. (2002). The ESAT-6/WXG100 superfamily - And a new Gram-positive secretion system? *Trends in Microbiology*, *10*(5), 209–212.

Pang, Y. Y. … Nauseef, W. M. (2010). Agr-dependent interactions of Staphylococcus aureus USA300 with human polymorphonuclear neutrophils. *Journal of Innate Immunity*, *2*(6), 546–559.

Panizzi, P. … Weissleder Ralph. (2011). In vivo detection of Staphylococcus aureus endocarditis by targeting pathogen-specific prothrombin activation. *Nature Medicine*, *17*(9), 1142–1147.

Papanikou, E., Karamanou, S., & Economou, A. (2007). Bacterial protein secretion through the translocase nanomachine. *Nature Reviews Microbiology*, *5*(11), 839–851.

Pappelbaum, K. I. … Schneider, S. W. (2013). Ultralarge von willebrand factor fibers mediate luminal staphylococcus aureus adhesion to an intact endothelial cell layer under shear stress. *Circulation*, *128*(1), 50–59.

Parsons, J. B., Yao, J., Frank, M. W., Jackson, P., & Rock, C. O. (2012). Membrane disruption by antimicrobial fatty acids releases low-molecular-weight proteins from staphylococcus aureus. *Journal of Bacteriology*, *194*(19), 5294–5304.

Patti, J. M., Allen, B. L., McGavin, M. J., & Hook, M. (1994). MSCRAMM-medicated adherence of microorganisms to host tissues. *Annual Review of Microbiology*, *48*, 585–617.

Pavillon, N. … Marquety, P. (2010). Cell morphology and intracellular ionic homeostasis explored with a multimodal approach combining epifluorescence and digital holographic microscopy. *Journal of Biophotonics*, *3*(7), 432–436.

Pavillon, N. … Marquet, P. (2012). Early cell death detection with digital holographic microscopy. *PLoS ONE*, *7*(1).

Pearson, J. S. ... Hartland, E. L. (2013). A type III effector antagonizes death receptor signalling during bacterial gut infection. *Nature*, *501*(7466), 247–251.

Periasamy, S. ... Otto, M. (2012). How Staphylococcus aureus biofilms develop their characteristic structure. *PNAS*, *109*(4), 1281–1286.

Peschel, A. ... Van Strijp, J. A. G. (2001). Staphylococcus aureus resistance to human defensins and evasion of neutrophil killing via the novel virulence factor MprF is based on modification of membrane lipids with L-lysine. *Journal of Experimental Medicine*, *193*(9), 1067–1076.

Pidwill, G. R., Gibson, J. F., Cole, J., Renshaw, S. A., & Foster, S. J. (2021). The Role of Macrophages in Staphylococcus aureus Infection. *Frontiers in Immunology*, *11*(January), 1–30.

Ploeger, D. T. ... Bank, R. A. (2013). Cell plasticity in wound healing: Paracrine factors of M1/ M2 polarized macrophages influence the phenotypical state of dermal fibroblasts. *Cell Communication and Signaling*, *11*(1).

Polat, G., Ugan, R. A., Cadirci, E., & Halici, Z. (2017). Sepsis and Septic Shock: Current Treatment Strategies and New Approaches. *Eurasian Journal of Medicine*, *49*(1), 53–58.

Pollitt, E. J. G., Szkuta, P. T., Burns, N., & Foster, S. J. (2018). Staphylococcus aureus infection dynamics. *PLoS Pathogens*, *14*(6).

Pollock, G. L. ... Hartland, E. L. (2017). Distinct roles of the antiapoptotic effectors NleB and NleF from enteropathogenic Escherichia coli. *Infection and Immunity*, *85*(4).

Portal-Celhay, C. ... Philips, J. A. (2016). Mycobacterium tuberculosis EsxH inhibits ESCRT-dependent CD4+ T-cell activation. *Nature Microbiology*, *2*.

Poulsen, C., Panjikar, S., Holton, S. J., Wilmanns, M., & Song, Y. H. (2014). WXG100 protein superfamily consists of three subfamilies and exhibits an α-helical C-terminal conserved residue pattern. *PLoS ONE*, *9*(2), e89313.

Powers, M. E., Kim, H. K., Wang, Y., & Wardenburg, J. B. (2012). ADAM10 mediates vascular injury induced by staphylococcus aureus α-hemolysin. *Journal of Infectious Diseases*, *206*(3), 352–356.

Proctor, R. A., Van Langevelde, P., Kristjansson, M., Maslow, J. N., & Arbeit, R. D.

(1995). Persistent and relapsing infections associated with small-colony variants of staphylococcus aureus. *Clinical Infectious Diseases*, *20*(1), 95–102.

Proctor, R. A. ... Peters, G. (2006). Small colony variants: A pathogenic form of bacteria that facilitates persistent and recurrent infections. *Nature Reviews Microbiology*, *4*(4), 295–305.

Public Health England. (2019). *MRSA and MSSA bacteraemia: annual data*. Staphylococcus Aureus: Guidance, Data and Analysis. https://www.gov.uk/government/collections/staphylococcus-aureus-guidance-data-and-analysis

Pym, A. S., Brodin, P., Brosch, R., Huerre, M., & Cole, S. T. (2002). Loss of RD1 contributed to the attenuation of the live tuberculosis vaccines Mycobacterium bovis BCG and Mycobacterium microti. *Molecular Microbiology*, *46*(3), 709–717.

Pym, A. S. ... Cole, S. T. (2003). Recombinant BCG exporting ESAT-6 confers enhanced protection against tuberculosis. *Nat Med*, *9*(5), 548–553.

Qazi, S. N. A. ... Hill, P. J. (2001). Agr Expression Precedes Escape of Internalized Staphylococcus Aureus From the Host Endosome. *Infection and Immunity*, *69*(11), 7074–7082.

Ramachandran, R. P. ... Aroeti, B. (2020). Mitochondrial targeting of the enteropathogenic escherichia coli map triggers calcium mobilization, adam10-map kinase signaling, and host cell apoptosis. *MBio*, *11*(5), 1–18.

Rathkey, J. K. ... Abbott, D. W. (2018). Chemical disruption of the pyroptotic pore-forming protein gasdermin D inhibits inflammatory cell death and sepsis. *Science Immunology*, *3*(26).

Rathman, M., Sjaastad, M. D., & Falkow, S. (1996). Acidification of phagosomes containing Salmonella typhimurium in murine macrophages. *Infection and Immunity*, *64*(7), 2765–2773.

Ray, G. T., Suaya, J. A., & Baxter, R. (2013). Incidence, microbiology, and patient characteristics of skin and soft-tissue infections in a U.S. population: A retrospective population-based study. *BMC Infectious Diseases*, *13*(1), 1.

Reddy, K., & Ross, J. M. (2001). Shear stress prevents fibronectin binding protein-

mediated Staphylococcus aureus adhesion to resting endothelial cells. *Infection and Immunity*, *69*(5), 3472–3475.

Redi, D., Raffaelli, C. S., Rossetti, B., De Luca, A., & Montagnani, F. (2018). Staphylococcus aureus vaccine preclinical and clinical development: current state of the art. *New Microbiologica*, *41*, 1121–7138.

Renshaw, P. S. … Carr, M. D. (2005). Structure and function of the complex formed by the tuberculosis virulence factors CFP-10 and ESAT-6. *The EMBO Journal*, *24*(14), 2491–2498.

Rice, L. B. (2008). Federal funding for the study of antimicrobial resistance in nosocomial pathogens: No ESKAPE. *Journal of Infectious Diseases*, *197*(8), 1079–1081.

Richardson, A., Libby, S. J., & Fang, F. C. (2008). A Nitric Oxide–Inducible Lactate Dehydrogenase Enables Staphylococcus aureus to Resist Innate Immunity. *Science*, *319*, 1672–1676.

Rittirsch, D., Flierl, M. A., & Ward, P. A. (2008). Harmful molecular mechanisms in sepsis. *Nature Reviews Immunology*, *8*(10), 776–787.

Romagnoli, A. … Coccia, E. M. (2012). ESX-1 dependent impairment of autophagic flux by Mycobacterium tuberculosis in human dendritic cells. *Autophagy*, *8*(9), 1357–1370.

Rostam, H. M. … Ghaemmaghami, A. M. (2016). The impact of surface chemistry modification on macrophage polarisation. *Immunobiology*, *221*(11), 1237–1246.

Roux, K. J., Kim, D. I., Burke, B., & May, D. G. (2018). BioID: A Screen for Protein-Protein Interactions. *Current Protocols in Protein Science*, *91*(1), 19.23.1-19.23.15.

Roy, S., Ghatak, D., Das, P., & BoseDasgupta, S. (2020). ESX secretion system: The gatekeepers of mycobacterial survivability and pathogenesis. *European Journal of Microbiology and Immunology*, *10*(4), 202–209.

Rudkin, J. K., McLoughlin, R. M., Preston, A., & Massey, R. C. (2017). Bacterial toxins: Offensive, defensive, or something else altogether? *PLoS Pathogens*, *13*(9).

Rühl, S. … Broz, P. (2018). ESCRT-dependent membrane repair negatively

regulates pyroptosis downstream of GSDMD activation. *Science*, *362*(6417), 956–960.

Safdar, N., & Bradley, E. A. (2008). The Risk of Infection after Nasal Colonization with Staphylococcus Aureus. *American Journal of Medicine*, *121*(4), 310–315.

Salgado-Pabón, W., & Schlievert, P. M. (2014). Models matter: The search for an effective Staphylococcus aureus vaccine. *Nature Reviews Microbiology*, *12*(8), 585–591.

Saxena, S. … Sharland, M. (2010). Increasing skin infections and Staphylococcus aureus complications in children, England, 1997-2006. *Emerging Infectious Diseases*, *16*(3), 530–533.

Scherr, T. D., Heim, C. E., Morrison, J. M., & Kielian, T. (2014). Hiding in plain sight: Interplay between staphylococcal biofilms and host immunity. *Frontiers in Immunology*, *5*(37), 1–7.

Schildberger, A., Rossmanith, E., Eichhorn, T., Strassl, K., & Weber, V. (2013). Monocytes, peripheral blood mononuclear cells, and THP-1 cells exhibit different cytokine expression patterns following stimulation with lipopolysaccharide. *Mediators of Inflammation*, *2013*.

Schnaith, A. … Krut, O. (2007). Staphylococcus aureus subvert autophagy for induction of caspase-independent host cell death. *Journal of Biological Chemistry*, *282*(4), 2695–2706.

Schulthess, B., Bloes, D. A., & Berger-Bächi, B. (2012). Opposing roles of σ b and σ b-controlled SpoVG in the global regulation of esxA in Staphylococcus aureus. *BMC Microbiology*, *12*.

Schultze, M. … Yakovlev, V. S. (2010a). Delay in photoemission. *Science*, *328*(5986), 1658–1662.

Schultze, M. … Yakovlev, V. S. (2010b). Delay in photoemission. *Science*, *328*(5986), 1658–1662.

Schwandner, R., Dziarski, R., Wesche, H., Rothe, M., & Kirschning, C. J. (1999). Peptidoglycan- and lipoteichoic acid-induced cell activation is mediated by Toll-like receptor 2. *Journal of Biological Chemistry*, *274*(25), 17406–17409.

Schwartz, J., Leidal, K. G., Femling, J. K., Weiss, J. P., & Nauseef, W. M. (2009). Neutrophil Bleaching of GFP-Expressing Staphylococci: Probing the Intraphagosomal Fate of Individual Bacteria. *The Journal of Immunology*, *183*(4), 2632–2641.

Schwarz-Linek, U., Höök, M., & Potts, J. R. (2004). The molecular basis of fibronectin-mediated bacterial adherence to host cells. *Molecular Microbiology*, *52*(3), 631–641.

Schwarz-Linek, U. ... Potts, J. R. (2003). Pathogenic bacteria attach to human fibronectin through a tandem β-zipper. *Nature*, *423*(6936), 177–181.

Sejvar, J. J. (2013). Neuroinfections (What Do I Do Now?). *Emerging Infectious Diseases*, *19*(9), 1553–1553.

Sendi, P., & Proctor, R. A. (2009). Staphylococcus aureus as an intracellular pathogen: the role of small colony variants. *Trends in Microbiology*, *17*(2), 54–58.

Shen, F. ... Yu, L. (2016). Fosfomycin enhances phagocyte-mediated killing of Staphylococcus aureus by extracellular traps and reactive oxygen species. *Scientific Reports*, *6*(August 2015), 1–15.

Shi, J. ... Shao, F. (2015). Cleavage of GSDMD by inflammatory caspases determines pyroptotic cell death. *Nature*, *526*(7575), 660–665.

Shimada, T. ... Underhill, D. M. (2010). Staphylococcus aureus Evades Lysozyme-Based Peptidoglycan Digestion that Links Phagocytosis, Inflammasome Activation, and IL-1β Secretion. *Cell Host and Microbe*, *7*(1), 38–49.

Shompole, S. ... Bayles, K. W. (2003). Biphasic intracellular expression of Staphylococcus aureus virulence factors and evidence for Agr-mediated diffusion sensing. *Molecular Microbiology*, *49*(4), 919–927.

Shrestha, J. ... Ebrahimi Warkiani, M. (2019). A rapidly prototyped lung-on-a-chip model using 3D-printed molds. *Organs-on-a-Chip*, *1*(December 2019), 100001.

Shrivastava, S. R., Shrivastava, P. S., & Ramasamy, J. (2018). World health organization releases global priority list of antibiotic-resistant bacteria to guide research, discovery, and development of new antibiotics. *JMS - Journal of Medical Society*, *32*(1), 76–77.

Si, L. ... Ingber, D. E. (2020). Human organs-on-chips as tools for repurposing approved drugs as potential influenza and COVID19 therapeutics in viral pandemics. *BioRxiv*, 2020.04.13.039917.

Si, L. ... Ingber, D. E. (2019). Discovery of influenza drug resistance mutations and host therapeutic targets using a human airway chip. *BioRxiv*, 685552.

Sibbald, M. J. J. B. ... van Dijl, J. M. (2006). Mapping the Pathways to StaphylococcalPathogenesis by Comparative Secretomics. *Microbiology and Molecular Biology Reviews*, *70*(3), 755–788.

Siboo, I. R., Chaffin, D. O., Rubens, C. E., & Sullam, P. M. (2008). Characterization of the accessory sec system of Staphylococcus aureus. *Journal of Bacteriology*, *190*(18), 6188–6196.

Sidhaye, V. K., Schweitzer, K. S., Caterina, M. J., Shimoda, L., & King, L. S. (2008). Shear stress regulates aquaporin-5 and airway epithelial barrier function. *Proceedings of the National Academy of Sciences of the United States of America*, *105*(9), 3345–3350.

Singh, R., Letai, A., & Sarosiek, K. (2019). Regulation of apoptosis in health and disease: the balancing act of BCL-2 family proteins. *Nature Reviews Molecular Cell Biology*, *20*(3), 175–193.

Sinha, B. ... Krause, K. H. (1999). Fibronectin-binding protein acts as Staphylococcus aureus invasin via fibronectin bridging to integrin α5β1. *Cellular Microbiology*, *1*(2), 101–117.

Sinha, B. ... Herrmann, M. (2000). Heterologously expressed staphylococcus aureus fibronectin-binding proteins are sufficient for invasion of host cells. *Infection and Immunity*, *68*(12), 6871–6878.

Sinha, B., & Fraunholz, M. (2010). Staphylococcus aureus host cell invasion and post-invasion events. *International Journal of Medical Microbiology*, *300*(2–3), 170–175.

Skolimowski, M. ... Emnéus, J. (2012). Modular microfluidic system as a model of cystic fibrosis airways. *Biomicrofluidics*, *6*(3), 0341091–03410911.

Skowyra, M. L., Schlesinger, P. H., Naismith, T. V., & Hanson, P. I. (2018). Triggered recruitment of ESCRT machinery promotes endolysosomal repair. *Science*, *360*(6384).

Sokolovska, A. … Stuart, L. M. (2013). Activation of caspase-1 by the NLRP3 inflammasome regulates the NADPH oxidase NOX2 to control phagosome function. *Nature Immunology*, *14*(6), 543–553.

Soyer, M., & Duménil, G. (2011). Introducing shear stress in the study of bacterial adhesion. *Journal of Visualized Experiments*, *55*(55), e3241.

Spaan, A. N., Surewaard, B. G. J., Nijland, R., & van Strijp, J. A. G. (2013). Neutrophils Versus Staphylococcus aureus : A Biological Tug of War . *Annual Review of Microbiology*, *67*(1), 629–650.

Stallings, C. L. … McKinney, J. D. (2020). A lung-on-chip model of early Mycobacterium tuberculosis infection reveals an essential role for alveolar epithelial cells in controlling bacterial growth. *ELife*, *9*, e59961.

Stanley, S. A., Johndrow, J. E., Manzanillo, P., & Cox, J. S. (2007). The Type I IFN Response to Infection with Mycobacterium tuberculosis Requires ESX-1-Mediated Secretion and Contributes to Pathogenesis . *The Journal of Immunology*, *178*(5), 3143–3152.

Stanley, S. A., Raghavan, S., Hwang, W. W., & Cox, J. S. (2003). Acute infection and macrophage subversion by Mycobacterium tuberculosis require a specialized secretion system. *Proceedings of the National Academy of Sciences of the United States of America*, *100*(22), 13001–13006.

Stelzner, K., Hertlein, T., … Rudel, T. (2020). Intracellular Staphylococcus aureus employs the cysteine protease staphopain A to induce host cell death in epithelial cells. *BioRxiv*.

Stelzner, K., Winkler, A. C., … Rudel, T. (2020). Intracellular staphylococcus aureus perturbs the host cell Ca2+ homeostasis to promote cell death. *MBio*, *11*(6), 1–24.

Stoll, H., Dengjel, J., Nerz, C., & Götz, F. (2005). Staphylococcus aureus deficient in lipidation of prelipoproteins is attenuated in growth and immune activation. *Infection and Immunity*, *73*(4), 2411–2423.

Strobel, M. … Niemann, S. (2016). Post-invasion events after infection with Staphylococcus aureus are strongly dependent on both the host cell type and the infecting S. aureus strain. *Clinical Microbiology and Infection*, *22*(9), 799–809.

Stuart, L. M. ... Moore, K. J. (2005). Response to Staphylococcus aureus requires CD36-mediated phagocytosis triggered by the COOH-terminal cytoplasmic domain. *Journal of Cell Biology*, *170*(3), 477–485.

Stutz, M. D. ... Pellegrini, M. (2018). Necroptotic signaling is primed in Mycobacterium tuberculosis-infected macrophages, but its pathophysiological consequence in disease is restricted. *Cell Death and Differentiation*, *25*(5), 951–965.

Sun, J. ... Niederweis, M. (2015). The tuberculosis necrotizing toxin kills macrophages by hydrolyzing NAD. *Nature Structural and Molecular Biology*, *22*(9), 672–678.

Sun, L. ... Wang, X. (2012). Mixed lineage kinase domain-like protein mediates necrosis signaling downstream of RIP3 kinase. *Cell*, *148*(1–2), 213–227.

Sundaramoorthy, R., Fyfe, P. K., & Hunter, W. N. (2008). Structure of Staphylococcus aureus EsxA Suggests a Contribution to Virulence by Action as a Transport Chaperone and/or Adaptor Protein. *Journal of Molecular Biology*, *383*(3), 603–614.

Sunuwar, L. ... Raffatellu, M. (2019). Mechanical Stimuli Affect Escherichia coli Heat-Stable Enterotoxin-Cyclic GMP Signaling in a Human Enteroid Intestine-Chip Model. *Infection and Immunity*, *88*(3), e00866-19.

Sutcliffe, I. C. (2011). New insights into the distribution of WXG100 protein secretion systems. *Antonie van Leeuwenhoek, International Journal of General and Molecular Microbiology*, *99*(2), 127–131.

Taabazuing, C. Y., Okondo, M. C., & Bachovchin, D. A. (2017). Pyroptosis and Apoptosis Pathways Engage in Bidirectional Crosstalk in Monocytes and Macrophages. *Cell Chemical Biology*, *24*(4), 507-514.e4.

Takahashi, N. ... Vandenabeele, P. (2012). Necrostatin-1 analogues: Critical issues on the specificity, activity and in vivo use in experimental disease models. *Cell Death and Disease*, *3*(11).

Talan, D. A. ... Moran, G. J. (2011). Comparison of staphylococcus aureus from skin and soft-tissue infections in us emergency Department patients, 2004 and 2008. *Clinical Infectious Diseases*, *53*(2), 144–149.

Tam, V. C. ... Gold, E. S. (2020). PPARα exacerbates necroptosis, leading to

increased mortality in postinfluenza bacterial superinfection. *Proceedings of the National Academy of Sciences of the United States of America*, *117*(27), 15789–15798.

Tamoutounour, S. … Henri, S. (2013). Origins and functional specialization of macrophages and of conventional and monocyte-derived dendritic cells in mouse skin. *Immunity*, *39*(5), 925–938.

Tan, H. Y. … Feng, Y. (2016). The Reactive Oxygen Species in Macrophage Polarization: Reflecting Its Dual Role in Progression and Treatment of Human Diseases. *Oxidative Medicine and Cellular Longevity*, *2016*.

Tang, D., Kang, R., Berghe, T. Vanden, Vandenabeele, P., & Kroemer, G. (2019). The molecular machinery of regulated cell death. *Cell Research*, *29*(5), 347–364.

Tavana, H., Zamankhan, P., Christensen, P. J., Grotberg, J. B., & Takayama, S. (2011). Epithelium damage and protection during reopening of occluded airways in a physiologic microfluidic pulmonary airway model. *Biomedical Microdevices*, *13*(4), 731–742.

Taylor, R. C., Cullen, S. P., & Martin, S. J. (2008). Apoptosis: Controlled demolition at the cellular level. *Nature Reviews Molecular Cell Biology*, *9*(3), 231–241.

Tehranirokh, M., Kouzani, A. Z., Francis, P. S., & Kanwar, J. R. (2013). Microfluidic devices for cell cultivation and proliferation. *Biomicrofluidics*, *7*(5).

Tekaia, F. … Cole, S. T. (1999). Analysis of the proteome of Mycobacterium tuberculosis in silico. *Tubercle and Lung Disease*.

Thacker, V. V. … McKinney, J. D. (2020). A lung-on-chip infection model reveals protective and permissive roles of alveolar epithelial cells in tuberculosis. *BioRxiv*.

Thammavongsa, V., Kim, H. K., Missiakas, D., & Schneewind, O. (2015). Staphylococcal manipulation of host immune responses. *Nature Reviews Microbiology*, *13*(9), 529–543.

Thwaites, G. E., & Gant, V. (2011). Are bloodstream leukocytes Trojan Horses for the metastasis of Staphylococcus aureus? *Nature Reviews Microbiology*, *9*(3), 215–222.

Tinevez, J. Y. … Eliceiri, K. W. (2017). TrackMate: An open and extensible platform for single-particle tracking. *Methods*, *115*, 80–90.

Tkaczyk, C. … Sellman, B. R. (2013). Staphylococcus aureus Alpha Toxin Suppresses Effective Innate and Adaptive Immune Responses in a Murine Dermonecrosis Model. *PLoS ONE*, *8*(10).

Tong, S. Y. C., Davis, J. S., Eichenberger, E., Holland, T. L., & Fowler, V. G. (2015). Staphylococcus aureus infections: Epidemiology, pathophysiology, clinical manifestations, and management. *Clinical Microbiology Reviews*, *28*(3), 603–661.

Torre, A. … Bensi, G. (2015). Four-component Staphylococcus aureus vaccine 4C-staph enhances fcγ receptor expression in neutrophils and monocytes and mitigates S. aureus infection in neutropenic mice. *Infection and Immunity*, *83*(8), 3157–3163.

Tranchemontagne, Z. R., Camire, R. B., O'Donnell, V. J., Baugh, J., & Burkholder, K. M. (2015). Staphylococcus aureus strain USA300 perturbs acquisition of lysosomal enzymes and requires phagosomal acidification for survival inside macrophages. *Infection and Immunity*, *84*(1), 241–253.

Tuchscherr, L. … Löffler, B. (2011). Staphylococcus aureus phenotype switching: An effective bacterial strategy to escape host immune response and establish a chronic infection. *EMBO Molecular Medicine*, *3*(3), 129–141.

Tucker, K. A., Reilly, S. S., Leslie, C. S., & Hudson, M. C. (2006). Intracellular Staphylococcus aureus induces apoptosis in mouse osteoblasts. *FEMS Microbiology Letters*, *186*(2), 151–156.

Tufariello, J. A. M. … Jacobs, W. R. (2016). Separable roles for Mycobacterium tuberculosis ESX-3 effectors in iron acquisition and virulence. *Proceedings of the National Academy of Sciences of the United States of America*, *113*(3), E348–E357.

Turner, N. A. … Fowler, V. G. (2019). Methicillin-resistant Staphylococcus aureus: an overview of basic and clinical research. *Nature Reviews Microbiology*, *17*(4), 203–218.

Ulhuq, F. R. … Palmer, T. (2020). A membrane-depolarizing toxin substrate of the Staphylococcus aureus type VII secretion system mediates intraspecies competition. *Proceedings of the National Academy of Sciences of the United States of America*, *117*(34), 20836–20847.

Unnikrishnan, M., Constantinidou, C., Palmer, T., & Pallen, M. J. (2017). The Enigmatic Esx Proteins: Looking Beyond Mycobacteria. *Trends in Microbiology*, *25*(3), 192–204.

Uribe-Quero, E., & Rosales, C. (2017). Control of phagocytosis by microbial pathogens. *Frontiers in Immunology*, *8*, 1368.

van der Wel, N. … Peters, P. J. (2007). M. tuberculosis and M. leprae Translocate from the Phagolysosome to the Cytosol in Myeloid Cells. *Cell*, *129*(7), 1287–1298.

van Kesse, K. P., Bestebroer, J., & van Strijp, J. A. G. (2014). Neutrophil-mediated phagocytosis of Staphylococcus aureus. *Frontiers in Immunology*, *5*(SEP).

Vance, R. E., Isberg, R. R., & Portnoy, D. A. (2009). Patterns of Pathogenesis: Discrimination of Pathogenic and Nonpathogenic Microbes by the Innate Immune System. *Cell Host and Microbe*, *6*(1), 10–21.

VanCleave, T. T., Pulsifer, A. R., Connor, M. G., Warawa, J. M., & Lawrenz, M. B. (2017). Impact of gentamicin concentration and exposure time on intracellular Yersinia pestis. *Frontiers in Cellular and Infection Microbiology*, *7*(DEC), 505.

Vanden Berghe, T., Kaiser, W. J., Bertrand, M. J. M., & Vandenabeele, P. (2015). Molecular crosstalk between apoptosis, necroptosis, and survival signaling. *Molecular and Cellular Oncology*, *2*(4), e975093.

Vandenesch, F., Lina, G., & Henry, T. (2012). Staphylococcus aureus hemolysins, bi-component leukocidins, and cytolytic peptides: a redundant arsenal of membrane-damaging virulence factors? *Frontiers in Cellular and Infection Microbiology*.

Vandenesch, F. … Etienne, J. (2003). Community-acquired methicillin-resistant staphylococcus aureus carrying panton-valentine leukocidin genes: Worldwide emergence. *Emerging Infectious Diseases*, *9*(8), 978–984.

Ventura, C. L. … DeLeo, F. R. (2010). Identification of a novel Staphylococcus aureus two-component leukotoxin using cell surface proteomics. *PLoS ONE*, *5*(7), 11634.

Verma, D. … Hua, S. Z. (2012). Interplay between Cytoskeletal Stresses and Cell Adaptation under Chronic Flow. *PLoS ONE*, *7*(9).

Vicar, T., Raudenska, M., Gumulec, J., & Balvan, J. (2020). The Quantitative-Phase Dynamics of Apoptosis and Lytic Cell Death. *Scientific Reports*, *10*(1), 1–12.

Viela, F. … Dufrênea, Y. F. (2019). Binding of staphylococcus aureus protein a to von willebrand factor is regulated by mechanical force. *MBio*, *10*(2).

Viganò, E. … Mortellaro, A. (2015). Human caspase-4 and caspase-5 regulate the one-step non-canonical inflammasome activation in monocytes. *Nature Communications*, *6*.

Villenave, R. … Ingber, D. E. (2017). Human gut-on-a-chip supports polarized infection of coxsackie B1 virus in vitro. *PLoS ONE*, *12*(2).

Volkman, H. E. … Ramakrishnan, L. (2004). Tuberculous granuloma formation is enhanced by a Mycobacterium virulence determinant. *PLoS Biology*, *2*(11).

Volz, T. … Biedermann, T. (2010). Natural Staphylococcus aureus-derived peptidoglycan fragments activate NOD2 and act as potent costimulators of the innate immune system exclusively in the presence of TLR signals. *FASEB Journal*, *24*(10), 4089–4102.

Voyich, J. M. … DeLeo, F. R. (2005). Insights into Mechanisms Used by Staphylococcus aureus to Avoid Destruction by Human Neutrophils . *The Journal of Immunology*, *175*(6), 3907–3919.

Walker, G. M., Zeringue, H. C., & Beebe, D. J. (2004). Microenvironment design considerations for cellular scale studies. *Lab on a Chip*, *4*(2), 91–97.

Walsh, E. J., Miajlovic, H., Gorkun, O. V., & Foster, T. J. (2008). Identification of the Staphylococcus aureus MSCRAMM clumping factor B (ClfB) binding site in the αC-domain of human fibrinogen. *Microbiology*, *154*(2), 550–558.

Walsh, E. J., O'Brien, L. M., Liang, X., Hook, M., & Foster, T. J. (2004). Clumping factor B, a fibrinogen-binding MSCRAMM (microbial surface components recognizing adhesive matrix molecules) adhesin of Staphylococcus aureus, also binds to the tail region of type I cytokeratin 10. *Journal of Biological Chemistry*, *279*(49), 50691–50699.

Wang, R. … Otto, M. (2007). Identification of novel cytolytic peptides as key virulence determinants for community-associated MRSA. *Nature Medicine*, *13*(12), 1510–1514.

Wang, X., Eagen, W. J., & Lee, J. C. (2020). Orchestration of human macrophage

NLRP3 inflammasome activation by Staphylococcus aureus extracellular vesicles. *Proceedings of the National Academy of Sciences of the United States of America*, *117*(6), 3174–3184.

Wang, Y. … Li, M. (2016). Role of the ESAT-6 secretion system in virulence of the emerging community-associated Staphylococcus aureus lineage ST398. *Scientific Reports*, *6*.

Wardenburg, J. B., Patel, R. J., & Schneewind, O. (2007). Surface proteins and exotoxins are required for the pathogenesis of Staphylococcus aureus pneumonia. *Infection and Immunity*, *75*(2), 1040–1044.

Wardenburg, J. B., & Schneewind, O. (2008). Vaccine protection against Staphylococcus aureus pneumonia. *Journal of Experimental Medicine*, *205*(2), 287–294.

Warne, B. … Holden, M. T. G. (2016). The Ess/Type VII secretion system of Staphylococcus aureus shows unexpected genetic diversity. *BMC Genomics*, *17*(1).

Weinrick, B. … Novick, R. P. (2004). Effect of Mild Acid on Gene Expression in. *Journal of Bacteriology*, *186*(24), 8407–8423.

Wemyss, M. A., & Pearson, J. S. (2019). Host Cell Death Responses to Non-typhoidal Salmonella Infection. *Frontiers in Immunology*, *10*(July), 1758.

Wertheim, H. F. L. … Van Belkum, A. (2008). Key role for clumping factor B in Staphylococcus aureus nasal colonization of humans. *PLoS Medicine*, *5*(1), 0104–0112.

Wertheim, H. F. … Nouwen, J. L. (2005). The role of nasal carriage in Staphylococcus aureus infections. *The Lancet Infectious Diseases*, *5*(12), 751–762.

Werz, O. … Serhan, C. N. (2018). Human macrophages differentially produce specific resolvin or leukotriene signals that depend on bacterial pathogenicity. *Nature Communications*, *9*(1).

Wesson, C. A. … Trumble, W. R. (2000). Apoptosis induced by Staphylococcus aureus in epithelial cells utilizes a mechanism involving caspases 8 and 3. *Infection and Immunity*, *68*(5), 2998–3001.

Wesson, C. A. … Bayles, K. W. (1998). Staphylococcus aureus Agr and Sar global

regulators influence internalization and induction of apoptosis. *Infection and Immunity*, *66*(11), 5238–5243.

White, C. R., & Frangos, J. A. (2007). The shear stress of it all: The cell membrane and mechanochemical transduction. *Philosophical Transactions of the Royal Society B: Biological Sciences*, *362*(1484), 1459–1467.

Whitesides, G. M. (2006). The origins and the future of microfluidics. *Nature*, *442*(7101), 368–373.

Wilke, G. A., & Wardenburg, J. B. (2010). Role of a disintegrin and metalloprotease 10 in Staphylococcus aureus α-hemolysin - Mediated cellular injury. *Proceedings of the National Academy of Sciences of the United States of America*, *107*(30), 13473–13478.

Wilmer, M. J. … Masereeuw, R. (2016). Kidney-on-a-Chip Technology for Drug-Induced Nephrotoxicity Screening. *Trends in Biotechnology*, *34*(2), 156–170.

Wong Fok Lung, T. … Prince, A. (2020). Staphylococcus aureus small colony variants impair host immunity by activating host cell glycolysis and inducing necroptosis. *Nature Microbiology*, *5*(1), 141–153.

Wong, K.-W. (2017). The Role of ESX-1 in Mycobacterium tuberculosis Pathogenesis. *Microbiology Spectrum*, *5*(3).

Wong, K. W., & Jacobs, W. R. (2011). Critical role for NLRP3 in necrotic death triggered by Mycobacterium tuberculosis. *Cellular Microbiology*, *13*(9), 1371–1384.

Yang, E. S. … Miller, L. G. (2010). Body site colonization in patients with community-associated methicillin-resistant Staphylococcus aureus and other types of S. aureus skin infections. *Clinical Microbiology and Infection*, *16*(5), 425–431.

Yao, R. … Wang, Z. (2020). Pathogenic effects of inhibition of mTORC1/ STAT3 axis facilitates Staphylococcus aureus-induced pyroptosis in human macrophages. *Cell Commun Signal*, *18*, 187.

Yates, R. M., Hermetter, A., & Russell, D. G. (2005). The kinetics of phagosome maturation as a function of phagosome/lysosome fusion and acquisition of hydrolytic activity. *Traffic*, *6*(5), 413–420.

Yokoyama, R. ... Onozaki, K. (2012). Staphylococcal superantigen-like protein 3 binds to the toll-like receptor 2 extracellular domain and inhibits cytokine production induced by Staphylococcus aureus, cell wall component, or lipopeptides in murine macrophages. *Infection and Immunity*, *80*(8), 2816–2825.

Yoon, K. H. ... Goldman, R. D. (2001). Insights into the dynamic properties of keratin intermediate filaments in living epithelial cells. *Journal of Cell Biology*, *152*(3), 503–516.

Young, E. W. K., & Beebe, D. J. (2010). Fundamentals of microfluidic cell culture in controlled microenvironments. *Chemical Society Reviews*, *39*(3), 1036–1048.

Zamprogno, P. ... Guenat, O. T. (2021). Second-generation lung-on-a-chip with an array of stretchable alveoli made with a biological membrane. *Communications Biology*, *4*(1).

Zhang, B. Z. ... Huang, J. D. (2015). Recombinant ESAT-6-like proteins provoke protective immune responses against invasive Staphylococcus aureus disease in a murine model. *Infection and Immunity*, *83*(1), 339–345.

Zheng Jian Li, Mohamed, N., & Ross, J. M. (2000). Shear stress affects the kinetics of Staphylococcus aureus adhesion to collagen. *Biotechnology Progress*, *16*(6), 1086–1090.

Zheng, W., Wang, Z., Zhang, W., & Jiang, X. (2010). A simple PDMS-based microfluidic channel design that removes bubbles for long-term on-chip culture of mammalian cells. *Lab on a Chip*, *10*(21), 2906–2910.

Zhou, C. ... Fey, P. D. (2019). Urease is an essential component of the acid response network of Staphylococcus aureus and is required for a persistent murine kidney infection. *PLoS Pathogens*, *15*(1), 1–23.

Zhou, H. ... Zhu, X. (2013). EsxA might as a virulence factor induce antibodies in patients with Staphylococcus aureus infection. *Brazilian Journal of Microbiology*, *44*(1), 267–271.

Zhu, X. ... Jiang, Q. (2019). Inhibition of pyroptosis attenuates Staphylococcus aureus-induced bone injury in traumatic osteomyelitis. *Annals of Translational Medicine*, *7*(8), 170–170.

Zoltner, M. … Hunter, W. N. (2016). EssC: domain structures inform on the elusive translocation channel in the Type VII secretion system. *Biochemical Journal*, *473*(13), 1941–1952.

Zoltner, Martin, Fyfe, P. K., Palmer, T., & Hunter, W. N. (2013). Characterization of Staphylococcus aureus EssB, an integral membrane component of the Type VII secretion system: Atomic resolution crystal structure of the cytoplasmic segment. *Biochemical Journal*, *449*(2), 469–477.
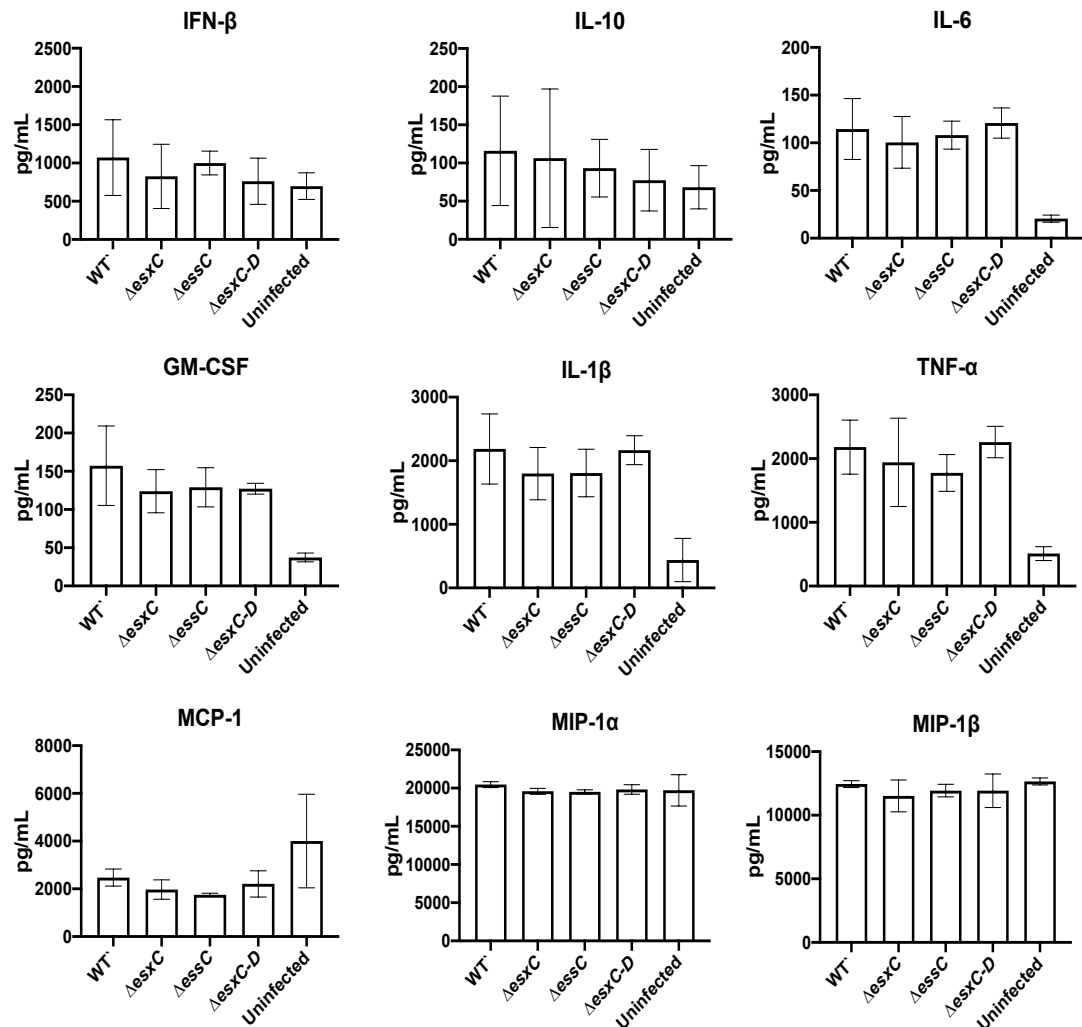
8. Appendix

Figure S1: Macrophage cytokine and chemokine response to *S. aureus* WT and T7SS mutants.

Levels of IFN-β, IL-10, IL-6, GM-CSF, IL-1β, TNF-α, MCP-1, MIP-1α, MIP-1β released into supernatant by THP-1 uninfected cells and THP-1 cells infected with WT JE2 or Δ*esxC*, Δ*essC,* Δ*esxC-D* isogenic mutants quantified after 24 hrs as quantified by MSD multiplex analysis. Graphs show mean $\pm$SD. Non-significant results were determined with one-way ANOVA.
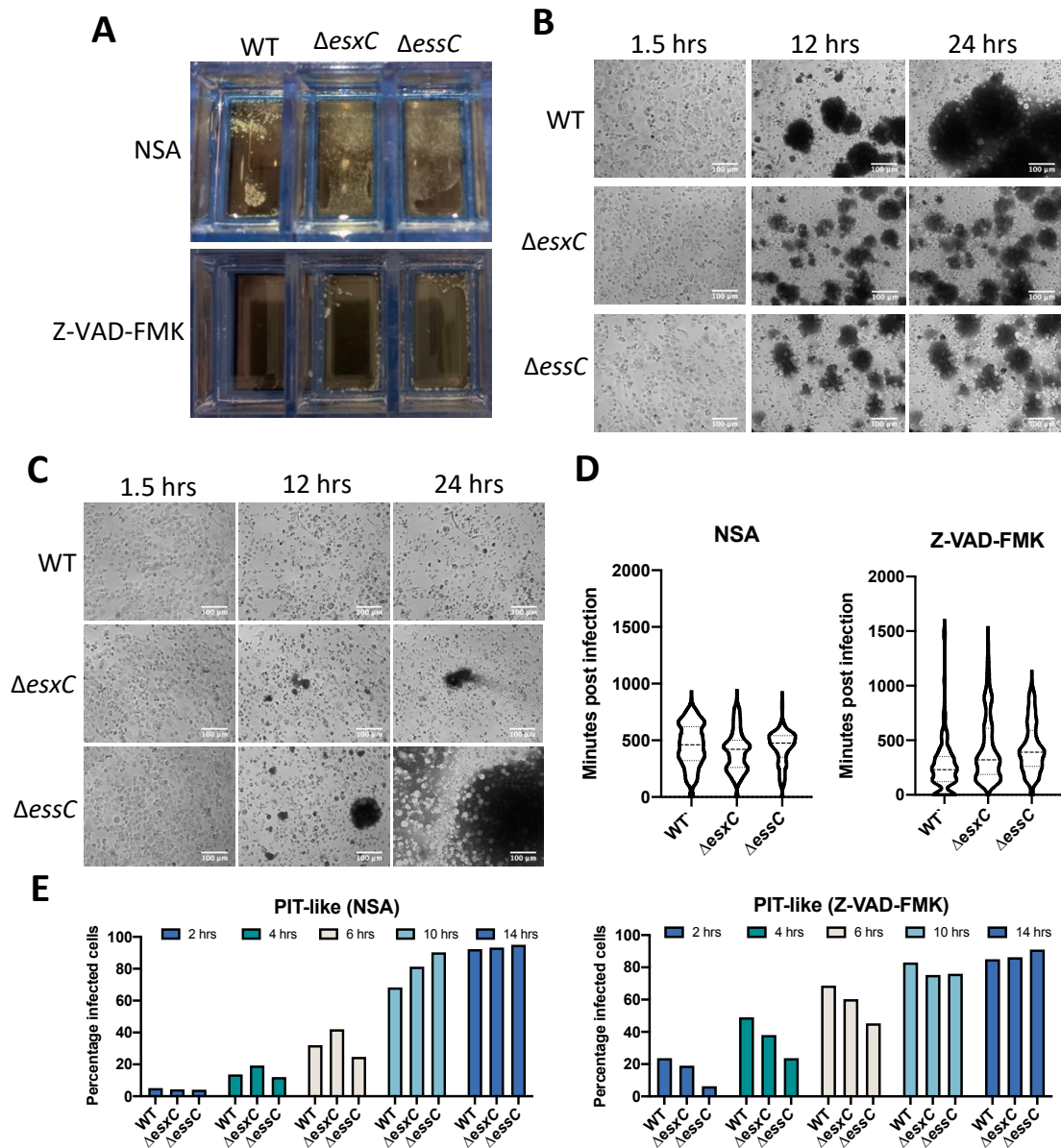
Figure S2: Inhibiting MLKL reverses the effect of the T7SS on microcolony formation.

THP-1 macrophages cultured on RS treated glass chamber slides were incubated with either Z-VAD-FMK or NSA for 1 hour prior to infection. THP-1 cells were then incubated with *S. aureus* JE2 WT or isogenic ΔesxC, Δ*essC* mutant strains at MOI 10:1 for 1 hour. Bacteria were then killed, cells washed and refreshed with RPMI media with NSA or Z-VAD-FMK for 24 hours. A total of 300 cells were analysed in 1 independent experiment. (A) Images of infection assays carried out on chamber slides, microcolonies are visible to the eye (yellow colonies). (B) Microscope images of THP-1 macrophages treated with NSA and infected with WT or T7SS mutant *S. aureus*. (C) Microscope images of THP-1 macrophages treated with Z-VAD-FMK and infected with WT or T7SS mutant *S.*

aureus. (D) Percentage of infected macrophages with PIT-like morphologies at indicated timepoints. All bar graphs show mean ±SD, n=1.
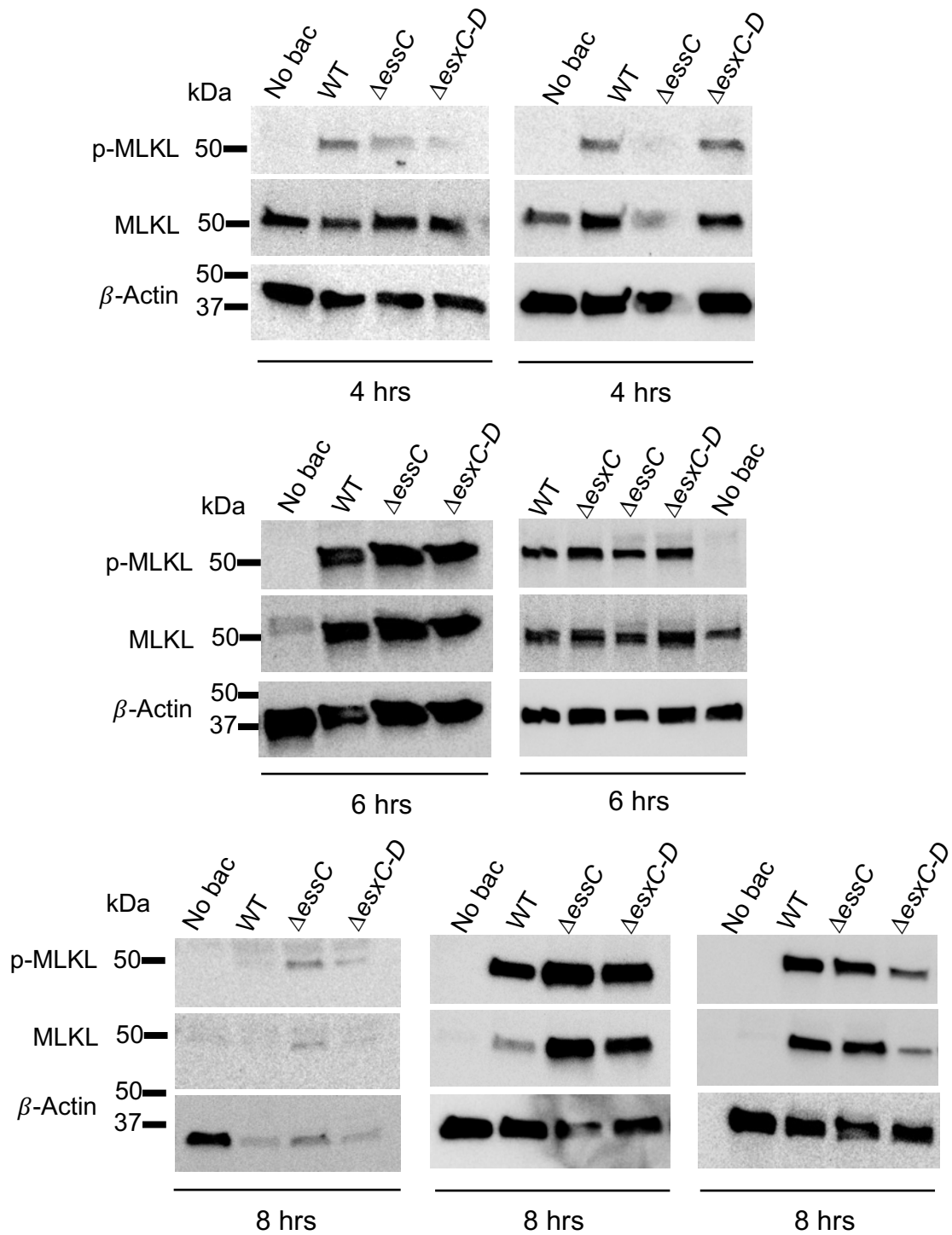
Figure S3: Western blots probing the necroptosis pathway.

Biological replicates of Western blots of phosphorylated MLKL (p-MLKL), MLKL and β-actin, from non-infected (no bac), WT and T7SS mutant infected THP-1 cells 4 hrs, 6hrs and 8 hrs post infection.
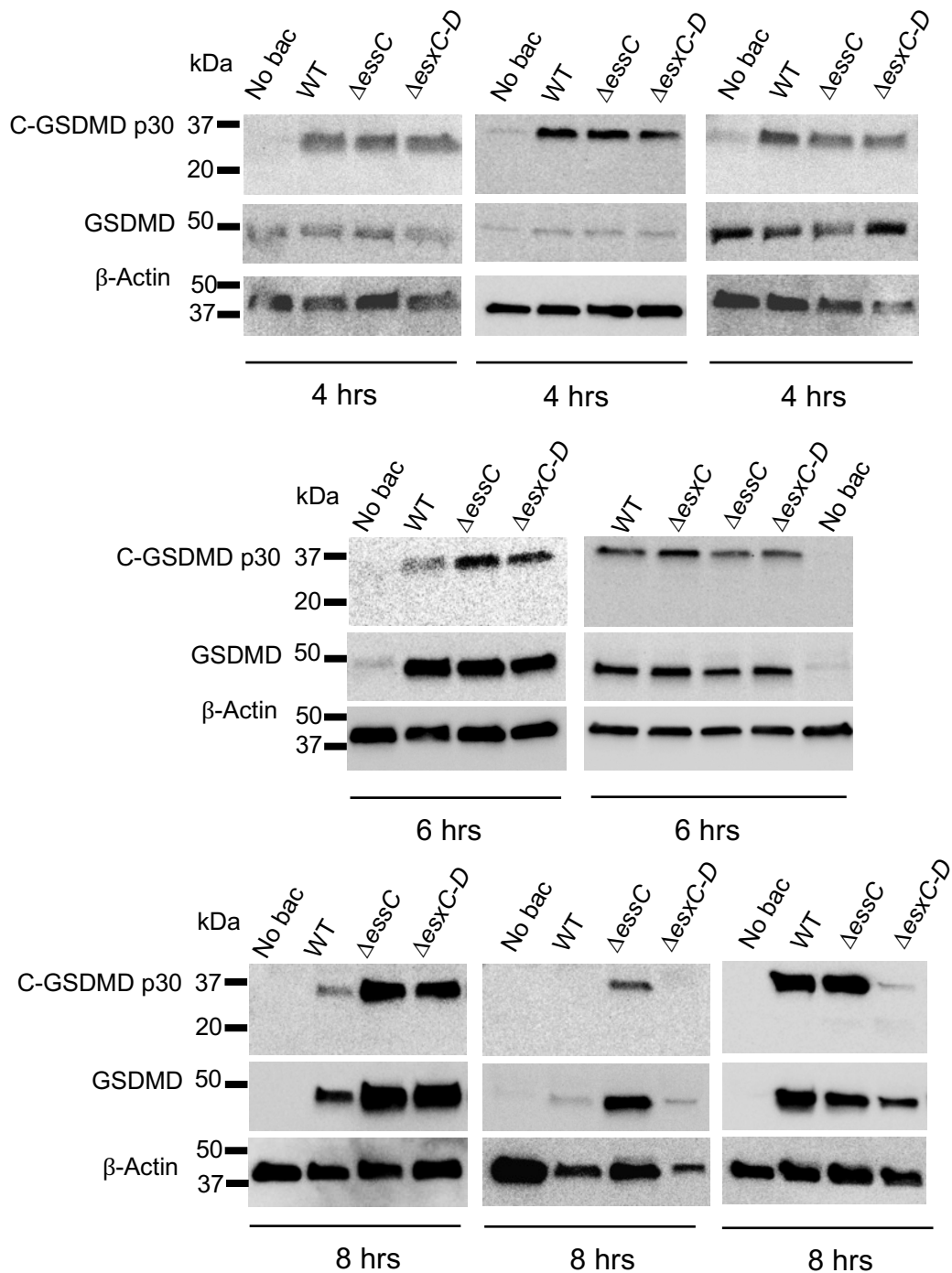
Figure S4: Western blots to show pyroptosis in *S. aureus* infections of THP-1 macrophages.

Biological repeats of western blots showing cleaved GSDMD (c-GSDMD), GSDMD and β-actin, from non-infected (no bac), WT and T7SS mutant infected THP-1 cells 4 hrs, 6hrs and 8 hrs post infection.
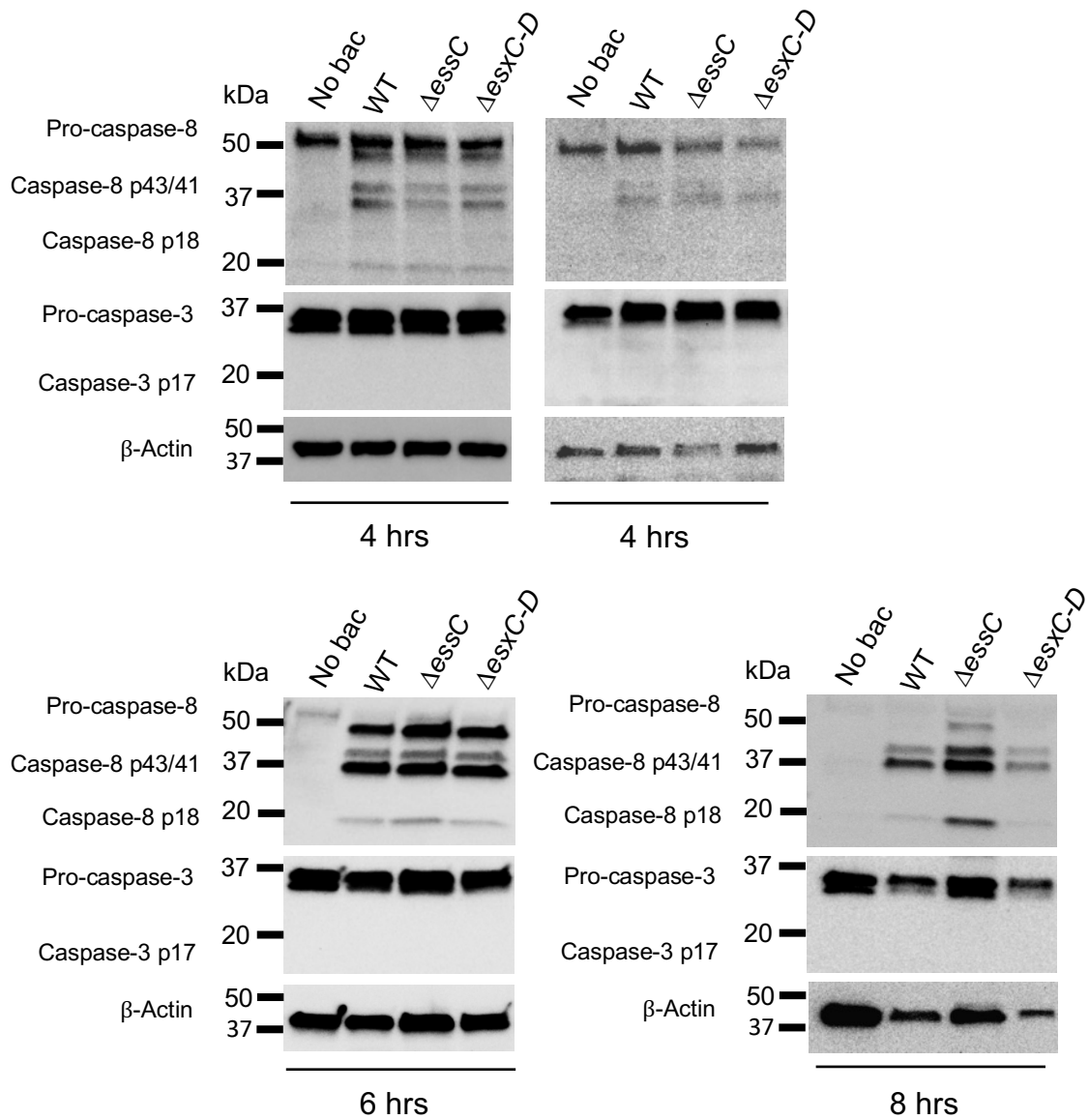
Figure S5: Western blots to show activation of apoptosis in infected macrophages.

Biological replicates of Western blots showing pro-caspase-3 and pro-caspase-8 plus corresponding cleaved subunits from non-infected (no bac) or infected WT and T7SS mutant THP-1 cell lysates at 4 hrs, 6hrs and 8 hrs post infection.